Development of nanostructured catalysts for the oxidative coupling of methane

(Desenvolvemento de catalisadores nanoestructurados para a conversão oxidativa do metano)

Víctor José Ferreira Ferreira

Dissertation presented for the Ph.D. Degree in

Chemical and Biological Engineering at the

Faculty of Engineering, University of Porto, Portugal

Supervisors: José Luís Cabral da Conceição Figueiredo

Joaquim Luís Bernardes Martins de Faria

LCM – Laboratório de Catálise e Materiais

Laboratório Associado LSRE/LCM

Department of Chemical Engineering

Faculty of Engineering

University of Porto

Portugal

2013

Dedicado a ti Papá…..

Abstract

There are large resources of natural gas which show a trend to increase, rivaling those of crude oil. Currently, natural gas is underutilized, since there are no feasible routes to convert large amounts of CH_4, the main component of natural gas, into value added products. Oxidative coupling of methane (OCM) to produce C_2H_6 and C_2H_4 (C_2 hydrocarbons) is a possible reaction. However, several challenges have limited its commercialization, such as high temperatures, limitations of methane conversion/yield and low selectivity at high CH_4 conversion. The main objective of this work was the development of catalysts for the OCM reaction, by testing several catalysts in conventional reactors with a feed current of molecular oxygen and methane to produce C_2 hydrocarbons, and then in an electrocatalytic system in which oxygen was produced in situ by water electrolysis.

The first goal of this thesis was the development of Ce-based mixed oxides and supported catalysts, with activity and selectivity to produce C_2 hydrocarbons, in order to select the most promising catalytic system for further developments. It was observed that the incorporation of Li, Na and Ca in CeO_2 influenced the acid/base properties of the catalyst surface, leading to a significant increase in the C_2 hydrocarbons selectivity and yield. The results obtained showed that the incorporation of metals, such as Mg, Ca and Sr, plays an important role in the creation of active sites on the CeO_2 surface, improving their performance in OCM. These active sites are related to surface oxygen species, namely O_2^{2-} and O_2^-. A linear relationship between the total amount of basic sites and the relative amount of electrophilic oxygen species and lattice oxygen on the surface of the catalyst, $[(O_2^{2-} + O_2^-)/ O^{2-}]$, was found. In addition, it was demonstrated that methane conversion and C_2 hydrocarbon selectivity are controlled by that ratio. A Ce-doped La_2O_3 catalyst with a Ce/La molar ratio of 1:3 was prepared by two methods, namely the solvothermal and citrate methods.

Both allowed the formation of a solid solution ($La_xCe_{1-x}O_{1.5+\delta}$). The solvothermal method created O^- oxygen species, while the citrate method created both O_2^{2-} and O^-. The results showed that the different oxygen species created are related to the different types of surface cerium ions (Ce^{3+} or Ce^{4+}). The O^- oxygen species predominant on the catalyst are suggested to be responsible for higher C_2 yield in the OCM.

The supported catalysts (Ce and Na_2WO_4 on SiO_2) revealed to be active and selective to the OCM, particularly the catalyst containing 5wt%Ce, which showed a good performance when compared to results reported in literature. This is related to an adequate mixture of both amorphous and α-crystobalite phases present in the catalyst and the tungstate-metal interactions formed during the crystallization process to create active centres for the OCM reaction. The best catalysts were then tested under a CH_4 wet atmosphere in the OCM reaction. The 5wt%Ce-5wt%Na_2WO_4/SiO_2 catalyst revealed the best performance . The presence of steam did not improve significantly the OCM performance over $Ca_{0.5}Ce_{0.5}O$. Nevertheless, steam showed to have a poisoning effect over $La_{0.75}Ce_{0.25}O$.

These results prompted the evaluation of the 5wt%Ce-5wt%Na_2WO_4/SiO_2 catalyst in two different solid electrolyte-fixed bed reactor configurations. In these configurations, O^{2-} ions were produced *in situ* by water electrolysis to react with a wet CH_4 atmosphere (single chamber) or with CH_4 alone (double chamber) over 5wt%Ce-5wt%Na_2WO_4/SiO_2. The results showed that C_2 hydrocarbons and H_2 were simultaneously produced in the single chamber and then produced and separated in the double chamber. In both configurations, the presence of this catalyst strongly increased the catalytic activity and the overall configuration (solid electrolyte cell + catalyst bed) was found to be stable for long operating times (24 h).

Resumo

Existem grandes recursos de gás natural com uma tendência em aumento rivalizando o petróleo. Atualmente, o gás natural é pouco subutilizado, uma vez que não há rotas viáveis para converter grandes quantidades de CH_4, o principal componente do gás natural, em produtos de valor acrescentado. O acoplamento oxidativo do metano (AOM) para produzir hidrocarbonetos C_2 (C_2H_6 e C_2H_4) é uma possível reação. No entanto, vários desafios têm limitado a sua comercialização, tais como, altas temperaturas, as limitações de conversão de metano / rendimento e baixa seletividade a uma conversão de CH_4 elevada.

O principal objetivo deste trabalho foi o desenvolvimento de catalisadores para a reação de AOM. Vários catalisadores foram testados em reatores convencionais com uma corrente de alimentação constituída por metano e oxigénio molecular para produzir hidrocarbonetos C_2 e depois num sistema eletrocatalítico em que o oxigénio é produzido *in situ* através do processo de eletrólise da água. O primeiro objetivo desta tese foi o desenvolvimento de óxidos mistos baseados em Ce e catalisadores suportados, ativos e seletivos para produzir hidrocarbonetos C_2 com a finalidade de selecionar o sistema catalítico mais promissor para futuros desenvolvimentos.

Observou-se que a incorporação de Li, Na e Ca no CeO_2 influência nas propriedades ácido / base da superfície do catalisador, o que fez aumentar significativamente a seletividade e rendimento para formar hidrocarbonetos C_2. Os resultados obtidos mostraram que a incorporação de metais, tais como Mg, Ca e Sr, desempenha um papel importante na formação de sítios ativos na superfície do CeO_2, melhorando o seu performance no AOM. Estes sitios ativos estão relacionados com as espécies de oxigénio na superfície, nomeadamente O_2^{2-} e O_2^-. Uma razão linear foi encontrada entre a quantidade total de sítios básicos e a quantidade relativa de espécies de oxigénio e oxigénio eletrofílico sobre a superfície do catalisador, [(O_2^{2-} + O_2^-) / O_2^-]. Além disso, demonstrou-se que a conversão do metano e a seletividade de hidrocarbonetos C_2 são controlados pela mencionada razão.

Um catalisador formado por La_2O_3 modificado com Ce numa razão molar de 1:3 Ce / La foi preparado por dois métodos, nomeadamente, os métodos solvotérmico e citrato. Os dois métodos permitiram a formação de uma solução sólida ($La_xCe_{1-x}O_{1.5\ \delta+}$). O método solvotérmico formou espécies de oxigénio O^-, enquanto o método de citrato formou O_2^{2-} assim como O^-. Os resultados mostraram que as diferentes espécies de oxigénio produzidos estão relacionados com os diferentes tipos de iões de cério (Ce^{3+} ou de Ce^{4+}). As espécies predominantes de oxigénio no catalisador são sugeridas ser responsáveis pelo maior rendimento de hidrocarbonetos C_2 na reação de AOM. Os catalisadores suportados (Ce e Na_2WO_4 em SiO_2) mostraram atividade e seletividade para o AOM, especialmente o catalisador com 5wt% Ce mostrou melhor performance quando comparado com os resultados encontrados na literatura. Este resultado está relacionado com uma mistura adequada de sílica amorfa e α-cristobalita presentes no catalisador e as interações tungstato-metal formadas durante o processo de cristalização para produzir centros ativos para a reação de AOM. Os melhores catalisadores foram testados sob uma atmosfera húmida de CH_4 na reação do AOM. O catalisador 5wt%Ce-5wt%Na_2WO_4/SiO_2 mostrou melhor performance. A presença de vapor de água não melhorou significativamente o performance do AOM sobre $Ca_{0.5}Ce_{0.5}O$. No entanto, o vapor teve um efeito de envenenamento sobre o $La_{0.75}Ce_{0.25}O$.

Estes resultados levaram a avaliação do catalisador 5wt%Ce-5wt% Na_2WO_4/SiO_2 em duas diferentes configurações de reator de leito fixo de electrólito sólido. Nessas configurações, os íones O^{2-} foram produzidos *in situ* através do processo de eletrólise da água para reagir com uma atmosfera húmida de CH_4 (câmara simples) ou com CH_4 só (câmara dupla) sobre o catalisador 5wt%Ce-5wt% Na_2WO_4/SiO_2. Os resultados mostraram que os hidrocarbonetos C_2 e H_2 foram produzidos simultaneamente na câmara simples e, em seguida, produzido e separado na câmara dupla. Nas duas configurações, a presença deste catalisador aumentou significativamente a actividade catalítica. Finalmente, a configuração, célula de electrólito sólido + leito de catalisador, foi encontrado ser estável por longos tempos de operação (24 h).

Résumé

Il existe d'importantes ressources de gaz naturel qui montrent une tendance à augmenter, rivalisant avec ceux du pétrole brut. Actuellement, le gaz naturel est sous-utilisé, car il n'y a pas de routes possibles pour convertir les grandes quantités de CH_4, principal composant du gaz naturel, en produits à valeur ajoutée. Le couplage oxydant du méthane (OCM) pour produire du C_2H_6 et du C_2H_4 (C_2 hydrocarbures) est une réaction possible. Toutefois, plusieurs défis ont limité sa commercialisation, comme les températures élevées, les limitations de conversion/rendement du méthane et une faible sélectivité pour de haute conversion de CH_4.L'objectif principal de ce travail a été le développement de catalyseurs pour la réaction OCM, à travers le test de plusieurs catalyseurs dans des réacteurs conventionnels sous courant d'oxygène moléculaire et de méthane pour produire des hydrocarbures C_2, puis dans un système électrocatalytique dans lequel l'oxygène est produit in situ par électrolyse de l'eau.

Le premier objectif de cette thèse a été le développement d'oxydes mixtes à base de Ce et de catalyseurs supportés, présentant une activité et une sélectivité pour produire des hydrocarbures C_2, afin de sélectionner le système catalytique la plus prometteur pour de nouveaux développements. Il a été observé que l'incorporation de Li, Na et Ca au sein de CeO_2 influence les propriétés acide/base de la surface du catalyseur, ce qui conduit à une augmentation significative de la sélectivité et le rendement des hydrocarbures C_2. Les résultats obtenus ont montré que l'incorporation de métaux, tels que le Mg, Ca et Sr, joue un rôle important dans la création de sites actifs sur la surface de CeO_2, améliorant leur performance dans l'OCM. Ces sites actifs sont liés aux espèces oxygénées de surface, à savoir O_2^{2-} et O_2^-. Une relation linéaire entre le nombre total de sites basiques et la quantité relative d'oxygène électrophile et du réseau d'oxygène à la surface du catalyseur, $[(O_2^{2-} + O_2^-)/ O^{2-}]$, a été trouvée. Additionnellement, il a été démontré que la conversion du méthane et la sélectivité en hydrocarbures

C_2 sont contrôlés par ce ratio. Un catalyseur La_2O_3 dopé avec du cérium et ayant un rapport molaire Ce/La de 1:3 a été préparé par deux méthodes, à savoir les méthodes solvothermale et citrate.

Toutes deux ont permis la formation d'une solution solide ($La_xCe_{1-x}O_{1.5+\delta}$). La méthode solvothermale a mené à la création d'oxygène O^-, tandis que la méthode citrate créa les deux espèces O_2^{2-} and O^-. Les résultats ont montré que les différentes espèces d'oxygène créés sont liés aux différents types d'ions cérium de surface (Ce^{3+} or Ce^{4+}). L'espèce prédominante d'oxygène O^- sur le catalyseur a été proposée comme responsable du rendement élevé de C_2 dans l'OCM.

Les catalyseurs supportés (Ce et Na_2WO_4 sur SiO2) ont révélé être actif et sélectif pour l'OCM, en particulier le catalyseur contenant 5% de Ce qui a montré une bonne performance par rapport aux résultats rapportés dans la littérature. Ceci est lié à un mélange adéquat des deux phases, amorphes et α-cristobalite, présentes dans le catalyseur et aux interactions tungstène-métal formées pendant le processus de cristallisation qui mène à la création des centres actifs pour la réaction OCM. Les meilleurs catalyseurs ont ensuite été testés sous une atmosphère humide de CH_4 dans la réaction OCM. Le catalyseur 5%Ce-5%Na_2WO_4/SiO_2 a révélé la meilleure performance. La présence de vapeur d'eau n'améliore pas significativement les performances de l'OCM sur $Ca_{0.5}Ce_{0.5}O$. Néanmoins, la vapeur a montré avoir un effet d'empoisonnement sur $La_{0.75}Ce_{0.25}O$.

Ces résultats ont incité l'évaluation du catalyseur 5%Ce-5% Na_2WO_4/SiO_2 en deux configurations de réacteurs électrolytique solide à lit fixe différents. Dans ces configurations, les ions O^{2-} étaient produits in situ par électrolyse de l'eau pour réagir avec une atmosphère humide de CH_4 (chambre unique) ou avec le CH_4 seul (double chambre) en présence de 5%Ce-5%Na_2WO_4/SiO_2. Les résultats ont montré que les hydrocarbures C_2 et H_2 étaient produits simultanément dans la chambre unique et puis produits et séparés dans la double chambre. Dans les deux configurations, la présence de ce catalyseur a fortement augmenté l'activité catalytique et la configuration globale (cellule d'électrolyte solide + lit de catalyseur) a été stable pour de longues durées de fonctionnement (24 h).

Agradecimentos

Em primeiro lugar aos meus orientadores, Professor Doutor José Luís Figueiredo e Professor Doutor Joaquim Luís de Faria agradeço o apoio, disponibilidade, conhecimentos, sugestões e criticas que aportaram durante estes quatro anos para conseguir a realização deste trabalho.

A Fundação para a Ciência e Tecnologia (FCT), agradeço a concessão da bolsa de doutoramento (SFRH/BD/33647/2009). Ao Professor Doutor José Luís Figueiredo, Coordenador Científico do Laboratório de Catalise e Materiais, agradeço as facilidades concedidas para a realização deste trabalho.

A todos os colegas que conformam o grupo de investigação do LCM, aos que foram passando e aos que ainda estão, agradeço toda a ajuda e companheirismo. Em particular a Raquel, Salomé, Elodie, Juliana, Alexandra, Carla, Rita, Maria José, Luisa, Sergio, Miguel, Tiago, Ricardo e João, agradeço a amizade, toda vossa ajuda e os bons momentos.

A Doutora Cláudia Silva pela ajuda na realização e interpretação das análises DRIFT.

Ao Professor Pedro Tavares (da Universidade trás-os-montes e Alto Douro) pela ajuda com as análises XRD.

Ao Doutor Carlos Sá (Centro de Materiais da Universidade do Porto) e seu pessoal pela ajuda nas análises XPS e SEM-EDS.

A minha Mãe, Pai e irmã, que apesar da distância durante todos estes anos foram cada dia fonte de inspiração e força para continuar e chegar ao fim. Especialmente a meu irmão pela sua presença e apoio neste último ano.

Table of Contents

List of Figures

List of Tables

PART I

INTRODUCTION

1 Introduction

Oxidative coupling of methane has been considered as an alternative reaction for the production of higher hydrocarbons from natural gas. Although this reaction does not present thermodynamic constraints, it is a catalysed reaction. Thus, several approaches have taken to maximise the yields of the catalysts towards the desired products (ethane and ethylene) to make an approved industrial application. In this first chapter, a review of the work performed in this area is presented. Several aspects of catalyst design and mechanisms, such as types of metal oxides, supported metals and surface oxygen species are revised. The influence of operating conditions, such as reaction temperature and partial press are among the many important factors discussed in this chapter. In addition, new technologies based on the design of electrolyte membrane reactors, in which the oxidative coupling of methane reaction is integrated, are also discussed.

1.1 Natural Gas

Natural gas is a combustible mixture of hydrocarbon gases. The composition of natural gas can vary widely. A typical composition, before refinement, is shown in Table 1.1.

Table 1.1 Typical composition of natural gas.

Methane	CH_4	70-90%
Ethane	C_2H_6	
Propane	C_3H_8	0-20%
Butane	C_4H_{10}	
Carbon Dioxide	CO_2	0-8%
Oxygen	O_2	0-0.2%
Nitrogen	N_2	0-5%
Hydrogensulphide	H_2S	0-5%
Rare gases	A, He, Ne, Xe	trace

As observed in the above table, CH_4 is the main component of natural gas which is considered as a source of energy and organic carbon. The registered reserves of natural gas have increased in recent years. Figure 1.1 shows a trend of the natural gas reserve increase compared to that of oil reserves. This latter is because gas is often found alongside petroleum. On the other hand, the production, refinement, transportation, and storage of crude oil are also a source of CH_4 emissions. It means that natural gas is available and produced mostly in remote areas. However, natural gas has currently been made ready for use either as ordinary gas in pipelines or as physically liquefied gas shipped in tankers. Liquefied gas was really the only viable alternative when the reserves were located far from the major customers. Nevertheless, a constraint on the growth of liquefied gas has always been the slow build-up of the liquefied gas and the construction of re-gasification capacity [1]. On the other words, natural gas transportation over long distances is energy and capital intensive and in some case is not economically feasible. Thus, it would be desirable to convert methane on site to useful chemicals or fuels easily transportable involving oxidative or non-oxidative activation of methane.

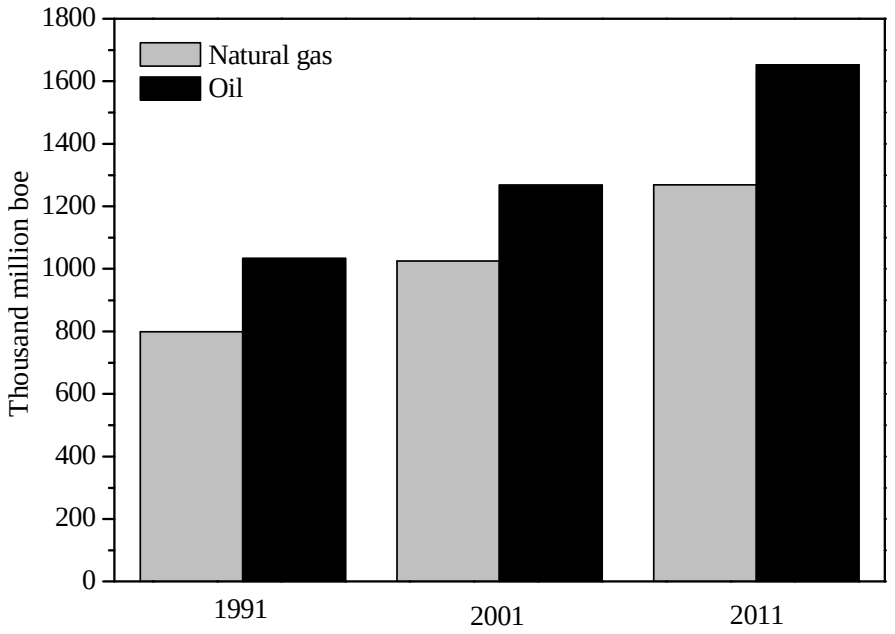

Figure 1.1 Natural gas and Oil registered reserves in 1991, 2001 and 2011 (source: BP Statistical Review of World Energy, June 2012).

1.2 Natural gas conversion process

Natural gas conversion is divided into direct and indirect conversion. Most of the processes related to direct conversion are still in development whereas the others were well-established in the industry 60 or 70 years ago.

1.2.1 Natural gas indirect conversion process

The indirect conversion process of natural gas comprises two steps. Steam reforming and then the subsequent production of hydrocarbons in low-temperature exothermic process. Steam reforming is the chemical conversion of methane to synthesis gas (syngas) which is a mixture of CO and H_2 in varied ratios to fit the particular process. In the second step, syngas is used as a raw material base to produce methanol and its many product derivatives including gasoline range hydrocarbons and methyl-t-butyl ether (MTBE), Fischer-Tropsch hydrocarbons, hydroformy-lation (oxosynthesis) products, formaldehyde, hydrogen source for ammonia, and a further wide spectrum of industrial chemicals [2]. A diagram highlighting the specific processes of syngas is showed in Figure 1.2.

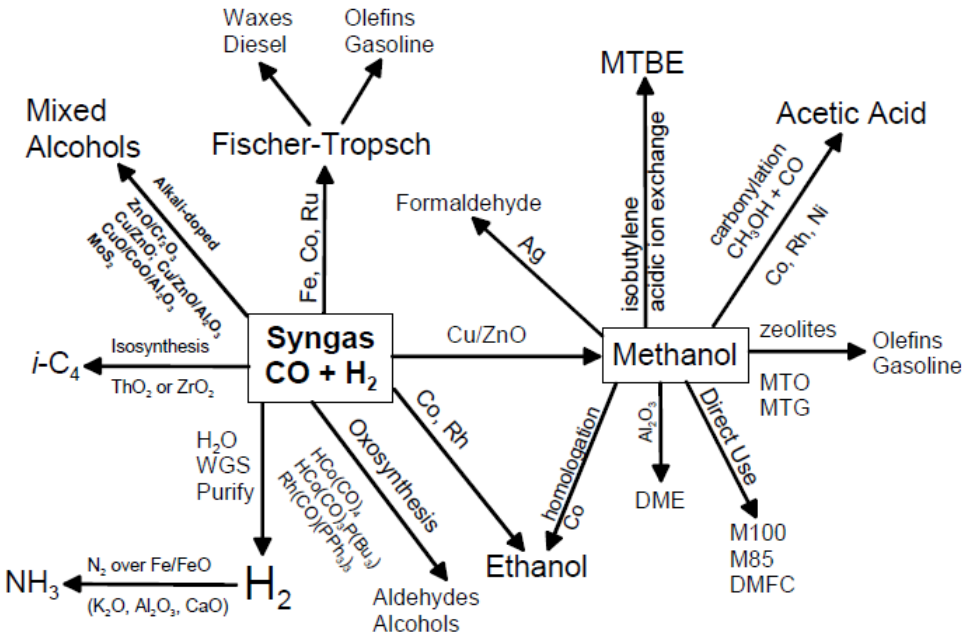

Figure 1.2 Scheme of syngas conversion process [3].

1.2.2 Natural gas direct conversion process

The direct conversion consists in the one-step transformation of methane to higher hydrocarbons and chemical derivatives. The systematic study of the direct conversion of methane to obtain more valuable products started at the beginning of the past century and considerable researches were carried out in the 1920s and 1930s [4]. Thus, direct methane conversion may be grouped into two categories: thermal cracking reaction and catalytic conversion of oxygen. The thermal cracking reactions are endothermic and temperature which must be above 1000 ^{o}C. These conditions require large quantities of energy making this process costly. Thermal conversion of methane by oxygen can lead to methanol, formaldehyde and C_2 hydrocarbons, but selectivities to these products are quite low due to deep oxidation reactions.

However, after several decades, this process continues to be intensively researched worldwide as a possible source of liquid fuels and chemical raw materials based on natural gas. A classification of the direct conversion was proposed by Kuo in 1987 [5] as follows:

1) Partial oxidation (to formaldehyde, methanol, methyl halogenated and others) using different oxidant agents (O_2, Nitrogen Oxides, Halogens, Super acids as catalysts);

2) Oxidative Coupling of Methane (OCM) to ethane and ethylene;

3) Direct conversion to acetylene or others higher hydrocarbons, for example: direct conversion to acetylene by thermal pyrolysis, by using electric arc or plasma, via partial oxidation and direct conversion to others higher hydrocarbons;

4) Other processes of direct conversion as hydrocarbon alkylation.

Relevant direct processes are methane partial oxidation to formaldehyde or methanol with oxygen, pyrolytic process, halogenated production and oxidative coupling of methane (OCM). However, this latter has received considerable attention since the pioneering work of Keller and Bhasin in 1982 [6], as a new selective oxidation technology to directly produce higher hydrocarbons.

1.3 Oxidative coupling of methane

Production of C_2 hydrocarbons (ethane and ethylene) from the OCM offers a potential route for utilization of the huge reservoirs of natural gas as liquid fuels, chemical and petrochemical feedstock. As mentioned above, CH_4 is the main constituent of natural gas. It is a stable alkane hydrocarbon and its direct conversion in C_2H_6 is a reaction with a positive variation of the Gibbs free energy:

$$CH_4 \rightarrow 1/2C_2H_6 + 1/2H_2 \qquad \Delta G° = \text{kJ mol}^{-1} \qquad 1.1$$

However, this thermodynamic disadvantage can be avoided using an oxidant:

$$CH_4 + 1/4O_2 \rightarrow 1/2C_2H_6 + 1/2H_2O \quad \Delta G° = -76 \text{ kJ mol}^{-1} \qquad 1.2$$

The last reaction, the oxidative condensation of methane, known as OCM, is a direct and exothermic process not limited by any thermodynamic constraints. Ethane (C_2H_6) is the main product, although it can be dehydrogenated to ethylene (C_2H_4) according to the following equation:

$$C_2H_6 \rightarrow C_2H_4 + H_2 \qquad \Delta G° = -115 \text{ kJ mol}^{-1} \qquad 1.3$$

Nevertheless, from a thermodynamic point of view, CH_4 and C_2 hydrocarbon oxidation to CO_x (CO and CO_2 products) is more favoured, since it presents higher Gibbs free energy as showed in the following equations:

$$CH_4 + 3/2O_2 \rightarrow CO + 2H_2O \qquad \Delta G° = -544 \text{ kJ mol}^{-1} \qquad 1.4$$

$CH_4 + 2O_2 \rightarrow CO_2 + 2H_2O \qquad \Delta G° = -801 \text{ kJ mol}^{-1}$ 1.5

$C_2H_6 + C_2H_4 + H_2 + 6O_2 \rightarrow 2CO + 2CO_2 + 6H_2O \qquad \Delta G° << 0$ 1.6

1.3.1 Challenges for the OCM commercialization

Although OCM process promises to be an alternative route for production of higher hydrocarbon, several challenges have limited its commercialization [7]. The most highlights challenges are listed as follows:

1) High temperature (750-800) ^oC to achieve high C_2 yield;

2) Removal of heat generated by the highly exothermic reactions (Eqs. 1.2-1.6) to control the hot-spot temperature which limits the highest oxygen inlet concentration and decreases the selectivity;

3) Limitation of CH_4 conversion (<40%) and C_2 yield (<25%) imposed by the explosion limit concentration in the feed;

4) Low concentration of ethylene in the stream (<7-8%) making the product separation by conventional cryogenic process uneconomical;

5) Low selectivity at high conversion, which makes to achieve good selectivity and conversion extremely difficult.

From the point of view of engineering and economics, OCM depends critically on the conversion and selectivity, as well as the price of natural gas compared to that of crude oil. Therefore, single-pass conversions of 35-37% and selectivities of 85-88%, equivalent to >30% C_2 yield, are required to make the OCM process commercially feasible [8,9].

1.3.2 Methane activation

The mentioned above drawback can be overcome by using a suitable catalyst. It is known that OCM over metal oxide catalysts is a heterogeneous–homogeneous reaction. According to the accepted mechanism, the methane activation in the catalytic OCM process involves an abstraction of H-atom from methane due surface defects on the catalyst, leading to the formation of methyl radicals ($CH_3\cdot$); the two desorbed methyl radicals are coupled (gas phase reactions) to form an ethane molecule [10-12] (Figure 1.3). These gas phase reactions are partly responsible for C_2H_6 dehydrogenation to C_2H_4 and formation CO_x products (CO and CO_2). In

addition, the $CH_3^{\bullet}$ secondary reactions can also contribute to produce CO_x [13].

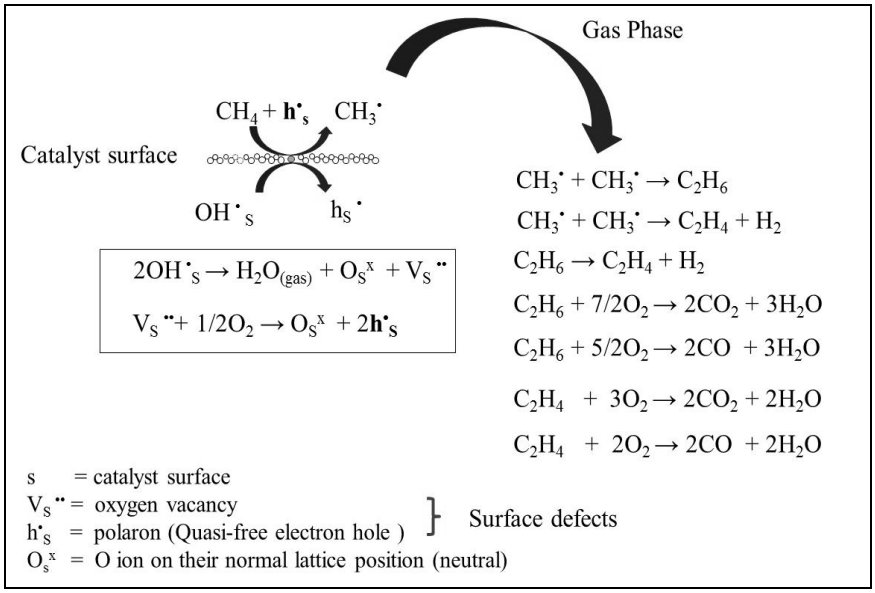

Figure 1.3 OCM reaction pathways. The notation used for defects is from Kröger and Vink [14].

1.4 Catalysts used in OCM

The conversion of methane is highly affected by the characteristics of catalysts. Thus, a large number of catalysts have been evaluated for their performance in OCM with the objective developing a catalyst highly active, selective and stable [15]. Oxides, such as alkaline, alkaline earth [16,17] and rare earth metal [18-20] , single, modified or mixed as perosvkites [21,22], have shown to be good catalysts for the OCM reaction. The productivity of these systems is attributed either to the catalyst basicity or the availability of active sites such as oxygen vacancies and/or other defects, which are important for CH_4 activation [23].

It has been generally established that on metal oxide catalysts the surface oxygen species may consist of lattice oxygen (O^{2-}), peroxide (O_2^{2-}), superoxide (O_2^-) and besides carbonate (CO_3^{2-}) and hydroxide (OH^-). Therefore, different viewpoints concerning the reaction mechanism are centred mainly on the participation of different oxygen species in the OCM reaction. The sources of these species are the adsorbed oxygen over the

catalyst (oxygen molecule and neutral atom) and the oxygen species present on the catalyst surface, such as, lattice oxygen O^{2-}, superoxide O_2^- and species formed by the filling of oxygen vacancies ($Vs^{\bullet\bullet}$) by molecular oxygen to form a polaron species. This reaction can be written as:

$$V_S^{\bullet\bullet} + 1/2O_2 \rightarrow O_S^x + 2h^{\bullet}_S \qquad 1.7$$

where $2\mathbf{h}^{\bullet}$ is a small polaron species, i.e., either $2(O^- = O_S^{\bullet})$ or $O_2^{2-} = (O_2)_S^{\bullet\bullet}$ [24].

The O^- species were shown to be the active centres on Li/MgO or Na/MgO systems [25]. Cation radii in the Li/MgO catalyst are similar ($r_{Li}^+ = 0.68$ Å, $r_{Mg}^{2+} = 0.66$ Å). They can be replaced by each other and therefore the electrical neutrality is maintained when the numbers of O^- and Li^+ ions into the oxide lattice are the same. A relationship between $[Li^+O^-]$ - active centres and the number of $CH_3^{\bullet}$ was found [26]. Lee and Oyama [27] reported that these active centres are formed by vacancies which are created between the O^{2-} and Li^+ as follows:

$$2Li^+O^{2-} + 1/2\ O_2 \rightarrow O_S^{2-} + 2[Li^+O^-] \qquad 1.8$$

$$[Li^+O^-] + CH_4 \rightarrow Li^+OH^- + CH_3\bullet \qquad 1.9$$

The regeneration of $[Li^+O^-]$ centre occurs by the reaction:

$$Li^+OH^- + 1/2O_2 \rightarrow [Li^+O^-] + H_2O \qquad 1.10$$

The surface O^- species (in the active centres Li^+O^-) are responsible for CH_4 activation.

The O_2^{2-} peroxide ions was also proposed to be an active species, especially at temperatures higher than 750 °C on catalytic systems such as Na_2O_2, Na/La_2O_3 and La_2O_3, Ba/MgO [28]. Finally, superoxide species O_2^- were also observed on other catalysts such as LaOF [29], Ba/Nd_2O_3 and Y_2O_3-CaO catalysts [30].

On the other hand, the oxides of the transition metals have been also used for the OCM. Although they are usually effective alone only as catalysts for no selective oxidation, they are particularly used as catalysts to promote the activity in the OCM. Especially when supported, or presented as composite materials or with alkali metals. For example, Gong et al. [31] studied the

effect of Li, La, Mn and W added to TiO_2 on the catalytic performance for the OCM reaction. The results showed that Li-La-Mn-W/TiO_2 system exhibited a methane conversion of 41.6%, C_2 selectivity of 61.7% and C_2 yield of 25.6% at 770°C with a gas hourly space velocity (GHSV) of 14400 h^{-1}. Murata et al. [32] studied the Li-doped sulfated-zirconia catalysts for the OCM reaction. A maximum C_2 yield was attributed over the catalysts containing 6 wt% sulphate in the calcination temperature range of 650-700 ^oC and they found that the catalyst performances were dependent on the sulfate content and calcination temperature. The results were closely related to the preparation conditions of sulfated-ZrO_2 as solid super-acids. In addition, when the performances of the Li-doped sulfated-ZrO2 (Li/SZ) catalysts were tested at 750 ^oC as a function of reaction time, both the C_2 and CO_x selectivity remained constant during 8 h but the CH_4 conversion decreased from 17.5% to 11.9%.

All mentioned above catalysts are only a few examples of the large amount of catalysts studied in the OCM. It can be found in literature over hundreds of different catalytic materials and numerous metal or metal-oxide loadings. The studies have been focused on the intrinsic reactions between reactants and catalyst surfaces. Most of the initial experimental work on catalyst screening was done from 1985 to 1995 in laboratory-scale catalytic fixed-bed reactors and a great deal of effort has been devoted to overcome the hurdle of the economic constraints of low C_2 yield [33]. Recently, a statistical analysis of past catalytic data on oxidative for new insights into the composition of high-performance catalysts was carried out by Zavyalova et al. [33]. In the study, they mention 24 different catalysts that provide C_2 yield $\geq$ 25%. Some of these catalysts are close to the target for the industrial application of the OCM process: single-pass conversions of methane of at least 30% and C_2 selectivity of around 80% (See Figure 1.4).

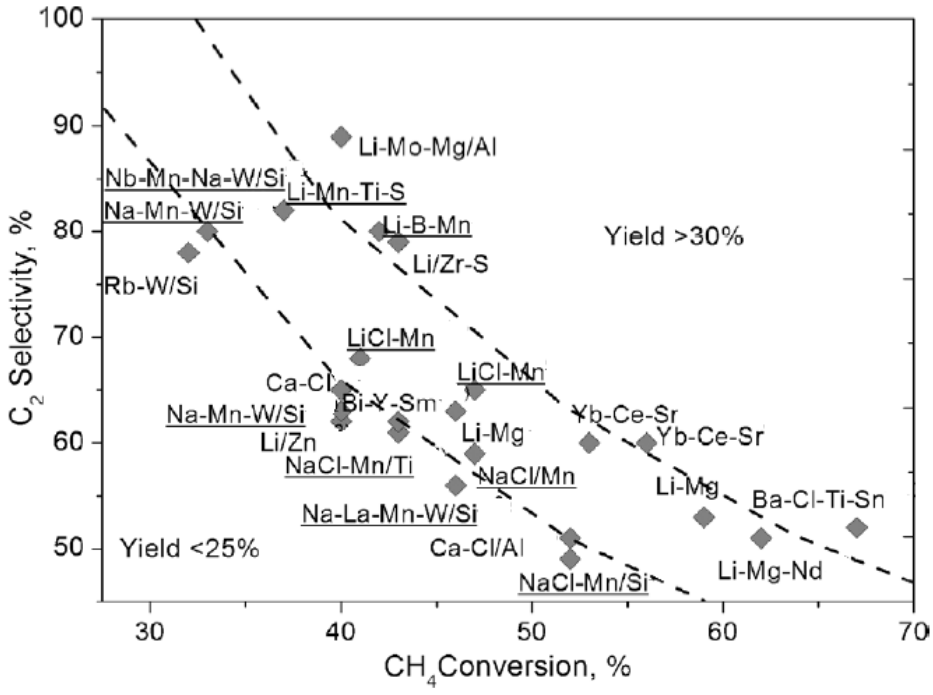

Figure 1.4 OCM catalysts with C_2 yield ≥ 25%. All the catalysts were tested in a fixed-bed reactor in the co-feed mode under atmospheric pressure at temperatures from 670 to 950 ^oC, CH_4/O_2=1.7–9.0 [33].

Although most of these catalysts showed an acceptable performance, the catalyst stability in OCM was often not reported. For instance, Li/MgO is one of the most frequently investigated catalysts for OCM, but in many publications, the information and experiments on the stability were neglected [34]. In fact, it has been shown that Li/MgO undergoes an intrinsic instability which prevents any practical application [34,35].

However, the Mn-Na_2WO_4/SiO_2 catalyst is one of the effective catalysts for OCM reaction consisting of alkali and transition metal oxides. This catalyst not only has an appropriate performance (CH_4 conversions of 20 - 35% and C_2 selectivities of 70 - 80%) but also is stable for long periods under reaction at high temperatures which is required for the OCM. This fact has been confirmed by different research groups [36-40]. In this type of catalysts the major component, W, has variable oxidation states, this represents a new type of oxidation catalyst on which the lattice oxygen O^{2-} may be responsible for methane activation. Thus, several subjects on the nature of this catalyst have been studied during the last twenty years such as: structure

activity relationship, active centres and mechanisms, composition variation and promoter components.

The relationship between the structure and the performance of Na-W-Mn/SiO_2 catalysts for the OCM was studied by Ji et al. [41]. They identified complex active phases, $Na_2WO_4/Na_2W_2O_7/Mn_2O_3$, in a large variation of the composition where the resulting catalytic activity does not change significantly. That composition range was reported as follows: Na (0.4–2.3) wt%, W (2.2–8.9) wt%, and Mn (0.5–3.0wt) wt %, respectively.

On the other hand, a critical influence of the amorphous silica to cristobalite phase transition in Na_2WO_4-Mn/SiO_2 catalysts for the OCM reaction was reported by Palermo et al. [42]. They found that during calcinations of OCM catalyst precursor, the presence of Na induced crystalline SiO_2 (α-cristobalite) from the amorphous silica. The results revealed that amorphous silica allowed obtaining active, but unselective catalysts, whereas α-cristobalite generated active and highly selective catalysts with respect to the formation of ethylene. The explanation of the phase transition of SiO_2 in the presence of Na was later given by Mazzara et al. [43].

Amorphous silica acts mainly to burn methane and hydrocarbon products, while α- cristobalite SiO_2 is effectively inert under OCM reaction [42]. Furthermore, α-cristobalite, produced during phase transition, was superior to that α -cristobalite used as starting material, indicating that dispersing and stabilizing tungsten surface species, possibly WO_4, has a positive influence in OCM. Ji et al. [41] reported that tetrahedral WO_4 was first formed with the presence of Na and Mn when the W content was low. While increasing W led to the presence of both tetrahedral WO_4 and octahedral WO_6 on the catalyst surface. However, tetrahedral WO_4 was more active and selective for the OCM reaction. The formation of surface cluster species of tetrahedral WO_4 species, with one W=O bond and three W-O-Si bonds have been assumed to be the active site [44,45]. Moreover, tetrahedral WO_4 species distortion was also attributed to be responsible for the activity [46].

On the other hand, a redox mechanism involving W^{6+}/W^{4+} species together with W-O-Si bonds were suggested by Jinjang et. al. [47] (see Figure 1.5). They investigated oxygen species and tetrahedrally coordinated molecules of the WO_4 by EPR and Raman spectroscopy techniques, respectively.

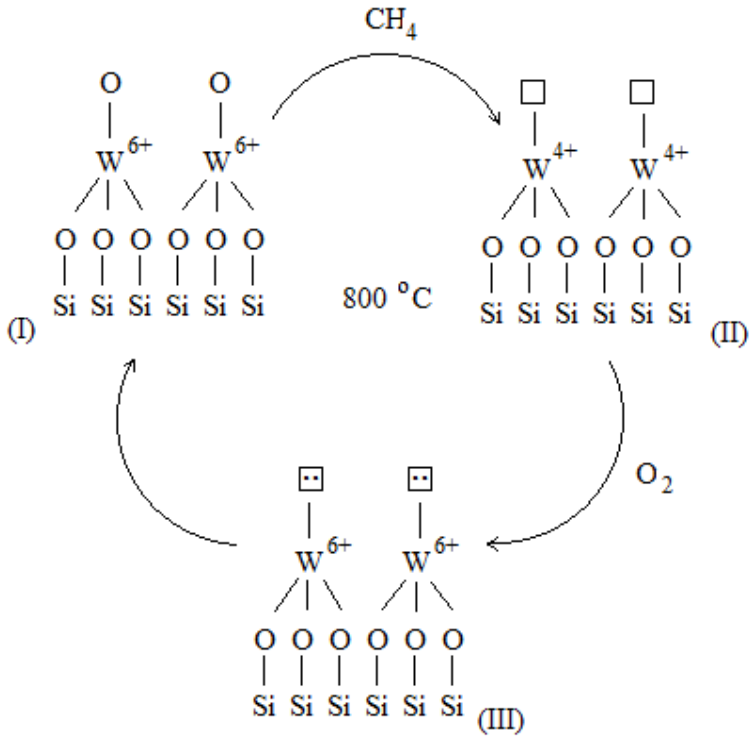

Figure 1.5 The proposed redox mechanism of Mn-Na_2WO_4/SiO_2 [47].

The mechanism is started with the process of breaking of top W-O bond which occurs by reduction of Species (I) in the presence of CH_4 to form Species (II). These latter are oxygen vacancies. When O_2 from the gas phase is involved in the process two electrons are transferred from the tungsten atom to the vacancy to generate the F-centre form (an oxygen ion vacancy with two trapped electrons) or Species (III). Molecular oxygen is activated in the F-centre to produce lattice oxygen, Species (I) form, and thus the redox cycle is completed. The role of Mn was suggested to increase the mobility of surface lattice oxygen.

Although above redox mechanism is based on W^{6+}/W^{+4} species, in other publications a mechanism of W^{6+}/W^{5+} was discussed [40]. For example, a redox mechanism for the generation of methyl radicals from CH_4 over Mn-Na_2WO_4/SiO_2 was suggested by Li et al. [48]. They reported that the activation of CH_4 takes place on W^{6+} sites and the activation of gas phase O_2 on Mn^{3+} sites, i.e., the mechanism proposed in Figure 1.5 was extended based on a two metal site model for this catalyst (see Figure 1.6). In this

model, it is suggested that oxygen spill-over, from Mn_2O_3 to the Na_2WO_4, increases the activity of the Mn-Na_2WO_4/SiO_2.

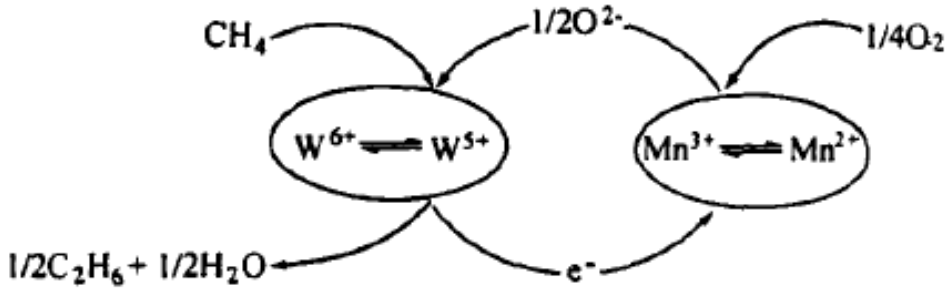

Figure 1.6 Two metal site model for OCM reaction on Mn-Na_2WO_4/SiO_2 catalyst from literature [48].

1.5 Operating mode of the OCM

In conventional reactors two different operating modes of the OCM have been studied:

- Sequential feeding methane and oxygen (the reactants are not together) and;
- Co-feeding where both reactants coincide at the same time-space over the catalyst.

Keller and Bhasin tested both operating modes. In the sequential feeding, reducible metallic oxide was utilized as the O_2 source. Then, the reduced metallic oxide is deoxidised using a gaseous oxygen stream. The typical reactions are:

$$2CH_4 + MO_{2+x} \rightarrow C_2H_4 + 2H_2O + MO_x \quad 1.11$$

$$MO_x + O_2 \rightarrow MO_{2+x} \quad 1.12$$

That sequential combination is the methane coupling reaction:

$$2CH_4 + O_2 \rightarrow C_2H_4 + 2H_2O \quad 1.13$$

On this route, methane and the coupling products are not in contact with gaseous oxygen and therefore the total oxidation reactions do not occur. However, methane conversion and C_2 hydrocarbons selectivities are not constant (unsteady state). Therefore, CH_4 conversion and selectivity vary in

the time. On the other hand, the amount of the catalyst and the reaction rate in (1.12) must be optimized.

Regarding the Co-feeding of CH_4 and O_2 in reactor inlet, different operating modes to contact both reactants on the catalyst surface were investigated. For that, some reactors have been designed to mix a hydrocarbon with a powerful oxidant reagent under safety conditions and to control the generated energy from the process (see section 1.8).

1.6 Kinetics of the OCM reaction

Numerous kinetic studies with different reaction steps, component types, operating conditions and rate equations have been performed for a description of the OCM reaction network. Thus, kinetic studies to elucidate the reaction mechanisms can be found in literature [15,49,50]. These models were derived either at low temperatures and/or at low conversions which are limited by Eq. 1.2. However, as mentioned in section 1.3.1, high temperatures are necessary to achieve high C_2 yield, but these temperatures favour the deep oxidation and methane consecutive reactions. These reactions can detriment the high C_2 selectivity and limit the achievable C_2 yields. Therefore, these should be considered in both reactor design and definition of kinetic models [51].

Kinetic models proposed in the literature differ in the reaction schemes applied and in the number of product compounds considered. Based in this, five models are briefly presented in this section to describe their complexity and understand because a reaction scheme applicable for all catalysts performed in OCM had been not found. Table 1.2 shows the reactions of each model. The first model was proposed by Stansch et al. [52] over La_2O_3/CaO catalyst. This was developed in a wide temperature range of 700 - 950 ^oC. Figure 1.7 shows the scheme which includes nine heterogeneously catalysed and one homogeneous non-catalytic (reaction 7 in Figure 1.7) reaction. Reactions of ethane and ethylene to higher hydrocarbons (C_{3+}) were neglected.

A second model was suggested by Sohrabi et al. [53] for OCM on $CaTiO_3$ in the temperature range of 760–780 °C. This model consists of four heterogeneous reaction steps. Methane is converted in four parallel reactions, including coupling of methane to ethylene. Reactions of ethane and ethylene to higher hydrocarbons (C_{3+}) are also neglected. The third

model was proposed by Lacombe et al. [54] and was based on their previous study of OCM on La_2O_3 catalyst at 750 °C. This model consists of seven heterogeneous reaction steps, including total and partial oxidation of ethane to carbon dioxide and to carbon monoxide, respectively.

Table 1.2 Stoichiometric equations of reaction models.

#	Reaction	Model				
		1	2	3	4	5
(1)	$2CH_4+1/2O_2\rightarrow C_2H_6+H_2O$	x	x	x	x	x
(2)	$CH_4+O_2\rightarrow CO+H_2O+H_2$	x			x	
(3)	$CH_4+1/2O_2\rightarrow CO+2H_2O$		x			x
(4)	$CH_4+2O_2\rightarrow CO_2+2H_2O$	x	x	x	x	
(5)	$2CH_4+O_2\rightarrow C_2H_4+2H_2O$		x			
(6)	$CO+1/2O_2\rightarrow CO_2$	x		x		
(7)	$C_2H_6+1/2O_2\rightarrow C_2H_4+H_2O$	x		x		x
(8)	$C_2H_6+O_2\rightarrow 2CO+3H_2$			x		
(9)	$C_2H_6+5/2O_2\rightarrow 2CO+3H_2O$				x	
(10)	$C_2H_6+7/2O_2\rightarrow 2CO_2+3H_2O$			x	x	
(11)	$C_2H_6\rightarrow C_2H_4+H_2$	x			x	x
(12)	$C_2H_4+O_2\rightarrow 2CO+2H_2$			x		
(13)	$C_2H_4+2O_2\rightarrow 2CO+2H_2O$	x			x	
(14)	$C_2H_4+3O_2\rightarrow 2CO_2+2H_2O$				x	
(15)	$C_2H_4+2H_2O\rightarrow 2CO+4H_2$	x				
(16)	$CO_2+H_2\rightarrow CO+H_2O$	x				x
(17)	$CO+H_2O\rightarrow CO_2+H_2$	x				x

Model 1 = Stansch et al. over La_2O_3/CaO [52], Model 2 = Sohrabi et al. over $CaTiO_3$ [53], Model 3 = Lacombe et al. over La_2O_3 [54], Model 4 = Olsbye et al. over $BaCO_3/La_2O_n(CO_3)_{3-n}$ (nN1.5) [55], Model 5 = Traykova et al. over La_2O_3/MgO [18].

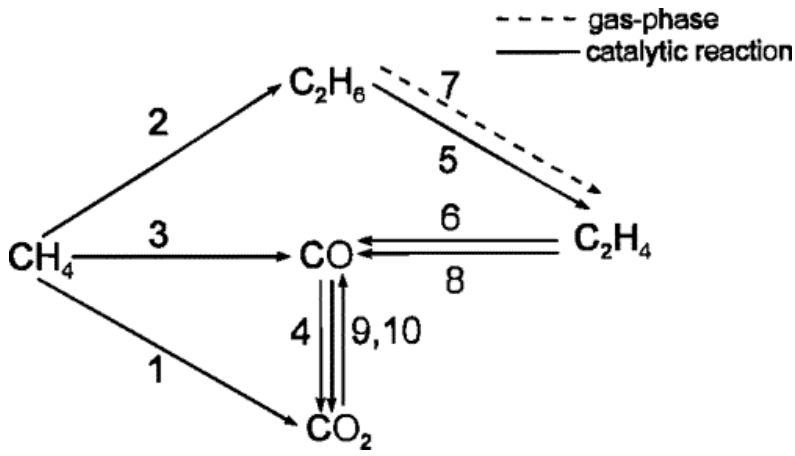

Figure 1.7 Reaction scheme of the OCM over the La_2O_3/CaO catalyst [52].

A reaction scheme proposed by Olsbye et al. [55] for OCM over $BaCO_3/La_2O_n(CO_3)_{3-n}$ (nN1.5) was developed at 680 to 800 °C. This consists of seven heterogeneous and one homogenous reaction steps, including total and partial oxidation of ethane to carbon dioxide and carbon monoxide and total and partial oxidation of ethylene to carbon dioxide and carbon monoxide. Finally, the last model is the kinetic model of Traykova et al. [18] over La_2O_3/MgO catalyst. They suggested five heterogeneous and one homogeneous reaction steps at 700–825 °C, including partial oxidation of ethane to ethylene, water gas shift.

The kinetic models presented above include almost all reaction steps considered in other models with the exception of the Model 2. The network reactions consist of homogenous and heterogeneous reaction steps with different mechanisms. With respect to the primary steps, methane oxidation by two parallel reactions to C_2H_6 and CO_x is the dominant reaction scheme However, great differences occur in the treatment of the consecutive reactions. Since, it is frequently assumed that ethane is converted consecutively to ethylene, either by dehydrogenation or oxy-dehydrogenation (reactions 7 and 11 in Table 1.2), CO and CO_2. The temperature range for the models is valid and depends on the catalyst; the majority of the models are valid for temperatures above 700°C. However, only a few models found in literature, were performed at temperatures above 800°C. Reactions of ethane and ethylene to higher hydrocarbons (C_{3+}) were

neglected since experimentally determined C_{3+} selectivities were generally lower than 5%.

Later in 2009, Daneshpayeh et. al. [56] developed a kinetic model of OCM over $Mn/Na_2WO_4/SiO_2$ catalyst based on the above five models. They used a decimal genetic algorithm [57] to estimate the parameters of the rate equations of all mentioned above models using the experimental data of $Mn/Na_2WO_4/SiO_2$ catalyst. In addition, the average absolute relative deviation (AARD) % and R-square (R^2) were calculated for all reaction networks of each model. They found that the reaction network of Stansch et al. [52] had lower AARD and higher R^2 when compared with others. Therefore, considering almost all reaction steps, Stansch et al.´s model resulted to be the most suitable reaction network. However, it was considered that AARD and higher R^2 was not enough for discriminating among the models, since the number of parameters are different from one model to another. Thus, a statistical method was applied taking into account both the number of parameters and the squared residuals to judge among the models. They found that the reaction network of Stansch et al. had a better validation compared to other models, i.e., this model had a more realistic description of OCM reaction behaviours. Kinetics of ethane formation were described by using Hougen-Watson type equation in which took into account the inhibiting effects of oxygen and carbon dioxide. This model was able to predict the OCM reaction in a wide range of operating conditions.

1.7 Effect of operating conditions on C_2 hydrocarbon selectivity and yield

OCM is a complex reaction network of parallel and consecutive, heterogeneous and homogeneous reaction steps in where the selectivity to C_2 hydrocarbons strongly depends on the operating conditions. They are determined by kinetic relationships described in the kinetic studies mentioned above. Thus, operating conditions, such as temperature, GHSV and CH_4/O_2 ratio play an important role on the catalytic performance of OCM.

1.7.1 Influence of the temperature

A similar trend of C_2 selectivity and yield is observed at a determined temperature range for most catalysts investigated. Both C_2 selectivity and yield increase as temperature increases passing through a maximum or

reaches a plateau [58-60]. The temperature of maximum selectivity is specific for each catalyst and also depends on the partial pressures of reactants as well as on mixing patterns which are different in various reactor types [61]. The increase in selectivity with growing temperature results from the higher activation energy of the selective, primary reaction step compared to that non-selective reactions [62]. Therefore, production of C_2 hydrocarbons increases stronger with temperature when compared to CO_x products [61]. A decrease of the selectivity at high temperatures is caused by consecutive reactions which occur also in the gas phase. When complete conversion of oxygen is realized, the increasing C_2 selectivity is accompanied by an increase in methane conversion. This effect results from the stoichiometry of the OCM reaction; the selective reaction consumes less oxygen than the oxidation to CO_2. However, a decrease of selectivity at high temperatures can be caused by oxidation of C_2 hydrocarbons and this decrease is associated with a decrease of methane conversion for stoichiometric reasons [61,63].

1.7.2 Influence of the CH_4/O_2 ratio

The effect of the CH_4/O_2 ratio on the catalytic performance was investigated for a large number of catalysts [64-70,7,71]. In general, the CH_4 conversion is limited to an industrial application by $CH_4/O_2 \geq$ 2-4, as well as, selectivity and hence, the amount of heat released. As shown in Figure 1.8, high CH_4/O_2 ratio promotes high C_2 selectivity but low conversion. This dependence which is common to various catalysts and reactor designs can be explained by the different apparent reaction orders for primary selective and non-selective reaction steps with respect to oxygen and methane. The dependence of C_2 yield on CH_4/O_2 ratios is accompanied with methane conversion, which means that the highest C_2 yields were achieved at highest conversion of methane but not at the highest C_2 selectivities.

1.7.3 Effect of the GHSV

The contact time is another parameter investigated in OCM due to the secondary oxidation of the hydrocarbons products. Thus, in several works the influence of resident time has been investigated by varying the volumetric feed flow rate in term of GHSV [52,72,73]. Reactants would have a longer contact time with low space GHSV.

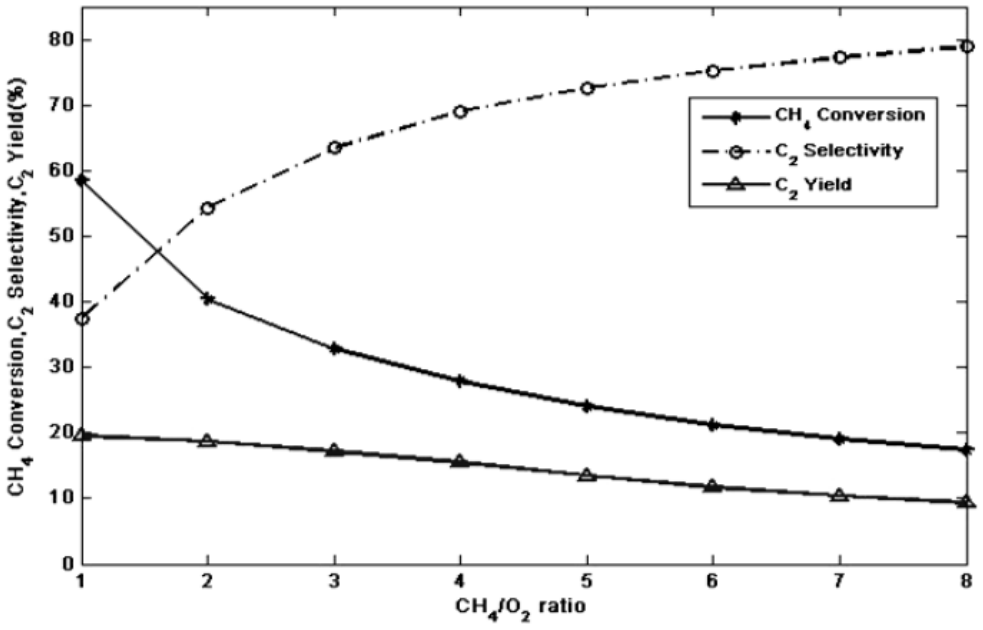

Figure 1.8 Influence of CH_4/O_2 ratio and temperature on the conversion of methane and the selectivity and yield of C_2 product [74].

Conversion of oxygen increased gradually with the contact time (low GHSV) and the course of methane conversion corresponded to that of oxygen [72,52]. When oxygen conversion was completed, no further increase of methane conversion is found with the contact time. Selectivity of ethylene increased with the contact time while the selectivity of ethane was found almost stable and slightly dropped with the contact time. However, it was found that oxygen achieved total conversion at 20 kg s m^{-3} at 830 ^oC, and C_2 yield reached the maximum. A similar behaviour of the OCM parameters (CH_4 and O_2 conversion and C_2H_6 and C_2H_4 selectivity) was reported by Shahri et al. [75] in the kinetic study of the OCM on the $Mn/Na_2WO_4/SiO_2$ catalyst. However, they found that oxygen was completely consumed at a higher contact time (350 $kg \cdot s \cdot m^{-3}$) in the temperature range of 800-900 ^oC. They noticed that ethane depends on the temperature at longer contact times passing through a maximum value is also strongly influenced by consecutive reactions especially at higher temperatures. The dependence of the yield of ethylene on the contact time at low values of this parameter seems to confirm the generally accepted thesis that ethylene is formed in a consecutive reaction of ethane already reported by Stansch et. al. [52].

1.8 Reactor design, distributed feed of oxygen and the membrane reactors for the OCM.

From a practical point of view, the first drawback mentioned in section 1.3.1 can be overcome with the use of a better catalyst and improved reaction engineering. However, the second drawback (the enormous heat effect) can only be solved by an enhanced reactor design, since it is also influenced by thermodynamics and fluid dynamics. As mentioned in section 1.4, in the past 30 years, huge efforts have been put in catalyst development for the OCM process. The results reviewed by [61,76,77] show that yields of less than 25% still represent the maximum one can expect from a conventional OCM reactor. From these reviews it would seem that the catalyst development does not allow further yield increase because of the interplay between heterogeneous and gas phase reactions. Thus, oxidation of both methane and higher hydrocarbons in reaction products would seem to be unavoidable in the case of higher oxygen content in the feed.

Therefore, a control of temperature and the heat management is one of the key challenges for the industrial application. Proposed methods to cope with the heat removal problem include the use of fixed bed and single or multi-stage fluidized bed reactors. On the other hand, membrane reactors allow better distribution of oxygen to improve the C_2 hydrocarbon yield.

1.8.1 Fixed - bed tubular reactors

Fixed-bed tubular reactor has been frequently studied in the OCM reaction. Several fixed-bed reactor designs have been proposed to control the high exothermicity exhibited in the most of the catalyst performed in the OCM reaction. Thin-bed reactor [78], sintered metal packing [79] and monolith reactor [80] have been used in laboratory-scale and their catalytic performances have allowed assuming projections at industrial-scale units, such as multi-tubular and multistage adiabatic fixed beds. In fixed bed reactors, the temperature control and heat management are crucial. Since, large exothermicity steep axial and radial temperature gradients can occur in the reactor bed. On the other hand, the inlet concentration of oxygen is limited to 20% in order to keep the hot-spot temperature below 1000 °C.

It was reported that the required tube diameter should be too small to be practical at laboratory scale [81]. In fact, Tye et al. [72] studied the effect of the tube reactor diameter under non-isothermal/non-adiabatic mode which is

closer to practical operating conditions. They reported that increasing reactor diameter caused a drop in the C_2 yield and reached a constant value (see Figure 1.9). Bigger tube diameter leads to higher temperature. It was attributed to more reactions occurring on a same surface area in catalyst bed and more heat was released at the same time.

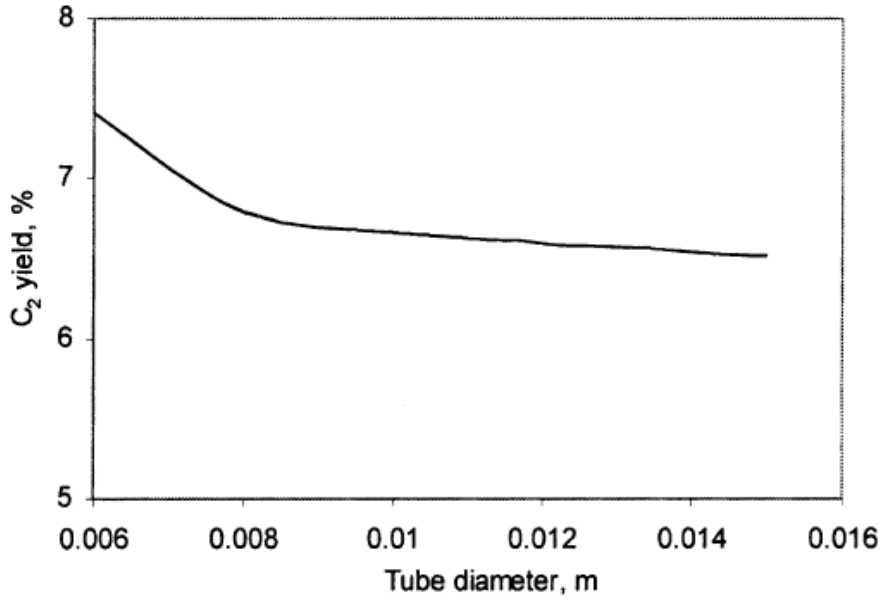

Figure 1.9 C_2 yield vs. different reactor tube diameter. CH_4/O_2 = 10, T = 700 ^oC [72].

The tube diameter has to be small in order to avoid steep axial and radial temperature gradients and to avoid reactor runaway condition, i.e., sudden and considerable change in the process variables [61,72]. Dautzenberg et al. [81] designed a multitubular reactor with 2000 tubes of diameter 24mm and length 2m for OCM on an industrial scale. However, these are impractical dimensions but required to control heat transfer and avoid temperature runaway when compared to the reactors that will be discussed in the next section.

1.8.2 Fluidised bed reactors

The fluidized bed reactor has been designated by different authors as the best reactor concept for OCM reaction [61,81]. Unlike any fixed bed reactor, the fluidised bed reactor allows managing of the huge reaction heat and presents the ability to operate in isothermal conditions and avoids a temperature

runaway at the same time to continuously re-circulate or even to change deactivated catalyst. There have been a number of investigations in the 90s around the fluidized bed reactor concept [82-85,63,86]. However, all of these studies showed that only a yield of less than 19.4% was accessible in a fluidized bed reactor, and thus, limiting its yield to the similar restriction as in the case of a fixed bed reactor.

Fluidised bed reactor design and scale-up has been an issue for more than 50 years [87-89]. However, industrial application of OCM reactors has only been discussed briefly in some published works [61,88,90]. Several cases of poor scale-up of fluidised bed reactors for different application has been reported in book of Kunni and Levenspiel [88] and the root of these failures was basically poor knowledge of fluidised bed hydrodynamics.

1.8.3 Membrane reactors

It is known that the membrane reactors present a potential to advance the process industry by enhancing selectivity and yield, reducing energy consumption, improving operational safety, and miniaturizing the reactor system. Membrane reactors made of inert porous or dense membrane tube with a regular OCM catalyst have been studied as oxygen distributor to improve the C_2 hydrocarbon yield [91,92]. On the other hand, studies on OCM in inorganic membrane reactors have not only led to a breakthrough in obtaining a higher C_2 yield, but also improve the understanding of the reaction mechanism. For instance, catalytically active membrane was used to change the OCM reaction mechanism and minimize the presence of the gas-phase oxygen in the methane stream [93-95].

Nevertheless, membrane reactors present inability to obtain high C_2 hydrocarbon yields. This because of problems inherent to the membrane reactors, such as: poor membrane surface catalytic properties and unfavourable reactor configuration. To solve this problem, it was necessary designing news of membrane reactors with a large permeation surface area to volume ratio.

However, all these studies, involving the different oxygen species present on the catalyst surface and reactors used in the OCM, have shown that the selectivity to C_2 hydrocarbons decreases as the overall conversion of methane increases. Thus the C_2 yield, which is the product of selectivity and the conversion, is usually limited to about 25%. Several innovative reactor

design approaches have been proposed and very high yields (>60%) were reported [96,97]. Nevertheless, the problem of low yields *per pass* remains unsolved.

On the other hand, the study of the types and state of oxygen to supply to the OCM reaction has also been of crucial importance to try achieving industrially acceptable C_2 hydrocarbon yields. An interesting alternative is the electrochemically supplied oxygen (O^{2-}) by the use of the solid electrolyte membrane reactor.

1.8.4 Solid Electrolyte Membrane Reactor (SEMR)

A SEMR consists in a fuel cell applied as chemical reactor that has a membrane selectively permeated by at least one of the components of a mixture to which it is exposed. In this reactor at least one of the reactants or products are supplied or removed partly or wholly through a membrane. Consequently, this means that the membrane serves as the wall or as part of the reactor wall.

According to permselectivity and permeability, membranes can be classified into two types: porous and dense membranes. Porous membranes offer a high permeability to molecules but with low permselectivity. The typical gas transport mechanisms in porous membranes are: molecular diffusion and viscous flow, capillary condensation, Knudsen diffusion as well as surface diffusion. Porous membranes have been widely successfully employed in many oxidation reactions, such as oxidative coupling of methane [98], oxidative dehydrogenation of ethane [99] propane [100], etc.

On the other hand, dense membranes have a rather high permselectivity to some special species but normally a lower permeability compared to porous membranes. The transport process in a dense membrane involves oxygen diffusion or ionic jumping in the lattice. The solid oxide dense membranes can be classified into two types: solid electrolytes and mixed ion electron conductors (MIEC). Unlike MIEC, the dominant characteristic of the solid electrolytes is the ionic conductivity. In fact, it is usually two or more orders of magnitude higher than the electronic conductivity. Therefore, their classification is based on the conducting anion. Many conductors have been discovered (H^+, K^+, Na^+, Cu^+, Ag^+, Li^+, O^{2-}, and F^-). However, H^+ and O^{2-} ion conductors have been mainly used in SEMRs [101-103].

The typical configuration of a SEMR is illustrated in Figure 1.10; the membrane is an oxygen-ion conductive solid electrolyte. The cathode is exposed to oxygen-containing gas, e.g., air, and the anode is exposed to the reactants, e.g., hydrocarbons. The two electrodes are connected to a circuit in three operation modes. Open-circuit mode in which the two electrodes are connected to a voltmeter (case 1a), closed-circuit connected to an external resistive load (case 1b), or to an external power source (case 1c). This last mode of operation is called electrochemical oxygen "pumping".

In the open-circuit mode, there is no net current through an electrolyte. The difference in chemical potential is converted into the open-circuit electromotive force of the cell.

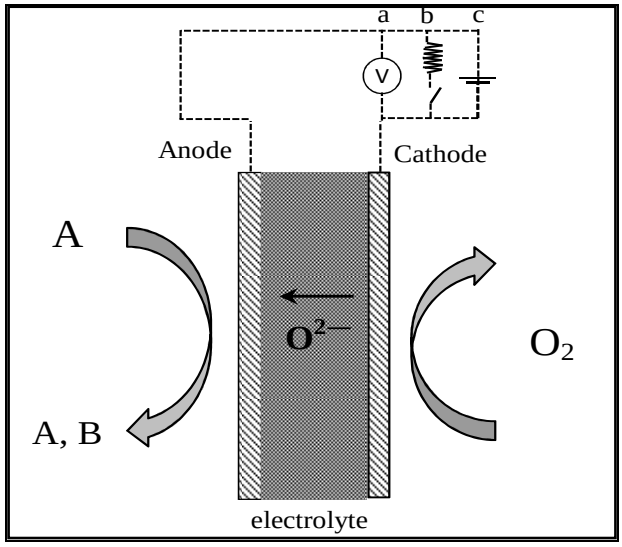

Figure 1.10 Schematic diagram of a SEMR: (a) open-circuit operation mode; (b) closed-circuit operation in a fuel cell mode; (c) closed-circuit operation in "pumping" mode.

If the primary goal is the production of electricity the fuel cell operates in a closed-circuit to convert directly chemical energy into electrical energy. This latter is also called fuel cell mode of operation. On the other hand, if the primary goal is the production of B chemicals, an external power source can be used to impose a current through the cell in the desired direction (case 1c).These operational modes generate three basic applications of the SEMRs as shown in Figure 1.10.

1) Solid electrolyte potentiometry (SEP),
2) SOFCs , and
3) Electrochemical oxygen “pumping”.

Solid electrolyte potentiometry can be applied to study the heterogeneous catalysis by the measurement of the activity of oxygen on metal and metal oxide catalysts. The basic principle of SEP is the in-situ measurement of the chemical potential difference between the two electrodes.

SOFCs combine the concepts of a fuel cell and a chemical reactor to produce valuable chemicals from the anodic reaction with co-generation of electrical energy instead of pure thermal energy. In SOFCs, several fuels can be used such as H_2, CO, CH_4, and CH_3OH. It is because SOFCs can be operated at high temperatures (<1073 K).

In electrochemical oxygen “pumping”, the SEMR also operate under closed-circuit conditions to carry out a reaction and produce useful chemicals rather than electrical energy. When the current is generated spontaneously and is either very low or in the undesired direction, an external power source is used to direct and control the current.

Solid electrolyte membrane reactors present several advantages such as: increased catalytic activity and selectivity, simultaneous reaction and separation in the same advice, better process integration, reduced feedstock, and easy reaction rate control [91]. These studies provided new possible alternatives to increase R&D activities to convert methane into useful chemicals or the co-generation of electric energy and useful chemicals.

Thus, selective oxidation of methane in SOFCs has been studied to co-generate electric power and C_2 hydrocarbons. As mentioned above, a SOFC is a SEMR operating in closed circuit (fuel cell mode). The power electrical and valuable chemicals such ethylene can be produced when the ionic charge through the electrolyte is balanced by the flow electronic charge through an outside circuit (Figure 1.10). Pujare and Sammellsn were the first to report the use of SOFCs for co-generation of C_2 hydrocarbons and electrical power [104]. They obtained high C_2 hydrocarbon selectivity (>90%) and relatively low methane conversion.

In a SOFC the electrolyte material is interposed between two thin electrodes (porous anode and cathode). Therefore, direct chemical combustion is prevented by the electrolyte that separates the fuel (CH_4) and from oxidant

(O_2). The oxygen is reduced to oxygen ion O^{2-} on the cathode as lattice oxygen and migrates across electrolyte, which also serves as a barrier to gas diffusion. The permeated oxygen is then activated on the anode catalyst to react with methane to form valuable C_2 hydrocarbons. Many studies have been reported focusing the catalyst preparation, characterization and reactor performance test. Conventional solid electrolytes used in most studies are O_2 ion conductors like yttria stabilized zirconia (YSZ) [105,106] or CeO_2 [107]. Catalysts such as KF, $BaCO_3$, $NaCl/MnO_2$, Sm_2O_3 deposited on the Au-electrode were tested by Otsuka et al. [108,109] and they found that the most active and selective catalyst was $BaCO_3$ on Au, which showed high selectivity to C_2 hydrocarbons, but further studies were needed to stabilize the catalytic activity. In addition, anode catalysts for an oxidative coupling of methane in SOFC become an important goal to improve the conversion, selectivity, yield and stability of the reactor. Xui-Mei et al. [110] combined 1wt%Sr/La_2O_3 and Bi_2O_3-Ag as the catalyst-electrode and they showed that the fuel cell was operated for an extended period of time with selectivity to C_2 hydrocarbons and CH_4 conversion relatively constant. Wiyaratn et al. [111], reported a possibility the simultaneous generation of electrical energy and C_2 hydrocarbons over $Au/La_{1-x}Sr_xMnO_3$ nanocomposites in an SOFC reactor. They showed that Au nanoparticles could significantly improve the catalytic performance of the composite to be used in a partial oxidation fixed bed reactor and an SOFC reactor.

Membranes were also used in SOFCs for the OCM reaction. Guo et al. [110] studied the effect of the Sr/La_2O_3-Bi_2O_3-Ag-YSZ membrane composition and revealed that an increase in the current generated was accompanied by a decrease in C_2 selectivity and an increase in CH_4 conversion. On the other hand, fuel cell type temperature-programmed desorption (FC-TPD) technique was used to investigate oxygen species. Kiatkittipong et al. [112] suggested that SOFC for oxidative coupling of methane is a good reactor for C_2 production and co-generation of electric power. However, the obtained electricity was far from a typical SOFC which solely for electricity generation. Several conventional fixed bed reactors (FBR), porous membrane reactor (PMR) and mixed ionic and electronic conducting membrane reactor (MIEMR) were compared with solid oxide fuel cell reactor. This latter improved C_2 selectivity compared to FBR. However,

PMR was superior to the other reactors at low temperature (<877 ^{o}C) while MIEMR was attractive at high temperature (>877 ^{o}C) [113].

1.9 Objectives and thesis outline

OCM is one of the main processes proposed for the direct CH_4 conversion to higher hydrocarbons. Despite enormous efforts, it has not yet proved to be commercially attractive. However, there is still a need to further optimize and create a new engineering process in which OCM can be integrated to achieve a practical application in which active and selective catalysts play an important role. Therefore, the main objective of this work is the development of catalysts nanostructured for the oxidative coupling of methane. The work started with the development of mixed oxide and supported catalysts active and selective for the OCM reaction. Subsequently the best catalysts were assessed in OCM under a wet atmosphere and then tested in an electrocatalytic system. The catalysts were studied and characterised. The practical feasibility of the OCM was addressed as a process integrated with efficient simultaneous production of C_2 hydrocarbons and H_2 using a single chamber under CH_4 humid atmosphere. Finally, similar studies are carried out in a double chamber solid oxide electrolysis cell to separately produce C_2 hydrocarbons and H_2.

The manuscript is organised in four parts and nine Chapters. The main core of this thesis is composed of Chapters 2 to 8. This introductory Chapter is Part I (Chapter 1). Part II includes Chapters 2, 3 and 4 and they report the use of mixed oxide for the OCM, whereas, in Part III (Chapter 5), supported catalysts tested in OCM were described, and Part IV (Chapters 6, 7 and 8) in where the efficient electrocatalytic simultaneous production of C_2 hydrocarbons and H_2 was achieved by using of the best catalyst. The catalytic experiments were carried out in several tube reactors, described along the manuscript, in gas-phase and atmospheric pressure.

More precisely, Chapter 2 is dedicated to the assessment of cerium oxide modified with alkaline, earth alkaline and transition metal more frequently used in OCM.

Chapter 3 consists in the study of surface oxygen species responsible for the OCM over cerium oxide modified with three earth alkaline metals and their relationship with the catalytic activity and surface basic sites.

Chapter 4 describes the structural modification of lanthanum oxide with cerium and the influence of two preparation methods to create surface oxygen species identified in the previous chapter.

Chapter 5, the effect of the amount of Ce on Na_2WO_4/SiO_2 for the OCM is studied.

Using the best catalysts reported in previous chapters, Chapter 6 shows their performance in the OCM under a CH_4 wet atmosphere.

In Chapter 7, the catalyst reported to have the best performance in OCM under CH_4 humid atmosphere is assessed in a solid electrolyte-fixed bed reactor configuration for the simultaneous production of C_2 hydrocarbons and H_2.

Similar studies to those reported in Chapter 7 but using methane in a double chamber solid oxide electrolysis cell are discussed in Chapter 8.

Finally, Chapter 9 summarises and integrates the main conclusions taken out from this work and the prospects for further investigations.

References

[1] Heng HC, Idrus S, *The future of gas to liquids as a gas monetisation option*. Journal of Natural Gas Chemistry **13** (2004) 63-70.

[2] Riegel ER, Kent JA, Riegel's handbook of industrial chemistry. Kluwer Academic/Plenum Publishers, Edited by, (2003)

[3] Spath PL, Dayton DC (2003) Preliminary Screening -- Technical and Economic Assessment of Synthesis Gas to Fuels and Chemicals with Emphasis on the Potential for Biomass-Derived Syngas. Other Information: PBD: 1 Dec 2003.

[4] Gesser HD, Hunter NR, Prakash CB, *The direct conversion of methane to methanol by controlled oxidation*. Chemical Reviews **85** (1985) 235-244.

[5] Kuo JCW (1987) Evaluation of direct methane conversion to higher hydrocarbons and oxygenates: Final report. Other Information: Portions of this document are illegible in microfiche products. Original copy available until stock is exhausted.

[6] Keller GE, Bhasin MM, *Synthesis of ethylene via oxidative coupling of methane: I. Determination of active catalysts*. Journal of Catalysis **73** (1982) 9-19.

[7] Choudhary V, Uphade B, *Oxidative Conversion of Methane/Natural Gas into Higher Hydrocarbons*. Catalysis Surveys from Asia **8** (2004) 15-25.

[8] Matheme JL, Culp GL, Methane conversion by oxidative processes: fundamental and engineering aspects. Edited by Wolf EE, (1992) 483

[9] Kuo JCW, Methane coupling by oxidative processes: fundamental and engineering aspects. Van Nostrand Reinhold Catalysis Series, Van Nostrand Reinhold, Edited by Wolf EE, (1992)

[10] Lunsford JH, *Catalytic conversion of methane to more useful chemicals and fuels: a challenge for the 21st century*. Catalysis Today **63** (2000) 165-174.

[11] Campbell KD, Morales E, Lunsford JH, *Gas-phase coupling of methyl radicals during the catalytic partial oxidation of methane*. Journal of the American Chemical Society **109** (1987) 7900-7901.

[12] Feng Y, Niiranen J, Gutman D, *Kinetic studies of the catalytic oxidation of methane. 1. Methyl radical production on 1% strontium/dilanthanum trioxide*. The Journal of Physical Chemistry **95** (1991) 6558-6563.

[13] Guczi L, Van Santen RA, Sarma KV, *Low-Temperature Coupling of Methane*. Catalysis Reviews **38** (1996) 249-296.

[14] Kröger FA, Vink HJ (1956) Relations between the Concentrations of Imperfections in Crystalline Solids. In: Frederick S, David T (eds) Solid State Physics, vol Volume 3. Academic Press, pp 307-435.

[15] Amenomiya Y, Birss VI, Goledzinowski M, Galuszka J, Sanger AR, *Conversion of Methane by Oxidative Coupling*. Cheminform **22** (1991) 341-341.

[16] Yamamura M, Okado H, Tsuzuki N, Wakatsuki T, Otsuka K, *Oxidative coupling of methane over ternary metal oxide catalysts consisting of Groups I, III and V elements in the Periodic Table*. Applied Catalysis A: General **122** (1995) 135-149.

[17] Kondratenko EV, Maksimov NG, Selyutin GE, Anshits AG, *Oxidative coupling of methane over oxides of alkali earth metals using N2O as oxidant*. Catalysis Today **24** (1995) 273-275.

[18] Traykova M, Davidova N, Tsaih J-S, Weiss AH, *Oxidative coupling of methane – the transition from reaction to transport control over La2O3/MgO catalyst*. Applied Catalysis A: General **169** (1998) 237-247.

[19] Au PCT, Liu YW, Ng CF, *Raman Spectroscopic and TPR Studies of Oxygen Species over BaO- and BaX_2(X=F, Cl, Br)-Promoted Nd_2O_3Catalysts for the Oxidative Coupling of Methane*. Journal of Catalysis **176** (1998) 365-375.

[20] Kuś S, Otremba M, Taniewski M, *The catalytic performance in oxidative coupling of methane and the surface basicity of La_2O_3, Nd_2O_3, ZrO_2 and Nb_2O_5*. Fuel **82** (2003) 1331-1338.

[21] Shamsi A, Zahir K, *Oxidative coupling of methane over perovskite-type oxides and correlation of Tmax for oxygen desorption with C2 selectivity*. Energy & Fuels **3** (1989) 727-730.

[22] Myung-Jin Lee J-HJ, Jin-Seung Jung, Yong-Rok Kim, Lee aS-H, *Catalytic Activities of Perovskite-type $LaBO_3$ (B = Fe, Co, Ni) Oxides for Partial Oxidation of Methane*. Bull Korean Chem Soc **26** (2005) 1591-1596.

[23] Voskresenskaya EN, Roguleva VG, Anshits AG, *Oxidant Activation Over Structural Defects of Oxide Catalysts in Oxidative Methane Coupling*. Catalysis Reviews **37** (1995) 101-143.

[24] Gellings PJ, Bouwmeester HJM, *Solid state aspects of oxidation catalysis*. Catalysis Today **58** (2000) 1-53.

[25] Lunsford JH, *The catalytic conversion of methane to higher hydrocarbons*. Catalysis Today **6** (1990) 235-259.

[26] Driscoll DJ, Martir W, Wang J-X, Lunsford J (1985) The Production of Gas Phase Methyl Radicals Over Lithium-Promoted Mg0. In: Che M, Bond GC (eds) Studies in Surface Science and Catalysis, vol Volume 21. Elsevier, pp 403-408.

[27] Lee JS, Oyama ST, *Oxidative Coupling of Methane to Higher Hydrocarbons*. Catalysis Reviews **30** (1988) 249-280.

[28] Sinev MY, Korchak VN, Krylov OV, *Highly selective ethane formation by reduction of BaO_2 with methane*. Journal Name: Kinet Catal (Engl Transl); (United States); Journal Volume: 27:5; Other Information: Translated from Kinet Katal; 27: No 5, 1274(Sep-Oct 1986) (1987) Medium: X; Size: Pages: 1110.

[29] Weng W, Chen M, Wan H, Liao Y, *High-temperature in situ FTIR spectroscopy study of LaOF and BaF_2/LaOF catalysts for methane oxidative coupling*. Catalysis Letters **53** (1998) 43-50.

[30] Osada Y, Koike S, Fukushima T, Ogasawara S, Shikada T, Ikariya T, *Oxidative coupling of methane over Y_2O_3CaO catalysts*. Applied Catalysis **59** (1990) 59-74.

[31] Gong MC, Xu XH, Chen YQ, Zhou JL, Chen Y, *Study on oxidative coupling of methane. Effect of additives on TiO_2-based catalytic performance*. Catalysis Today **24** (1995) 263-264.

[32] Murata K, Hayakawa T, Hamakawa S, Suzuki K, *Lithium-doped sulfated-zirconia catalysts for oxidative coupling of methane to give ethylene and ethane*. Catalysis Today **45** (1998) 41-45.

[33] Zavyalova U, Holena M, Schlögl R, Baerns M, *Statistical Analysis of Past Catalytic Data on Oxidative Methane Coupling for New Insights into the Composition of High-Performance Catalysts*. ChemCatChem **3** (2011) 1935-1947.

[34] Arndt S, Laugel G, Levchenko S, Horn R, Baerns M, Scheffler M, Schlögl R, Schomäcker R, *A Critical Assessment of Li/MgO-Based Catalysts for the Oxidative Coupling of Methane*. Catalysis Reviews **53** (2011) 424-514.

[35] Arndt S, Simon U, Heitz S, Berthold A, Beck B, Görke O, Epping JD, Otremba T, Aksu Y, Irran E, Laugel G, Driess M, Schubert H, Schomäcker R, *Li-doped MgO From Different Preparative Routes for the Oxidative Coupling of Methane*. Top Catal **54** (2011) 1266-1285.

[36] Lin JZ, Gu JF, Yang DX, Zhang CW, Yang YL, Chu YL, Li aSB, *Stability test of W-Mn/SiO_2 catalyst for oxidative coupling of methane*. Shiyou Huagong **24** (1995) 293-298.

[37] Wang XL, Zhang JN, Yang DX, Zhang CW, Lin JZ, Li aSB, *Oxidative coupling of methane over w-mn/sio2 catalyst in a bench-*

scale stainless steel fluidized-bed reactor. Shiyou Huagong **26** (1997) 361-367.

[38] Pak S, Qiu P, Lunsford JH, *Elementary Reactions in the Oxidative Coupling of Methane over $Mn/Na_2WO_4/SiO_2$and $Mn/Na_2WO_4/MgO$ Catalysts*. Journal of Catalysis **179** (1998) 222-230.

[39] Liu H, Wang X, Yang D, Gao R, Wang Z, Yang J, *Scale up and stability test for oxidative coupling of methane over Na_2WO_4-Mn/SiO_2 catalyst in a 200 ml fixed-bed reactor*. Journal of Natural Gas Chemistry **17** (2008) 59-63.

[40] Li S-B, *Oxidative Coupling of Methane over W-Mn/SiO_2 Catalyst*. Chinese Journal of Chemistry **19** (2001) 16-21.

[41] Ji S-f, Xiao T-c, Li S-b, Xu C-z, Hou R-l, Coleman KS, Green MLH, *The relationship between the structure and the performance of Na-W-Mn/SiO_2 catalysts for the oxidative coupling of methane*. Applied Catalysis A: General **225** (2002) 271-284.

[42] Palermo A, Holgado Vazquez JP, Lee AF, Tikhov MS, Lambert RM, *Critical influence of the amorphous silica-to-cristobalite phase transition on the performance of $Mn/Na_2WO_4/SiO_2$ catalysts for the oxidative coupling of methane*. Journal of Catalysis **177** (1998) 259-266.

[43] Mazzara C, Jupille J, Flank AM, Lagarde P, *Stereochemical Order around Sodium in Amorphous Silica*. The Journal of Physical Chemistry B **104** (2000) 3438-3445.

[44] Jiang ZC, Yu CJ, Fang XP, Li SB, Wang HL, *Oxide/support interaction and surface reconstruction in the sodium tungstate(Na_2WO_4)/silica system*. The Journal of Physical Chemistry **97** (1993) 12870-12875.

[45] H.S. Chen, J.Z. Niu, B. Zhang, Li SB, *Dft study on the active sites in Mn-Na_2WO_4/SiO_2 catalyst*. Acta Physico-Chimica Sinica **17** (2001) 111-115.

[46] Wu J, Li S, *The Role of Distorted WO_4 in the Oxidative Coupling of Methane on Supported Tungsten Oxide Catalysts*. The Journal of Physical Chemistry **99** (1995) 4566-4568.

[47] Wu J, Li S, Niu J, Fang X, *Mechanistic study of oxidative coupling of methane over $Mn_2O_3/Na_2WO_4SiO_2$ catalyst*. Applied Catalysis A: General **124** (1995) 9-18.

[48] Jiang Z-c, Gong H, Li S-b (1997) Methane activation over Mn_2O_3-Na_2WO_4/SiO_2 catalyst and oxygen spillover. In: Can L, Qin X (eds) Studies in Surface Science and Catalysis, vol Volume 112. Elsevier, pp 481-490.

[49] Wendt G, Schaffarczyk S, *Oxidative dimerisierisierung von Methan an mischoxiden*. Chem Technik **43** (1991) 131-140.

[50] Lehmann L, Berns M, *Kinetic studies of the oxidative coupling of methane over a NaOH/CaO catalyst*. Journal of Catalysis **135** (1992) 467-480.

[51] van Kasteren JMN, Geerts JWMH, der Wiele Kv (1991) Methane Oxidative Coupling Using Li/MgO Catalysts: The Importance of Consecutive Reactions. In: A. Holmen KJJ, Kolboe S (eds) Studies in Surface Science and Catalysis, vol Volume 61. Elsevier, pp 139-146.

[52] Stansch Z, Mleczko L, Baerns M, *Comprehensive Kinetics of Oxidative Coupling of Methane over the La_2O_3/CaO Catalyst*. Industrial & Engineering Chemistry Research **36** (1997) 2568-2579.

[53] Sohrabi M, Dabir B, Eskandari A, Golpasha RD, *Some aspects of kinetics and mechanism of the oxidative coupling of methane*. Journal of Chemical Technology & Biotechnology **67** (1996) 15-20.

[54] Lacombe S, Durjanova Z, Mleczko L, Mirodatos C, *Kinetic modelling of the oxidative coupling of methane over lanthanum oxide in connection with mechanistic studies*. Chemical Engineering & Technology **18** (1995) 216-223.

[55] Olsbye U, Desgrandchamps G, Jens K-J, Kolboe S, *A kinetic study of the oxidative coupling of methane over a $BaCO_3$ / $La_2On(CO_3)_{3-n}$ catalyst: I. Determination of a global reaction scheme and the influence of heterogeneous and homogeneous reactions*. Catalysis Today **13** (1992) 209-218.

[56] Daneshpayeh M, Khodadadi A, Mostoufi N, Mortazavi Y, Sotudeh-Gharebagh R, Talebizadeh A, *Kinetic modeling of oxidative coupling of methane over $Mn/Na_2WO_4/SiO_2$ catalyst*. Fuel Processing Technology **90** (2009) 403-410.

[57] Boozarjomehry RB, Masoori M, *Which method is better for the kinetic modeling: Decimal encoded or Binary Genetic Algorithm?* Chemical Engineering Journal **130** (2007) 29-37.

[58] Baerns M, Mleczko L, Zanthoff H, Commission of the European Communities. Directorate-General for Science R, Development, Oxidative Coupling of Methane to C_{2+} Hydrocarbons: Basis of Catalyst Mode of Operation and Process Optimization : Final Report. Office for Official Publications of the European Communities, Edited by, (1993)

[59] Shahri SMK, Pour AN, *Ce-promoted $Mn/Na_2WO_4/SiO_2$ catalyst for oxidative coupling of methane at atmospheric pressure*. Journal of Natural Gas Chemistry **19** (2010) 47-53.

[60] Rane VH, Chaudhari ST, Choudhary VR, *Oxidative coupling of methane over La-promoted CaO catalysts: Influence of precursors and catalyst preparation method*. Journal of Natural Gas Chemistry **19** (2010) 25-30.

[61] Mleczko L, Baerns M, *Catalytic oxidative coupling of methane—reaction engineering aspects and process schemes*. Fuel Processing Technology **42** (1995) 217-248.

[62] Amenomiya Y, Goledzinowski Vibam, Galuszka J, Sanger Ar, *Conversion of Methane by Oxidative Coupling*. CATAL REV-SCI ENG **32** (1990) 163-227.

[63] Andorf R, Mleczko L, Schweer D, Baerns M, *Oxidative coupling of methane in a bubbling fluidized bed reactor*. The Canadian Journal of Chemical Engineering **69** (1991) 891-897.

[64] Labinger JA, Ott KC, *Mechanistic studies on the oxidative coupling of methane*. The Journal of Physical Chemistry **91** (1987) 2682-2684.

[65] Labinger JA, Ott KC, Mehta S, Rockstad HK, Zoumalan S, *Oxidative coupling of methane: the role of solid state chemistry*. Journal of the Chemical Society, Chemical Communications **0** (1987) 543-545.

[66] Lin CH, Campbell KD, Wang JX, Lunsford JH, *Oxidative dimerization of methane over lanthanum oxide*. The Journal of Physical Chemistry **90** (1986) 534-537.

[67] Otsuka K, Jinno K, Morikawa A, *Active and selective catalysts for the synthesis of C_2H_4 and C_2H_6 via oxidative coupling of methane*. Journal of Catalysis **100** (1986) 353-359.

[68] Otsuka K, Nakajima T, *Oxidative coupling of methane over samarium oxides using N_2O as the oxidant*. Journal of the Chemical Society, Faraday Transactions 1: Physical Chemistry in Condensed Phases **83** (1987) 1315-1321.

[69] Asami K, Hashimoto S, Shikada T, Fujimoto K, Tominaga H-o, *Selective Oxidative Coupling of Methane over Supported Lead Oxide Catalyst*. Chemistry Letters **15** (1986) 1233-1236.

[70] Ito T, Wang J, Lin CH, Lunsford JH, *Oxidative dimerization of methane over a lithium-promoted magnesium oxide catalyst*. Journal of the American Chemical Society **107** (1985) 5062-5068.

[71] Amorebieta VT, Colussi AJ, *Kinetics and mechanism of the catalytic oxidation of methane over lithium-promoted magnesium oxide*. The Journal of Physical Chemistry **92** (1988) 4576-4578.

[72] Tye CT, Mohamed AR, Bhatia S, *Modeling of catalytic reactor for oxidative coupling of methane using La_2O_3/CaO catalyst*. Chemical Engineering Journal **87** (2002) 49-59.

[73] Yaghobi N, *The role of gas hourly space velocity and feed composition for catalytic oxidative coupling of methane: Experimental study*. Journal of King Saud University - Engineering Sciences **25** (2013) 1-10.

[74] Sirikarn T, WiyaratnWisitsree, Assabumrungrat S, Amornchai A (2011) Simulation and Optimization of Oxidative Coupling of Methane in a Dense Tubular Membrane Reactor. Paper presented at the TIChE International Conference 2011, Hatyai, Songkhla THAILAND,

[75] Shahri SMK, Alavi SM, *Kinetic studies of the oxidative coupling of methane over the $Mn/Na_2WO_4/SiO_2$ catalyst*. Journal of Natural Gas Chemistry **18** (2009) 25-34.

[76] Olivier L, Haag S, Pennemann H, Hofmann C, Mirodatos C, van Veen AC, *High-temperature parallel screening of catalysts for the oxidative coupling of methane*. Catalysis Today **137** (2008) 80-89.

[77] Ertl G, Knözinger H, Weitkamp J, Handbook of heterogeneous catalysis. vol. 4, VCH, Edited by, (1997)

[78] Leyshon DW (1991) Thin Bed Reactor for Conversion of Methane to Higher Hydrocarbons. In: A. Holmen KJJ, Kolboe S (eds) Studies in Surface Science and Catalysis, vol Volume 61. Elsevier, pp 497-507. doi:10.1016/s0167-2991(08)60116-0

[79] van Looij F, Mulder A, Boon AQM, Scheepens JF, Geus JW (1993) Fixed Bed Catalytic Reactors Based on Sintered Metals. In: L. Guczi FS, P T (eds) Studies in Surface Science and Catalysis, vol Volume 75. Elsevier, pp 1377-1389. doi:10.1016/s0167-2991(08)64458-4

[80] M. Aigler J, H. Lunsford J, *Oxidative dimerization of methane over MgO and Li+/MgO monoliths*. Applied Catalysis **70** (1991) 29-42.

[81] Dautzenberg FM, Schlatter JC, Fox JM, Rostrup-Nielsen JR, Christiansen LJ, *Catalyst and reactor requirements for the oxidative coupling of methane*. Catalysis Today **13** (1992) 503-509.

[82] Mleczko L, Pannek U, Niemi VM, Hiltunen J, *Oxidative Coupling of Methane in a Fluidized-Bed Reactor over a Highly Active and Selective Catalyst*. Industrial & Engineering Chemistry Research **35** (1996) 54-61.

[83] Mleczko L, Pannek U, Rothaemel M, Baerns M, *Oxidative coupling of methane over a La_2O_3/CaO catalyst. Optimization of reaction conditions in a bubbling fluidized-bed reactor*. The Canadian Journal of Chemical Engineering **74** (1996) 279-287.

[84] Pannek U, Mleczko L, *Comprehensive model of oxidative coupling of methane in a fluidized-bed reactor*. Chemical Engineering Science **51** (1996) 3575-3590.

[85] Pannek U, Mleczko L, *Reaction Engineering Simulations of Oxidative Coupling of Methane in a Circulating Fluidized-Bed Reactor*. Chemical Engineering & Technology **21** (1998) 811-821.

[86] Edwards JH, Tyler RJ, White SD, *Oxidative coupling of methane over lithium-promoted magnesium oxide catalysts in fixed-bed and fluidized-bed reactors*. Energy & Fuels **4** (1990) 85-93.

[87] Levenspiel O, Chemical Reaction Engineering, 3rd Ed. Wiley India Pvt. Limited, Edited by, (2006)

[88] Kunii D, Levenspiel O, Fluidization engineering. Butterworth-Heinemann Limited, Edited by, (1991)

[89] Werther J, Hartge E-U, *Modeling of Industrial Fluidized-Bed Reactors*. Industrial & Engineering Chemistry Research **43** (2004) 5593-5604.

[90] Pak S, Lunsford JH, *Thermal effects during the oxidative coupling of methane over $Mn/Na_2WO_4/SiO_2$ and $Mn/Na_2WO_4/MgO$ catalysts*. Applied Catalysis A: General **168** (1998) 131-137.

[91] Coronas J, Menendez M, Santamaria J, *Development of ceramic membrane reactors with a non-uniform permeation pattern. Application to methane oxidative coupling*. Chemical Engineering Science **49** (1994) 4749-4757.

[92] Lu Y, Dixon AG, Moser WR, Ma YH, Balachandran U, *Oxygen-permeable dense membrane reactor for the oxidative coupling of methane*. Journal of Membrane Science **170** (2000) 27-34.

[93] Nozaki T, Fujimoto K, *Oxide ion transport for selective oxidative coupling of methane with new membrane reactor*. AIChE Journal **40** (1994) 870-877.

[94] Zeng Y, Lin YS, Swartz SL, *Perovskite-type ceramic membrane: synthesis, oxygen permeation and membrane reactor performance for oxidative coupling of methane*. Journal of Membrane Science **150** (1998) 87-98.

[95] Shao Z, Dong H, Xiong G, Cong Y, Yang W, *Performance of a mixed-conducting ceramic membrane reactor with high oxygen permeability for methane conversion*. Journal of Membrane Science **183** (2001) 181-192.

[96] Jiang Y, Yentekakis IV, Vayenas CG, *Methane to ethylene with 85 percent yield in a gas recycle electrocatalytic reactor-separator*. Science **264** (1994) 1563-1566.

[97] Garagounis I, Kyriakou V, Anagnostou C, Bourganis V, Papachristou I, Stoukides M, *Solid Electrolytes: Applications in Heterogeneous Catalysis and Chemical Cogeneration*. Industrial & Engineering Chemistry Research **50** (2010) 431-472.

[98] Ramachandra AM, Lu Y, Ma YH, Moser WR, Dixon AG, *Oxidative coupling of methane in porous Vycor membrane reactors*. Journal of Membrane Science **116** (1996) 253-264.

[99] Klose F, Wolff T, Thomas S, Seidel-Morgenstern A, *Operation modes of packed-bed membrane reactors in the catalytic oxidation of hydrocarbons*. Applied Catalysis A: General **257** (2004) 193-199.

[100] Kölsch P, Noack M, Schäfer R, Georgi G, Omorjan R, Caro J, *Development of a membrane reactor for the partial oxidation of hydrocarbons: direct oxidation of propane to acrolein*. Journal of Membrane Science **198** (2002) 119-128.

[101] Stoukides M, *Solid-Electrolyte Membrane Reactors: Current Experience and Future Outlook*. Catalysis Reviews - Science and Engineering **42** (2000) 1-70.

[102] Marnellos G, Stoukides M, *Catalytic studies in electrochemical membrane reactors*. Solid State Ionics **175** (2004) 597-603.

[103] Munder B, Ye Y, Rihko-Struckmann L, Sundmacher K, *Solid electrolyte membrane reactor for controlled partial oxidation of hydrocarbons: Model and experimental validation*. Catalysis Today **104** (2005) 138-148.

[104] Pujare NU, Sammells AF, *Methane activation to C_2 hydrocarbon species in solid oxide fuel cell*. Journal of the Electrochemical Society **135** (1988) 2544-2545.

[105] Tsiplakides D, Neophytides S, Vayenas CG, *Investigation of electrochemical promotion using temperature-programmed desorption and work function measurements*. Solid State Ionics **136–137** (2000) 839-847.

[106] Vernoux P, Gaillard F, Bultel L, Siebert E, Primet M, *Electrochemical Promotion of Propane and Propene Oxidation on Pt/YSZ*. Journal of Catalysis **208** (2002) 412-421.

[107] Petrolekas PD, Balomenou S, Vayenas CG, *Electrochemical promotion of ethylene oxidation on Pt catalyst films deposited on CeO_2*. Journal of the Electrochemical Society **145** (1998) 1202-1206.

[108] Otsuka K, Yokoyama S, Morikawa A, *Catalytic activity- and selectivity-control for oxidative coupling of methane by oxygen-*

pumping through yttria-stabilized zirconia. Chemistry Letters **14** (1985) 319-322.

[109] Otsuka K, Suga K, Yamanaka I, *Oxidative coupling of methane applying a solid oxide fuel cell system*. Catalysis Today **6** (1990) 587-592.

[110] Guo X-M, Hidajat K, Ching C-B, *An experimental study of oxidative coupling of methane in a solid oxide fuel cell with 1 wt%Sr/La_2O_3-Bi_2O_3-Ag-YSZ membrane*. Korean Journal of Chemical Engineering **15** (1998) 469-473.

[111] Wiyaratn W, Appamana W, Charojrochkul S, Kaewkuekool S, Assabumrungrat S, *Au/$La_{1-x}Sr_xMnO_3$ nanocomposite for chemical-energy cogeneration in solid oxide fuel cell reactor*. Journal of Industrial and Engineering Chemistry **18** (2012) 1819-1823.

[112] Kiatkittipong W, Tagawa T, Goto S, Assabumrungrat S, Silpasup K, Praserthdam P, *Comparative study of oxidative coupling of methane modeling in various types of reactor*. Chemical Engineering Journal **115** (2005) 63-71.

[113] Kirubakaran A, Jain S, Nema RK, *A review on fuel cell technologies and power electronic interface*. Renewable and Sustainable Energy Reviews **13** (2009) 2430-2440.

PART II

MIXED OXIDE CATALYSTS FOR THE OXIDATIVE COUPLING OF METHANE

2 Ce based oxide catalysts for the Oxidative Coupling of Methane

Metals (Li, Na, Ca, Ba and Ti) have been used frequently to improve the performance of catalyst oxides for the oxidative coupling of methane. In this work these metals were used to prepare Ce based oxides. It was found that the incorporation of Li, Na and Ca influences the basic properties of the catalysts. Catalytic tests were carried out at different temperatures (600-800) ^{o}C. It was observed that C_2 selectivity increased with temperature passing through a maximum around 750 ◦C on the catalysts with better performance. The Ca-doped CeO_2 showed the highest C_2 yield at 750 ^{o}C. It seems that the intermediate basic sites play a key role in the OCM reaction.

2.1 Introduction

Production of C_2 hydrocarbons (ethane and ethylene) through the OCM has been studied in the last 30 years [1-6]. In fact, the first fundamental work was published by Keller and Bashin in 1982 [1]. Although, this reaction represents a promising route for using natural gas, the OCM is still not used for commercial practice due to low overall yield [7-10]. The main reason is due to several thermodynamic constraints. First, in the absence of oxygen the energy changes for the gas phase conversion of methane to C_2 hydrocarbons are unfavourable at temperatures below 1250 ^oC. Then, in the presence of oxygen the conversion of methane to C_2 hydrocarbons becomes thermodynamically favourable [7]. However the overall thermodynamically favoured products are carbon oxides and water. Therefore, in order to obtain the intermediate products, such as C_2 hydrocarbons or even methanol, a greater degree of reaction control must be gained. The use of active and selective catalysts would offer a possibility to achieve such reaction control.

A large number of metal oxides and mixed metal oxides have been reported to catalyse the OCM [1,11-14,3,15]. It was reported that solid single or mixed oxides can be active/selective catalysts in the OCM [2]. The choice of catalytic components has been one of the many fundamental aspects studied in the OCM reaction [7,8]. However, the essential features for an optimal composition remain unknown. Alkaline, earth alkaline and transition metal oxides such as Li, Na, Ca, Ba and Ti, have been reported in the literature to be efficient catalyst for the OCM [16-20].

On the other hand, in several research works, CeO_2 exhibited very low C_2 selectivity [2,21,22]. For example, Pacheco et al. [23] reported CH_4 conversion of 10 % and selectivity to C_2 hydrocarbons of 6 % at 750 ^oC. Nevertheless, Ce has been used in small amounts to promote catalysts for the OCM reaction due to its ability for transporting charges as reported by Bartsch and Hofmann [24]. Nowadays, few works have been carried out using CeO_2 modified with metals which are known to promote a higher C_2 hydrocarbons selectivity. Therefore, in this work Li, Na, Ca, Ba and Ti metals are incorporated to CeO_2 to study their performance in the OCM reaction at different temperatures (600-800) ^oC. Temperature Programmed Reduction (TPR) and Temperature Programmed Desorption of CO_2 (CO_2-

TPD) were used to investigate the reducibility and the base strength distribution of the oxide catalysts and their effects in OCM.

2.2 Experimental section

2.2.1 Catalyst preparation

Citrate method was used to prepare the oxide catalysts. This method has been used in literature to prepare multicomponent oxides [25]. It involves the formation of a mixed-ions citrate that due to the three-ligand nature of the citric acid results in a transparent three-dimensional network which allows preparation of highly dispersed mixed oxides from the individual cations in the desired stoichiometric ratio [26-28]. Thus, the oxides were obtained from $Ce(NO_3)_3 \cdot 6H_2O$ (99% Aldrich), $LiNO_3$ (Sigma-Aldrich 99%), $NaNO_3$ (Sigma-Aldrich 99%), $Ca(NO_3)_2 \cdot 4H_2O$ (99% Fluka), $Ba(NO_3)_2$ (Riedel-de Haen 99%) and $TiCl_4$ (Fluka98%). Figure 2.1 shows schematically the citrate method procedure.

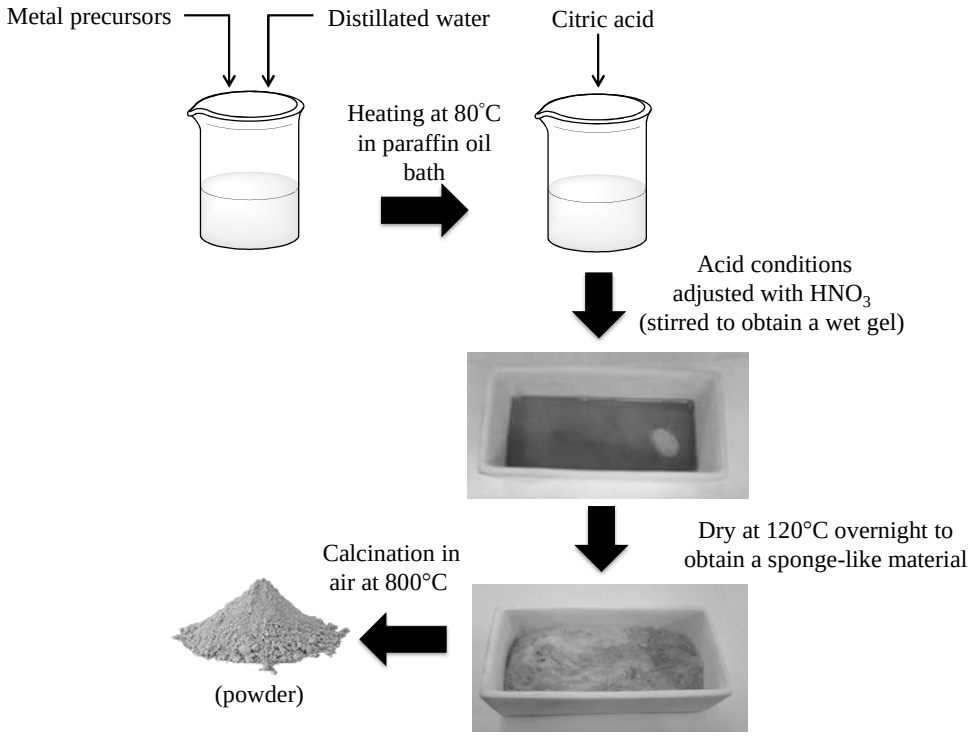

Figure 2.1 Schematic procedure of the oxide preparation.

Firsts, the precursors were added to distilled water in the appropriate amounts to obtain a M:Ce molar ratio of 1:1. Citric acid was added with a

molar ratio of acid/(Ce + M) = 1.5. Then, acid conditions were adjusted using HNO_3 (pH=2). The solution was heated up to 80 °C in a paraffin bath under constant stirring to evaporate superfluous water, the volume of the solution decreased and a viscous gel was obtained. The gel was dried at 120 °C overnight to form a spongy material and finally it was calcined at 800 °C during 6 h. The oxides are denoted as $M_{0.5}Ce_{0.5}O$ (M=Li, Na, Ca, Ba and Ti).

2.2.2 Catalyst characterisation

Reducibility and the base strength distribution of the catalyst oxides were investigated by Temperature Programmed Reduction (TPR) and CO_2 Temperature Programmed Desorption CO_2 (CO_2-TPD). Both TPR and CO_2-TPD experiments were carried out in an Altamira Instruments (AMI-200) apparatus. The surface basicity/base strength distribution of the catalyst was measured by Temperature Programmed Desorption (TPD) of CO_2 chemisorbed at 100 °C for 2 h on 100 mg of catalyst placed in a U-shaped quartz tube located inside an electrical furnace, and subsequently heated up from 100 °C to 1000 °C with a linear heating rate of 10 °C min^{-1} and argon (25 cm^3 min^{-1}) as the carrier gas. The chemisorbed amount of CO_2 was defined as the amount retained on the pre-saturated catalyst. Then, it was swept with pure argon (25 cm^3 min^{-1}) for a period of 1.5 h at 100 °C. The CO_2 desorbed was measured quantitatively by the MS signal (m/e: 44) monitored by a Dycor Dymaxion mass spectrometer.

For TPR experiments, a mixture of 5 vol.% H_2/Ar was used, at a total flow rate of 30 cm^3min^{-1}, with 100 mg of catalyst. The temperature was increased at a rate of 5 °C min^{-1} from room temperature to 1000°C, while the hydrogen consumption was monitored.

2.2.3 Catalyst evaluation

The catalytic performance of the prepared oxides for the OCM was studied in a quartz tube reactor of i.d = 25 mm as shown in Figure 2.2 which was filled with 0.2 g of catalyst held by quartz wool placed on a support in the shape of a cross.

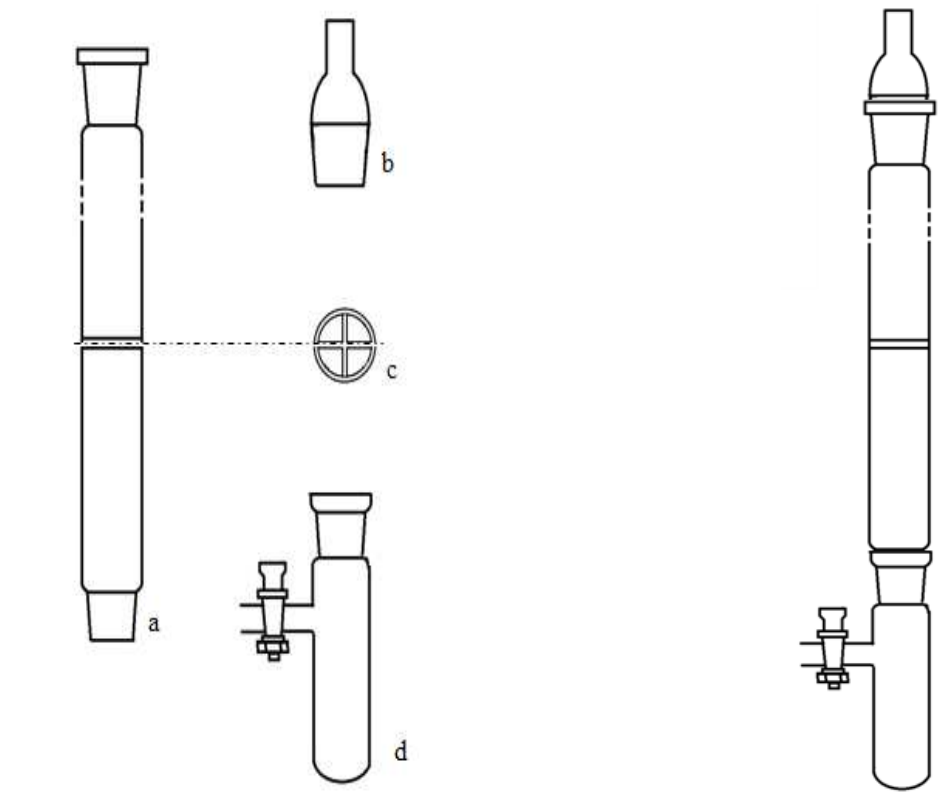

Figure 2.2 Left: (a) quartz tube reactor, (b) reduction adaptor, (c) support in the shape of a cross and (d) cold trap. Right: coupled reactor system elements.

The reactor was placed into an electrical heater as showed in Figure 2.3. Methane, helium and oxygen flow rates were regulated by mass flow controllers (HI-TEC). The mixture of methane and oxygen (CH_4/O_2 molar ratio of 4) diluted in Helium (75% of the total flow) was passed through the catalyst bed with a total flow rate of 50 cm^3 min^{-1}. A cold trap was placed at the outlet of the quartz tube to separate any condensed water vapour from the reaction products. The OCM study stared when the temperature reached 600 °C. The product stream containing carbon monoxide, carbon dioxide, ethane, ethylene, unreacted oxygen and methane was analysed by an on-line gas chromatograph (GC) equipped with a thermal conductivity (TC) detector, using a capillary column (Carboxen 1010 Plot. Supelco).

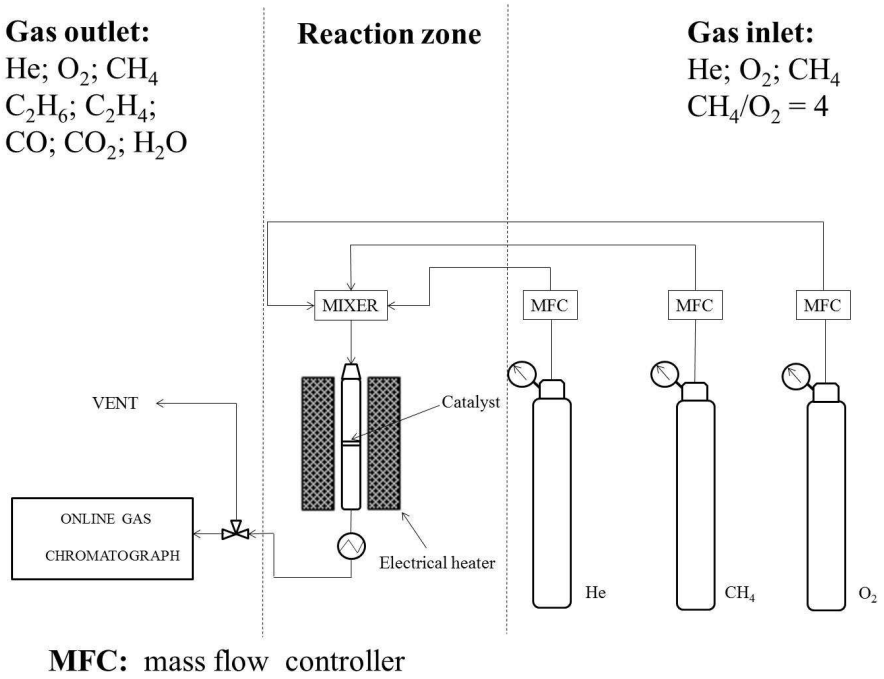

Figure 2.3 Schematic diagram of the OCM setup.

It was assumed that carbon and /or hydrogen in methane were only converted into ethane, ethylene carbon monoxide, carbon dioxide and/or molecular hydrogen and water. Then, the conversion of CH_4 and the selectivity of the products were defined, respectively, as follows:

$$\text{CH}_4 \text{ conversion} = \frac{2F_{C_2H_4} + 2F_{C_2H_6} + F_{CO} + F_{CO_2}}{F_{CH_{4inlet}}} x100\% \qquad 2.1$$

$$\text{C}_2 \text{ selectivity} = \frac{2F_{C_2H_4} + 2F_{C_2H_6}}{2F_{C_2H_4} + 2F_{C_2H_6} + F_{CO} + F_{CO_2}} x100\% \qquad 2.2$$

$$\text{C}_2 \text{ yield} = (\text{CH}_4 \text{ conversion}) \text{ x } (\text{C}_2 \text{ selectivity})/100 \qquad 2.3$$

where F_i is the flow of the species i (mol min^{-1}).

2.3 Results and discussion

2.3.1 Characterisation

2.3.1.1 Temperature programmed reduction (TPR)

As mentioned before, TPR was used to study the reduction of Ce-based oxide catalysts in the presence of hydrogen. A peak at high temperature (about 850 °C) is observed in the CeO_2 TPR profile (Figure 2.4) which can be attributed to CeO_2 bulk oxygen (O^{2-}) [29]. The peak shape differs for the $Ti_{0.5}Ce_{0.5}O$ and $Na_{0.5}Ce_{0.5}O$ catalysts. This latter is shifted by 19 ^oC towards higher temperature, compared with CeO_2. It can be also observed that the introduction of Ti generated small peaks at about 620 and 675 ^oC. The reason for these results may be due to the influence of the additives Ti and Na, in both cases, leading differences in the metal-metal interaction.

On the other hand, the $Ba_{0.5}Ce_{0.5}O$, $Ca_{0.5}Ce_{0.5}O$ and $Li_{0.5}Ce_{0.5}O$ also show different TPR profiles, compared to CeO_2. Two reduction peaks at high temperatures (850 and 976 ^oC) are observed in the $Ba_{0.5}Ce_{0.5}O$ TPR profile. It was reported in literature that BaO is not reduced at temperatures below 800 ^oC [30]. Therefore the reduction peak at 976 ^oC can be attributed to bulk oxygen reduction of BaO indicating no formation of a binary oxide. As mentioned above, the peak at 850 ^oC is assigned to the reduction of bulk cerium oxide.

Two peaks are also observed in the profiles of the $Ca_{0.5}Ce_{0.5}O$ and $Li_{0.5}Ce_{0.5}O$ catalysts (590 and 785 ^oC) and (729 and 870 ^oC) respectively. It is reported that calcium oxide exhibits very high reduction temperatures (> 1000 ^oC) [31]. Therefore, the peak at about 870 ^oC could be also attributed to the bulk oxygen of ceria and the peaks at temperatures below 870 ^oC would correspond to lower temperature of ceria surface shell reduction or the most easy reduction of surface oxygen species known as capping oxygen [32]. Moreover, a large difference in hydrogen consumption is observed upon comparison of the peak intensities of $Ti_{0.5}Ce_{0.5}O$, $Ba_{0.5}Ce_{0.5}O$ and $Li_{0.5}Ce_{0.5}O$. The addition of Ti, Ba and Li seems to increase the amount of hydrogen consumed for Ce^{4+} reduction, but this may be partly due to moderate reduction of those metals in their ionic state in the same temperature range.

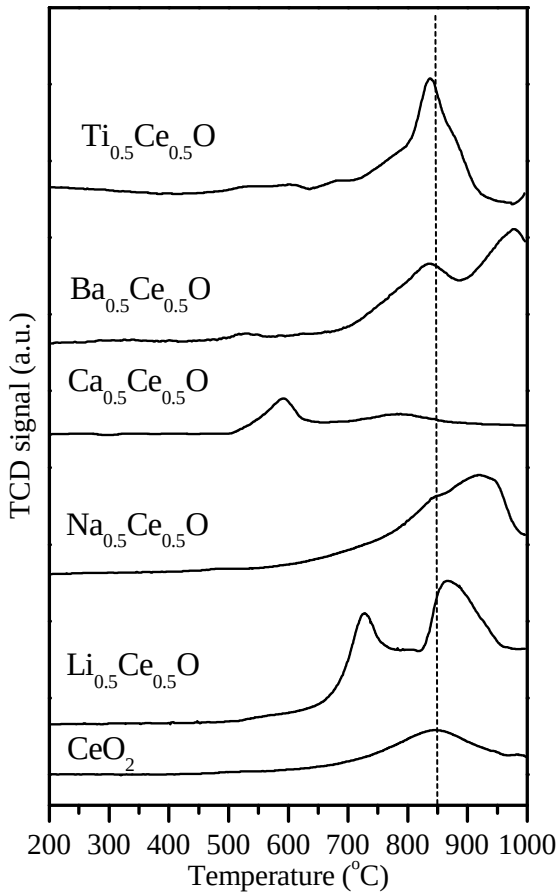

Figure 2.4 TPR profiles of the Ce-based binary oxide catalysts.

2.3.1.2 CO_2 Temperature programmed desorption (CO_2-TPD)

Temperature programmed desorption with CO_2 as acid probe was used to measure the acid-basic properties of the catalysts. Figure 2.5 shows the CO_2-TPD profiles of the Ce based oxide catalysts. From this figure, it can be observed that there is much larger amount of desorbed CO_2 in the $Ca_{0.5}Ce_{0.5}O$ and $Li_{0.5}Ce_{0.5}O$ catalyst profiles at temperatures above 500 ^oC. Two main peaks are found; centred at 650 and 950 ^oC respectively. On the other hand; $Na_{0.5}Ce_{0.5}O$ shows a peak at lower temperature (200 ^oC). The CeO_2, $Ba_{0.5}Ce_{0.5}O$ and $Ti_{0.5}Ce_{0.5}O$ catalysts did not reveal significant amounts of desorbed CO_2.

These peaks can represent the base strength distribution of different catalysts. For a catalyst having a broad site energy distribution, the adsorbate adsorbed on weaker basic sites is desorbed at lower temperatures and that

adsorbed on stronger basic sites is desorbed at higher temperatures. Therefore, the strength of the particular group of basic sites can be expressed in terms of the temperature interval in which the CO_2 chemisorbed on the basic sites is desorbed. These basic sites can be classified into three intervals: weak (100-500) °C, intermediate (500-750) °C and strong (750-950) °C. Then, based in that classification, it can be suggested that $Na_{0.5}Ce_{0.5}O$, $Ca_{0.5}Ce_{0.5}O$ and $Li_{0.5}Ce_{0.5}O$ catalysts present weak, intermediate and strong basic sites respectively. It means that the difference in the amount of desorbed CO_2 and the base strength distribution is strongly influenced by incorporation of Li^+, Na^+, and Ca^{2+} when compared to Ba^{2+} and Ti^{+4} ions, which revealed no basicity as evidenced by the horizontal lines with no peaks in Figure 2.5.

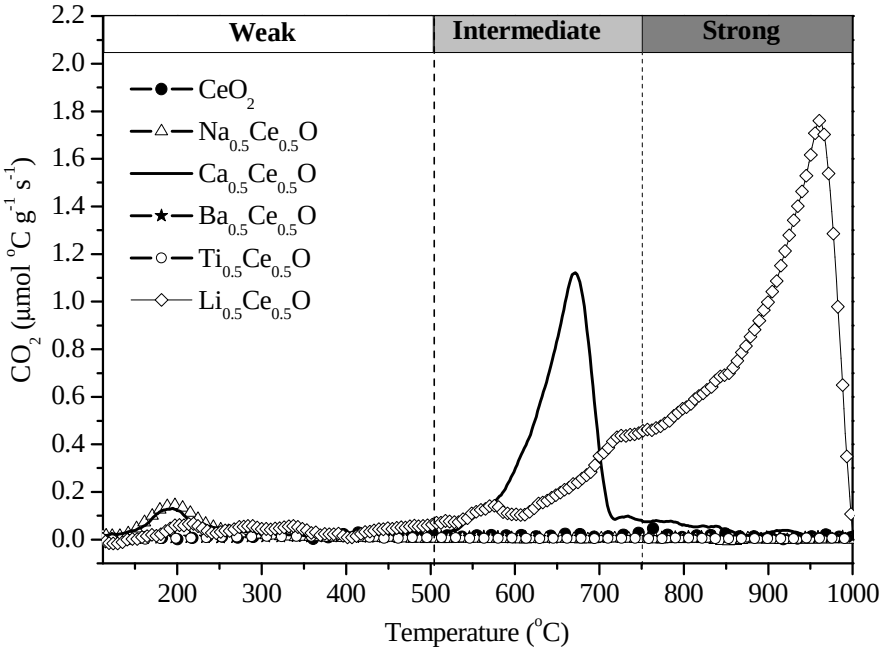

Figure 2.5 TPD-CO2 profiles of the catalysts.

Therefore, both the TPR and CO_2-TPD results suggest that $Li_{0.5}Ce_{0.5}$ and $Ca_{0.5}Ce_{0.5}O$ are more reducible and more basic by having considerable amounts of intermediate and strong basic sites compared to other catalysts.

2.3.2 Catalytic tests

The performance of pure CeO_2 and Ce-based oxide catalysts is shown in Figure 2.6. The reactions were carried out at different temperatures (600-800) ^oC. It can be observed that the methane conversion increased with temperature, particularly in the temperature range of 600−750 $^\circ C$, but in the case of the $Li_{0.5}Ce_{0.5}O$, $Na_{0.5}Ce_{0.5}O$ and $Ca_{0.5}Ce_{0.5}O$ catalysts, it slightly decreased at 800 ^oC. Similar behaviour was observed for the C_2 selectivity and yield of these catalysts. In fact, C_2 selectivity increased with temperature and passed through a maximum around 750 $^\circ C$.

A similar behaviour also was reported in literature [6] when Ce was used to promote a $Mn\text{-}Na_2WO_4/SiO_2$ catalyst. In that work, the temperature of maximum C_2 selectivity was found at 820 ^oC. L. Mleczko and M. Baerns [4], evaluated several engineering aspects in order to make OCM process technically feasible. They point out that, in several catalysts used in OCM, with increasing temperature, C_2 selectivity as well as yield pass through a maximum or even reach a plateau. The temperature of maximum selectivity is specific for each catalyst and depends on the partial pressures of reactants as well as on mixing patterns which are different in various reactor types [4].

The increase in C_2 selectivity with growing temperature up to 700 ^oC would result from the higher activation energy of the selective primary reaction step when compared to the non-selective ones [4], i.e., the formation of C_2 hydrocarbons can be considered as primary reaction step compared to the non-selective ones, and therefore C_2 hydrocarbons increases more with temperature than CO_x. However, Lin et al. [16] pointed out that the formation of C_2 hydrocarbons is of second order for $CH_3\cdot$ radicals whereas that of CO_x is of first order. When the rate of $CH_3\cdot$ radical production increases with temperature, relatively more C_2 hydrocarbons than CO_x are formed, compared to lower temperatures. Therefore, the C_2 hydrocarbon production increases more strongly with temperature than CO_x.

On the other hand, a decrease of the selectivity at higher temperatures (>750 ^oC) can be caused by consecutive reactions of oxidation which occur also in the gas phase as shown in the following equations:

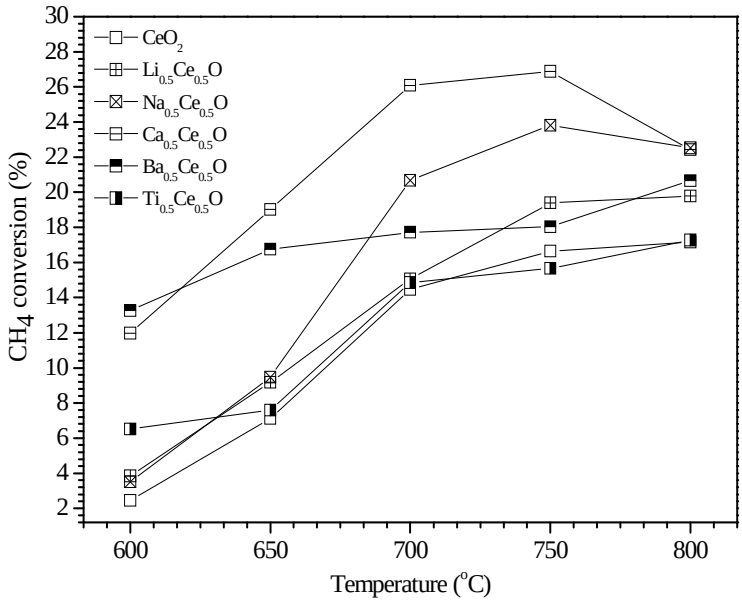

(a)

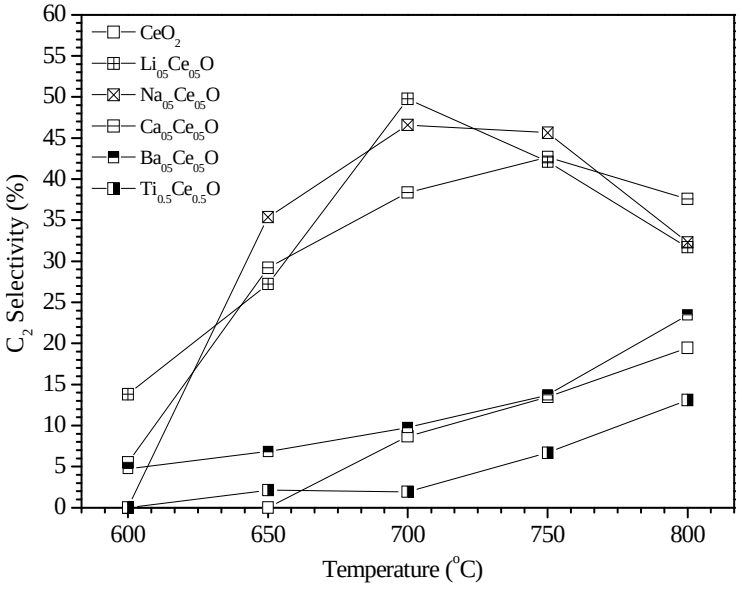

(b)

Figure 2.6 Performance of the catalysts at different temperature. (a) Methane conversion, (b) C_2 selectivity, (c) C_2 yield and (d) C_2H_4/C_2H_6 ratio.

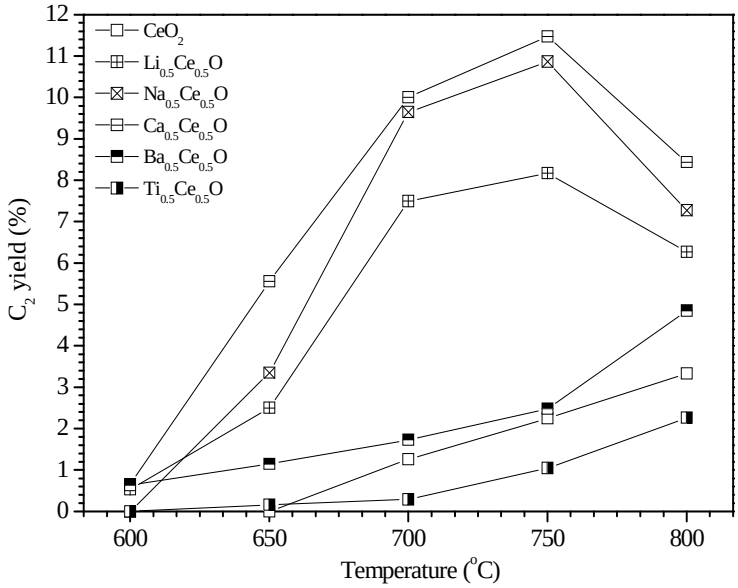

(c)

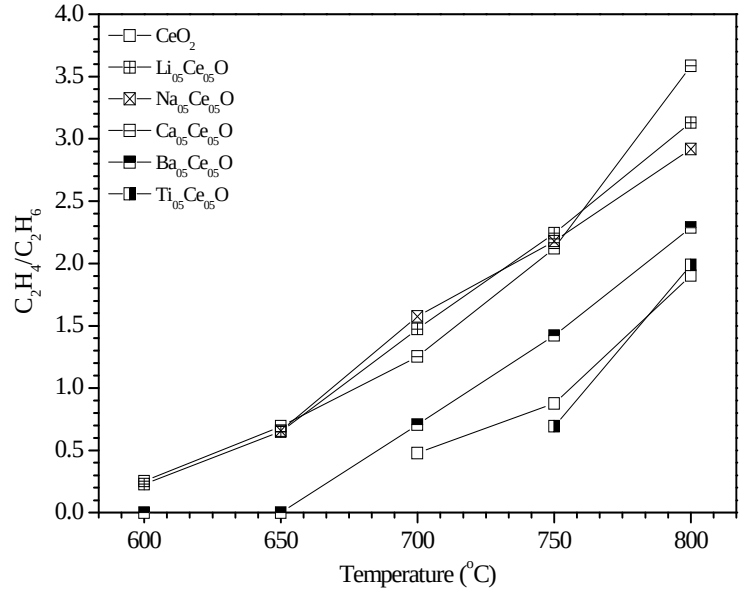

(d)

Figure 2.6 (Cont.) Performance of the catalysts at different temperature. (a) Methane conversion, (b) C_2 selectivity, (c) C_2 yield and (d) C_2H_4/C_2H_6 ratio.

$C_2H_6 + 7/2O_2 \rightarrow 2CO_2 + 3H_2O$ 2.4

$C_2H_6 + 5/2O_2 \rightarrow 2CO + 3H_2O$ 2.5

$C_2H_4 + 3O_2 \rightarrow 2CO_2 + 2H_2O$ 2.6

$C_2H_4 + 2O_2 \rightarrow 2CO + 2H_2O$ 2.7

It can be also explained by oxygen conversion. Complete conversion of oxygen was observed in the catalysts studied in this work. When complete conversion of oxygen was achieved, the increasing C_2 selectivity was accompanied by an increase in methane conversion in the temperature range of 600 and 700 ^oC. This effect can result from the selective reactions (Eqs. 2.8 and 2.9) of the OCM [4].

$CH_4 + 1/4O_2 \rightarrow 1/2C_2H_6 + ½\ H_2O$ 2.8

$C_2H_6 + 1/2O_2 \rightarrow C_2H_4 + H_2O$ 2.9

However, oxidation of C_2 hydrocarbons can occur at high temperature (800 ^oC) by the above equations (2.4-2.7), which cause a decrease of selectivity. These oxidation reactions have been reported in literature [33]. When a decrease of selectivity at high temperatures was caused by oxidation of C_2 hydrocarbons this decrease was also associated to a decrease of methane conversion for stoichiometric reasons [4].

On the other hand, the catalytic results showed higher CH_4 conversion, C_2 yield and C_2H_4/C_2H_6 ratio for the $Li_{0.5}Ce_{0.5}O$, $Na_{0.5}Ce_{0.5}O$ and $Ca_{0.5}Ce_{0.5}O$ catalysts when compared with pure CeO_2, $Ba_{0.5}Ce_{0.5}$ and $Ti_{0.5}Ce_{0.5}O$. These results suggest that doping of CeO_2 with Li, Na, and Ca increases the activity and selectivity of methane coupling specially at 700 and 750^{0}C. It can be related with the results obtained from TPR and CO_2-TPD techniques. As observed in Figure 2.4, the incorporation of metals (Li, Na and Ca) in CeO_2 has a significant effect on the reducibility of bulk mixed oxide, which reflects in a difference in the TPR profiles. The incorporation of these metals would generate probably different defects on surface in each catalyst. These defects can create important active/selective sites for the OCM reaction. It was reported that these active/selective sites are related with the basicity of the oxides [34], and this latter, plays an important role in OCM [21]. Therefore, the CO_2-TPD results showed that the addition of Li, Na and Ca to create higher basicity when compared to CeO_2.

However, the $Li_{0.5}Ce_{0.5}O$ catalyst TPD profile reveals the highest amount of desorbed CO_2, and therefore the highest basicity. It would seem that this catalyst showed be much more active. However, the catalytic results showed that $Li_{0.5}Ce_{0.5}O$ was less active when compared to $Ca_{0.5}Ce_{0.5}O$ and $Na_{0.5}Ce_{0.5}O$ catalysts, as shown in Figure 2.5a, which can be related to the base strength distribution. As mentioned above, $Li_{0.5}Ce_{0.5}O$ has a large amount of desorbed CO_2 in an interval of high temperature, (750-1000 ^oC). Large amounts of strong basic sites could be detrimental to the OCM activity due to CO_2 produced during the OCM reaction being strongly adsorbed on the strong basic sites and therefore would block the catalyst surface.

On the other hand, the $Ca_{0.5}Ce_{0.5}O$ catalyst revealed higher amount of intermediate basic sites and had better performance. This could suggest that weak and intermediate basic sites play an important role for the oxidative coupling of methane than strong basic sites. Then, $Na_{0.5}Ce_{0.5}O$ catalyst showed only weak basic sites and no intermediate and strong basic sites. However, it revealed higher activity than $Li_{0.5}Ce_{0.5}O$, which exhibit intermediate basic sites than $Na_{0.5}Ce_{0.5}O$. Therefore, the correlation between the basicity and the activity or C_2 yield is rather poor. This points out the fact that other factors than basicity are also important in determining the catalytic performance of Ce-based oxide catalyst in oxidative coupling of methane.

2.4 Conclusions

Modification of CeO_2 with Li, Na, Ca, Ba and Ti was investigated in the OCM reaction. It was evidenced that incorporation of Li, Na and Ca increased significantly the C_2 selectivity and yield when compared CeO_2. This effect could be attributed to the basicity created on the catalyst surface and higher reducibility of the catalysts. It was found that C_2 selectivity and yield pass through a maximum in the range of temperature between 700 and 750 ^oC on the $Li_{0.5}Ce_{0.5}O$, $Na_{0.5}Ce_{0.5}O$ and $Ca_{0.5}Ce_{0.5}O$ catalysts. The $Ca_{0.5}Ce_{0.5}O$ catalyst showed the best performance in the OCM reaction. It could be attributed to its easy reducibility and large amount of intermediate basic sites.

These results reveal important information about modification of CeO_2 surface. Incorporation of metals seems to be the key, not only to improve performance, but also can help to study the nature of the active sites created on the catalyst surface by incorporation of other metals.

References

[1] Keller GE, Bhasin MM, *Synthesis of ethylene via oxidative coupling of methane: I. Determination of active catalysts*. J. Catal. **73** (1982) 9-19.

[2] DeBoy JM, Hicks RF, *The oxidative coupling of methane over alkali, alkaline earth, and rare earth oxides*. Ind. Eng. Chem. Res. **27** (1988) 1577-1582.

[3] Dubois J-L, Cameron CJ, *Common features of oxidative coupling of methane cofeed catalysts*. Appl. Catal. **67** (1990) 49-71.

[4] Mleczko L, Baerns M, *Catalytic oxidative coupling of methane—reaction engineering aspects and process schemes*. Fuel Process. Technol. **42** (1995) 217-248.

[5] Ji S, Xiao T, Li S, Chou L, Zhang B, Xu C, Hou R, York APE, Green MLH, *Surface WO_4 tetrahedron: the essence of the oxidative coupling of methane over MW·Mn/SiO_2 catalysts*. J. Catal. **220** (2003) 47-56.

[6] Shahri SMK, Pour AN, *Ce-promoted Mn/Na_2WO_4/SiO_2 catalyst for oxidative coupling of methane at atmospheric pressure*. J. Nat. Gas Chem. **19** (2010) 47-53.

[7] Methane conversion by oxidative processes fundamental and engineering aspects / edited by E.E. Wolf. Van Nostrand Reinhold catalysis series, (1992). Van Nostrand Reinhold, New York

[8] Maitra AM, *Critical performance evaluation of catalysts and mechanistic i mplications for oxidative coupling of methane*. Appl. CataL. A Gen. **104** (1993) 11-59.

[9] Zhang Z, Verykios XE, Baerns M, *Effect of electronic properties of catalysts for the oxidative coupling of methane on their selectivity and activity*. Catal. Rev. **36** (1994) 507-556.

[10] Alvarez-Galvan MC, Mota N, Ojeda M, Rojas S, Navarro RM, Fierro JLG, *Direct methane conversion routes to chemicals and fuels*. Catal. Today **171** (2011) 15-23.

[11] Chan TK, Smith KJ, *Oxidative coupling of methane over cobalt—magnesium and manganese—magnesium mixed oxide catalysts*. Appl. Catal. **60** (1990) 13-31.

[12] Wu J, Zhang H, Qin S, Hu C, *La-promoted $Na_2WO_4/Mn/SiO_2$ catalysts for the oxidative conversion of methane simultaneously to ethylene and carbon monoxide*. Appl. Catal. A Gen. **323** (2007) 126-134.

[13] Matsuura I, Utsumi Y, Nakai M, Doi T, *Oxidative Coupling of Methane over Lithium-Promoted Zinc Oxide Catalyst*. Chem. Lett. **15** (1986) 1981-1984.

[14] Palermo A, Holgado Vazquez JP, Lee AF, Tikhov MS, Lambert RM, *Critical influence of the amorphous silica-to-cristobalite phase transition on the performance of $Mn/Na_2WO_4/SiO_2$ catalysts for the oxidative coupling of methane*. J. Catal. **177** (1998) 259-266.

[15] Liu H, Wang X, Yang D, Gao R, Wang Z, Yang J, *Scale up and stability test for oxidative coupling of methane over Na_2WO_4-Mn/SiO_2 catalyst in a 200 ml fixed-bed reactor*. J. Nat. Gas Chem. **17** (2008) 59-63.

[16] Lin C-H, Wang J-X, Lunsford JH, *Oxidative dimerization of methane over sodium-promoted calcium oxide*. J. Catal. **111** (1988) 302-316.

[17] Korf SJ, Roos JA, Derksen JWHC, Vreeman JA, Van Ommen JG, Ross JRH, *Oxidative coupling of methane over Ba/CaO catalysts: A comparison with Li/MgO*. Appl. Catal. **59** (1990) 291-309.

[18] Choudhary VR, Rane VH, *Surface Properties of CaO (or BaO)–La_2O_3–MgO Catalysts and Their Performance in Oxidative Coupling of Methane*. J. Chem. Technol. Biotechnol. **69** (1997) 63-69.

[19] Dissanayake D, Lunsford JH, Rosynek MP, *Oxidative coupling of methane over oxide-supported barium catalysts*. J. Catal. **143** (1993) 286-298.

[20] Wang Z, Zou G, Luo X, Liu H, Gao R, Chou L, Wang X, *Oxidative coupling of methane over $BaCl_2$-TiO_2-SnO_2 catalyst*. J. Nat. Gas Chem. **21** (2012) 49-55.

[21] Choudhary VR, Mulla SAR, Uphade BS, *Oxidative coupling of methane over alkaline earth oxides deposited on commercial support precoated with rare earth oxides*. Fuel **78** (1999) 427-437.

[22] Zhou X, Zhang W, Wan H, Tsai K, *Methane oxidative coupling over fluoro-oxide catalysts*. Catal. Lett. **21** (1993) 113-122.

[23] Pacheco Filho JGA, Eon J, Schmal M, *Oxidative coupling of methane on Ce/Na/CaO catalysts*. Catal. Lett. **68** (2000) 197-202.

[24] Bartsch S, Falkowski J, Hofmann H, *Catalyst development for oxidative methane coupling*. Catal. Today **4** (1989) 421-431.

[25] Aoki A, Ohno S, Muramatsu Y, *Preparation of YBaCu oxide precursor by the citrate gel process*. J. Non-Cryst Solids **147–148** (1992) 720-723.

[26] Marcilly C, Courty P, Delmon B, *Preparation of highly dispersed mixed oxides and oxide solid solutions by pyrolysis of amorphous organic precursors*. J. Am. Ceram. Soc. **53** (1970) 56-57.

[27] Yu M, Lin J, Zhou YH, Wang SB, *Citrate–gel synthesis and luminescent properties of $ZnGa_2O_4$ doped with Mn^{2+} and Eu^{3+}*. Mater. Lett. **56** (2002) 1007-1013.

[28] Segal D, *Chemical synthesis of ceramic materials*. J. Mater. Chem. **7** (1997) 1297-1305.

[29] Liotta LF, Di Carlo G, Longo A, Pantaleo G, Venezia AM, *Support effect on the catalytic performance of $Au/Co_3O_4–CeO_2$ catalysts for CO and CH_4 oxidation*. Catal. Today **139** (2008) 174-179.

[30] Tu Y-J, Chen Y-W, *Effects of alkaline-earth oxide additives on silica-supported copper catalysts in ethanol dehydrogenation*. Ind. Eng. Chem. Res. **37** (1998) 2618-2622.

[31] Ruckenstein E, Wang HY, *Carbon dioxide reforming of methane to synthesis gas over supported cobalt catalysts*. Appl. Catal. A Gen. **204** (2000) 257-263.

[32] Yao HC, Yao YFY, *Ceria in automotive exhaust catalysts: I. Oxygen storage*. J. Catal. **86** (1984) 254-265.

[33] Andorf R, Mleczko L, Schweer D, Baerns M, *Oxidative coupling of methane in a bubbling fluidized bed reactor*. Can. J. Chem. Eng. **69** (1991) 891-897.

[34] Choudhary VR, Mulla SAR, Uphade BS, *Influence of support on surface basicity and catalytic activity in oxidative coupling of methane of Li–MgO deposited on different commercial catalyst carriers*. J. Chem. Technol. Biotechnol. **72** (1998) 99-104.

3 Effect of Mg, Ca and Sr on CeO_2 based catalysts for the oxidative coupling of methane: investigation on the oxygen species responsible for catalytic performance[1]

CeO_2 catalysts modified with earth alkaline metals (M= Mg, Ca and Sr) were prepared by the citrate method. Different analytical techniques including DR UV-Vis and DRIFT spectroscopy, XPS, XRD and TPD-CO_2 were used for the characterisation of the catalysts. These materials were tested in the OCM at 700 and 750 ^{o}C. Results of calcined samples revealed that the charge transfer from cerium to oxygen ions is shifted when CeO_2 is doped, indicating defects on the catalyst surface. A linear correlation was found between the amount of surface basic sites and the ratio of the oxygen species O_2^- and O_2^{2-} to lattice oxygen. This behaviour is crucial for CH_4 conversion and selectivity to C_2H_6 and C_2H_4 at 700 and 750 ^{0}C. Ca-doped CeO_2 catalyst revealed the best performance in the OCM, which could be attributed to the similar ionic radii of Ca^{2+} and Ce^{4+}.

---

[1] Ferreira VJ, Tavares P, Figueiredo JL, Faria JL (2012), Effect of Mg, Ca, and Sr on CeO_2 Based Catalysts for the Oxidative Coupling of Methane: Investigation on the Oxygen Species Responsible for Catalytic Performance. Ind. Eng. Chem. Res. **51** (2012) 10535-10541

3.1 Introduction

Oxidative coupling of methane is a promising route for the production of C_2 or higher hydrocarbons from natural gas. It is known that CH_4 is the most stable alkane, and its direct conversion to higher hydrocarbons, e.g. ethane (C_2H_6), is a reaction with positive free energy change. In the OCM reaction, methane and oxygen react on catalysts between 700 and 750 °C to form C_2H_6, which is the main product and can be subsequently dehydrogenated to ethylene (C_2H_4). Ethylene is an important base chemical for the petrochemical industry, and there is an increasing demand for ethylene in both developed and developing countries. A relevant aspect, the OCM reaction is highly exothermic, and is favoured from the thermodynamic point of view. However, in the presence of O_2, CH_4 can be completely oxidised to CO and CO_2.

According to Ito et al. [1], who published the accepted mechanism, the oxidative activation of methane in the catalytic OCM process involves the abstraction of a H-atom from methane, leading to the formation of methyl radicals ($CH_3\cdot$) on the catalyst surface; two desorbed methyl radicals are coupled in the gas phase to form ethane.

Basic oxides, such as alkaline, alkaline earth and rare earth metal oxides, single or mixed, are good catalysts for the OCM reaction. The productivity of these systems is attributed either to the catalyst basicity or to the availability of active sites such as oxygen vacancies and/or other defects, which are important for oxygen activation [2-5]. It has been generally established that on metal oxide catalysts the surface oxygen species may consist of lattice oxygen O^{2-}, peroxide O_2^{2-}, superoxide O_2^{-}, carbonate CO_3^{2-}, hydroxide OH^- ions, etc. The O^- species were shown to be the active centres on Li/MgO or Na/CaO systems [6-8]. The O_2^{2-} peroxide ion was also proposed to be an active species, especially at temperatures higher than 750 °C on catalytic systems such as Na_2O_2 [9], Ba/MgO, Na/La_2O_3 and La_2O_3 [10].On the other hand, superoxide species O_2^{-} were observed on catalysts such as LaOF [4], Ba/Nd_2O_3 [3] and Y_2O_3-CaO catalysts [11].

The influence of cerium on the oxide systems for the oxidative coupling of methane is of particular interest, due to its excellent redox properties. Cerium added to Li/MgO and Na/MgO was studied by Radha et al. [12], who observed an improved activity and selectivity towards C_2 hydrocarbons.

This behaviour was attributed to the presence of different active sites. Shahri et al. [13] showed that 5%wtCe promotes the activity and stability of the Mn-Na_2WO_4/SiO_2 catalyst. However, from the catalytic point of view, other studies revealed that CeO_2 exhibited low selectivity to coupled hydrocarbon products [14], and Choudhary et al [15] studied the influence of the rare earth oxide(s) pre-coated on catalyst support on the conversion, selectivity, yield and product C_2H_4/C_2H_6 and CO/CO_2 ratios. They reported a poor performance when CeO_2 was precoated on the commercial support (CH_4 conversion < 0.1%).

Although there are many reports on alkaline earth oxides doped with small amounts of Ce for the oxidative coupling of methane, few papers focus on the modification of CeO_2 using alkaline earth metals, and up to now, no evidence was presented to explain the surface features of such catalysts [16]. Therefore, the aim of this chapter is to investigate the structural and surface modifications due to three alkaline earth metals (Mg, Ca and Sr) that may explain the improved performance of doped CeO_2 in the OCM reaction. These metals were chosen due their ionic radii. It is known that the ionic radius varies with the coordination number [17]. Ca^{2+} and Ce^{4+} have similar ionic radii, while Mg^{2+} has a lower ionic radius and Sr^{2+} has a higher ionic radius than Ce^{4+}.

Therefore, the effect of the above mentioned metals on the structural and textural properties of the samples was studied, the Ce^{4+} coordination number being shifted by incorporation of these metals. In particular, various oxygen species are formed by adjusting the ratio of Mg^{2+}, Ca^{2+}, and Sr^{2+} cations in the catalyst surface. X-ray photoelectron spectroscopy (XPS) and Temperature Programmed Reduction (TPR) were used to identify and quantify the surface oxygen species. Moreover, the surface basicity/base strength distribution was studied using Temperature Programmed Desorption of CO_2 (CO_2-TPD). Diffuse Reflectance Ultraviolet-Visible (DR UV-Vis) spectroscopy was performed to study the nature and the coordination state of the surface oxide species, and X-ray diffraction (XRD) to corroborate the existence of different surface distortions on the modified ceria crystals. Diffuse Reflectance infrared Fourier Transform (DRIFT) spectroscopy was used to qualitatively characterise the material's surface. Along these lines, the relationship between the surface oxygen species and the catalyst performance for methane coupling is discussed.

3.2 Experimental section

3.2.1 Catalyst preparation

Preparation of materials was carried out by the citrate method. This is used to prepare multicomponent oxides [18], allowing the preparation of highly dispersed mixed oxides from the individual cations in the desired stoichiometric ratio [19,20]. In addition, this method involves the formation of a mixed-ions citrate that, due to the three-ligand nature of citric acid, yields a transparent three-dimensional network [19,21]. The catalysts were obtained from $Ce(NO_3)_3 \cdot 6H_2O$ (99% Aldrich), $Mg(NO_3)_2 \cdot 6H_2O$ (98% Fluka), $Ca(NO_3)_2 \cdot 4H_2O$ (99% Fluka) and $Sr(NO_3)_2$ (Sigma-Aldrich). These precursors were dissolved in distilled water in the appropriate amounts to obtain a M:Ce molar ratio of 1:1 (M= Mg, Ca and Sr). Citric acid was added with a molar ratio of acid/(Ce + M) = 1.5. Acid conditions were adjusted using HNO_3. The solution was heated up to 80 °C in a paraffin bath under constant stirring to evaporate superfluous water, the volume of the solution decreased and a viscous gel was obtained. The gel was dried at 120 °C overnight to form a spongy material and then it was calcined at 800 °C during 6 h (See Figure 2.1).

3.2.2 Catalyst characterisation

As mentioned in section 3.1, the surface oxygen species formed and the surface basicity/base strength distribution were studied by means of spectroscopic techniques such as Diffuse Reflectance Ultraviolet-Visible (DR UV-Vis), Diffuse Reflectance Infrared Fourier Transform (DRIFT) and X-Ray Photoelectron Spectroscopy (XPS), together with X-Ray Diffraction (XRD), Temperature Programmed Reduction (TPR) and CO_2 Temperature Programmed Desorption (CO_2-TPD) techniques.

The DR UV-Vis spectra of the powder solids were measured with a Jasco V-650 UV-Vis spectrophometer equipped with an integrating sphere attachment (JASCO ISV-469). The spectra were recorded in diffuse reflectance mode and transformed by the instrument software (JASCO) to equivalent absorption Kubelka-Munk units over the wavelength range λ=200-800 nm.

On the other hand, DRIFT spectroscopic analyses of the solid materials were done on a Nicolet 510P FTIR Spectrometer, with a KBr beam splitter for

mid-IR range and a pyroelectric detector with deuterated tri-glycine sulfate (DTGS) and KBr windows equipped with a special beam collector (COLLECTOR from SpectraTech), fixed on a plate for consistent experimental conditions. The collection angle is a full pi steradian, collecting a maximum 50% of the available diffuse energy and reducing the spot size of the FTIR beam by 1/6. When required, the specular component was dealt with the blocker device, which minimises distortion. The instrument was always purged with dry air which was passed through a filter to partially remove CO_2 and moisture (Balston air purifier with filter). Samples were ground and "diluted" with KBr powder, with pure KBr powder used as the blank. Then, the samples were used in a micro-cup and spectra taken at room temperature. Typically, about 256 scans were recorded for each spectrum with a 4 cm^{-1} resolution. The instrument software (OMINC) converted the interferograms to equivalent absorption units in the Kubelka–Munk scale.

CO_2-TPD and TPR experiments were carried out in an Altamira Instruments (AMI-200) apparatus. The surface basicity/base strength distribution on the catalyst was measured by temperature programmed desorption (TPD) of CO_2 chemisorbed at 100 °C for 2 h on 100 mg of catalyst placed in a U-shaped quartz tube located inside an electrical furnace, and subsequently heated up from 100 °C to 1000 °C with a linear heating rate of 10 °C min^{-1} and argon (25 cm^3 min^{-1}) as the carrier gas. The chemisorbed amount of CO_2 was defined as the amount retained on the pre-saturated catalyst after it was swept with pure argon (25 cm^3 min^{-1}) for a period of 1.5 h at 100 °C. The CO_2 desorbed was measured quantitatively by the MS signal (m/e: 44) monitored by a mass spectrometer (Dymaxion 200 ami. Ametek). A mixture of 5 vol.% H_2/Ar was used for TPR experiments, at a total flow rate of 30 cm^3min^{-1}, with 100 mg of catalyst. The temperature was increased at a rate of 5 °C min^{-1} from room temperature to 1000°C, while the hydrogen consumption was monitored.

Patterns of XRD diffraction were used to identify the crystallographic phases present and calculate the crystallite size. The XRD spectra were recorded on a PANalytical X'Pert MPD equipped with a X'Celerator detector and secondary monochromator (Cu Kα λ = 0.154 nm, 50 kV, 40 mA; data recorded at a 0.017° step size, 100 s/step). Rietveld refinement with PowderCell software was used

Finally, XPS analyses were performed with a VG Scientific ESCALAB 200A spectrometer. The O 1s envelopes were deconvoluted into the contributions of corresponding surface oxygen species using the software XPS-peak. For all the computer fits, the XPS peaks were assumed to have 80% Gaussian plus 20% Lorentzian peak shape. The correctness of the analysis method was checked by deconvolution of a simulated peak composed of four single peaks with known binding energy and peak width values.

3.2.3 Catalyst evaluation

The catalytic performance of the prepared oxides for the oxidative coupling of methane was studied in a quartz tube reactor of i.d = 25mm as shown in Figure 2.2 which was filled with 0.2 g of catalyst held by quartz wool. The reactor was placed into an electrical furnace (see Figure 2.3). Methane, helium and oxygen flow rates were regulated by mass flow controllers (HI-TEC). The mixture of methane and oxygen (CH_4/O_2 molar ratio of 4) diluted in Helium (75% of the total flow) was passed through the catalyst bed with a total flow rate of 50 cm^3 min^{-1}. A cold trap was placed at the outlet of the quartz tube to separate any condensed water vapour from the reaction products.

The OCM study started when the temperature reached 600 °C. The product stream containing carbon monoxide, carbon dioxide, ethane, ethylene, unreacted oxygen and methane was analysed by an on-line gas chromatograph (GC) equipped with a thermal conductivity (TC) detector, using a capillary column (Carboxen 1010 Plot. Supelco). It was assumed that carbon and /or hydrogen in methane were only converted into ethane, ethylene carbon monoxide, carbon dioxide and/or molecular hydrogen and water. Then, the conversion of CH_4 and the selectivity of the products were defined, respectively, as follows:

$$\text{CH}_4 \text{ conversion} = \frac{2F_{C_2H_4} + 2F_{C_2H_6} + F_{CO} + F_{CO_2}}{F_{CH_{4inlet}}} x100\% \qquad 3.1$$

$$\text{C}_2 \text{ selectivity} = = \frac{2F_{C_2H_4} + 2F_{C_2H_6}}{2F_{C_2H_4} + 2F_{C_2H_6} + F_{CO} + F_{CO_2}} x100\% \qquad 3.2$$

where F_i is the flow of the species i (mol min^{-1}).

3.3 Results and discussion

3.3.1 Characterisation

3.3.1.1 Diffuse Reflectance Ultraviolet-Visible spectroscopy (DR UV-Vis)

Diffuse Reflectance Ultraviolet-Visible spectroscopy was used to explain changes in the coordination number of the surface oxides. Figure 3.1 shows the DRUV spectra. Bands at 250 and 354 nm for CeO_2 can be attributed to the charge transfer $Ce^{3+} \leftarrow O^{2-}$ and $Ce^{4+} \leftarrow O^{2-}$ respectively [12].The DR-UV results showed that the absorption bands are affected by incorporation of Ca and Mg. The presence of band shifts suggests different coordination numbers for the oxide [12].

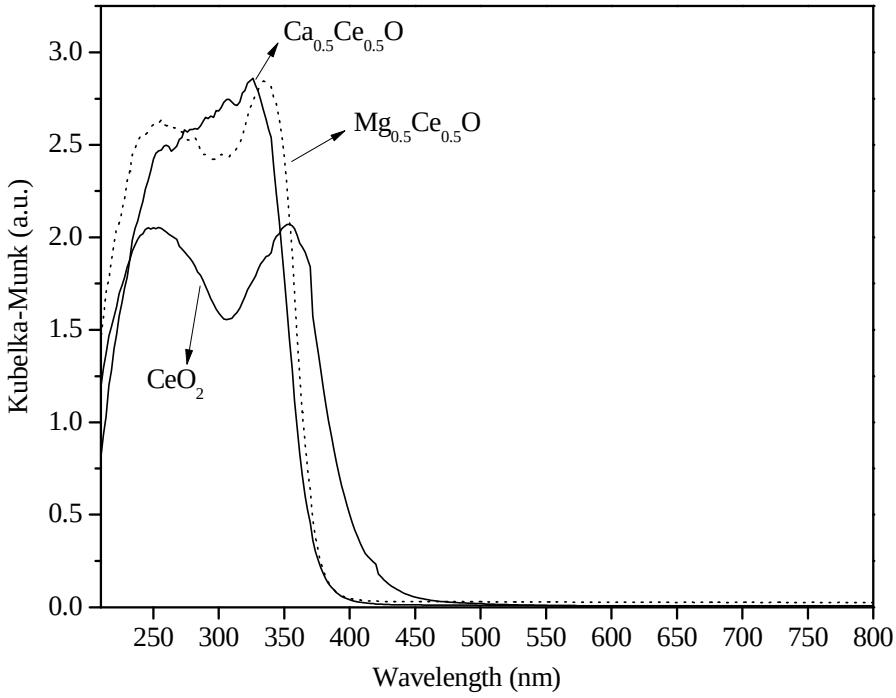

Figure 3.1 DR-UV spectra of $Ca_{0.5}Ce_{0.5}O$, $Mg_{0.5}Ce_{0.5}O$ and CeO_2 catalysts.

The addition of Ca shifts absorption bands of Ce^{3+} from 249 nm to 258 nm and C^{4+} from 354 nm to 325 nm in the $Ca_{0.5}Ce_{0.5}O$ catalyst. These absorption band shitfts can be assigned to the bands with lower (about 8) coordination number. This suggests the formation of surface defects in the Ca-doped

CeO_2 leading to surface imperfections. Similarly, Mg shifts the 354 nm absorption band to 334 nm in $Mg_{0.5}Ce_{0.5}O$, suggesting less surface imperfections.

3.3.1.2 Diffuse reflectance infrared Fourier transform (DRIFT) spectroscopy

From the DRIFT experimental results, the O_2^{2-} species was detected by the band of 873 cm^{-1} on $Ca_{0.5}Ce_{0.5}O$ and 860 cm^{-1} on the $Sr_{0.5}Ce_{0.5}O$ catalyst (Figure 3.2). This band is attributed to the vibration of dioxygen as in adsorbed peroxide species ($O_2^{2-}{}_{ads}$) [22].

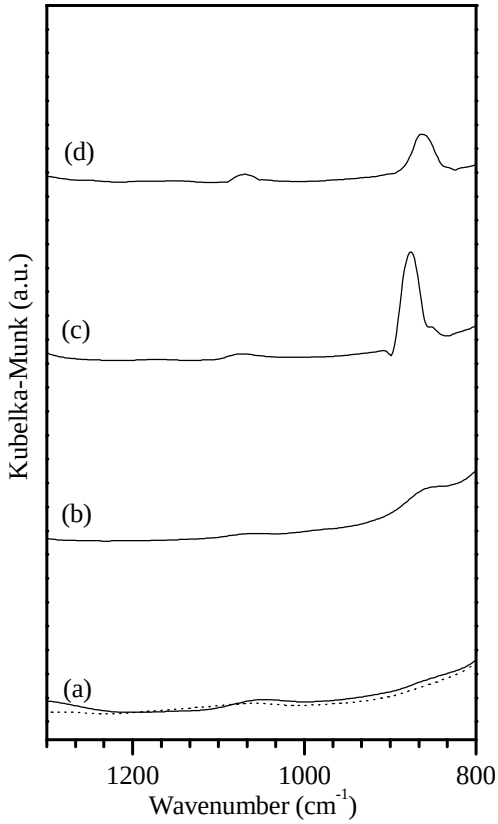

Figure 3.2 DRIFT spectra of the catalysts (a) synthesised (—) and commercial (·····) CeO_2; (b) $Mg_{0.5}Ce_{0.5}O$; (c) $Ca_{0.5}Ce_{0.5}O$; (d) $Sr_{0.5}Ce_{0.5}O$.

The region 970-700 $cm^{-1}$for dioxygen adsorption is typical for O_2^{2-} in metal complexes [22]. In the $Mg_{0.5}Ce_{0.5}O$ catalyst, the band corresponding to O_2^{2-} species occurs with lower intensity when compared to the above mentioned materials. In the synthesised and commercial CeO_2 the band attributed to

O_2^{2-} species was not detected. Therefore, vibrational spectra by DRIFT confirms structural modifications by the introduction of Mg, Ca and Sr. The vibrational structure of the surface being more affected by Ca and less by Mg.

3.3.1.3 X-Ray photoelectron spectroscopy (XPS)

As mentioned above, XPS technique was used to investigate the surface of the $Mg_{0.5}Ce_{0.5}O$, $Ca_{0.5}Ce_{0.5}O$, $Sr_{0.5}Ce_{0.5}O$ and CeO_2 catalysts. Their binding energies are summarised in Table 3.1. The O 1s spectra of the samples, as shown in Figure 3.3, are used to identify the coexisting oxygen species on the surface of the catalysts. As can be observed, the FWHM (full widths at half maximum) of the O 1s measured spectra are larger than that of the single species, which was between 1.8-2.0 eV. For this purpose, the O 1s spectra of the $Mg_{0.5}Ce_{0.5}Ce$, $Ca_{0.5}Ce_{0.5}O$ and $Sr_{0.5}Ce_{0.5}O$ catalysts could be deconvoluted in four peaks corresponding to the different oxygen species. These can be assigned to O_2^-, CO_3^{2-}, O_2^{2-} and O^{2-} [23-27], the actual values being given in Table 3.2

Table 3.1 XPS binding energies (eV) and corresponding FWHM (between brackets).

Catalyst	Ca^{2+} ($2p_{3/2}$)	Ca^{2+} ($2p_{3/2}$)	Mg^{2+} (2p)	Sr^{2+} ($3d_{5/2}$)	Sr^{2+} ($3d_{3/2}$)	CeIV ($3d_{5/2}$)	CeIV ($3d_{3/2}$)
$Ca_{0.5}Ce_{0.5}O$	350.2 (2.2)	346.7 (2.3)	-----	-----	----	882.0 (3.0)	900.2 (2.9)
$Mg_{0.5}Ce_{0.5}O$	----	----	49.4 (2.7)	-----	-----	882.3 (2.6)	900.8 (2.7)
$Sr_{0.5}Ce_{0.5}O$	----	-----	----	133.4 (2.1)	135.2 (2.2)	882.2 (2.8)	900.7 (2.9)

Table 3.2 Curve-fitting results from XPS data.

Catalyst	O 1s binding energies (eV) FWHM (between brackets) Relative amount of the oxygen species (%)				$(O_2^{2-} + O_2^{-})/O^{2-}$
	O^{2-}	O_2^{2-}	CO_3^{2-}	O_2^{-}	
CeO_2	529.15 (1.9) 76.86	530.75 (1.6) 12.30	532.01 (2.1) 10.84	---	0.16
$Mg_{0.5}Ce_{0.5}O$	529.20 (1.9) 51.48	530.78 (1.8) 11.62	531.89 (2.0) 27.72	533.01 (2.0) 9.18	0.40
$Ca_{0.5}Ce_{0.5}O$	528.88 (2.0) 40.34	530.93 (2.0) 49.99	532.00 (1.9) 6.76	533.05 (2.0) 2.91	1.31
$Sr_{0.5}Ce_{0.5}O$	528.5 (2.1) 54.23	530.6 (2.1) 37.56	531.90 (2.0) 6.41	533.03 (1.8) 1.81	0.73

The fit observed in Figure 3.3 shows the contribution of single species which was computed using an experimental methodology assigning fixed binding energy and reasonable peak width to each species. Based on these primary results, the software allowed to adjust the binding energy and the peak widths of the four peaks. Thus, the binding energies and peak widths obtained typically differed by less than 0.32 eV. This confirms the goodness of the fit to the experimental data; therefore, reasonable physical meanings can be derived.

The relative amounts (%) of the oxygen species were calculated from the areas under the curves for each sub-peak. The relative amounts of the O_2^{2-} and O_2^{-} oxygen species vary much more when compared with the lattice oxygen species. It is known that the electrophilic oxygen species are active for the OCM. Thus the ratio of surface electrophilic oxygen to lattice oxygen species, i.e. $(O_2^{2-} + O_2^{-})/ O^{2-}$ was estimated. These results are summarised in Table 3.2. Significant variation of the ratio for the different catalysts is

observed, indicating the influence of the incorporated metal on the relative amount of electrophilic oxygen.

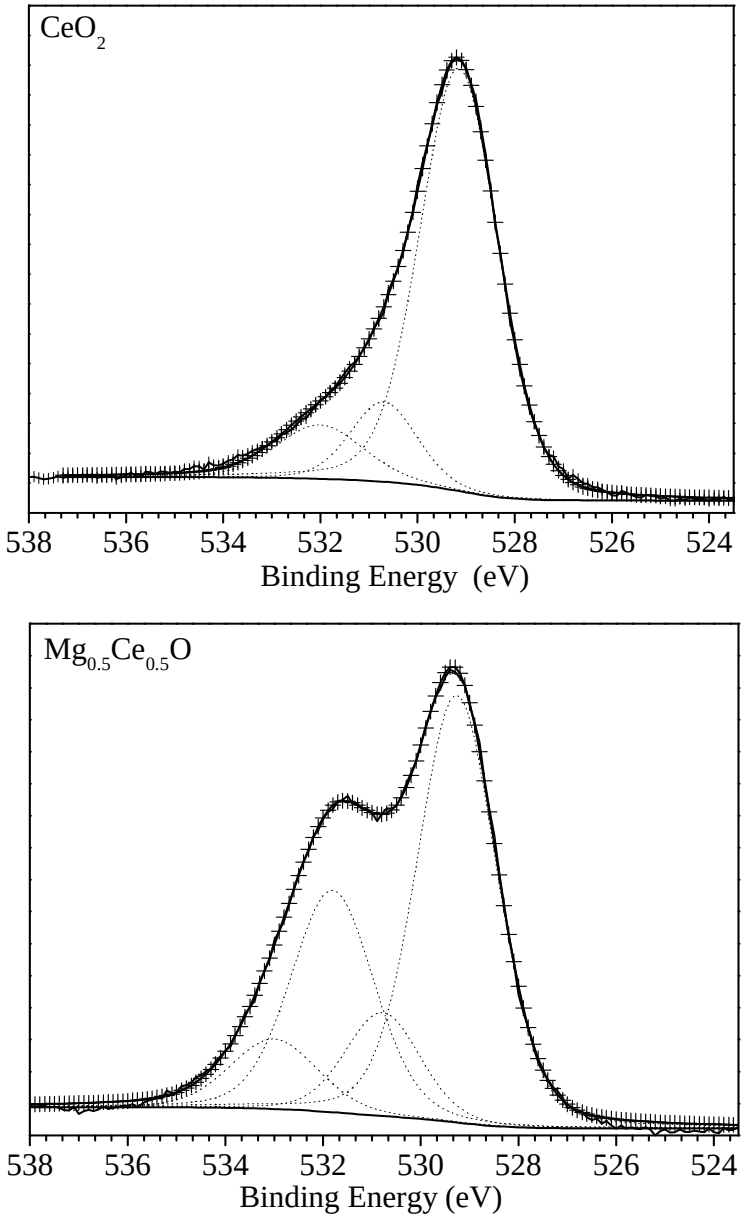

Figure 3.3 O1s binding energy spectra of the various samples (—) referring to experimental data, (····) showing contribution of single species, (+++) showing sum of the computer fitted contribution of each single species. (For sample identification see the left upper corner of each spectrum).

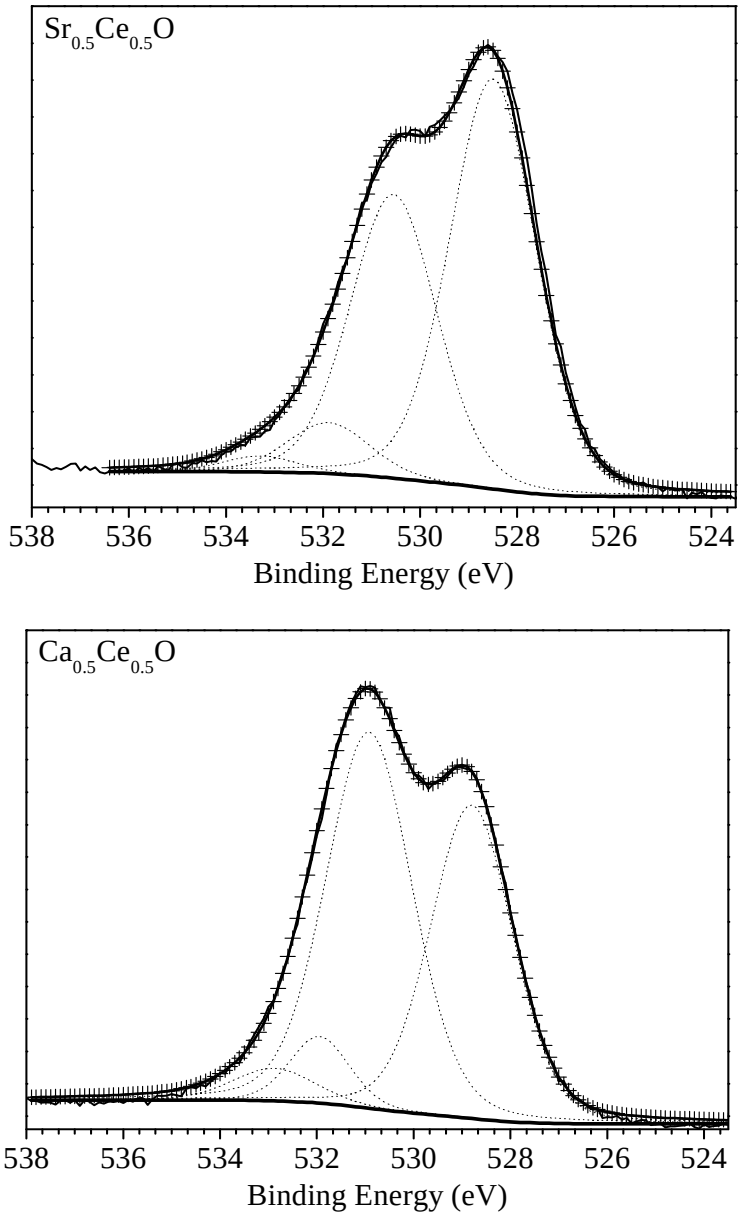

Figure 3.3 (Cont.) O1s binding energy spectra of the various samples (—) referring to experimental data, (···) showing contribution of single species, (+++) showing sum of the computer fitted contribution of each single species. (For sample identification see the left upper corner of each spectrum).

3.3.1.4 X-Ray diffraction (XRD)

The XRD technique was used to study the effect of the incorporation of metals such as Mg and Ca in CeO_2. Figure 3.4 shows XRD patterns of samples with nominal compositions of CeO_2, $Ca_{0.5}Ce_{0.5}O$ and $Mg_{0.5}Ce_{0.5}O$. The diffraction lines correspond to the cubic structure of CeO_2 and the Ca, Mg doped CeO_2. Figure 3.4 (inset) shows that $Ca_{0.5}Ce_{0.5}O$ and $Mg_{0.5}Ce_{0.5}O$ revealed a larger peak broadening when compared with CeO_2 (see peaks attributed to the (1 1 1) and (2 0 0) reflecting planes). In the case of $Ca_{0.5}Ce_{0.5}O$, the line broadening analysis indicated a decrease in crystallite size from 45.9 to 29.8 nm, while $Mg_{0.5}Ce_{0.5}O$ revealed a decrease from 45.9 to 26.5 nm (calculated from XRD pattern). Lattice parameter shifts were not observed in the oxides, indicating that lattice distortions were not produced by incorporation of the metals. In addition, $Ca_{0.5}Ce_{0.5}O$ displayed diffraction peaks of $CaCO_3$, meaning no formation of binary oxide. However, the shifts of the absorption bands in the DR-UV spectra and the decrease in the crystallite size suggest important surface modifications due to the incorporation of Ca and Mg.

Noal et al. [28], studied the interaction of Mg with the CeO_2 surface and suggested that the incorporation of Mg in the surface creates localised distortions around the Mg lattice site—Mg-O distances. They also showed that the geometry of the surface oxygen atoms, while distorted by their motion towards Mg, remains quite symmetric upon doping. In addition, a lower valent dopant substitutes a higher valent cation, generating an oxygen hole polaron, compensating the lower valence of Mg and Ca by the formation of oxygen vacancies [28]. On the other hand, the DR-UV results are consistent with the binding energies of the cations in the catalysts obtained by XPS analysis (Table 3.1), which indicate that the metal cations are in their higher oxidation states, i.e., Ce^{4+} Mg^{2+}, Sr^{2+} and Ca^{2+}.

Nevertheless, it can be observed in Table 3.1 that $Ca_{0.5}Ce_{0.5}O$ showed lower Ce($3d_{5/2}$) binding energy when compared with $Mg_{0.5}Ce_{0.5}O$ and both have lower energy when compared with literature[29] ~882.5 eV. The Ce($3d_{5/2}$) binding energy shift from high to low energy can be attributed to the shift of the Ce 3d chemical environment [30] meaning that the electron cloud density of Ce was increased. This result indicates that both Mg and Ca may be bonded to Ce^{4+} on the oxide surface.

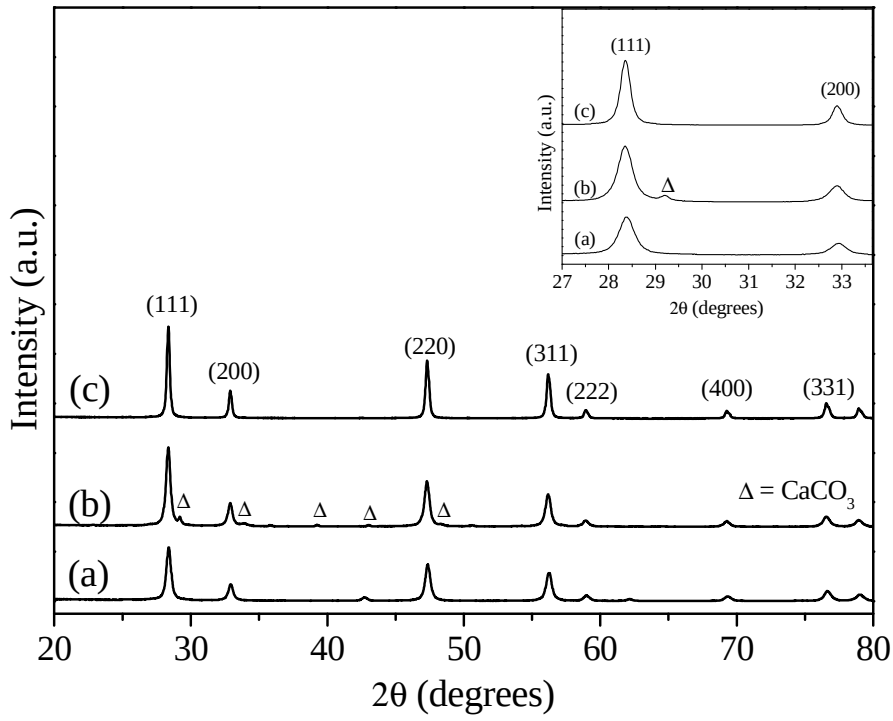

Figure 3.4 X-ray diffraction profiles of (a) $Mg_{0.5}Ce_{0.5}O$, (b) $Ca_{0.5}Ca_{0.5}O$ and (c) CeO_2, showing the effect of calcium and magnesium doping on the crystal structure of CeO_2. Notice in the inset, as the peak intensity decreases.

3.3.1.5 Temperature programmed reduction (TPR)

The presence of the O_2^-, O_2^{2-} and O^{2-} species was also confirmed by TPR of the samples (Figure 3.5). A high-temperature peak (~850 °C) of the CeO_2 TPR profile was observed corresponding to the reduction of bulk oxygen (O^{2-}) and the formation of cerium oxides of lower oxidation state [31,32]. The high temperature peak is also observed (825 and 800 °C) when cerium is doped with Mg and Ca.

On the other hand, cerium doped with Ca has a large peak in the ~500–600 °C temperature range. This can be assigned to lower temperature catalyst surface shell reduction or reduction of surface O_2^- and O_2^{2-} species [33]. The size of the low temperature peak would be dependent on the method of preparation and on the amount of surface oxygen anions attached to surface Ca^{2+} and Ce^{4+} ions. However, $Mg_{0.5}Ce_{0.5}O$ exhibited two low temperature peaks (~500 and 610 °C) which are much smaller than the large peak of low temperature corresponding to $Ca_{0.5}Ce_{0.5}O$ registered in the above mentioned

temperature range. This would indicate that in the $Mg_{0.5}Ce_{0.5}O$ catalyst the amount of bulk oxygen (O^{2-}) is larger when compared with the other oxygen species, which is supported by the relative amount (%) of the oxygen species calculated from the $Mg_{0.5}Ce_{0.5}O$ and $Sr_{0.5}Ce_{0.5}O$ O 1s spectra (Table 3.2).

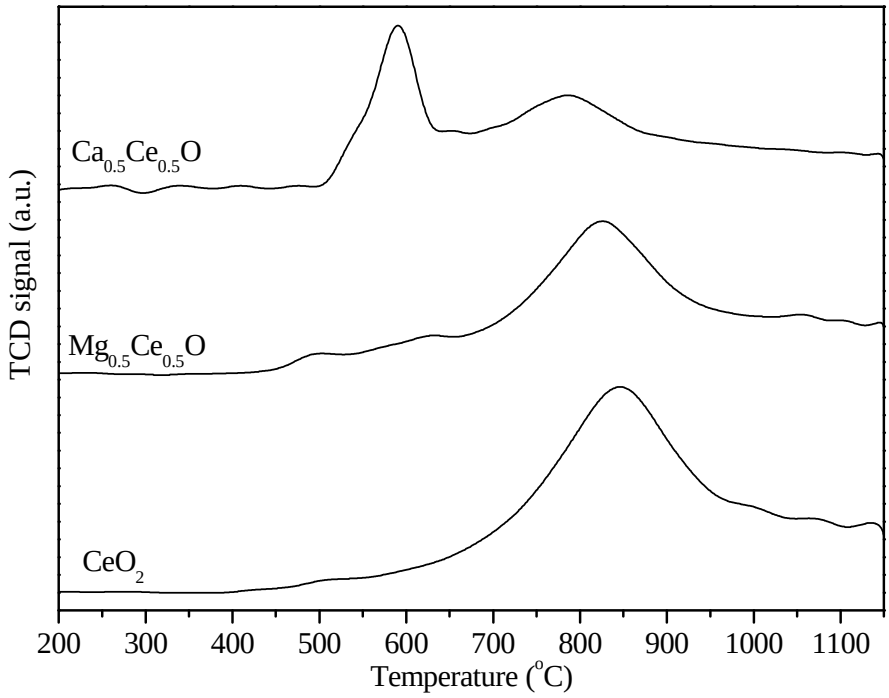

Figure 3.5 TPR profiles of the catalysts.

3.3.1.6 CO_2 Temperature programmed desorption (CO_2-TPD)

The acid-base properties of the catalysts were measured by TPD with CO_2 as acid probe. Figure 3.6 shows CO_2-TPD profiles of the catalysts which represent the amount of CO_2 desorbed ($\mu molg^{-1}s^{-1}$) vs. Temperature. For a catalyst having a broad site energy distribution, the CO_2 adsorbed on weaker basic sites is desorbed at lower temperatures and that adsorbed on stronger basic sites is desorbed at higher temperatures. Therefore, the strength of the particular group of basic sites can be expressed in terms of the temperature interval in which the CO_2 chemisorbed on the basic sites is desorbed.

The strength of the basic sites determined by CO_2 chemisorption was estimated from the area under the TPD curve, and classified into three intervals: weak (50-500°C), intermediate strength (500-750°C) and strong

(750-950°C). These intervals were chosen according to the TPD peaks observed for each catalyst.

A comparison of the catalysts for their basicity/basic sites of different strengths shows that the basicity and strength distribution are strongly influenced by introduction of Ca Mg and Sr when compared with CeO_2, which revealed 19 μmol g^{-1} of desorbed CO_2 (Table 3.3). The addition of Ca and Mg resulted in the creation of more intermediate basic sites when compared with strong basic sites. However, $Ca_{0.5}Ce_{0.5}O$ had larger amounts of total basic sites than $Mg_{0.5}Ce_{0.5}O$ and $Sr_{0.5}Ce_{0.5}O$ catalysts. This result could be related with the basicity attributed to the anions (O_2^-, O_2^{2-} and O^{2-}) exposed on the surface of the catalyst [34].

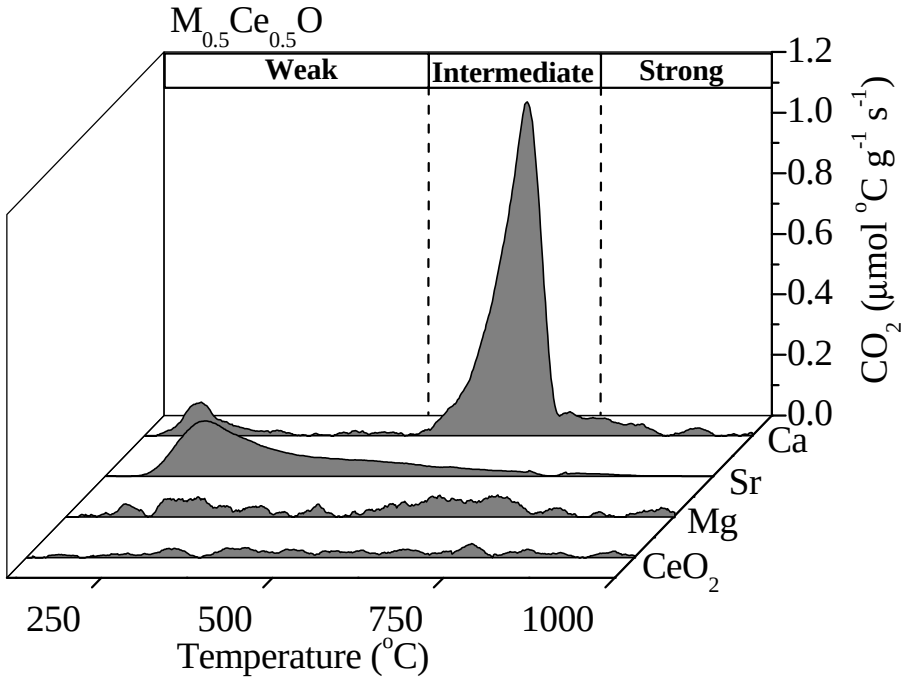

Figure 3.6 CO_2-TPD profiles of the catalysts. M=Mg, Ca and Sr.

This can be corroborated in Figure 3.7 where a linear relationship between the amount of total of basic sites and the (O_2^{2-} + O_2^-)/ O^{2-} ratio (evaluated from Table 3.2) was obtained.

Table 3.3 Surface basicity/base strength distribution

Catalyst	Basic Sites (μmol g^{-1})			
	(100-500) °C Weak	(500-750) °C Intermediate	(750-1000) °C Strong	Total
CeO_2	10	4	6	19
$Mg_{0.5}Ce_{0.5}O$	42	57	23	122
$Sr_{0.5}Ce_{0.5}O$	196	50	14	260
$Ca_{0.5}Ce_{0.5}O$	52	503	37	592

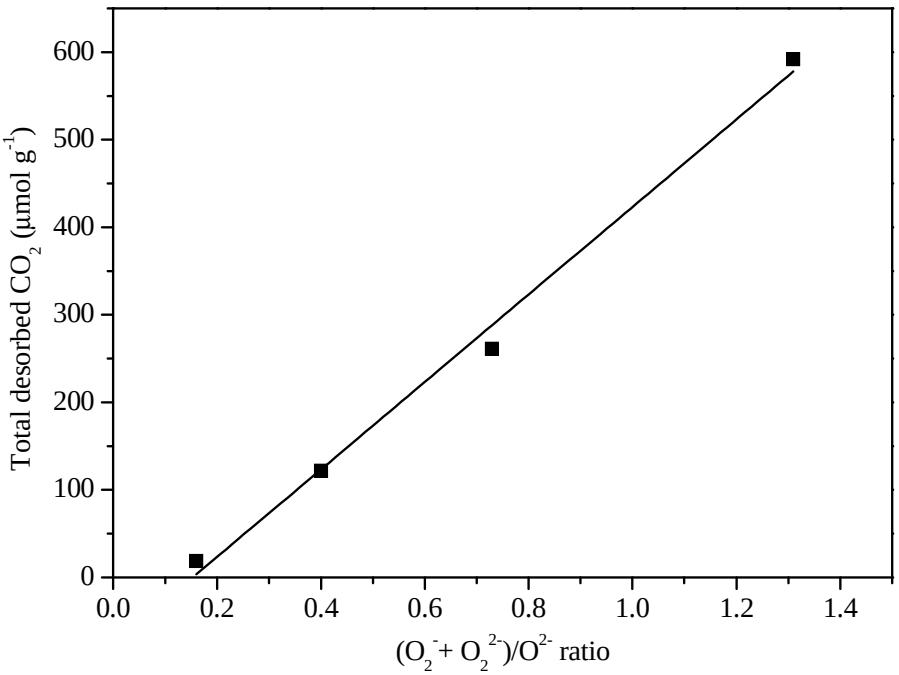

Figure 3.7 Linear relationship between the total amount of the basic sites and the $(O_2^{2-} + O_2^{-})/ O^{2-}$ ratio.

The basicity strength of the surface sites is considered to be dependent on the effective charge on the anions and /or their coordination number on the surface. Surface imperfections such as steps and kinks are expected to be responsible for the presence of sites of different basic strength [34]. All these results point to the fact that both atomic and molecular oxygen species with various charges are present on the surface of the catalysts.

3.3.2 Catalytic tests

Catalytic tests were carried out at two temperatures (700 and 750 ^{0}C). Figure 3.8 shows the conversion of methane and Figure 3.9 the selectivity for $Mg_{0.5}Ce_{0.5}O$, $Ca_{0.5}Ce_{0.5}O$, $Sr_{0.5}Ce_{0.5}O$ and pristine CeO_2.

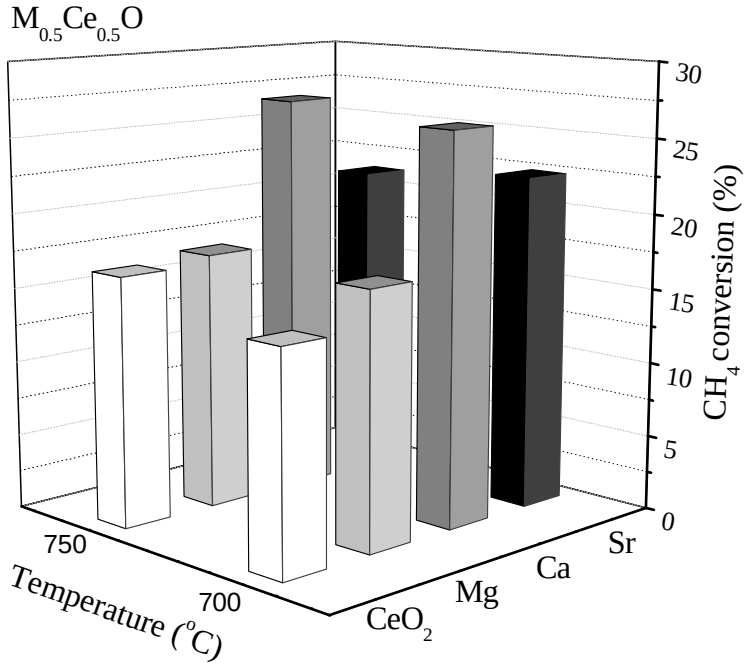

Figure 3.8 Methane conversion of the catalysts at 700 and 750 ^{o}C. M=Mg, Ca and Sr.

It can be observed that CH_4 conversion and C_2 selectivity on $Ca_{0.5}Ce_{0.5}O$ was much higher than CeO_2 and $Mg_{0.5}Ce_{0.5}O$. However, comparing $Sr_{0.5}Ce_{0.5}O$ with CeO_2 the effect of Sr on the conversion was about 30%. The same behaviour was observed for the selectivity towards C_2 hydrocarbons, suggesting that doping of CeO_2 with Ca and Sr increases the activity and selectivity of methane coupling at 700 and 750 ^{0}C.

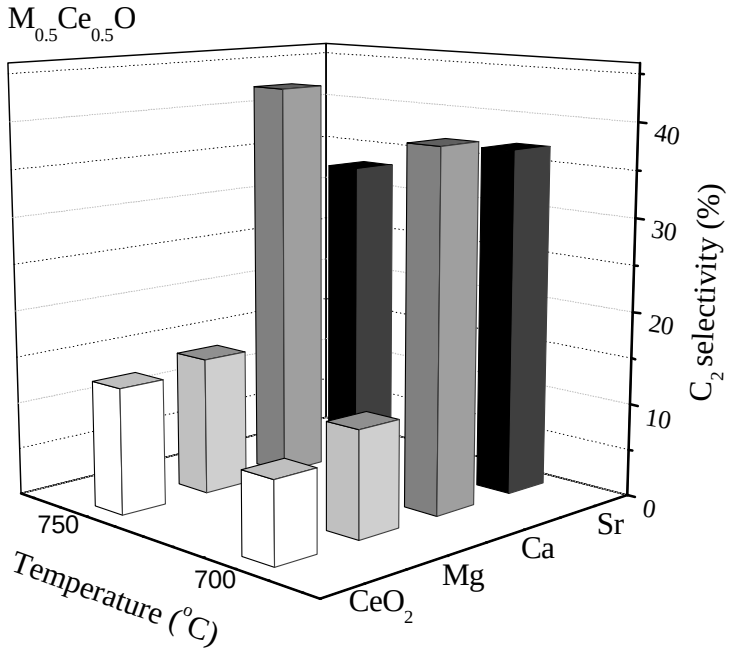

Figure 3.9 Selectivity of the catalysts at 700 and 750 ^{o}C. M=Mg, Ca and Sr.

Doping CeO_2 with Mg^{2+}, Ca^{2+} and Sr^{2+} cations can create interstitial oxygen, and therefore oxygen species in the oxide surface structure. The ratios of surface electrophilic oxygen to lattice oxygen species, i.e. $(O_2^{2-} + O_2^{-})/O^{2-}$, in CeO_2, $Mg_{0.5}Ce_{0.5}O$, $Sr_{0.5}Ce_{0.5}O$ and $Ca_{0.5}Ce_{0.5}O$ were evaluated from Table 2.2 and related to their corresponding CH_4 conversions as well as to the C_2H_6 and C_2 selectivity at the reaction temperatures of 700 and 750 ^{0}C. The results are shown in Figure 3.10. These results can help to identify the oxygen species that are responsible for the activity of methane oxidative coupling to C_2 hydrocarbons. The proportional relationship between the ratio and the conversion of methane points out to the effect of the surface oxygen species, as compared to lattice oxygen, on the activity of the catalyst. A similar trend can be observed for the selectivity to C_2H_6 and C_2 hydrocarons, with the exception of the $Mg_{0.5}Ce_{0.5}O$ sample, which shows a much lower selectivity to C_2 hydrocarbons than $Ca_{0.5}Ce_{0.5}O$, although slightly higher than CeO_2.

It is hard to distinguish the contribution of O_2^{-} or O_2^{2-} on the OCM reaction solely from the above results. Lunsford et al [5] claimed that O_2^{-} is stable around 200 ^{o}C. However, it is known that the reactivity of O_2^{-} increases with the temperature [5], and Osada et al. were able to show that

O_2^- species could be stable up to 750 °C to react with CH_4 over Y_2O_3-CaO catalysts [11]. On the other hand, several studies have evidenced the role of surface peroxide O_2^{2-} ions as the active species [35].

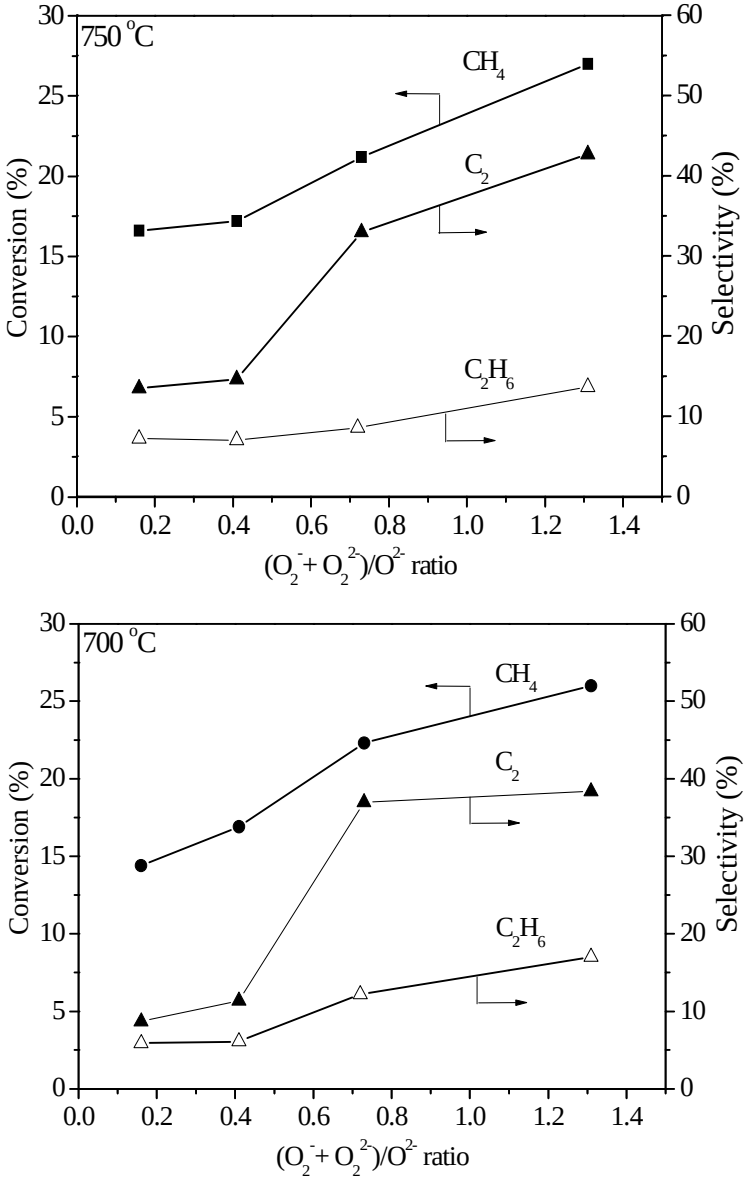

Figure 3.10 Conversion of methane and C_2H_6 and C_2 selectivity, versus the $(O_2^{2-} + O_2^-)/ O^{2-}$ ratio of the catalysts at 700 and 750 °C.

Otsuka et al. found that Na_2O_2, SrO_2 and BaO_2 were capable of converting CH_4 into C_2H_6 at temperature below 400 °C in the presence of O_2 [36].

On the other hand, Dubois et al. suggested that peroxycarbonate ions are formed in the reaction between superoxide ions and carbonate ions, formed from the CO_2 produced by methane oxidation and that these give rise to the formation of peroxide [27,35], i.e. O_2^{2-}, according to equations (3.3) and (3.4):

$$CO_3^{2-} + O_2^{-} \rightarrow CO_4^{2-} + O^{-} \quad 3.3$$

$$2O^{-} \rightarrow O_2^{2-} \quad 3.4$$

These authors then suggested that the peroxide ion could be the active species for the methane coupling reaction. In this work, the surface of CeO_2 was modified by the incorporation of Mg and Ca, creating O_2^{-} and O_2^{2-} species as corroborated by XPS. Catalytic results showed that the catalytic performance to form C_2 hydrocarbons depends on these surface oxygen species. Although O_2^{2-} ions can be formed by equations (3.3) and (3.4) during the OCM reaction, conversion through equations (3.3) and (3.4) should not be significant, since all the catalytic results revealed a higher CO_2 selectivity compared to CO.

Concerning the individual contributions of surface O_2^{-} or O_2^{2-} ions to the OCM reaction, $Ca_{0.5}Ce_{0.5}O$ revealed higher relative amounts of O_2^{2-} species than $Mg_{0.5}Ce_{0.5}O$, as shown in Table 2.2. Moreover, the doped CeO_2 catalysts present defects when Mg^{2+}, Ca^{2+} or Sr^{2+} substitutes Ce^{4+} surface ions. The XRD results suggest that Mg^{2+}, Ca^{2+} and Sr^{2+} ions would be incorporated into an “interstitial” site on the surface, as substitution ions on cerium sites, with oxygen vacancies for charge compensation. Then, filling of oxygen vacancies by molecular oxygen would form the O_2^{-} and O_2^{2-} species.

Finally, as mentioned before, DR UV spectra suggest that the coordination number (CN) of Ce^{4+} ions would shift to lower coordination number when metals are incorporated. Therefore, the ionic radius would decrease from 1.34 Å (CN=12) to 1.14 Å (CN=8) [37]. While the ionic radii of Ca and Ce are similar, Mg presents a lower ionic radius than Ce^{4+}, which may cause a different lattice distortion, thus affecting the type of active sites present in the samples. This is reflected in their catalytic activities. Calcium ion with an ionic radius of (1.12 Å), similar to the Ce ionic radius (1.14 Å), exhibited (in the $Ca_{0.5}Ce_{0.5}O$ catalyst) higher CH_4 conversion when compared with Sr^{2+} and Mg^{2+} ions, whose ionic radii are 1.26 and 0.89 Å (Figure 3.11). The

$Mg_{0.5}Ce_{0.5}O$ catalyst showed lower activity and selectivity. Similar behaviour is observed upon incorporation of Sr^{2+}, which has larger ionic radius than Ce^{4+}. This would indicate different lattice distortions and creation of less active sites with increasing difference between the dopant ionic radius and the Ce^{4+} ionic radius (Δri).

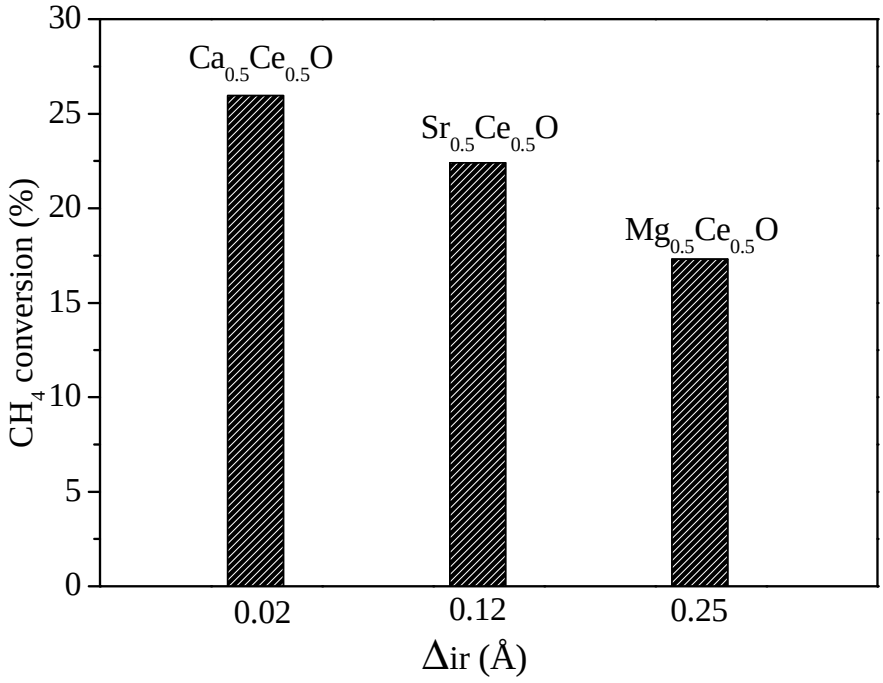

Figure 3.11 CH_4 conversion at 700 ^{0}C versus difference between ionic radius of the metal and Ce (Δri).

In other words, these different lattice distortions, detected on the catalysts through DR UV-Vis and XRD analyses, would be related with the creation of the surface oxygen species which were identified using TPR. Quantification by the XPS analysis allowed to explain the influence of the superoxide and peroxide species in the OCM reaction.

3.4 Conclusions

The oxygen species responsible for catalytic performance were investigated in OCM. It was evidenced that incorporation of Mg^{2+}, Ca^{2+} and Sr^{2+} cations into CeO_2 surface, as substitution ions on cerium, creates oxygen species in "interstitial" sites on the oxide surface. This leads to an abundance of electrophilic oxygen species (O_2^{2-} and O_2^-) on the catalyst surface. A linear relationship between the total amount of basic sites and the (O_2^{2-} + O_2^-)/

O^{2-} ratio was found. The amount of basic sites, CH_4 conversion, and selectivity to C_2H_6 and C_2H_4, are controlled by the relative amount of electrophilic oxygen species to lattice oxygen on the surface of the catalyst. It is possible that the metal ionic radius influences the lattice distortion, thus affecting the type of active sites present in the samples. Similarity between the Ca^{2+} and Ce^{2+} ionic radii suggests a lattice distortion to create higher amount of electrophilic oxygen species, which reflects in the best performance for the oxidative coupling of methane.

Results obtained in this work suggest that the control of the amount and type of surface oxygen species on CeO_2 based oxides allows to obtain catalysts active and selective catalysts to form C_2 hydrocarbons.

References

[1] Ito T, Wang J, Lin CH, Lunsford JH, *Oxidative dimerization of methane over a lithium-promoted magnesium oxide catalyst*. J. Am. Chem. Soc. **107** (1985) 5062-5068.

[2] Voskresenskaya EN, Roguleva VG, Anshits AG, *Oxidant activation over structural defects of oxide catalysts in oxidative methane coupling*. Catal. Rev. **37** (1995) 101-143.

[3] Au P. C. T., Liu Y. W., F. NC, *Raman spectroscopic and TPR studies of oxygen species over BaO-and BaX_2(X=F, Cl, Br)-promoted Nd_2O_3 catalysts for the oxidative coupling of methane*. J. Catal. **176** (1998) 365-375.

[4] Weng W, Chen M, Wan H, Liao Y, *High-temperature in situ FTIR spectroscopy study of LaOF and BaF_2/LaOF catalysts for methane oxidative coupling*. Catal. Lett. **53** (1998) 43-53.

[5] Iwamoto M, Lunsford JH, *Surface reactions of oxygen ions. 5. Oxidation of alkanes and alkenes by O_2^- on MgO*. J. Phys. Chem-us **84** (1980) 3079-3084.

[6] Lunsford JH, *The catalytic conversion of methane to higher hydrocarbons*. Catal. Today. **6** (1990) 235-259.

[7] Wang JX, Lunsford JH, *Characterization of [Li+O] centers in lithium-doped magnesium oxide catalysts*. J. Phys. Chem-us **90** (1986) 5883-5887.

[8] Driscoll DJ, Martir W, Wang JX, Lunsford JH, *Formation of gas-phase methyl radicals over magnesium oxide*. J. Am. Chem. Soc. **107** (1985) 58-63.

[9] Sinev MY, Korchak VN, Krylov OV, *Highly selective ethane formation by reduction of BaO_2 with methane*. Kinet. Catal. **27** (1987) 1110.

[10] Dissanayake D, Lunsford JH, Rosynek MP, *Oxidative coupling of methane over oxide-supported barium catalysts*. J. Catal. **143** (1993) 286-298.

[11] Osada Y, Koike S, Fukushima T, Ogasawara S, Shikada T, Ikariya T, *Oxidative coupling of methane over Y_2O_3CaO catalysts*. App. Catal. **59** (1990) 59-74.

[12] Gonçalves R, Muniz F, Passos F, Schmal M, *Promoting effect of Ce on the oxidative coupling of methane catalysts*. Catal. Lett. **135** (2010) 26-32.

[13] Shahri SMK, Pour AN, *Ce-promoted $Mn/Na_2WO_4/SiO_2$ catalyst for oxidative coupling of methane at atmospheric pressure*. J. Nat. Gas Chem. **19** (2010) 47-53.

[14] DeBoy JM, Hicks RF, *The oxidative coupling of methane over alkali, alkaline earth, and rare earth oxides*. Ind. Eng. Chem. Res. **27** (1988) 1577-1582.

[15] Choudhary V. R., Mulla S. A. R., Uphade B. S., *Oxidative coupling of methane over alkaline earth oxides deposited on commercial support precoated with rare earth oxides*. Fuel **78** (1999) 427-437

[16] Otsuka K, Komatsu T, Shimizu Y, *The cerium oxide cased catalysts active for oxidative coupling of methane*. Stud. Surf. Sci. Catal. **44** (1989) 43-50.

[17] Shannon R, *Revised effective ionic radii and systematic studies of interatomic distances in halides and chalcogenides*. Acta Crystallogr. Sect. A **32** (1976) 751-767.

[18] Aoki A, Ohno S, Muramatsu Y, *Preparation of YBaCu oxide precursor by the citrate gel process*. J. Non-Cryst. Solids **147–148** (1992) 720-723.

[19] Marcilly C, Courty P, Delmon B, *Preparation of highly dispersed mixed oxides and oxide solid solutions by pyrolysis of amorphous organic precursors*. J. Am Ceram. Soc. **53** (1970) 56-57.

[20] Yu M, Lin J, Zhou YH, Wang SB, *Citrate–gel synthesis and luminescent properties of $ZnGa_2O_4$ doped with Mn^{2+} and Eu^{3+}*. Mat. Lett. **56** (2002) 1007-1013.

[21] Segal D, *Chemical synthesis of ceramic materials*. J. Mat. Chem. **7** (1997) 1297-1305.

[22] Li C, Domen K, Maruya K, Onishi T, *Dioxygen adsorption on well-outgassed and partially reduced cerium oxide studied by FT-IR*. J. Am. Chem. Soc. **111** (1989) 7683-7687.

[23] Rodriguez JA, Hrbek J, Kuhn M, Sham TK, *Interaction of oxygen with lithium-gold and cesium-gold films: a photoemission and thermal desorption study*. J. Phys. Chem-us **97** (1993) 4737-4744.

[24] Gopinath CS, Hegde SG, Ramaswamy AV, Mahapatra S, *Photoemission studies of polymorphic $CaCO_3$ materials*. Mat. Res. Bull. **37** (2002) 1323-1332.

[25] Peng XD, Richards DA, Stair PC, *Surface composition and reactivity of lithium-doped magnesium oxide catalysts for oxidative coupling of methane*. J. Catal. **121** (1990) 99-109.

[26] Zhang X, He D, Zhang Q, Xu B, Zhu Q, *Comparative studies on direct conversion of methane to methanol/formaldehyde over La–Co–O and ZrO_2; supported molybdenum oxide catalysts*. Top. Catal. **32** (2005) 215-223.

[27] Dubois J.-L. BM, Mimoun H., Cameron C.J. , *The oxidative coupling of methane over alkali, alkaline earth, and rare earth oxides*. Chem. Lett. **19** (1990) 967.

[28] Nolan M, Lykhach Y, Tsud N, Skala T, Staudt T, Prince KC, Matolin V, Libuda J, *On the interaction of Mg with the (111) and (110) surfaces of ceria*. Phys. Chem. Chem. Phys. **14** (2012) 1293-1301.

[29] Abi-aad E, Bechara R, Grimblot J, Aboukais A, *Preparation and characterization of ceria under an oxidizing atmosphere. Thermal analysis, XPS, and EPR study*. Chem. Mat. **5** (1993) 793-797.

[30] Cui H, Hong G, Wu X, Hong Y, *Silicon dioxide coating of CeO_2 nanoparticles by solid state reaction at room temperature*. Mat. Res. Bull. **37** (2002) 2155-2163.

[31] Liotta LF, Di Carlo G, Longo A, Pantaleo G, Venezia AM, *Support effect on the catalytic performance of Au/Co_3O_4-CeO_2 catalysts for CO and CH_4 oxidation*. Catal. Today **139** (2008) 174-179.

[32] Andreeva D, Idakiev V, Tabakova T, Ilieva L, Falaras P, Bourlinos A, Travlos A, *Low-temperature water-gas shift reaction over Au/CeO_2 catalysts*. Catal. Today **72** (2002) 51-57.

[33] Linganiso LZ, Jacobs G, Azzam KG, Graham UM, Davis BH, Cronauer DC, Kropf AJ, Marshall CL, *Low-temperature water-gas shift: Strategy to lower Pt loading by doping ceria with Ca^{2+} improves formate mobility/WGS rate by increasing surface O-mobility*. App. Catal. A **394** (2011) 105-116.

[34] Nagamoto H, Shinoda E, Inoue H, *Methane oxidation over strontium cerium oxide ($SrCeO_3$) catalysts: effect of solid-state reaction temperature*. Ind. Eng. Chem. Res. **32** (1993) 1790-1794.

[35] Gellings PJ, Bouwmeester HJM, *Solid state aspects of oxidation catalysis*. Catal. Today **58** (2000) 1-53.

[36] Otsuka K SA, Jinno K, Komatsu T, *Peroxide anions as possible active species in oxidative coupling of methane*. Chem. Lett. **16** (1987) 77-80.

[37] Speight J Lange's Handbook of Chemistry, 70th Anniversary Edition. (2004). McGraw-Hill Education,

4 Ce-doped La_2O_3 based catalyst for the oxidative coupling of Methane: Influence of the preparation method on the surface oxygen species

In this chapter, the effect of ceria on the OCM with Ce-doped La_2O_3 in a La:Ce molar ratio of 75:25 using two preparation methods, namely citrate and solvothermal methods, is presented. DR UV-Vis, XRD and XPS techniques were used for the characterisation of the catalysts. Results revealed a high concentration of surface oxygen. In addition, different types of ions (Ce^{3+} + Ce^{4+}) were detected on catalyst surface. The occurrence of more surface Ce^{3+} and higher ratio (O_2^{2-} + O^-)/ O^{2-}) were obtained in the oxide synthesised by solvothermal method, affecting the OCM reaction in terms of higher C_2 hydrocarbons selectivity. This behaviour can be attributed to the higher relative amount of O^- species on the catalyst surface.

4.1 Introduction

Oxidative coupling of methane has been studied during the past three decades for the production C_2 hydrocarbons (C_2H_6 and C_2H_4), particularly C_2H_4 which is an important base chemical for the petrochemical industries. In this reaction, it is imperative to control the oxidation of CH_4 and C_2 hydrocarbons, in order to avoid further oxidation to CO and CO_2. The O_2^{2-}, O^- and O^{2-} ions are considered to be the oxygen species responsible for methane activation to form methyl radicals ($CH_3\cdot$), which are coupled to produce C_2 hydrocarbons [1-5].

It is known that La_2O_3 is an effective catalyst for the OCM reaction [6-12]. Gellings et al. [13] pointed out in their review that the activity of lanthanum oxide catalysts is correlated with their ability to (re)generate reactive oxygen hole centres (O_2^{2-} and O^-) by reaction between gaseous oxygen and oxygen vacancies at the surface. On the other hand, Yamashita et al. [8] suggested that O_2^{2-} species would be decomposed into active oxygen species, probably $2O^-$, which would interact with methane to form $CH_3\cdot$ radicals. However, these studies do not differentiate the contribution of the O_2^{2-} and O^- ions in the OCM reaction. The nature of the active oxygen species in La_2O_3 has been subject of debate, but there are only a few works focused on the study of the oxygen species which are the most active for the OCM over La_2O_3 based catalysts. CeO_2 has excellent redox properties due to the easy reduction of Ce^{+4} to Ce^{+3} associated to the formation of surface oxygen vacancies in the crystalline lattice [14] offering oxygen storage property/capacity [15,16] . For that reason, Ce has been used as doping agent in several catalysts to promote their performance in OCM [16-18]. In this work, La_2O_3 doped with Ce was prepared by two different methods (citrate and solvothermal methods) and the oxygen ions on the oxide surface were examined to explain the active sites for the OCM reaction.

Different techniques were used to achieve this objective. Diffuse Reflectance Ultraviolet-Visible (DR UV-Vis) spectroscopy was applied to study the nature and the coordination state of the surface oxide species. On the other hand, X-ray diffraction (XRD) was used to corroborate the existence of different lattice strains in modified La_2O_3 crystals and the XPS spectra of electrons of inner subshells Ce 3d and O 1s of the composite oxide were obtained by mean of X-ray photoelectron spectroscopy (XPS). Principal

component analysis and curve fitting were applied to determinate the oxidation states and their relative surface proportions. The characteristics of XPS Ce 3d and O 1s spectra were the focus of the study, in order to discuss the surface oxygen species and the catalyst performance on the OCM reaction.

4.2 Experimental section

4.2.1 Catalyst preparation

The citrate and solvothermal methods were used to prepare the materials. The citrate method allows the preparation of highly dispersed mixed oxides from the individual cations in the desired stoichiometric ratio [19,20], involving the formation of a mixed-ions citrate due to the three-ligand nature of citric acid, resulting in a transparent three-dimensional network for subsequent calcination. The second method used was the solvothermal method, which permits the modification of precipitates, gels or flocculates induced by temperature under aging or ripening in the presence of mother liquor (solvent) [21,22]. Reactions occur at temperatures above their normal boiling point containing the reaction mixture within a pressure vessel (autoclave) subjected to autogenous pressure [23,24]. The obtained solid is washed, dried and finally calcined at the desired temperature.

Thus, La-Ce mixed oxides were prepared from $Ce(NO_3)_3 \cdot 6H_2O$ (99% Aldrich) and $La(NO_3)_3 \cdot 6H_2O$ (99% Fluka) precursor solutions in appropriate amounts to obtain a La:Ce molar ratio of 75:25. In the first method, the precursors were dissolved in water and then citric acid was added in a molar ratio of acid/(Ce + La) = 1. The final solution was heated up to 80 °C under constant stirring to evaporate superfluous water until a viscous gel was obtained, which was dried at 120 °C overnight to form a spongy material that was calcined at 800 °C during 6 h (see Figure 2.1).

Using the second method mentioned above (solvothermal method), a solution was prepared by dissolving $La(NO_3)_3 \cdot 6H_2O$ and $Ce(NO_3)_3 \cdot 6H_2O$ in methanol in appropriate amounts to obtain the above mentioned molar ratio. Then, the alkaline conditions were adjusted using KOH (3M). The solution obtained was transferred to a teflon vessel inserted in the high pressure reactor (Figure 4.1) and heated up to the desired temperature (150 °C) under autogeneous pressure. The solution was then maintained at the above

mentioned temperature for 150 min under continuous stirring (300 rpm). The colloidal material obtained was washed with distillated water and dried at 120 °C overnight. The material was calcined at 800 °C during 6 h. Pure CeO_2 and La_2O_3 were also synthesised. The mixed oxide is denoted as $La_{0.75}Ce_{0.25}O$(CM) when prepared by the citrate method and (SM) by the solvothermal method.

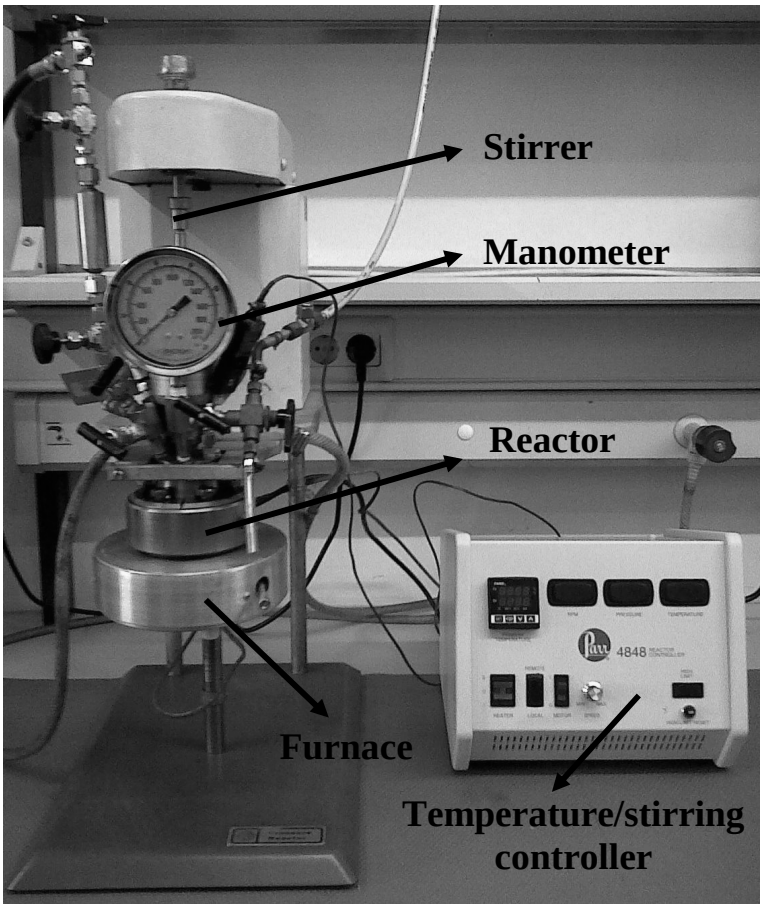

Figure 4.1 High pressure reactor system.

4.2.2 Catalyst characterisation

As previously mentioned, the oxygen ions on the oxide surface were investigated by using Diffuse Reflectance Ultraviolet-Visible (DR UV-Vis) spectroscopy, and X-ray photoelectron spectroscopy (XPS). The X-ray diffraction (XRD) technique was used to corroborate lattice strains into modified La_2O_3 oxide which can be reflected on catalyst surface, leading to the formation of different oxygen ion species.

Thus, DR-UV spectra of the powder solids were measured using a Jasco V-650 UV-Vis spectrophometer equipped with an integrating sphere attachment (JASCO ISV-469). The spectra were recorded in diffuse reflectance mode and transformed by the instrument software (JASCO) to equivalent absorption Kubelka-Munk units over the wavelength range λ=200-800 nm.

The XPS analysis was performed with a VG Scientific ESCALAB 200A spectrometer. XPS data corresponding to Ce 3d and O 1s spectra were fitted and envelopes were deconvoluted using the XPS-peak software. To minimise the number of degrees of freedom of the curve fitting procedure, constraints on the binding energy (BE), full width at half maximum (FWHM) and peak areas were applied to each doublet pair.

Finally, XRD diffractogram were recorded on a PANalytical X'Pert MPD equipped with a X'Celerator detector and secondary monochromator (Cu Kα λ = 0.154 nm, 50 kV, 40 mA; data recorded at a 0.017° step size, 100 s/step). Rietveld refinement with PowderCell software was used to identify the crystallographic phases present and to calculate the crystallite size from the XRD diffraction patterns.

4.2.3 Catalyst evaluation

The catalytic performance of the prepared oxides for the OCM was studied in a quartz tube reactor which was filled with 0.2 g of catalyst held by quartz wool as shown in Figure 2.2. Then, the reactor was placed into an electrical furnace (Figure 2.3). Methane, helium and oxygen flow rates were regulated by mass flow controllers (HI-TEC). The mixture of methane and oxygen (CH_4/O_2 molar ratio of 4) diluted in Helium (75% of the total flow) was passed through the catalyst bed with a total flow rate of 50 cm^3 min^{-1}. A cold trap was placed at the outlet of the quartz tube to separate any condensed water vapor from the reaction products. The OCM study starts when the temperature reaches 600 °C. The product stream containing carbon monoxide, carbon dioxide, ethane, ethylene, unreacted oxygen and methane was analysed by an on-line gas chromatograph (GC) equipped with a capillary column (Carboxen 1010 Plot. Supelco) and a thermal conductivity detector. It was assumed that carbon and /or hydrogen in methane were only converted into ethane, ethylene carbon monoxide, carbon dioxide and/or molecular hydrogen and water. Then, the conversion of CH_4, the selectivity

and yield of the products were defined, respectively, as in section 2.2.3 (Eqs. 2.1-2.3).

4.3 Results and discussion

4.3.1 Characterisation

4.3.1.1 Diffuse Reflectance Ultraviolet-Visible spectroscopy (DR UV-Vis)

Diffuse Reflectance Ultraviolet-Visible spectroscopy was used to explain possible shifts in the coordination number of the oxides. Figure 4.2 shows the DR-UV spectra. Bands at 250 and 354 nm for CeO_2 can be attributed to the charge transfer $Ce^{3+} \leftarrow O^{2-}$ and $Ce^{4+} \leftarrow O^{2-}$ respectively [25]. On the other hand, the band at 216 nm can be assigned to the charge transfer $La^{3+} \leftarrow O^{2-}$ [26]. The DR-UV results showed that the absorption bands are strongly affected by incorporation of Ce.

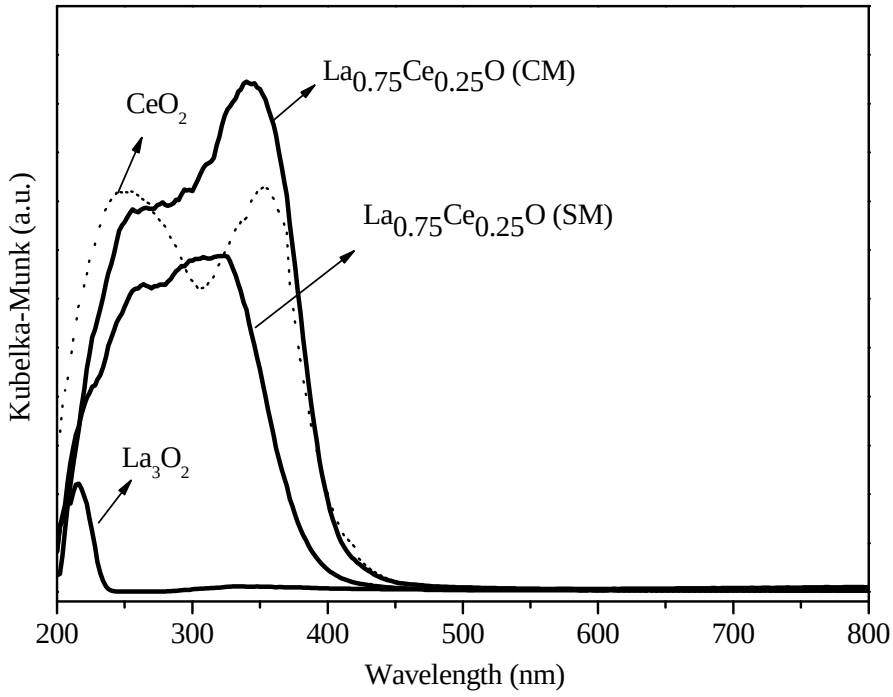

Figure 4.2 DR-UV spectra of $La_{07.5}Ce_{0.25}O$(CM), $La_{07.5}Ce_{0.25}O$(CM), La_3O_2 and CeO_2 oxides.

The addition of Ce shifts the absorption band of La_2O_3 from 216 nm to a broad absorption at 255 and 341 nm in the $La_{0.75}Ce_{0.25}O$(CM) catalyst

(Figure 4.2). Similarly, a shift of absorption band in $La_{0.75}Ce_{0.25}O$(SM) is observed from 216 nm to 262 and 323 nm. The emergence of these absorption bands can be due to the presence of Ce^{3+} and Ce^{4+} species in the coordinated oxide environment, which suggests different coordination numbers for the oxide [27]. Therefore, band shifts suggest the formation of defects in the Ce-doped La_2O_3 lattice, leading to surface imperfections, and therefore, formation of different surface oxygen species.

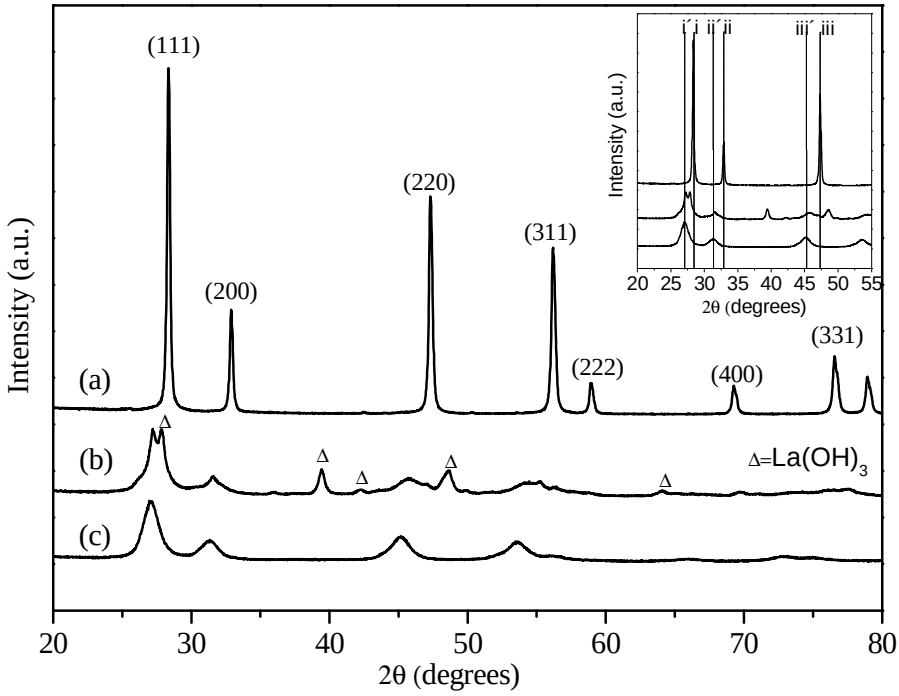

Figure 4.3 X-ray diffraction profiles of (a) CeO_2, (b) $La_{0.75}Ce_{0.25}O$(SM) and (c) $La_{0.75}Ce_{0.25}O$(CM), showing the effect of Ce doping into the lattice of La_2O_3. Note in the inset, as the peak intensity of the Ce-doped La_2O_3 is decreased and the peak position (2θ) is shifted.

4.3.1.2 X-Ray diffraction (XRD)

Cubic phases in the modified La_2O_3 oxide were detected by applying the XRD technique. Figure 4.3 shows the diffraction lines corresponding to the cubic structure of CeO_2, $La_{0.75}Ce_{0.25}O$ (SM) and $La_{0.75}Ce_{0.25}O$(CM) catalysts and Table 4.1 shows the detected phases and particle size. No second phases or additional reflections were found in $La_{0.75}Ce_{0.25}O$(CM) indicating the

formation of a single phase. However, the XRD diffractogram of the $La_{0.75}Ce_{0.25}O$ (SM) catalyst revealed additional reflections, which are in agreement with the standard patterns of $La(OH)_3$.

Table 4.1 Ce doped La_2O_3 phases and particle sizes determined by XRD.

Sample	Phases (Vol %)	Crystalline structure	Cell parameter (Å)	Crystallite size (nm)
$La_{0.75}Ce_{0.25}O$(CM)	$La_{0.75}Ce_{0.25}O_{1.5+\delta}$	Cubic	a= 5.64	10.3
$La_{0.75}Ce_{0.25}O$(SM)	$La(OH)_3$ 44.68	Hexagonal	a= 6.52 c= 3.85	27.8
	$La_{0.59}Ce_{0.41}O_{1.5+\delta}$ 55.32	Cubic	a= 5.59	8.8

In addition, a discernible diffraction peak shift toward lower 2θ values can be observed in the inset of Figure 4.3 (see drop-down lines for i - i', ii – ii' and iii-iii' peak shifts attributed to the (1 1 1), (2 0 0) and (220) reflecting planes), representing a change in the lattice parameter from 5.41 Å for pure CeO_2 to 5.64 Å for $La_{07.5}Ce_{0.25}O$ (CM) and 5.59 Å for $La_{07.5}Ce_{0.25}O$ (SM), i.e., an increase around 3%.

These results suggest the formation of a $La_xCe_{1-x}O_{1.5+\delta}$ solid solution present in $La_{0.75}Ce_{0.25}O$ catalysts prepared by both preparation methods. Table 4.2 shows the cubic cell parameter (a) and La content (x) in $La_xCe_{1-x}O_{1.5+\delta}$ reported in literature. Thus, a linear relationship between cubic lattice parameter and La content in a $La_xCe_{1-x}O_{1.5+\delta}$ solid solution can be found from these data (Figure 4.4).

Therefore, the La content in $La_xCe_{1-x}O_{1.5+\delta}$ could be estimated from Figure 4.4 (x=0.75), which corresponds a cubic cell parameter of 5.64 Å in $La_{07.5}Ce_{0.25}O$(CM). It can be observed that the estimated La content corresponds to the nominal composition which indicates the formation of a single phase of $La_{0.75}Ce_{0.25}O_{1.5+\delta}$ in $La_{07.5}Ce_{0.25}O$(CM). Similarly, the La content was estimated in $La_{0.75}Ce_{0.25}O$(SM) from Figure 4.3.

Table 4.2 Cubic cell parameter in $La_xCe_{1-x}O_{1.5+\delta}$.

Cubic cell parameter (nm)	(x) in $La_xCe_{1-x}O_{1.5+\delta}$	Reference
a=0.540	0.00	Kümmerle, E. A. et al. [28]
a=0.549	0.25	Sukharevskii B.Y. et al. [29]
a=0.557	0.50	McBride J. R. et al. [30]

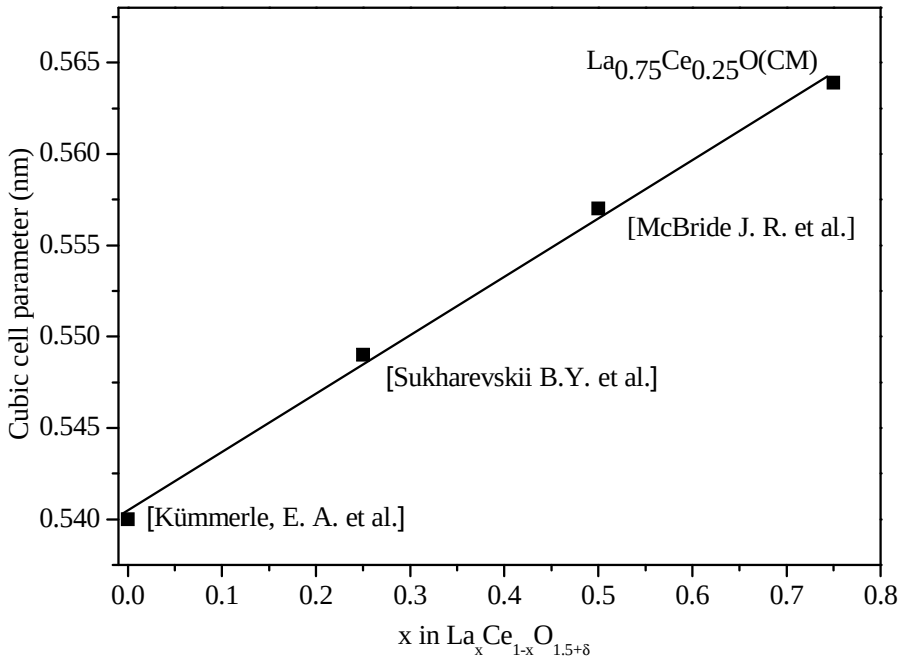

Figure 4.4 Linear relationship between cubic cell parameter and La content in $La_xCe_{1-x}O_{1.5+\delta}$.

In this case, La content is x=0.59 which corresponds a cubic cell parameter of 5.59 Å. This indicates the formation of $La_{0.59}Ce_{0.41}O_{1.5+\delta}$, besides $La(OH)_3$ phase, in the $La_{07.5}Ce_{0.25}O$(SM) catalyst.

On the other hand, a broadening of the mixed oxide reflexions can be observed, which indicates a decrease in crystallite size from 45.9 in CeO_2 to 10.32 nm the $La_{07.5}Ce_{0.25}O$ (CM) catalyst and from 45.9 to 8.8 in $La_{07.5}Ce_{0.25}O$(SM) (calculated from XRD pattern). The shift of the particle size and lattice strain can contribute to peak broadening in XRD, in particular for nanoparticles [31]. The lattice expansion can be attributed to a

combination of the effects of increasing number of oxygen vacancies due to La doping and the large ionic radius of La^{3+} versus Ce^{4+} [32].

4.3.1.3 X-Ray photoelectron spectroscopy (XPS)

The surface oxidation states of La and Ce species on the samples $La_{0.75}Ce_{0.25}O$(SM) and $La_{0.75}Ce_{0.25}O$(CM) were characterised by XPS analysis. The binding energies are summarised in Table 4.3. According to the literature [33,34], La is in its higher oxidation state (3+). On the other hand, Ce 3d spectra of the samples exhibit the characteristic features of the Ce(IV). However, the coexistence of both Ce(III) and Ce(IV) species must be considered in order to obtain a good fitting of the experimental data. As shown in Figure 4.5a and b, the Ce 3d XPS spectra exhibit three lobed envelopes (around 879-890 eV, 895-910 eV and approximately 916 eV) which is according with literature [35]. From these lobed envelopes, the coexistence of both Ce^{3+} and Ce^{4+} states are distinguishable, although the oxidation state 4+ is predominant [36]. Ce(IV) and Ce(III) always show peaks at ~882 and ~916 eV as well as at ~885 and ~903 eV, which are considered fingerprints characterising Ce(IV) and Ce(III), respectively [37].

Table 4.3 Binding energies for the La and Ce 3d by XPS analysis (FWHM) (eV**).**

Catalyst	La ($3d_{5/2}$)	La ($3d_{3/2}$)	Ce (IV)	Ce (IV)	Ce (III)	Ce (III)	[%Ce(III)]
$La_{07.5}Ce_{0.25}O$ (SM)	833.9 (3.1)	850.7 (3.5)	881.7 (3.0)	915.7 (2.9)	884.7 (3.3)	902.8 (3.1)	30.0
$La_{07.5}Ce_{0.25}O$ (CM)	833.8 (3.5)	850.5 (3.5)	881.4 (3.3)	915.5 (3.0)	884.3 (3.0)	902.4 (2.9)	26.1

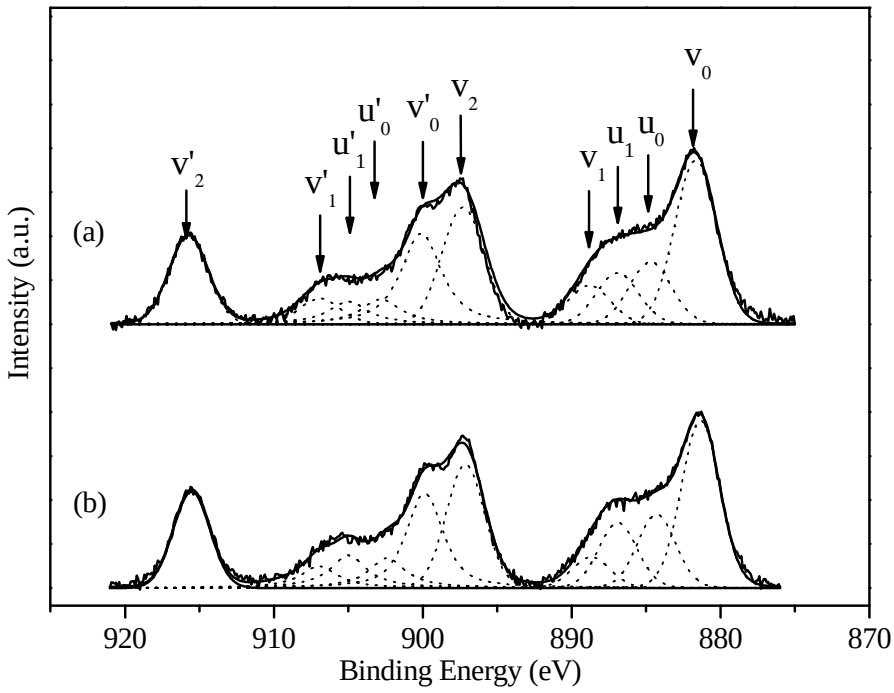

Figure 4.5 Cerium 3d XPS spectra for (a) $La_{0.75}Ce_{0.25}O$(CM) and (b) $La_{0.75}Ce_{0.25}O$(SM).

The Ce 3d spectra of the $La_{07.5}Ce_{0.25}O$(CM) and $La_{07.5}Ce_{0.25}O$(SM) catalysts were deconvoluted into 10 peaks corresponding to the different surface Ce species (Figure 4.5). The full width at half maximum (FWHM) of the single species peaks was fixed between 2.9-3.3 eV. In the Ce $3d_{3/2}$ spin-orbit split doublet of Ce(IV), v_o and v_2 components represent the intensive peaks, and v_1 a weak satellite. Correspondently, v'_o and v'_2 components characterise the Ce $3d_{5/2}$ doublet intensive peaks and v'_1 the associated weak satellite [38-41]. For Ce(III), the mean components u_o and u_1 characterise the Ce $3d_{5/2}$ and u'_o and u'_1 the Ce $3d_{5/2}$ contribution[38,42]. The concentration of Ce^{3+} in ceria can be determined from the following equations [43]:

$$\text{Ce(III)} = u_o + u'_o + u_1 + u'_1 \tag{4.1}$$

$$\text{Ce(IV)} = v_o + v'_o + v_1 + v'_1 + v_2 + v'_2 \tag{4.2}$$

$$\%\text{Ce[III]} = \frac{Ce(III)}{Ce(III) + Ce(IV)} \tag{4.3}$$

where Ce(III) and Ce(IV) represent the corresponding sums of the integrated peak areas related to the Ce^{3+} and Ce^{4+} XPS signals respectively. According

to the XPS results (Tale 4.3), it is possible to conclude that the Ce(IV)/Ce(III) redox couple exists on the surface of the Ce doped La_2O_3 catalysts using the two preparation methods. It is observed that the $La_{0.75}Ce_{0.25}O$(SM) catalyst has higher surface [%Ce(III)] when compared with $La_{0.75}Ce_{0.25}O$(CM), by about 12%.

On the other hand, the O 1s spectra of the samples, shown in Figure 4.6, are used to identify the coexisting oxygen species on the surface of the catalysts. The O 1s spectra of the $La_{07.5}Ce_{0.25}O$ (CM) and $La_{07.5}Ce_{0.25}O$ (SM) catalysts were deconvoluted into four peaks corresponding to the different oxygen species. These can be assigned to CO_3^{2-} at (531.5~532.5) eV, O_2^{2-} at (530.5 ~ 531.1) eV, O^- at (530.1~530.2) eV and O^{2-} at (528.0~529.0) eV, the actual values being given in Table 4.4 [44-49].

Table 4.4 Curve-fitting results from XPS data.

Catalyst	**O 1s binding energies (FWHM) (eV) Relative amount of the oxygen species (%)**				**$(O_2^{2-}+O^-)/O^{2-}$**
	O^{2-}	**O_2^{2-}**	**O^-**	**CO_3^{2-}**	
$La_{0.75}Ce_{0.25}O$ (SM)	528.09 (2.5) 28.8	-----	530.07 (2.4) 61.1	531.56 (2.0) 10.0	2.11
$La_{0.75}Ce_{0.25}O$ (CM)	528.09 (2.5) 40.5	530.60 (2.3) 35.6	530.07 (2.3) 8.7	531.60 (2.3) 15.1	1.25

The fitting of experimental data can be observed in Figure 4.6 showing the contribution of the aforementioned single species. From reasonable physical meanings, it can be concluded that $La_{07.5}Ce_{0.25}O$(CM) revealed the presence of three oxygen species (O_2^{2-}, O^- and O^{2-}), while, $La_{07.5}Ce_{0.25}O$(SM) revealed the presence of two oxygen species (O^- and O^{2-}).

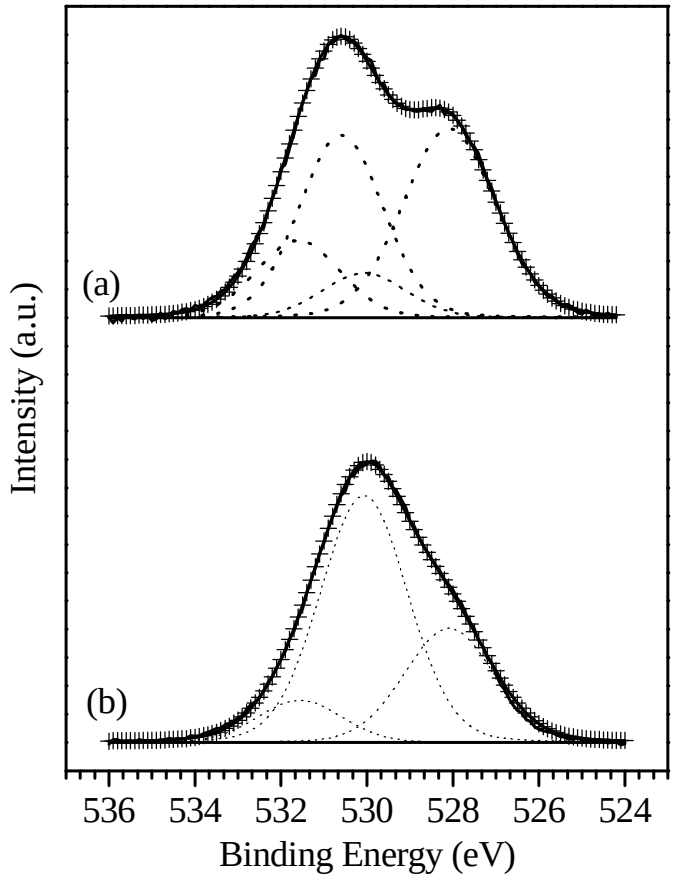

Figure 4.6 O 1s binding energy spectra of (a) $La_{0.75}Ce_{0.25}O$(CM) and (b) $La_{0.75}Ce_{0.25}O$(SM).

Then, the ratio of surface electrophilic oxygen to lattice oxygen species, i.e. $(O_2^{2-} + O^-)/ O^{2-}$, was estimated from the relative amounts (%) of the oxygen species calculated according to the areas under the curves for each sub-peak. Results summarised in Table 4.4 indicate an influence of the preparation method in the amount of electrophilic oxygen. $La_{0.75}Ce_{0.25}O$ (SM) revealed higher $((O_2^{2-} + O^-)/ O^{2-})$ ratio when compared with $La_{0.75}Ce_{0.25}O$ (CM), by around 69%.

These results would indicate that the oxygen species in the oxide structure were created by doping La_2O_3 with Ce. Islam et al. [50] studied methane oxidation on La_2O_3 as catalyst. They investigated the formation of O_2^{2-} and O^- peroxide species, as these are supposed to be responsible for methane activation on this material. The authors suggested that the catalytic activity

of doped La_2O_3 is correlated with its ability to (re)generate oxygen hole centres (O^- and O_2^{2-}) by reaction between gaseous oxygen and oxygen vacancies at the surface. In this work, it was possible to distinguish the contribution of each oxygen species (O^- and O_2^{2-}) in OCM from the above results. $La_{0.75}Ce_{0.25}O$(SM) show higher relative amount of the O^- oxygen species when compared with O_2^{2-} oxygen species, while $La_{0.75}Ce_{0.25}O$(CM) revealed lower relative amount of the O^- oxygen species.

On the other hand, the formation oxygen vacancies is accompanied by the change of oxidation state of Ce ions (Ce^{3+} or Ce^{4+}) [51], which influences the concentration of partially reduced oxygen species and content of vacancy defects. Therefore, Ce-doped La_2O_3 and the synthesis procedure, would explain the presence of different types of ions (Ce^{3+} + Ce^{4+}) on the catalyst surface and the occurrence of more Ce^{3+} leading higher ratio (O_2^{2-} + O^-)/ O^{2-} in the $La_{0.75}Ce_{0.25}O$ (SM), and therefore, better performance in OCM reaction.

4.3.2 Catalytic tests

The structure dependence of the catalytic behavior was investigated by examining the activity of CeO_2, La_2O_3 and Ce-doped La_2O_3 via two different synthesis procedures. The catalytic tests were carried out following the conversion of methane and selectivity at different reaction temperatures (600-750 ^{0}C). Figure 4.7 shows the conversion of methane as a function of temperature and Figure 4.8a and b shows the selectivity to form C_2 hydrocarbons for the $La_{0.75}Ce_{0.25}O$ catalyst prepared by both preparation methods. The catalytic results revealed a significant effect of the solvothermal method in the increasing of the methane conversion and the

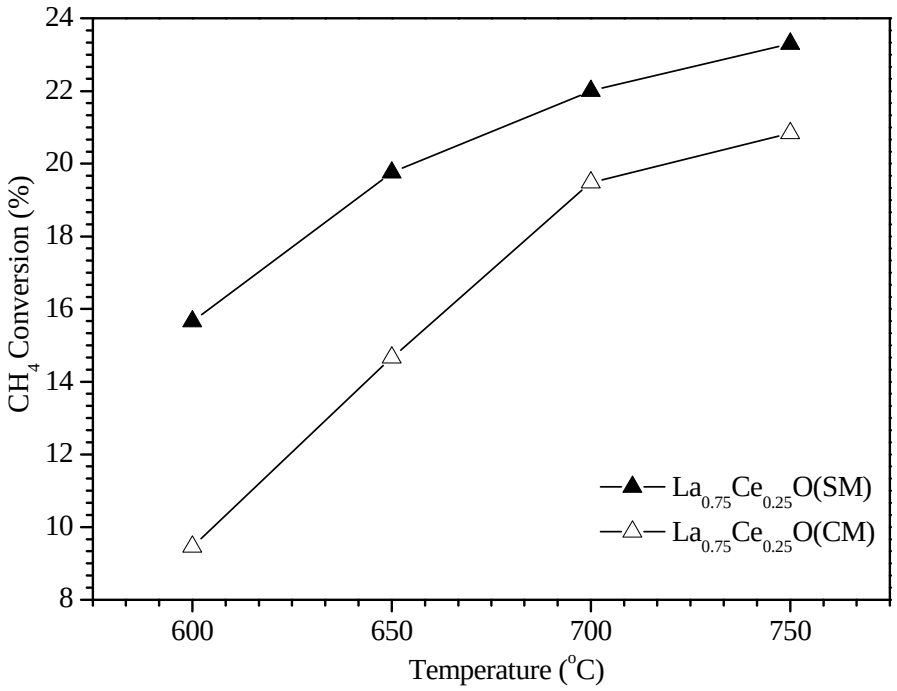

Figure 4.7 Methane conversion at different temperatures.

selectivity to form C_2 hydrocarbons when compared with the citrate method, particularly higher selectivity (by about 30%) at 750 ^{0}C. On the other hand, both catalysts revealed higher selectivity than the pristine oxides (CeO_2 and La_2O_3). Results of the reactions at 750 ^{0}C of the samples prepared using the citrate and solvothermal method are sumarised in Table 4.5.

Table 4.5 Catalytic activities of CeO_2, La_2O_3 and Ce-doped La_2O_3 on the OCM at 750 ^{0}C.

Catalyst	Conversion (%)		Selectivity (%)			C_2 yield (%)
	O_2	CH_4	CO_2	CO	C_{2+}	
CeO_2(CM)	96.6	16.7	85.1	1.4	13.5	2.3
La_2O_3(CM)	100.0	23.0	39.4	31.4	29.2	6.7
$La_{0.75}Ce_{0.25}O$(CM)	97.6	21.0	48.0	16.5	35.5	7.5
CeO_2(SM)	100.0	17.1	87.5	3.2	9.3	1.6
La_2O_3(SM)	100.0	23.5	57.0	12.1	30.9	7.3
$La_{0.75}Ce_{0.25}O$(SM)	100.0	23.3	53.0	1.8	45.1	10.5

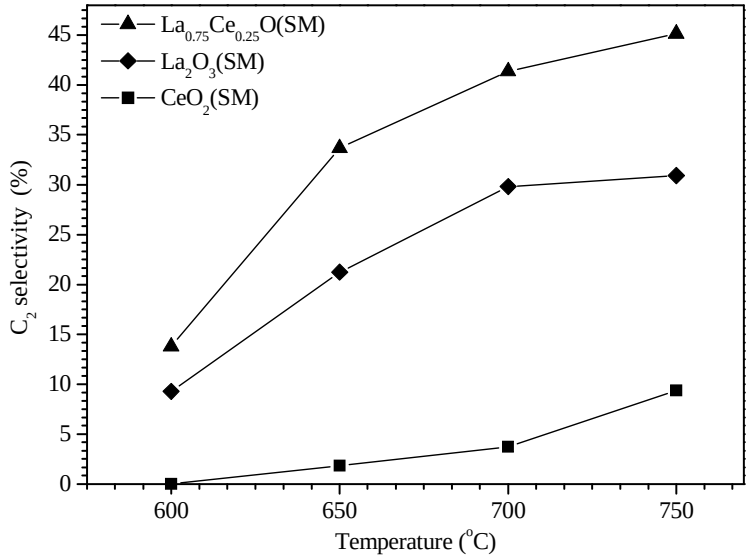

(a)

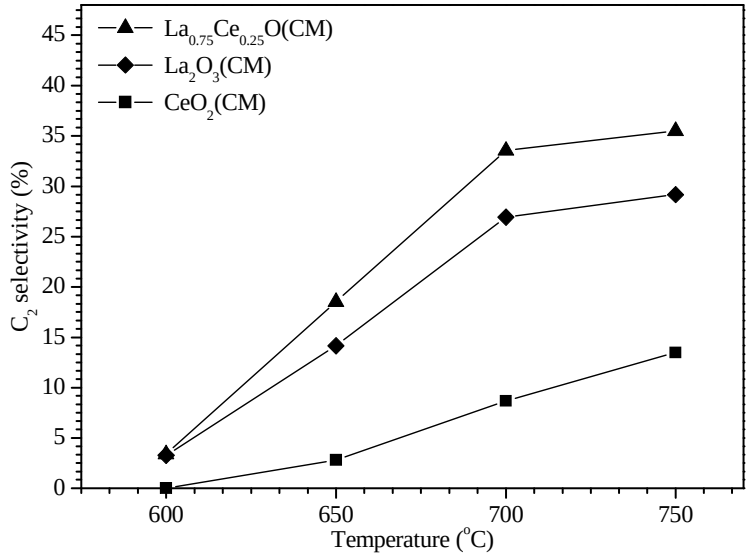

(b)

Figure 4.8 Selectivity at different temperatures of samples prepared using (a) solvothermal method (b) citrate method.

The $La_{0.75}Ce0._{25}O$ catalysts prepared using both methods revealed higher C_2 selectivity, particularly $La_{0.75}Ce0._{25}O$(SM), which showed selectivity of 45.1 and a C_2 yield of 10.5 (%).These catalysts also showed high O_2 conversion between 96-100% because of its high oxidising ability.

As mentioned above, XPS results indicate that interstitial oxygen and therefore surface oxygen species in the oxide structure were created by doping La_2O_3 with Ce. Particularly the solvothermal method showed a significant difference. The $La_{0.75}Ce_{0.25}O$(SM) catalyst showed to have higher $(O_2^{2-} + O^-)/ O^{2-}$ ratio when compared with $La_{0.75}Ce_{0.25}O$ (CM) catalyst. This was reflected in the catalytic results, since the $La_{0.75}Ce_{0.25}O$(SM) catalyst showed higher C_2 yield.

On the other hand, the different oxidation states of the Ce ions are related to the partially reduced oxygen species. The oxygen vacancies (decrease in O occupancy) are also formed together with the oxidation state change of Ce ions [51]. Then, the presence of different types of cerium ions (Ce^{3+} or Ce^{4+}) influences the concentration of partially reduced oxygen species and content of vacancies defects. This would be also reflected by the replacement of La^{3+} with Ce^{+4} suggested by the DR-UV and XRD pattern. As mentioned above, the XRD spectrum of the $La_{0.75}Ce_{0.25}O$ catalyst prepared by solvothermal method revealed higher strain, suggesting higher formation of defects in the Ce-doped La_2O_3 lattice, which leads to surface imperfections (oxygen vacancies). Therefore, Ce-doped La_2O_3 and the synthesis procedure, would explain the presence of different types of ions (Ce^{3+} + Ce^{4+}) and the occurrence of more Ce^{3+} leading to higher ratio $(O_2^{2-} + O^-)/ O^{2-}$ in $La_{0.75}Ce_{0.25}O$ (SM).

The oxygen species created different chemical and structural properties in the oxide, which improve the C_2 hydrocarbons selectivity of $La_{0.75}Ce_{0.25}O$ (SM) in the OCM reaction due the subsequent methane transformation into the products of dimerization (through the activation of the C-H bond), which is determined by the presence oxygen vacancies in the catalyst [52]. CeO_2 is an oxide having excellent redox properties owing to the very fast reduction of Ce^{4+} to Ce^{3+} associated with the formation of oxygen vacancies at the surface and in the solid. The oxygen mobility, reducibility and ionic conductivity are enhanced by doping La_2O_3 with CeO_2. Therefore, the catalyst surface with high oxygen vacancy lead, to the adsorption and activation of molecular oxygen to produce oxygen active species which in turn activate methane to produce methyl radicals ($CH_3\cdot$).

4.4 Conclusions

The Ce-doped La_2O_3 catalyst was examined for the OCM reaction. Both citrate and solvothermal method allowed the incorporation of Ce into the La_2O_3 lattice as substitution ions on La which creates interstitial oxygen species leading to an abundance of electrophilic oxygen species on the catalyst surface. The citrate method revealed creating O^- and O_2^{2-} oxygen species, while solvothermal method O^- oxygen species. These results would be related with the different types of cerium ions (Ce^{3+} or Ce^{4+}) on the oxide surface. The catalyst prepared by the solvothermal method showed higher concentration of [$\%Ce^{3+}$]. The O^- oxygen species predominant in the $La_{0.75}Ce_{0.25}O$(SM) catalyst would be responsible for higher C_2 yield (by 10.5 %) at 750 ^oC in the oxidative coupling of methane.

References

[1] Lunsford JH, *The catalytic conversion of methane to higher hydrocarbons*. Catalysis Today **6** (1990) 235-259.

[2] Weng W, Chen M, Wan H, Liao Y, *High-temperature in situ FTIR spectroscopy study of LaOF and BaF_2/LaOF catalysts for methane oxidative coupling*. Catal Lett **53** (1998) 43-53.

[3] Au P. C. T., Liu Y. W., F. NC, *Raman spectroscopic and TPR studies of oxygen species over BaO-and BaX_2 (X=F, Cl, Br)-promoted Nd_2O_3 catalysts for the oxidative coupling of methane*. Journal of Catalysis **176** (1998) 365-375.

[4] Osada Y, Koike S, Fukushima T, Ogasawara S, Shikada T, Ikariya T, *Oxidative coupling of methane over Y_2O_3CaO catalysts*. Applied Catalysis **59** (1990) 59-74.

[5] Ferreira VJ, Tavares P, Figueiredo JL, Faria JL, *Effect of Mg, Ca, and Sr on CeO_2 Based Catalysts for the Oxidative Coupling of Methane: Investigation on the Oxygen Species Responsible for Catalytic Performance*. Industrial & Engineering Chemistry Research **51** (2012) 10535-10541.

[6] Choudhary VR, Mulla SAR, Uphade BS, *Oxidative coupling of methane over alkaline earth oxides deposited on commercial support precoated with rare earth oxides*. Fuel **78** (1999) 427-437.

[7] Kuś S, Otremba M, Taniewski M, *The catalytic performance in oxidative coupling of methane and the surface basicity of La_2O_3, Nd_2O_3, ZrO_2 and Nb_2O_5*. Fuel **82** (2003) 1331-1338.

[8] Yamashita H, Machida Y, Tomita A, *Oxidative coupling of methane with peroxide ions over barium-lanthanum-oxygen mixed oxide*. Applied Catalysis A: General **79** (1991) 203-214.

[9] Louis C, Lin Chang T, Kermarec M, Le Vana T, Michel Tatibouët J, Chea M, *EPR study of the stability and the role of the O^{2-} species on La_2O_3 in the oxidative coupling of methane*. Catalysis Today **13** (1992) 283-289.

[10] Levan T, Che M, Tatibouet JM, Kermarec M, *Infrared Study of the Formation and Stability of $La_2O_2CO_3$ During the Oxidative Coupling of Methane on La_2O_3*. Journal of Catalysis **142** (1993) 18-26.

[11] Käßner P, Baerns M, *Comparative characterization of basicity and acidity of metal oxide catalysts for the oxidative coupling of methane by different methods*. Applied Catalysis A: General **139** (1996) 107-129.

[12] DeBoy JM, Hicks RF, *Oxidative coupling of methane over alkaline earth promoted La_2O_3*. Journal of the Chemical Society, Chemical Communications **0** (1988) 982-984.

[13] Gellings PJ, Bouwmeester HJM, *Solid state aspects of oxidation catalysis*. Catalysis Today **58** (2000) 1-53.

[14] Sun C, Li H, Chen L, *Nanostructured ceria-based materials: synthesis, properties, and applications*. Energy & Environmental Science **5** (2012) 8475-8505.

[15] Sobukawa H, *Development of Ceria-Zirconia Solid Solutions and Future Trends* R & D Review of Toyota CRDL **37** (2002) 1-5.

[16] Gholipour Z, Malekzadeh A, Hatami R, Mortazavi Y, Khodadadi A, *Oxidative coupling of methane over (Na_2WO_4+Mn or Ce)/SiO_2 catalysts: In situ measurement of electrical conductivity*. Journal of Natural Gas Chemistry **19** (2010) 35-42.

[17] Shahri SMK, Pour AN, *Ce-promoted Mn/Na_2WO_4/SiO_2 catalyst for oxidative coupling of methane at atmospheric pressure*. Journal of Natural Gas Chemistry **19** (2010) 47-53.

[18] Gonçalves RP, Muniz F, Passos F, Schmal M, *Promoting fffect of Ce on the oxidative coupling of methane catalysts*. Catal Lett **135** (2010) 26-32.

[19] Marcilly C, Courty P, Delmon B, *Preparation of Highly Dispersed Mixed Oxides and Oxide Solid Solutions by Pyrolysis of Amorphous Organic Precursors*. Journal of the American Ceramic Society **53** (1970) 56-57.

[20] Yu M, Lin J, Zhou YH, Wang SB, *Citrate–gel synthesis and luminescent properties of $ZnGa_2O_4$ doped with Mn^{2+} and Eu^{3+}*. Materials Letters **56** (2002) 1007-1013.

[21] Hu C, Gao Z, Yang X, *One-pot low temperature synthesis of MFe_2O_4 (M=Co, Ni, Zn) superparamagnetic nanocrystals*. Journal of Magnetism and Magnetic Materials **320** (2008) L70-L73.

[22] Peng Q, Dong Y, Deng Z, Sun X, Li Y, *Low-Temperature Elemental-Direct-Reaction Route to II−VI Semiconductor Nanocrystalline ZnSe and CdSe*. Inorganic Chemistry **40** (2001) 3840-3841.

[23] Yáñez-Vilar S, Sánchez-Andújar M, Gómez-Aguirre C, Mira J, Señarís-Rodríguez MA, Castro-García S, *A simple solvothermal synthesis of MFe_2O_4 (M=Mn, Co and Ni) nanoparticles*. Journal of Solid State Chemistry **182** (2009) 2685-2690.

[24] Silva AT, Machado B, Gomes H, Figueiredo J, Dražić G, Faria J, *Pt nanoparticles supported over Ce–Ti–O: the solvothermal and photochemical approaches for the preparation of catalytic materials*. J Nanopart Res **12** (2010) 121-133.

[25] Voskresenskaya EN, Roguleva VG, Anshits AG, *Oxidant activation over structural defects of oxide catalysts in oxidative methane coupling*. Catal Rev **37** (1995) 101-143.

[26] Li D, Chen G, Wang X, *Incorporation of lanthanum into SBA-15 and its catalytic activity in trichloroethylene combustion*. J Rar Eart **26** (2008) 717-721.

[27] Gonçalves R, Muniz F, Passos F, Schmal M, *Promoting effect of Ce on the oxidative coupling of methane catalysts*. Catal Lett **135** (2010) 26-32.

[28] Kümmerle EA, Heger G, *The Structures of C–$Ce_2O_{3+\delta}$, Ce_7O_{12}, and $Ce_{11}O_{20}$*. Journal of Solid State Chemistry **147** (1999) 485-500.

[29] Sukharevskii B.Y. S, A.M G, A.E Se, *Substitutional-interstitial-vacancy-type solid solutions in coordination crystals*. Sov Phys Crystallogr **25** (1980) 434-439.

[30] McBride JR, Hass KC, Poindexter BD, Weber WH, *Raman and x-ray studies of $Ce_{(1-x)}RE_xO_{(2-y)}$, where RE=La, Pr, Nd, Eu, Gd, and Tb*. Journal of Applied Physics **76** (1994) 2435-2441.

[31] Weidenthaler C, *Pitfalls in the characterization of nanoporous and nanosized materials*. Nanoscale **3** (2011) 792-810.

[32] Speight J Lange's Handbook of Chemistry, 70th Anniversary Edition. (2004). McGraw-Hill Education,

[33] Larachi Fç, Pierre J, Adnot A, Bernis A, *Ce 3d XPS study of composite $Ce_xMn_{1-x}O_{2-y}$ wet oxidation catalysts*. Applied Surface Science **195** (2002) 236-250.

[34] Zhang Z, Lu X, Luo J, Liu Y, Zhang C, *Preparation and characterization of La_2O_3 doped diamond-like carbon nanofilms (I): Structure analysis*. Diamond and Related Materials **16** (2007) 1905-1911.

[35] Reddy GK, Boolchand P, Smirniotis PG, *Sulfur tolerant metal doped Fe/Ce catalysts for high temperature WGS reaction at low steam to CO ratios – XPS and Mössbauer spectroscopic study*. Journal of Catalysis **282** (2011) 258-269.

[36] Creaser DA, Harrison PG, Morris MA, Wolfindale BA, *X-ray photoelectron spectroscopic study of the oxidation and reduction of a cerium(III) oxide/cerium foil substrate*. Catal Lett **23** (1994) 13-24.

[37] Abi-aad E, Bechara R, Grimblot J, Aboukaïs A, *Preparation and characterization of CeO_2 under an oxidizing atmosphere. Thermal analysis, XPS, and EPR study*. Chemistry of Materials **5** (1993) 793-797.

[38] Trudeau ML, Tschope A, Ying JY, *XPS investigation of surface oxidation and reduction in nanocrystalline $CexLa_{1-x}O_{2-y}$*. Surface and Interface Analysis **23** (1995) 219-226.

[39] Fujimori A, *Mixed-valent ground state of CeO_2*. Physical Review B **28** (1983) 2281.

[40] Teterin YA, Teterin AY, Lebedev AM, Utkin IO, *The XPS spectra of cerium compounds containing oxygen*. Journal of Electron Spectroscopy and Related Phenomena **88-91** (1998) 275-279.

[41] Orge CA, Órfão JJM, Pereira MFR, *Catalytic ozonation of organic pollutants in the presence of cerium oxide–carbon composites*. Applied Catalysis B: Environmental **102** (2011) 539-546.

[42] Barr TL, Fries CG, Cariati F, Bart JCJ, Giordano N, *A spectroscopic investigation of cerium molybdenum oxides*. Journal of the Chemical Society, Dalton Transactions (1983) 1825-1829.

[43] Zhang J, Ju X, Wu ZY, Liu T, Hu TD, Xie YN, Zhang ZL, *Structural characteristics of cerium oxide nanocrystals prepared by the microemulsion method*. Chemistry of Materials **13** (2001) 4192-4197.

[44] Rodriguez JA, Hrbek J, Kuhn M, Sham TK, *Interaction of oxygen with lithium-gold and cesium-gold films: a photoemission and thermal desorption study*. Journal of Physical Chemistry **97** (1993) 4737-4744.

[45] Gopinath CS, Hegde SG, Ramaswamy AV, Mahapatra S, *Photoemission studies of polymorphic $CaCO_3$ materials*. Materials Research Bulletin **37** (2002) 1323-1332.

[46] Peng XD, Richards DA, Stair PC, *Surface composition and reactivity of lithium-doped magnesium oxide catalysts for oxidative coupling of methane*. Journal of Catalysis **121** (1990) 99-109.

[47] Zhang X, He D, Zhang Q, Xu B, Zhu Q, *Comparative studies on direct conversion of methane to methanol/formaldehyde over La–Co–O and ZrO_2; supported molybdenum oxide catalysts*. Topics in Catalysis **32** (2005) 215-223.

[48] Dubois J.-L. BM, Mimoun H., Cameron C.J. , *The oxidative coupling of methane over alkali, alkaline earth, and rare earth oxides*. Chemistry Letters **19** (1990) 967.

[49] Zhang X, He DH, Zhang QJ, Xu BQ, Zhu QM, *Selective oxidation of methane to methanol using molecular oxygen on*

$MoOx/(LaCoO_3+Co_3O_4)$ catalysts. Chinese Chemical Letters **14** (2003) 1066-1069.

[50] Islam MS, Ilett DJ, Parker SC, *Surface structures and oxygen hole formation on the La_2O_3 catalyst. A computer simulation study*. Journal of Physical Chemistry **98** (1994) 9637-9641.

[51] Binet C, Badri A, Lavalley JC, *A spectroscopic characterization of the reduction of ceria from electronic transitions of intrinsic point defects*. Journal of Physical Chemistry **98** (1994) 6392-6398.

[52] Dedov AG, Loktev AS, Menshchikov VA, Kartasheva MN, Parkhomenko KV, Moiseev II, *The unusual ceria promoting influence on methane oxidative coupling catalysts*. Doklady Akademii Nauk **380** (2001) 791-795.

PART III

SUPPORTED CATALYSTS FOR THE OXIDATIVE COUPLING OF METHANE

5 Effect of Ce on Na_2WO_4/SiO_2 for the oxidative coupling of methane

Cerium is one of the rare earth metals used as doping agent in active and selective catalysts towards C_2 hydrocarbons. In this Chapter, Xwt%Ce-5wt%Na_2WO_4 /SiO_2 catalysts powders (X= 0, 2, 5 and 7) were synthesised. Then, the obtained catalyst powders were characterised and tested in the OCM reaction. Both DRIFT and XRD spectroscopy techniques were applied to detect phases of SiO_2 and formed metal species on the catalyst surface. In addition, TPR was used to analyse the interaction of metals and support. Results revealed that the addition of Ce affects the crystallization degree of SiO_2, which plays an important role in the OCM reaction. On the other hand, it was concluded that 5 wt%Ce seems to be the optimal concentration to obtain a mix of amorphous and α-crystobalite SiO_2 to provide higher activity and C_2 hydrocarbon selectivity.

5.1 Introduction

C_2 hydrocarbons, especially C_2H_4, can be used for production of petrochemicals and fuels [1-4]. On the other hand, methane is the main component of natural gas found in large world reservoir areas. The OCM is one of the best methods for the direct conversion of methane to higher hydrocarbons [5]. Methane conversion via OCM is a direct and exothermic process not limited by any thermodynamic constraints (Eq. 5.1) [2]. Nevertheless, the partial and total oxidation of CH_4 is favoured from a thermodynamic point of view, as shown in Eqs. 5.2 and 5.3.

$$CH_4 + 1/4O_2 \rightarrow 1/2C_2H_6 + 1/2H_2O \quad \Delta G° = -76 \text{ kJ mol}^{-1} \qquad 5.1$$

$$C_2H_6 \rightarrow C_2H_4 + 2\,H_2 \quad \Delta G° = -115 \text{ kJ mol}^{-1} \qquad 5.2$$

$$CH_4 + 1/2O_2 \rightarrow CO + 2H_2O \quad \Delta G° = -544 \text{ kJ mol}^{-1} \qquad 5.3$$

$$CH_4 + 2O_2 \rightarrow CO_2 + 2H_2O \quad \Delta G° = -801 \text{ kJ mol}^{-1} \qquad 5.4$$

This thermodynamic disadvantage, and the lack of an active, selective and stable catalyst, are the main reasons why, up to now, an economically viable process has not still been put into practice [6,1,7,8].

Among the many catalysts used in OCM, Li/MgO catalyst was intensely investigated, but its strong and fast deactivation prevents its industrial application [9,10]. In contrast, the Mn-Na_2WO_4/SiO_2 catalyst system is one of the very few suitable OCM catalysts which have demonstrated to achieve the required performance for possible industrial application [11-18]. Preparation methods [12,13,19], structure activity relationship [20-24], active centre & reaction mechanism [11,25,26] and additives [27-29] have been some of the studied subjects to drive progresses in the Mn-Na_2WO_4/SiO_2 catalyst system performance. On the other hand, variation of composition, such as substitution of Mn or support, is also an important subject to understand the relationships between bulk properties, surface properties and the performance in the OCM reaction. Thus, the catalytic performance and structural features for Na_2WO_4/SiO_2 doped with V, Cr, Mn, Fe, Co and Zn was investigated [30,31]. In both works, it was concluded that catalyst containing Mn oxide presented the best OCM performance, and the authors, attributed this finding to moderate interaction between Mn oxide-tungstate components. This interaction affects and controls the redox

properties of Mn oxide, tungstate and efficient oxygen spillover, which are important properties for a better performance in this type of catalyst.

On the other hand, Zeinab Gholipour et al. [32] carried out an experiment in which two different promoters were used, namely Mn and Ce. They reported similar textural, redox and catalytic properties which seem to be responsible for a similar O_2 and CH_4 activation sites. In other works, Ce as well as other components, such as Sn, La, S, P and Zr [29,33,34] were used as doping agents in the Mn-Na_2WO_4/SiO_2 catalyst [28]. They did not improve substantially the catalytic performance, which would increase the cost and a more complex system. In addition, it should be noted that SiO_2, particularly commercial SiO_2, is the support commonly used in all these works. Additionally, others supports also have been used giving a similar performance [35,36].

In general, it can be said that the Mn-Na_2WO_4/SiO_2 catalyst is a very complex system itself, and therefore, the support material with a variety of different materials, concentration, composition, or SiO_2 precursor is still under investigation to accomplish an optimal catalyst. Thus, based in the textural, redox and catalytic properties of Ce to promote catalysts for the OCM, three wt%Ce (2, 5 and 7) on 5wt%Na_2WO_4/SiO_2 were studied in this work. To this end, a SiO_2 support was synthesised in-house from tetraethylorthosilicate precursor and, therefore, commercial SiO_2 was not used as support in contrast previously to published works [25,32,37,30]. The incipient wetness impregnation method was used to prepare the catalyst powders. DRIFT and XRD spectroscopies were applied to study the effect of Ce on the degree crystallisation in amorphous SiO_2. In addition, TPR was used to study the reducibility of different metal oxide species on SiO_2 in the presence of H_2. The effect of Ce content on Na_2WO_4/SiO_2 was studied following the CH_4 conversion, C_2 selectivity and yield in the temperature range of 600-850 ^oC.

5.2 Experimental section

5.2.1 Catalyst preparation

Catalyst preparation was carried out in two steps, namely synthesis of SiO_2 support and the preparation of the catalyst powders. The synthesis of SiO_2 support was carried out following a procedure similar to that reported by

Wang et al. [38] which allows to obtain amorphous silica. A solution of H_2O (0.7 mL), ethanol (30 mL) and tetraethylorthosilicate 6 mL (99% Aldrich TEOS) was prepared at room temperature. Then, 10 mL of NH_4OH (25 % aqueous solution) containing 0.16 g of citric acid was added into the homogenous solution during 2 h under stirring at 300 rpm until a gel was obtained. The precipitate was washed in an up-flow mode system [39] as shown in Figure 5.1 using distilled water (50 mL min^{-1}) for 8 h. The material was dried overnight in an oven at 120 ^oC and finally the product was calcined at 500 ^oC for 2 h to obtain the SiO_2 support.

In the second step, the catalyst powder Xwt%Ce-5wt%Na_2WO_4/SiO_2 (X=0, 2, 5 and 7) was prepared by the incipient wetness impregnation method. This latter is a classic method used for catalyst preparation [28,40,32,41], which consists in the support impregnation with precursor solutions. These solutions contain salts of precursor agents, preferably anions, which may be eliminated easily by washing (chlorates, sulphates) or by decomposition at low temperatures (nitrates, carbonates). The required volume of solution to impregnate the support corresponds to the necessary quantity to fill the pore volume.

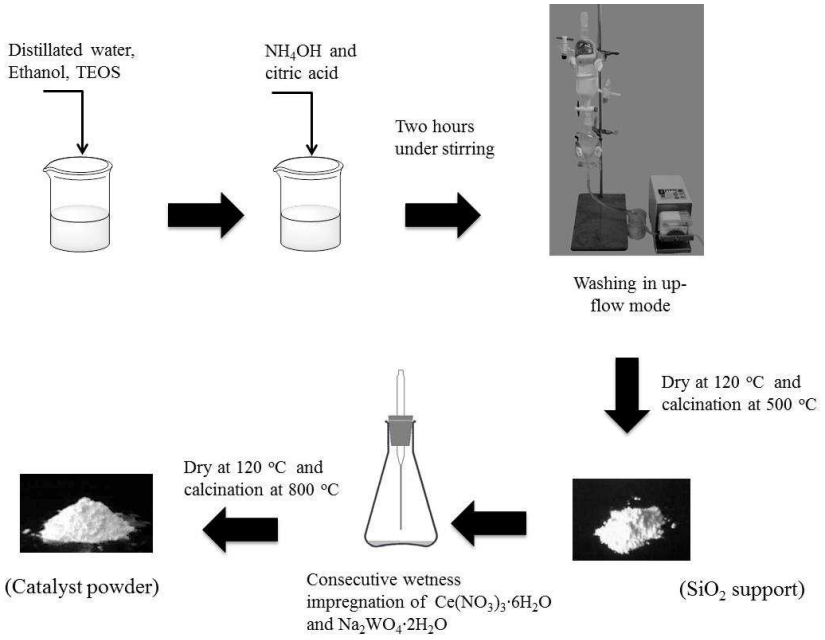

Figure 5.1 Schematic representation of the catalyst powder preparation.

This technique allows to obtain a uniform distribution of the metallic precursor on the support. The method was performed using aqueous solutions of $Ce(NO_3)_3 \cdot 6H_2O$ (99% Aldrich) and $Na_2WO_4 \cdot 2H_2O$ (99% Riedel-deHaën) in the appropriate concentration. Finally, the catalyst powders were dried at 120 °C after each impregnation overnight, followed by calcination at 800 °C for 8 h (see Figure 5.1).

5.2.2 Catalyst characterisation

As mentioned above, silica phases in presence of Ce and/or Na_2WO_4 were detected by Diffuse Reflectance Infrared Fourier Transform (DRIFT) spectroscopy. Then, the interactions with the SiO_2 support were studied by TPR technique and finally, phases present in the 5wt%Ce-5wt%Na_2WO_4/SiO_2 catalyst were identified by X-Ray Diffraction (XRD).

DRIFT spectroscopic analyses of the solid materials were done on a Nicolet 510P FTIR Spectrometer, with a KBr beam splitter for mid-IR range and an deuterated tri-glycine sulfate pyroelectric detector (DTGS) with KBr windows equipped with a special beam collector (COLLECTOR from SpectraTech), fixed on a plate for consistent experimental conditions. The collection angle is a full pi steradian, collecting a maximum 50% of the available diffuse energy and reducing the spot size of the FTIR beam by 1/6. When required, the specular component was dealt with the blocker device, which minimises distortion. The instrument was always purged with dry air, which was passed through a filter to partially remove CO_2 and moisture (Balston air purifier with filter). Samples were ground and "diluted" with KBr powder, with pure KBr powder used as the blank. Then the samples were used in a micro-cup and spectra taken at room temperature. Spectra were collected at 4 cm^{-1} resolution with 256 scans. The instrument software (OMINC) converted the interferograms to equivalent absorption units in the Kubelka–Munk scale.

Temperature programmed reduction (TPR) experiments were carried out in an Altamira Instruments (AMI-200) in which a mixture of 5 vol.% H_2/Ar was used, at a total flow rate of 30 $cm^3 min^{-1}$, with 100 mg of catalyst. The temperature was increased at a rate of 5 °C min^{-1} from room temperature to 1000 °C, while the hydrogen consumption was monitored. Finally, the X-ray diffraction (XRD) pattern of the fresh 5Ce-5Na_2WO_4/SiO_2 catalyst powder

was recorded on a Philips PW 1710 instrument using Ni-filtered Cu Kα radiation.

5.2.3 Catalyst evaluation

The catalytic performance of the prepared catalyst powder for the oxidative coupling of methane was studied in two quartz tube reactors which are denoted in this Chapter as AR and BR. A scheme of AR (i.d= 25 mm) was previously shown in Figure 2.2. Unlike AR, BR has an i.d of 10 mm and a porous disc to hold the catalyst (see Figure 5.2).

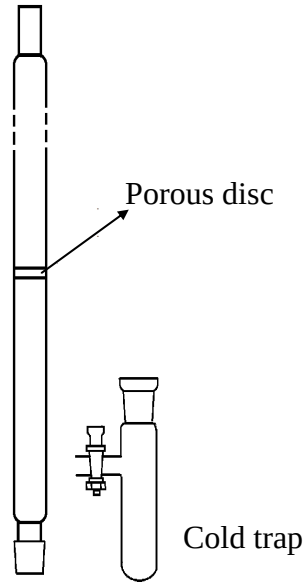

Figure 5.2 Quartz tube reactor (i.d=10 mm) with porous disc.

The oxide catalyst (mass=0.2 g) is placed inside the quartz tube reactor (AR or BR). Then, this latter is located into an electrical heater as shown in Figure 2.3. Methane, helium and oxygen flow rates were regulated by mass flow controllers (HI-TEC). The mixture of methane and oxygen (CH_4/O_2 molar ratio of 4) diluted in Helium (75% of the total flow) was passed through the catalyst bed with a total flow rate of 50 cm^3 min^{-1}. A cold trap was placed at the outlet of the quartz tube to separate any condensed water vapour from the reaction products. The OCM study started when the temperature reached 600 °C. The product stream containing carbon monoxide, carbon dioxide, ethane, ethylene, unreacted oxygen and methane

was analysed by an on-line gas chromatograph (GC) equipped with a thermal conductivity (TC) detector, using a capillary column (Carboxen 1010 Plot. Supelco). It was assumed that carbon and /or hydrogen in methane were only converted into ethane, ethylene carbon monoxide, carbon dioxide and/or molecular hydrogen and water. The conversion of CH_4, the C_2 selectivity and yield of the products were defined, respectively, as shown in section 2.2.3 (Eqs. 2.1-2.3).

5.3 Results and discussion

5.3.1 Characterisation

5.3.1.1 Diffuse reflectance infrared Fourier transform (DRIFT)

DRIFT spectra in the range of 1190-583 cm^{-1} of fresh catalysts are shown in Figures 5.3. It is known that peaks of α-crystobalite SiO_2 are around 1140, 1079, 793, 619 cm^{-1} [32,37].

The DRIFT bands of α-crystobalite SiO_2 are present in the 5wt%Na_2WO_4/SiO_2 catalyst (1149, 1075, 798 and 624 cm^{-1}). As mentioned in section 5.2.1, the calcination temperature of the catalysts was of 800 ^oC. This latter and the presence of Na_2WO_4 could lead the transformation of amorphous to crystalline α-cristobalite silica. This would be consistent with the literature, since transformation of amorphous silica to highly crystalline α-cristobalite occurs around 800-900 ^oC in the presence of an alkali like Na_2WO_4 acting as the mineralising agent [42,20,43].

Comparison with the DRIFT spectra of catalysts containing Ce (Figure 5.3b-d) revealed that the presence of Ce shifts the bands in the DRIFT spectra. A shift from 798 cm^{-1} to 802 cm^{-1} can be observed in the catalysts. This latter could be attributed to the presence of amorphous silica, which exhibits a wavenumber around 801 cm^{-1} [32]. Similarly, a slight shift is also observed from 624 cm^{-1} to higher wavenumber (629 cm^{-1}), suggesting that the interactions of the metal tungstate, cerium and α-crystobalite SiO_2 are strong in the catalyst. On the other hand, shifts occur in the bands in the range 1183-1000 cm^{-1}.

The band at 1145 cm^{-1} disappears with increasing Ce and the band at 1075 shifts to a lower wavenumber (1048 cm^{-1}) in the catalysts containing 2 and 7 wt%Ce (Figure 5.2b and d). It has been reported in literature that addition

of Ce to this type of catalyst can inhibit the crystallisation of α-cristobalite silica possibly because of interaction between Na_2WO_4 and support [28].

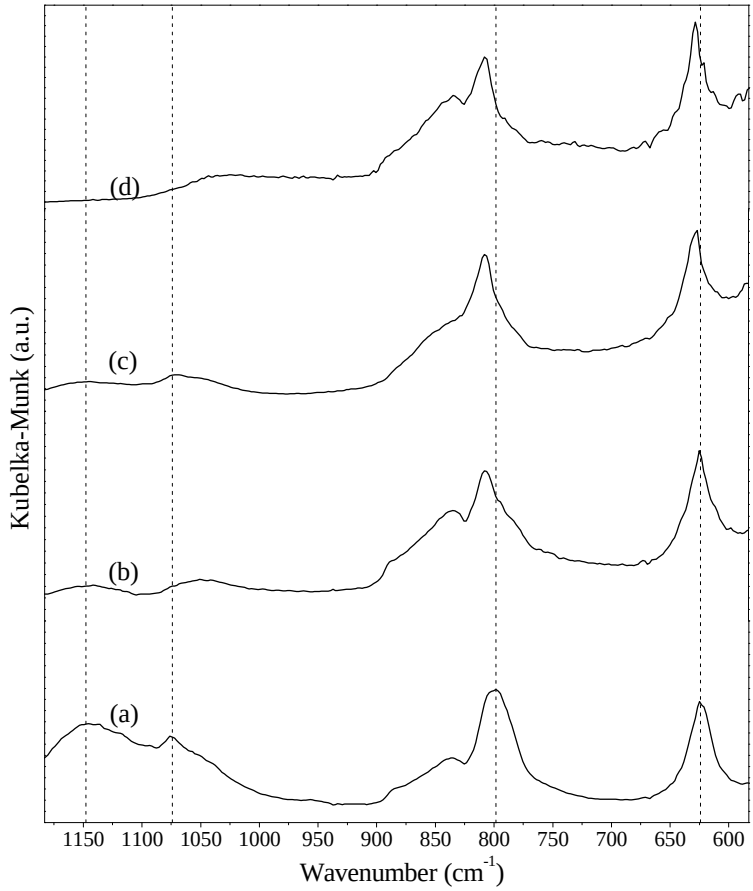

Figure 5.3 DRIFT spectra of the catalysts of Xwt%Ce-5wt%Na_2WO_4/SiO_2. (a) X=0, (b) X=2, (c) X=5 and (d) X=7. As typical for the DRIFTS technique, intensities are expressed in Kubelka–Munk units to correct for diffuse reflectance distortions that would otherwise appear in the absorption presents in the spectra [44].

Therefore, DRIFTs results suggest a close interaction of Ce with Na_2WO_4 and silica support, affecting the degree of crystallinity in α-cristobalite which would agree with observed interference with catalyst crystallization in (Na+Ce)/SiO_2 samples reported in literature [32,45].

5.3.1.2 Temperature programmed reduction (TPR)

As mentioned above, the technique of temperature programmed reduction was used to analyse the interaction of metals and support on the catalysts Xwt%Ce-5wt%Na_2WO_4/SiO_2 (X=0, 2, 5, and 7). Their profiles are shown in Figure 5.4, which show broad TPR patterns between 200 and 1000 ^oC. It can be observed that TPR patterns corresponding to the Xwt%Ce-5wt%Na_2WO_4/SiO_2 catalysts are similar to 5wt%Na_2WO_4/SiO_2. However, some differences can be detected.

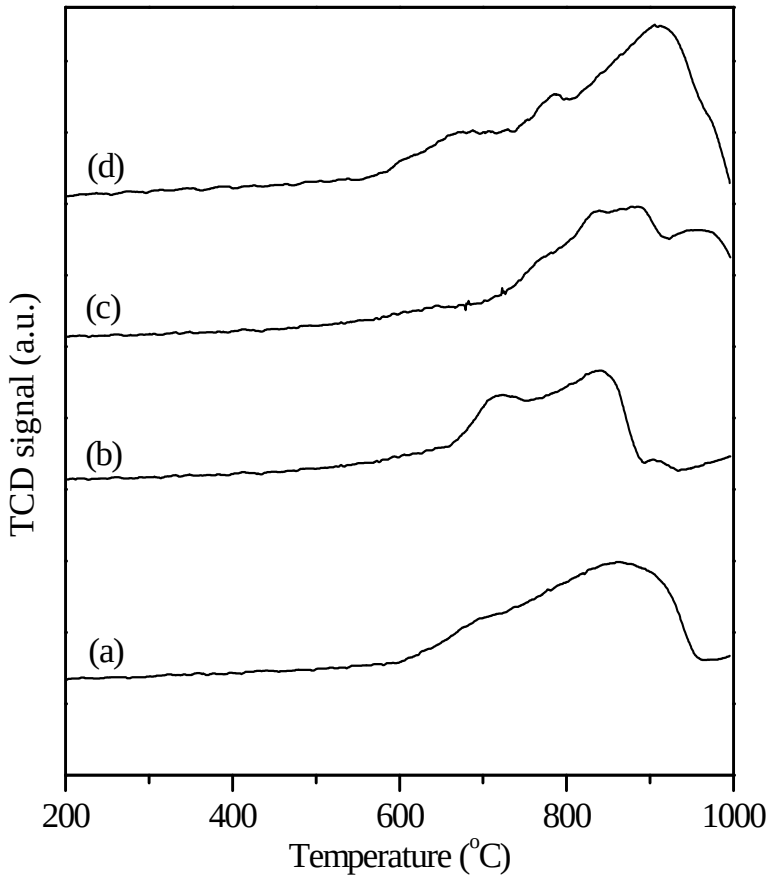

Figure 5.4 TPR profiles of the catalysts Xwt%Ce-5wt%Na_2WO_4/SiO_2. (a) X=0, (b) X=2, (c) X=5 and (d) X=7.

The TPR pattern of the catalyst containing 7 wt% of Ce is completed around of 1000 ^oC and has three peaks at 670, 786 and 900 ^oC. The TPR profile of catalyst containing 5wt% of Ce is not completed at 1000 ^oC and its TPR profile revealed peaks around 772, 883, 890 and 958 ^oC. In the case of 2

wt%Ce (Figure 5.4b), its TPR profile shows two peaks at 716 and 839 ^{o}C. These results suggest an important interaction of Ce with Na-W species. It seems that addition of a small amount (2wt%Ce) decreases the reduction temperature of Na-W species. This could be attributed to a suitable dispersion of such species. However, this is different when compared to the catalysts containing 5 and 7 wt%Ce. The fact that a higher reduction temperature in the case of 5wt%Ce (Figure 5.4c), compared to Na_2WO_4/SiO_2, suggests the possible formation of other species on the support surface. A similar interpretation can be given to the case of 7 wt%Ce (Figure 5.4d). However, a higher amount of consumed hydrogen can be observed with a peak at high temperature (around 900 ^{o}C) indicating the possible reduction of bulk oxygen in CeO_2 species formed on the support.

5.3.1.3 X-Ray Diffraction (XRD)

The XRD spectrum of catalyst 5wt%Ce-5wt%Na_2WO_4/SiO_2 is shown in Figure 5.5. According to Joint Committee on Powder Diffraction Standards (JCPDS), the presence of α-cristobalite SiO_2, CeO_2 and Na_2WO_4 was identified. In addition, amorphous silica could be identified by a wide peak (2θ = 15-25 º) following a similar trend as the base line of the diffractogram shown in Figure 5.5 which agrees with a similar broad halo of amorphous silica reported by Lee et al. [46]. This result would indicate the presence of amorphous silica together with α-cristobalite SiO_2, which would be consistent with obtained DRIFT results, suggesting that part of the amorphous SiO_2 support did not crystallize into α-cristobalite during the calcination process, i.e., amorphous features remain after the calcination of silica support in presence of Ce.

Therefore, DRIFT, TPR and XRD results would indicate different interactions between Ce and the other components in the Xwt%Ce-5wt%Na_2WO_4/SiO_2 catalysts. In addition, results suggest that adding Ce to Na_2WO_4/SiO_2 would affect in crystallinity degree in α-cristobalite. In fact, Ce is suggested as a crystallization inhibitor [32]. On the other hand, it was reported that amorphous SiO_2, with and without Na, is basically a total oxidation catalyst and the phase transition to α-cristobalite was considered as inert [47]. Therefore, based in the characterization results obtained in this work and in all those aspects found in literature, the preparation of a catalyst Ce-Na_2WO_4/SiO_2 with higher activity and selectivity towards C_2

hydrocarbons depends of the type of silica support and the appropriate amount of Ce added to Na_2WO_4/SiO_2.

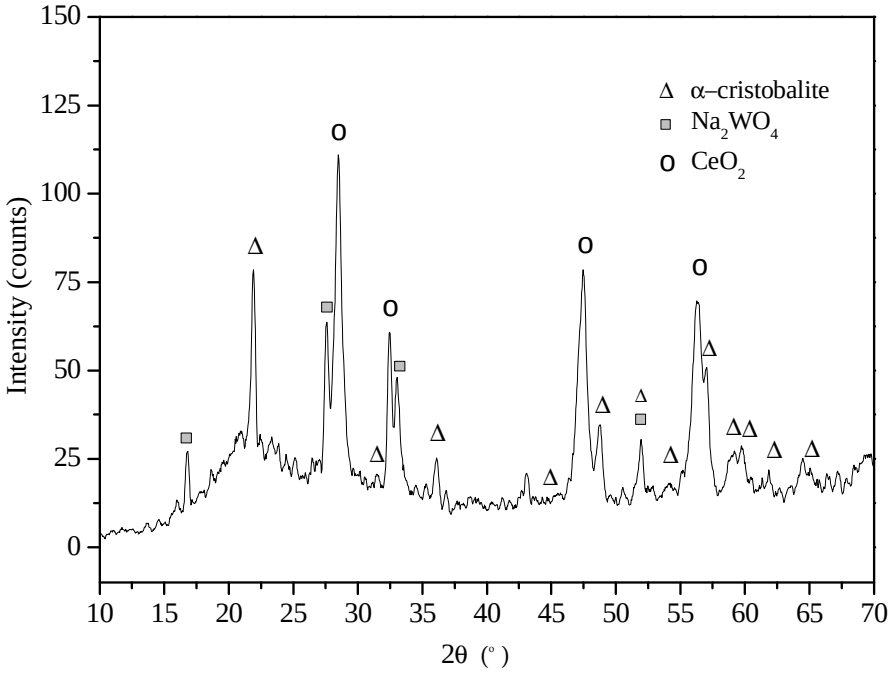

Figure 5.5 XRD pattern of 5Ce-5Na_2WO_4/SiO_2 catalyst.

5.3.2 Catalytic tests

5.3.2.1 Preliminary catalytic tests

The 5wt%Ce-5wt%Na_2WO_4/SiO_2 catalyst was tested in the OCM reaction using two reactors (AR and BR). The other parameters were maintained (CH_4/O_2=4, total flow=50 cm^{-3}, catalyst mass=0.2 g and composition of He as diluent = 75%). It can be observed in chapter II (section 2.3.2) that selectivity as well as yield of the Ce based oxide catalysts pass through a maximum (750 ^oC) in the temperature range of 600-800 ^oC. Such behaviour was even observed in the catalytic results of the oxide catalysts studied in chapter III and IV. For that reason, in these works the catalytic test results were reported up to 750 ^oC, since all these catalytic tests were performed in AR.

A similar behaviour was observed again when the 5wt%Ce-5wt%Na_2WO_4/SiO_2 catalyst was tested in the OCM reaction using the AR (see Figure 5.6a, b and c). The CH_4 conversion, C_2 selectivity and yield pass

through a maximum in the temperature range of 600-800 ^{o}C. This type of behaviour was discussed above in section 2.3.2. Nevertheless, different limiting mechanisms can lead to different conversion of methane and C_2

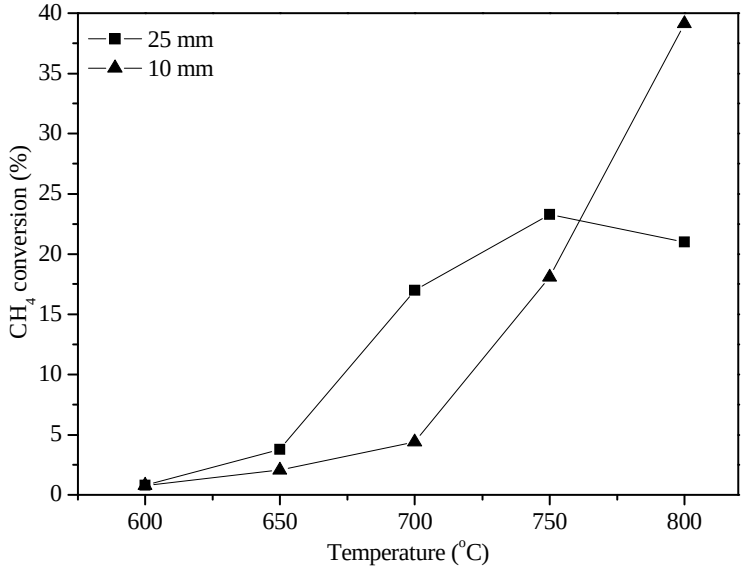

(a)

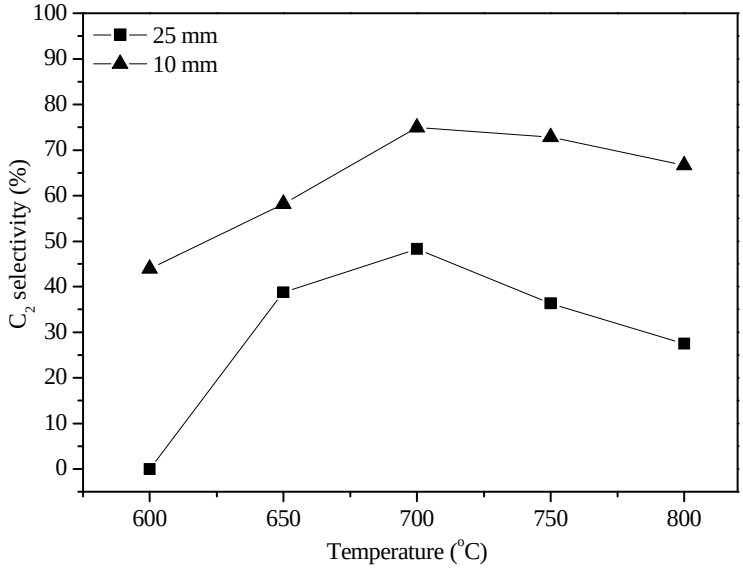

(b)

Figure 5.6 Catalytic performance of the 5Ce-5Na_2WO_4/SiO_2 catalyst at different temperatures using reactors of different inner diameter (25 and 10 mm). (a) CH_4 conversion (b) C_2 selectivity (c) C_2 yield.
Total flow=50 cm^3min^{-1}, CH_4/O_2=4 and $mass_{cat}$: 0.2 g.

selectivity using a smaller inner diameter as seen in Figure 5.6a and b. BR shows higher conversion of methane above 750 ^{o}C when compared to AR, even though total flow and other parameters remain constant for both reactors. On the other hand, higher C_2 selectivity was observed, in the temperature range of 600- 800 ^{o}C when compared to AR.

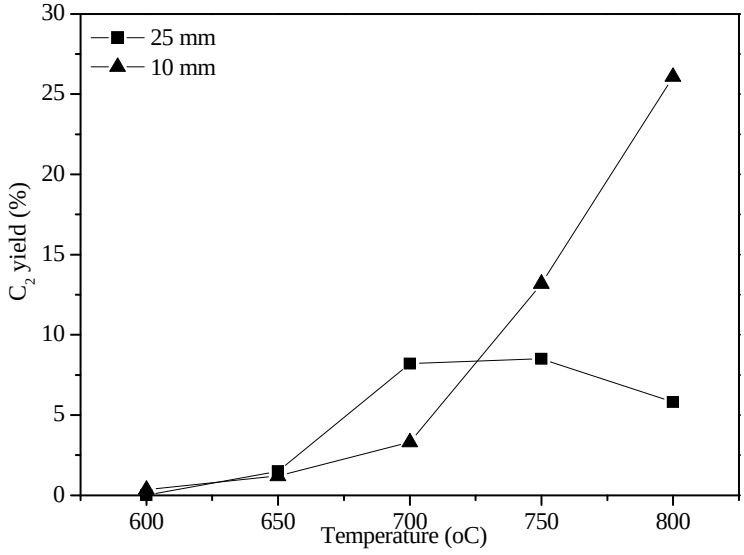

(c)

Figure 5.6 (Cont.) Catalytic performance of the 5Ce-5Na_2WO_4/SiO_2 catalyst at different temperatures using reactors of different inner diameter (25 and 10 mm). (a) CH_4 conversion (b) C_2 selectivity (c) C_2 yield. Total flow=50 cm^3min^{-1}, CH_4/O_2=4 and $mass_{cat}$: 0.2 g.

This latter could be attributed a higher linear rate of gas flow due to the smaller inner diameter of the reactor. The linear flow rate or superficial velocity (v), in cm min^{-1}, can be calculated using the following equation:

$$v = \frac{F}{\pi . R^2} \qquad 5.1$$

Where, F = volumetric flow rate (cm^3 min^{-1}) and R= reactor radius (cm). Therefore, for a F= 50 cm^3 min^{-1} used in both reactors, the superficial velocity in BR is 2.5 times higher than in AR. A gas flow linear rate increase would limit the possibility of deep oxidation of CH_4 and C_2 products. A competition between the combustion reaction in the gas phase and the catalytic reaction on the surface of the catalyst has been reported [2,48,49]. That competition can be controlled by adjusted reaction conditions, and plays an important role for the catalyst performance in the

OCM reaction. Thus, probably a lower inner diameter together with the other used conditions could lead to higher CH_4 conversion and C_2 yield.

5.3.2.2 Effect of Ce content on the catalytic activity at different temperatures

Catalytic tests concerning the effect of Ce content were carried out using BR. The other parameters, such as CH_4/O_2; total flow; catalyst mass; and composition of He as diluent, were maintained in all tests. Thus, Figure 5.7 shows the effect of temperature on CH_4 conversion, C_2 yield and C_2H_4/C_2H_6 ratio over Xwt%Ce-5Na_2WO_4/SiO_2 catalyst with different content of Ce (X= 0, 2, 5 and 7%). It can be observed that both CH_4 conversion and C_2 yield increased with temperature, particularly in the temperature range of 700−800 ^oC. However, in the catalysts containing Ce, the CH_4 conversion and C_2 yield decreased at higher temperature (850 ^oC). A maximum of CH_4 conversion and C_2 yield is then observed at 800 ^oC.

As mentioned in section 2.3.2, it is known that the influence of the temperature on C_2 yield is similar for a large number of investigated catalysts in the OCM reaction. With increasing temperature CH_4 conversions as well as yield pass through a maximum [2,28]. Therefore, the results obtained in this work confirm that the temperature of maximum selectivity is specific for each catalyst and not only depends on the partial pressures of reactants as well as on mixing patterns, but also of reactor type [2]. On the other hand, the C_2H_4/C_2H_6 ratio increased with a rise in temperature. This behaviour was also observed with other catalysts such as $Ca_{0.5}Ce_{0.5}O$ in section 2.3.2. It can be attributed to the homogeneous-heterogeneous pathways of the oxidative coupling reaction, which lead to the oxidative dehydrogenation of ethane (ODE) to produce ethylene [50,51].

It can be observed that catalysts containing Ce revealed higher CH_4 conversion and C_2 yield at 800 ^oC compared to 5wt%Na_2WO_4/SiO_2 catalyst. However, it seems that the amount of Ce has an important role on the performance of Ce-5wt%Na_2WO_4/SiO_2 catalyst. Thus, the maximum performance (CH_4 conv. = 39 % and C_2 yield = 26%) was observed for the catalyst with 5wt%Ce. Moreover, CH_4 conversion and C_2 yield showed to be higher when compared to a similar catalyst found in literature [32] which was studied under similar conditions. On the other hand, the 5wt%Ce-5wt%Na_2WO_4/SiO_2 catalyst showed an acceptable activity and C_2 selectivity

when compared to the Na-W-Mn/SiO_2 catalyst system which is known to have good performance for the OCM studied under different conditions [52,28].

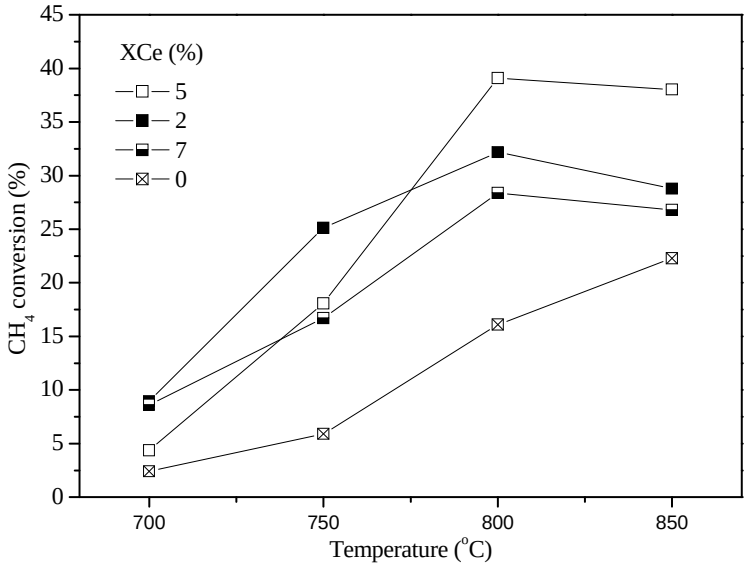

(a)

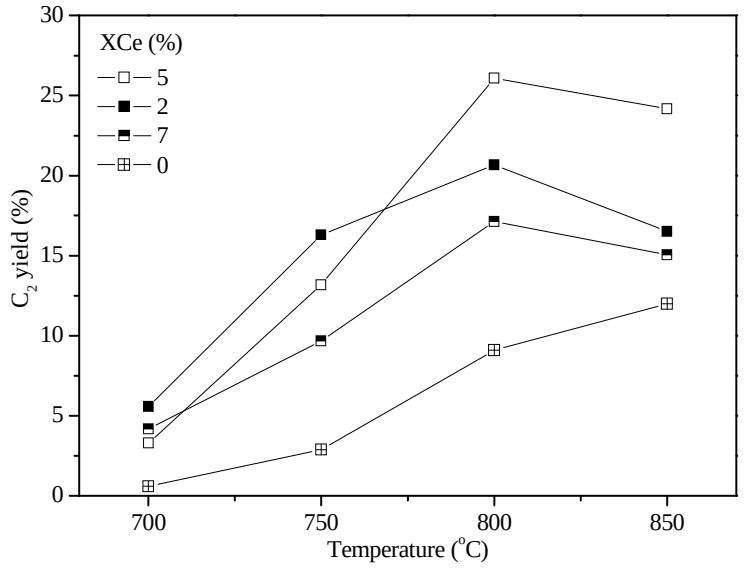

(b)

Figure 5.7 Catalytic performance of the XCe-5Na_2WO_4/SiO_2 catalyst at different temperatures (X= 0, 2, 5 and 7%). (a) CH_4 conversion (b). C_2 yield and (c) C_2H_4/C_2H_6 ratio. Total flow=50 cm^3min^{-1}, CH_4/O_2=4, i.d=10 mm and $mass_{cat}$: 0.2 g.

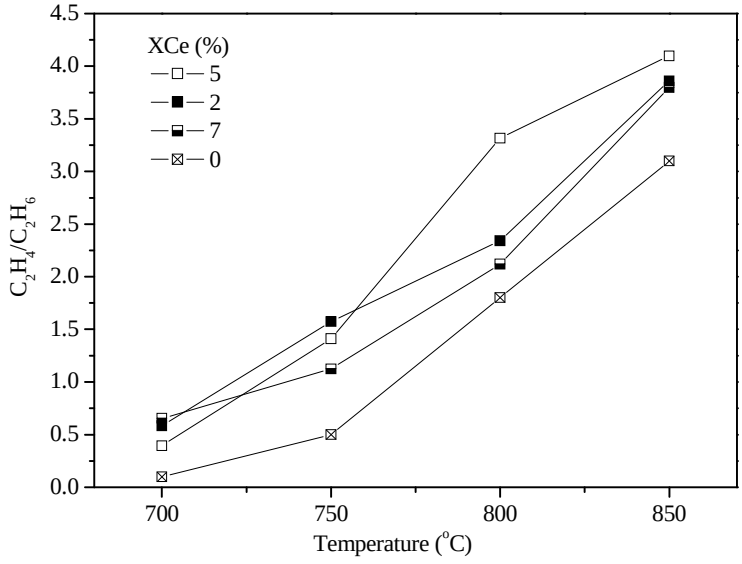

(c)

Figure 5.7 (Cont.) Catalytic performance of the XCe-5Na_2WO_4/SiO_2 catalyst at different temperatures (X= 0, 2, 5 and 7%). (a) CH_4 conversion (b). C_2 yield and (c) C_2H_4/C_2H_6 ratio. Total flow=50 cm^3min^{-1}, CH_4/O_2=4, i.d=10 mm and $mass_{cat}$: 0.2 g.

It has been reported in literature that cerium provides a better OCM performance in monometallic catalysts for the OCM reaction [32], which is attributed to its oxygen storage property to prevent the direct contact of methane and OCM products with gas phase oxygen, known as the pathway for the deep oxidation reactions (Eqs. 2.4-2.7). But cerium is also observed to provide a better OCM performance in a well-known catalyst (5wt%Na_2WO_4-2wt%Mn/SiO_2) used in OCM [28]. This results from the metal-metal and metal-support interactions, comprising tungstate-silica support and transition metal oxide, which are considered to be essential for the formation of an OCM active/selective catalyst [31]. However, in an other study [32], the [Na_2WO_4 + Ce)]/SiO_2 catalyst (using commercial silica as support) exhibited similar methane activator sites under different conditions, attributed to similar textural, redox and catalytic properties compared to [Na_2WO_4 + Mn)]/SiO_2, around 30 and 21% of CH_4 conversion and C_2 yield, respectively.

In this work, it was shown that using a suitable amount of Ce together with 5wt%Na_2WO_4 on synthetized SiO_2 led to higher CH_4 conversion and C_2

yield when compared to the results reported in literature [32]. The catalytic results obtained here can be explained in terms of the characterization obtained from DRIFTs, TPR and XRD techniques. As mentioned above, they suggest that the presence Ce affects the crystallinity degree of α-cristobalite. Therefore, the appropriate amount of Ce (around 5Wt%Ce) would minimise Ce inhibition of α-cristobalite SiO_2 crystallisation, creating a mix consisting on amorphous SiO_2 and α-cristobalite. Thus, the formation of an OCM active/selective catalyst can be due to tungstate-silica and tungstate-metal oxide interactions which occur during the crystallization process.

5.4 Conclusions

Oxidative coupling of methane was studied using 5wt%Ce-5wt%Na_2WO_4/SiO_2 catalyst in which the amount of Ce was varied in three concentrations (2, 5 and 7 wt%). DRIFT and XRD results revealed that the content of Ce affects the crystallization degree of amorphous SiO_2 and the type of formed species on the support, which is the key for a better performance in OCM. The catalyst containing 5wt%Ce showed the best performance, since CH_4 conversion and C_2 yield presented a maximum values (39 and 26 %, respectively) in the temperature range of 700-850 ^oC.

This work shows that the 5wt%Ce-5wt%Na_2WO_4/SiO_2 catalyst is adequate for the OCM reaction, due to its acceptable activity and selectivity when compared to those found in literature, which makes it a good catalyst to study under different operating conditions, and in applications where the OCM reaction is used to produce C_2 hydrocarbons.

References

[1] Maitra AM, *Critical performance evaluation of catalysts and mechanistic implications for oxidative coupling of methane*. Applied Catalysis A: General **104** (1993) 11-59.

[2] Mleczko L, Baerns M, *Catalytic oxidative coupling of methane—reaction engineering aspects and process schemes*. Fuel Processing Technology **42** (1995) 217-248.

[3] Lunsford JH, *The Catalytic Oxidative Coupling of Methane*. Angewandte Chemie International Edition in English **34** (1995) 970-980.

[4] Lunsford JH, *Catalytic conversion of methane to more useful chemicals and fuels: a challenge for the 21st century*. Catalysis Today **63** (2000) 165-174.

[5] Keller GE, Bhasin MM, *Synthesis of ethylene via oxidative coupling of methane: I. Determination of active catalysts*. Journal of Catalysis **73** (1982) 9-19.

[6] Methane conversion by oxidative processes : fundamental and engineering aspects / edited by E.E. Wolf. Van Nostrand Reinhold catalysis series, Van Nostrand Reinhold, Edited by, New York (1992)

[7] Zhang Z, Verykios XE, Baerns M, *Effect of electronic properties of catalysts for the oxidative coupling of methane on their selectivity and activity*. Catalysis Reviews **36** (1994) 507-556.

[8] Alvarez-Galvan MC, Mota N, Ojeda M, Rojas S, Navarro RM, Fierro JLG, *Direct methane conversion routes to chemicals and fuels*. Catalysis Today **171** (2011) 15-23.

[9] Arndt S, Laugel G, Levchenko S, Horn R, Baerns M, Scheffler M, Schlögl R, Schomäcker R, *A Critical Assessment of Li/MgO-Based Catalysts for the Oxidative Coupling of Methane*. Catalysis Reviews **53** (2011) 424-514.

[10] Arndt S, Simon U, Heitz S, Berthold A, Beck B, Görke O, Epping JD, Otremba T, Aksu Y, Irran E, Laugel G, Driess M, Schubert H, Schomäcker R, *Li-doped MgO From Different Preparative Routes for the Oxidative Coupling of Methane*. Top Catal **54** (2011) 1266-1285.

[11] Li S-B, *Oxidative Coupling of Methane over W-Mn/SiO_2 Catalyst*. Chinese Journal of Chemistry **19** (2001) 16-21.

[12] X.P. Fang, S.B. Li, J.Z. Lin, Chu aYL, *Oxidative coupling of methane on W-Mn catalysts*. Journal of Molecular Catalysis (China) **6** (1992) 427-433.

[13] Fang XP, Li SB, Lin JZ, Gu JF, Yan aDX, *Preparation and characterization of catalyst for oxidative coupling of methane*. Journal of Molecular Catalysis (China) **6** (1992) 255-262.

[14] Lin JZ, Gu JF, Yang DX, Zhang CW, Yang YL, Chu YL, Li aSB, *Stability test of W-Mn/SiO_2 catalyst for oxidative coupling of methane*. Shiyou Huagong **24** (1995) 293-298.

[15] Wang XL, Zhang JN, Yang DX, Zhang CW, Lin JZ, Li aSB, *Oxidative coupling of methane over w-mn/sio2 catalyst in a bench-scale stainless steel fluidized-bed reactor*. Shiyou Huagong **26** (1997) 361-367.

[16] Simon U, Görke O, Berthold A, Arndt S, Schomäcker R, Schubert H, *Fluidized bed processing of sodium tungsten manganese catalysts for the oxidative coupling of methane*. Chemical Engineering Journal **168** (2011) 1352-1359.

[17] Pak S, Qiu P, Lunsford JH, *Elementary Reactions in the Oxidative Coupling of Methane over Mn/Na_2WO_4/$SiO_2$and Mn/Na_2WO_4/MgO Catalysts*. Journal of Catalysis **179** (1998) 222-230.

[18] Liu H, Wang X, Yang D, Gao R, Wang Z, Yang J, *Scale up and stability test for oxidative coupling of methane over Na_2WO_4-Mn/SiO_2 catalyst in a 200 ml fixed-bed reactor*. Journal of Natural Gas Chemistry **17** (2008) 59-63.

[19] Wang J, Chou L, Zhang B, Song H, Zhao J, Yang J, Li S, *Comparative study on oxidation of methane to ethane and ethylene over Na_2WO_4–Mn/SiO_2 catalysts prepared by different methods*. Journal of Molecular Catalysis A: Chemical **245** (2006) 272-277.

[20] Jiang ZC, Yu CJ, Fang XP, Li SB, Wang HL, *Oxide/support interaction and surface reconstruction in the sodium tungstate(Na_2WO_4)/silica system*. The Journal of Physical Chemistry **97** (1993) 12870-12875.

[21] Jones CA, Leonard JJ, Sofranko JA, *The oxidative conversion of methane to higher hydrocarbons over alkali-promoted $MnSiO_2$*. Journal of Catalysis **103** (1987) 311-319.

[22] Sofranko JA, Leonard JJ, Jones CA, *The oxidative conversion of methane to higher hydrocarbons*. Journal of Catalysis **103** (1987) 302-310.

[23] Salehoun V, Khodadadi A, Mortazavi Y, Talebizadeh A, *Dynamics of catalyst in oxidative coupling of methane*. Chemical Engineering Science **63** (2008) 4910-4916.

[24] Palermo A, Holgado Vazquez JP, Lee AF, Tikhov MS, Lambert RM, *Critical influence of the amorphous silica-to-cristobalite phase transition on the performance of $Mn/Na_2WO_4/SiO_2$ catalysts for the oxidative coupling of methane*. Journal of Catalysis **177** (1998) 259-266.

[25] Jiang Z-c, Gong H, Li S-b (1997) Methane activation over Mn_2O_3-Na_2WO_4/SiO_2 catalyst and oxygen spillover. In: Can L, Qin X (eds) Studies in Surface Science and Catalysis, vol Volume 112. Elsevier, pp 481-490.

[26] Jiang Z-C, Feng L-B, Gong H, Wang H-L (1995) Evidence for the Production of Methyl Radicals on the Na_2WO_4/SiO_2 Catalyst Upon Interaction with Methane. In: Bhasin M, Slocum DW (eds) Methane and Alkane Conversion Chemistry. Springer US, pp 45-48. doi:10.1007/978-1-4615-1807-5_5

[27] Chou L, Cai Y, zhang B, Niu J, Ji S, Li S, *CeO_2-Promoted W-Mn/SiO_2 catalysts for conversion of methane to C3-C4 hydrocarbons at elevated pressure*. Chemical Communications **0** (2002) 996-997.

[28] Shahri SMK, Pour AN, *Ce-promoted $Mn/Na_2WO_4/SiO_2$ catalyst for oxidative coupling of methane at atmospheric pressure*. Journal of Natural Gas Chemistry **19** (2010) 47-53.

[29] Chou L, Cai Y, Zhang B, Niu J, Ji S, Li S, *Influence of SnO_2-doped W-Mn/SiO_2 for oxidative conversion of methane to high hydrocarbons at elevated pressure*. Applied Catalysis A: General **238** (2003) 185-191.

[30] Malekzadeh A, Khodadadi A, Abedini M, Amini M, Bahramian A, Dalai AK, *Correlation of electrical properties and performance of OCM $MO_x/Na_2WO_4/SiO_2$ catalysts*. Catalysis Communications **2** (2001) 241-247.

[31] Malekzadeh A, Dalai AK, Khodadadi A, Mortazavi Y, *Structural features of Na_2WO_4–MO_x/SiO_2 catalysts in oxidative coupling of methane reaction*. Catalysis Communications **9** (2008) 960-965.

[32] Gholipour Z, Malekzadeh A, Hatami R, Mortazavi Y, Khodadadi A, *Oxidative coupling of methane over (Na_2WO_4+Mn or Ce)/SiO_2 catalysts: In situ measurement of electrical conductivity*. Journal of Natural Gas Chemistry **19** (2010) 35-42.

[33] Wu J, Zhang H, Qin S, Hu C, *La-promoted Na_2WO_4/Mn/SiO_2 catalysts for the oxidative conversion of methane simultaneously to ethylene and carbon monoxide*. Applied Catalysis A: General **323** (2007) 126-134.

[34] Zheng W, Cheng D, Zhu N, Chen F, Zhan X, *Studies on the structure and catalytic performance of S and P promoted Na-W-Mn-Zr/SiO_2 catalyst for oxidative coupling of methane*. Journal of Natural Gas Chemistry **19** (2010) 15-20.

[35] Liu H, Yang D, Gao R, Chen L, Zhang S, Wang X, *A novel Na_2WO_4–Mn/SiC monolithic foam catalyst with improved thermal properties for the oxidative coupling of methane*. Catalysis Communications **9** (2008) 1302-1306.

[36] Yu ZQ, Yang XM, Lunsford JH, Rosynek MP, *Oxidative Coupling of Methane over Na_2WO_4/CeO_2 and Related Catalysts*. Journal of Catalysis **154** (1995) 163-173.

[37] Mahmoodi, Somayeh;, Ehsani, Reza M, *Effect of Additives on Mn/SiO_2 Based Catalysts on Oxidative Coupling of Methane*. Iran J Chem Chem Eng **30** (2011) 29-36.

[38] Wang L, Tomura S, Ohashi F, Maeda M, Suzuki M, Inukai K, *Synthesis of single silica nanotubes in the presence of citric acid*. Journal of Materials Chemistry **11** (2001) 1465-1468.

[39] Silva AT, Machado B, Gomes H, Figueiredo J, Dražić G, Faria J, *Pt nanoparticles supported over Ce–Ti–O: the solvothermal and photochemical approaches for the preparation of catalytic materials*. J Nanopart Res **12** (2010) 121-133.

[40] Gonçalves RP, Muniz F, Passos F, Schmal M, *Promoting Effect of Ce on the Oxidative Coupling of Methane Catalysts*. Catal Lett **135** (2010) 26-32.

[41] Chua YT, Mohamed AR, Bhatia S, *Oxidative coupling of methane for the production of ethylene over sodium-tungsten-manganese-supported-silica catalyst (Na-W-Mn/SiO_2)*. Applied Catalysis A: General **343** (2008) 142-148.

[42] Wang DJ, Rosynek MP, Lunsford JH, *Oxidative coupling of methane over oxide-supported sodium-manganese catalysts*. Journal of Catalysis **155** (1995) 390-402.

[43] Ji S, Xiao T, Li S, Chou L, Zhang B, Xu C, Hou R, York APE, Green MLH, *Surface WO_4 tetrahedron: the essence of the oxidative coupling of methane over M-W-Mn/SiO_2 catalysts*. Journal of Catalysis **220** (2003) 47-56.

[44] Olinger JM, Griffiths PR, *Effects of Sample Dilution and Particle Size/Morphology on Diffuse Reflection Spectra of Carbohydrate Systems in the Near- and Mid-Infrared. Part I: Single Analytes*. Appl Spectrosc **47** (1993) 687-694.

[45] Trovarelli A, Catalysis by ceria and related materials. Imperial College Press, Edited by, London (2002)

[46] Lee D-W, Ihm S-K, Lee K-H, *Mesoporous silica framed by sphere-shaped silica nanoparticles*. Microporous and Mesoporous Materials **83** (2005) 262-268.

[47] Arndt S, Otremba T, Simon U, Yildiz M, Schubert H, Schomäcker R, *Mn–Na_2WO_4/SiO_2 as catalyst for the oxidative coupling of methane. What is really known?* Applied Catalysis A: General **425–426** (2012) 53-61.

[48] Reyes S, Kelkar CP, Iglesia E, *Kinetic-transport models and the design of catalysts and reactors for the oxidative coupling of methane*. Catal Lett **19** (1993) 167-180.

[49] Reyes SC, Iglesia E, Kelkar CP, *Kinetic-transport models of bimodal reaction sequences—I. Homogeneous and heterogeneous pathways in oxidative coupling of methane*. Chemical Engineering Science **48** (1993) 2643-2661.

[50] Choudhary VR, Mulla SAR, *Coupling of thermal cracking with noncatalytic oxidative conversion of Ethane to Ethylene*. AIChE Journal **43** (1997) 1545-1550.

[51] Chao Z-S, Ruckenstein E, *Noncatalytic and catalytic conversion of ethane over V-Mg oxide catalysts prepared via solid reaction or mesoporous precursors*. Journal of Catalysis **222** (2004) 17-31.

[52] Thien CY, Mohamed AR, Bhatia S, *Process optimization of oxidative coupling of methane for ethylene production using response surface methodology*. Journal of Chemical Technology & Biotechnology **82** (2007) 81-91.

PART IV

ELECTROCATALYTIC SIMULTANEOUS PRODUCTION OF H_2 AND C_2 HYDROCARBONS

6 Effect of steam on the Oxidative Coupling of Methane over $Ca_{0.5}Ce_{0.5}O$, $La_{0.75}Ce_{0.25}O$ and 5wt%Ce-5wt%Na_2WO_4 /SiO_2 catalysts

The OCM reaction can be integrated into a process formed by a single chamber electrolysis cell for the production of H_2 and the simultaneous production of C_2 hydrocarbons from a CH_4 humid atmosphere. However, as occurred with other process of OCM integration which were studied in the past, it is necessary to make additional effort on the development of new catalysts to improve CH_4 conversion, C_2 selectivity, yield and stability of the system. In previous chapters, $Ca_{0.5}Ce_{0.5}O$, $La_{0.75}Ce_{0.25}O$ and 5wt%Ce-5wt%Na_2WO_4 /SiO_2 catalysts showed the best performance when tested on the OCM. However, the behaviour of these catalysts under humid atmosphere is unknown. Thus, this chapter is focused on the effect of steam on the above mentioned catalysts when are operating in the OCM reaction. Results reveal the presence of oxygen species, which were identified by XPS. It seems that steam does not affect the role of O_2^{2-} and O^- species in forming C_2 hydrocarbons. The presence of steam practically does not show any significant improvement in the performance of $Ca_{0.5}Ce_{0.5}O$. However, CH_4 conversion, C_2 selectivity as well as yield increased with the amount of steam over 5wt%Ce-5wt%Na_2WO_4 /SiO_2. This can be attributed to the suppression of the oxidation of CH_4 and C_2 hydrocarbons to form CO_x products. Steam showed to have a poisoning effect over $La_{0.75}Ce_{0.25}O$.

6.1 Introduction

The OCM has received considerable attention since Keller and Bhasin´s work in 1982 [1]. Most researchers have focused their attention on the catalyst efficiency for a possible industrial application. However, an acceptable catalytic performance (CH_4 conversions of 15-30% at C_2 selectivity of 50-80%) was only obtained with a few catalysts [2-7]. In addition, there are other difficulties for the commercialisation of the OCM, such as the high temperatures required (usually > 700 ^oC). These high temperatures increase the deep oxidation of CH_4 and C_2 products which generates a long amount of heat. Thus, some reactors have been designed and used to mix CH_4 with O_2 under safe conditions, and to control the energy generated from the process [8-12]. Membrane reactors are promising technology, with a high potential to enhance selectivity and yield, reducing energy consumption, improving operation safety, and miniaturising the reactor system. Moreover, membrane reactors provide for a better distribution of oxygen, which improves the C2 hydrocarbon yield [11,12].

On the other hand, the type of oxygen supplied to the OCM reaction has also been studied in order to achieve industrially acceptable C_2 hydrocarbon yields. An interesting alternative is the electrochemically supplied oxygen (O^{2-}) by the use of a solid electrolyte membrane reactor (SEMR) [13-16]. This kind of configuration allows to integrate the OCM reaction into other processes, in order to combine the possibility of electrochemical enhancement of C_2 selectivity, with simultaneous generation of electrical power and/or useful products, and to achieve better control over the reaction pathway. Recently, Caravaca et al. [17] introduced a new electrocatalytic concept which integrates a single chamber electrolysis cell for the production of H_2 and the simultaneous production of C_2 hydrocarbons. They used a single chamber solid electrolyte cell in which the electrodes (Pt/YSZ/Ag) are exposed to the same reaction atmosphere (a mixture of CH_4 and H_2O). However, although this system could to produce H_2 and C_2 hydrocarbons simultaneously, a low C_2 yield (7.5 %) was observed at 820 ^oC under a maximum current of - 450 mA.

All these works indicate that the development of catalysts and/or active and selective catalytic electrodes are essential to improve conversion, C_2 selectivity, yield and stability of the reactor. Previous chapters showed the

development of active and selective catalysts towards C_2 hydrocarbons. These catalysts could be used in a system as described by Caravaca et al. [17]. However, although their OCM performance has been evaluated, it is important to know their behaviour in OCM reaction under similar atmosphere ($CH_4 + H_2O$). Thus, the objective of this work is the study of the effect of steam over the best catalysts ($Ca_{0.5}Ce_{0.5}O$, $La_{0.75}Ce_{0.25}O$ and 5wt%Ce-5wt%Na_2WO_4 /SiO_2) to evaluate the viability of their application under similar conditions. To this end, the catalytic tests under humid atmosphere were carried out at the temperature of maximum CH_4 conversion and C_2 selectivity observed in the absence of steam. Surface oxygen species were investigated by X-Ray Photoelectron Spectroscopy (XPS) to explain the effect of steam.

6.2 Experimental section

6.2.1 Catalyst preparation

The catalysts studied in this work, $Ca_{0.5}Ce_{0.5}O$, $La_{0.75}Ce_{0.25}O$ and 5wt%Ce-5wt%Na_2WO_4 /SiO_2, named henceforward as A_{Cat}, B_{Cat} and C_{Cat} respectively, were prepared by different methods. The citrate method was used to prepare the first catalyst, the solvothermal method for the second one and the third catalyst was obtained by incipient wetness impregnation of silica support.

The citrate method has been used in literature to prepare multicomponent oxides [18-21]. It involves the formation of a mixed-ions citrate that due to the three-ligand nature of the citric acid results in a transparent three-dimensional network which allows preparation of highly dispersed mixed oxides from the individual cations in the desired stoichiometric ratio. Thus, A_{Cat} was obtained from $Ce(NO_3)_3 \cdot 6H_2O$ (99% Aldrich) and $Ca(NO_3)_2 \cdot 4H_2O$ (99% Fluka), Figure 2.1 showing schematically the citrate method procedure. The precursors were added to distilled water in the appropriate amounts to obtain a Ca:Ce molar ratio of 1:1. Citric acid was added with a molar ratio of acid/(Ce + Ca) = 1.5. Then, acid conditions were adjusted using HNO_3. The solution was heated up to 80 °C in a paraffin bath under constant stirring to evaporate superfluous water, the volume of the solution decreased and a viscous gel was obtained. The gel was dried at 120 °C overnight to form a spongy material and finally it was calcined at 800 °C during 6 h.

On the other hand, the solvothermal method permits the modification of precipitates, gels or flocculates induced by temperature under aging or ripening in the presence of mother liquor (solvent) [22,23]. Reactions occur at temperatures above their normal boiling points by containing the reaction mixture in a pressure vessel (autoclave) subjected to autogenous pressure [24,25]. The obtained solid is washed, dried and finally calcined at the desired temperature. Thus, B_{Cat} was prepared from $Ce(NO_3)_3 \cdot 6H_2O$ (99% Aldrich) and $La(NO_3)_3 \cdot 6H_2O$ (99% Fluka) precursor solutions in appropriate amounts to obtain a La:Ce molar ratio of 75:25. A solution was prepared by dissolving $La(NO_3)_3 \cdot 6H_2O$ and $Ce(NO_3)_3 \cdot 6H_2O$ in methanol in appropriate amounts to obtain the above mentioned molar ratio. Then, the alkaline conditions were adjusted using KOH (3M). The solution obtained was transferred to a Teflon vessel inserted in the high pressure reactor (Figure 4.1) and heated up to the desired temperature (150 °C) under autogeneous pressure. The solution was then maintained at the above mentioned temperature for 150 min under continuous stirring (300 rpm). The colloidal material obtained was washed with distilled water and dried at 120 °C overnight. The material was calcined at 800 °C during 6 h.

Support SiO_2 was synthesised using a similar method as reported in literature [26]. It consisted in the preparation of a solution mixing H_2O 0.7 mL, ethanol 30 and 6 mL of tetraethylorthosilicate (99% Aldrich TEOS) at room temperature. Then, 10 mL of NH_4OH (25 % aqueous solution) containing 0.16 g of citric acid was added to the homogenous solution during 2 h under stirring at 300 rpm until a gel was obtained. The obtained precipitated was washed in an up-flow mode system as shown in Figure 5.1 using distilled water (50 mL min^{-1}) for 8 h. The material was dried overnight in an oven at 120 ^oC and finally the product was calcined at 500 ^oC for 2 h to obtain the SiO_2 support.

Finally, C_{Cat} was prepared by the incipient wetness impregnation method. This latter is used for the catalyst preparation and consists in the support impregnation (in this case SiO_2) with precursor solutions. These solutions contain salts of precursor agents, preferably anions, which may be eliminated by easily washing (chlorates, sulphates) or decomposition to low temperatures (nitrates, carbonates). The required volume of the solution to impregnate the support corresponds to the necessary quantity to fill the pore volume. This technique allows the uniform distribution of the metallic

precursor on the support. Thus, the method was performed using aqueous solutions of $Ce(NO3)_3 \cdot 6H_2O$ (99% Aldrich) and $Na_2WO_4 \cdot 2H_2O$ (99% Riedel-deHaën) in the appropriate concentration. Finally, the catalyst powders were dried overnight at 120 °C, followed by calcination at 800 °C for 8 h (see Figure 5.1).

6.2.2 Catalyst characterisation

Surface oxygen species on the catalysts were investigated by X-Ray Photoelectron Spectroscopy (XPS) VG Scientific ESCALAB 200A spectrometer. Deconvolution of XPS spectral envelope into the contributions of corresponding surface oxygen species was made using the software XPS-peak to fit the O 1s envelope. For all the computer fits, the XPS peaks were assumed to have 80% Gaussian plus 20% Lorentzian peak shape. The correctness of the analysis method was checked by deconvolution of a simulated peak composed of four single peaks with known binding energy and peak width values.

6.2.3 Catalyst evaluation

The catalytic activity measurements over OCM were carried out with and without the presence of steam. A modification of the experimental setup, presented in previous chapters, was made to achieve this objective. A saturator as shown in Figure 6.1 was placed in the experimental setup adjusting all appropriate pipes, accessories and valves connecting the saturator and the reactor inlet. As mentioned above, the gases (methane, helium and oxygen) were regulated using mass flow controllers (HI-TEC). Water was introduced to feed stream by means of saturator using helium as carrier gas in order to achieve liquid–vapour equilibrium.

The content of water in the reaction mixture was controlled by using the vapour pressure of water at determined temperature in the saturator. All lines placed downstream from the saturator were heated above 100 °C via flexible electric resistances to prevent water condensation. The gases were introduced into the reactor in CH_4:O_2:He molar ratio of 4:1:15 with an overall gas flow rate of 50 cm^3 min^{-1}. All catalytic experiments were studied in a quartz tube reactor of i.d = 10 mm as shown in Figure 5.2 which was filled with 0.2 g of sample.

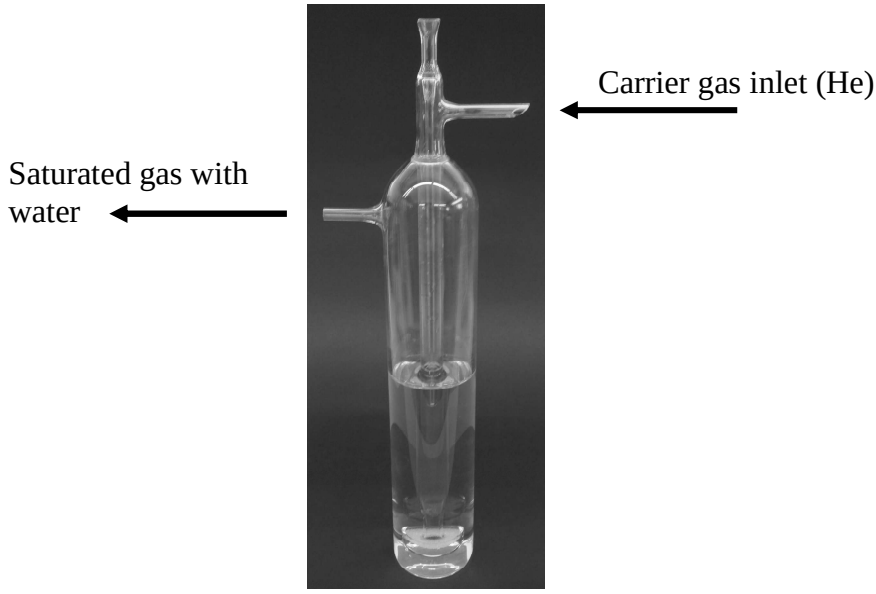

Figure 6.1 Saturator.

A cold trap was placed at the outlet of the quartz tube to separate condensed water vapour from the reaction products. The product stream containing carbon monoxide, carbon dioxide, ethane, ethylene, unreacted oxygen and methane was analysed by an on-line gas chromatograph (GC) equipped with a thermal conductivity (TC) detector, using a capillary column (Carboxen 1010 Plot. Supelco). It was assumed that carbon and /or hydrogen in methane were only converted into ethane, ethylene carbon monoxide, carbon dioxide and/or molecular hydrogen and water. Then, the CH_4 conversion, C_2 selectivity and yield of the products were defined, respectively, as showed in Eqs. 2.1-2.3.

6.3 Results and discussion

6.3.1 Characterisation

In this work, the type of surface oxygen species was the relevant difference found between catalysts. These were identified by applying X-ray photoelectron spectroscopy. The O 1s spectra of A_{Cat}, B_{Cat} and B_{Cat} are shown in Figure 6.3. Such as described in the sections 3.3.1.3 and 4.3.1.3, the spectra corresponding to A_{cat} and B_{cat} were deconvoluted in single peaks corresponding to the different oxygen species which can be assigned to CO_3^{2-} at (531.5~532.5) eV, O_2^{2-} at (530.5 ~ 531.1) eV, O^- at

(530.1~530.2) eV and O^{2-} at (528.0~529.0) eV, the values being summarised in Table 6.1.

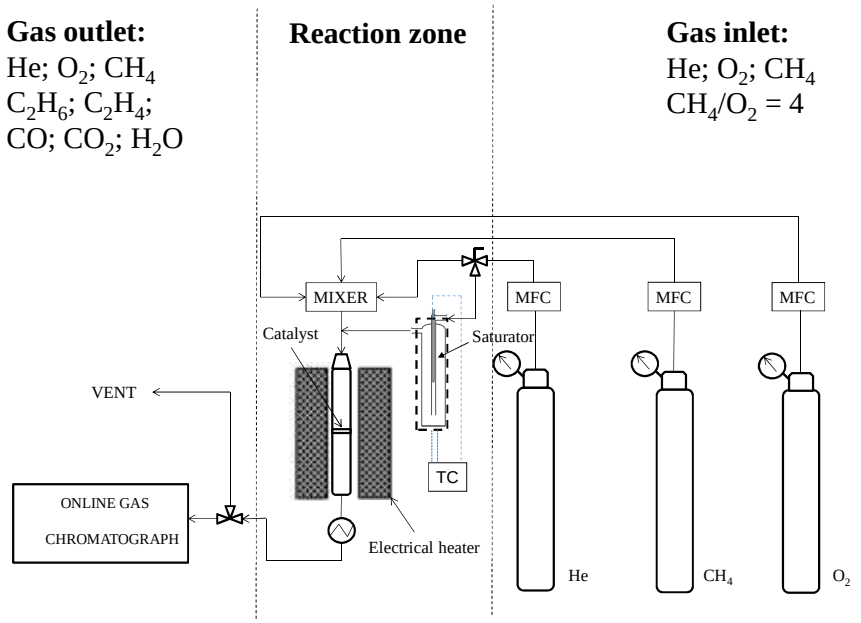

MFC: mass flow controller
TC: Temperature controller

Figure 6.2 Schematic representation of the OCM setup after modification to introduce steam into the reactor.

The fitting of experimental data observed in Figure 6.3 shows the contribution of the aforementioned single species. From reasonable physical meanings, it can be derived that A_{cat} revealed the presence of three oxygen species (O_2^-, O_2^{2-}, and O^{2-}) while, B_{cat} showed to have the O^- and O^{2-} oxygen species.

However, the C_{cat} O1s XPS spectrum only revealed the presence of two peaks. On the one hand, one small peak with binding energy of ca. 529 eV which would correspond to O atom in metal oxides (MO_x) and, on the other hand, another peak of ca. 532.5 eV corresponding to bulk O atom in SiO_2 that is in agreement with literature, since the binding energy between O-Si in SiO_2 has been reported to be in the range of (530-533) eV [27-29]. In other words, the C_{cat} XPS spectrum showed that O_2^-, O_2^{2-} and O^- species are absent (Figure 6.3).

It was reported in Chapters III and IV that the identification of the surface oxygen species O_2^- and O_2^{2-} on A_{cat} and O^- on B_{cat} allowed to explain why these catalysts showed a better performance in the OCM reaction. On the other hand, C_{cat} showed to have the highest performance (see chapter V). This was attributed to the appropriate amount of Ce on the catalyst surface, revealing to play an important role in the crystallisation of α-cristobalite SiO_2 besides the tungstate-metal oxide interactions which occur during crystallisation process, which are important for the OCM. Hence, the above XPS results, showing different oxygen species in the A_{cat} and B_{cat} and the absence of O_2^-, O_2^{2-} and O^- oxygen species in C_{cat} could help to understand the behaviour of catalysts in the OCM in the presence of steam.

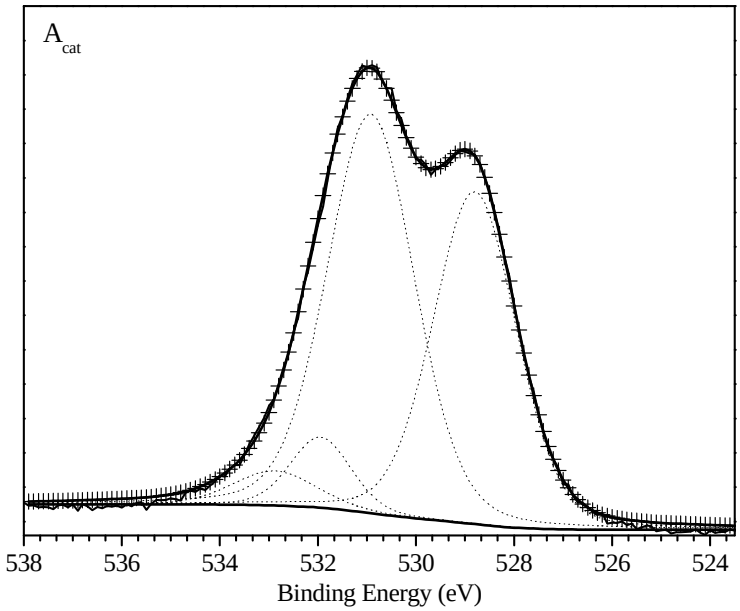

Figure 6.3 O1s binding energy spectra of the various samples, (—) referring to experimental data, (····) showing contribution of single species, (+++) showing the sum of the computer fitted contributions of all single species. (For sample identification see the left upper corner of each spectrum).

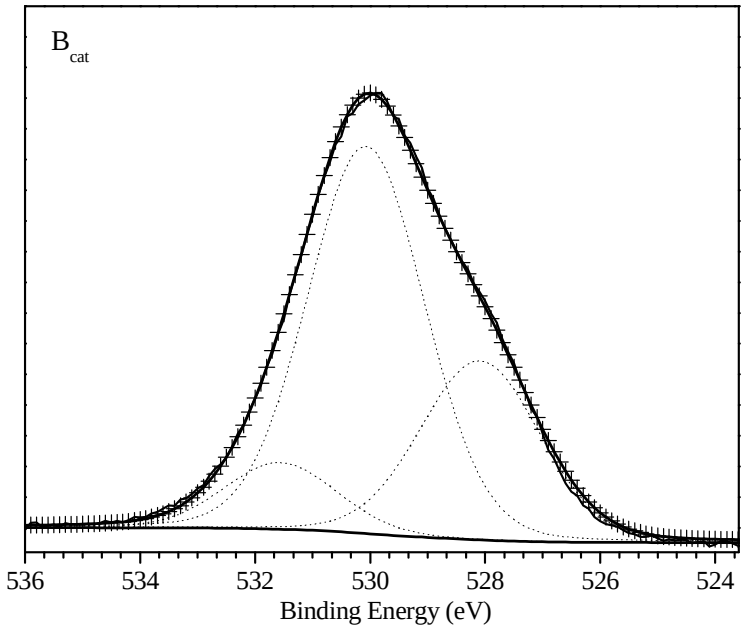

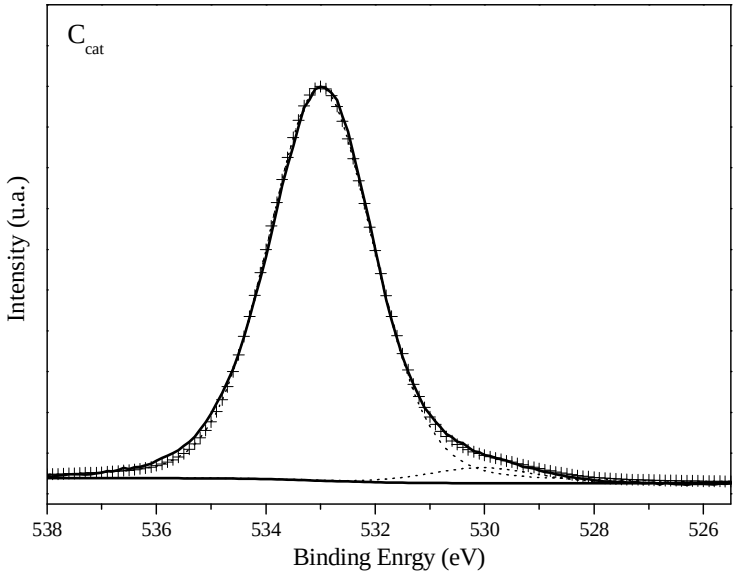

Figure 6.3 (cont) O1s binding energy spectra of the various samples, (—) referring to experimental data, (····) showing contribution of single species, (+++) showing sum of the computer fitted contributions of all single species. (For sample identification see the left upper corner of each spectrum).

Table 6.1 O 1s binding energy from XPS data.

Catalyst	O 1s binding energies (eV) FWHM (between brackets)				
	O^{2-}	O_2^{2-}	O^-	CO_3^{2-}	O_2^-
A_{cat}	528.88 (2.0)	530.93 (2.0)	----	532.00 (1.9)	533.05 (2.0)
B_{cat}	528.09 (2.5)	----	530.07 (2.4)	531.56 (2.0)	----
C_{cat}	532.7 (2.2) 529.1 (2.2)	----	----	----	----

6.3.2 Catalytic tests

6.3.2.1 Effect of temperature in the absence of steam

The effect temperature on OCM was studied over A_{cat} and B_{cat} without steam. Figure 6.4 shows the CH_4 conversion, C_2 selectivity and yield in the temperature range of 650-850 ^oC. It can be observed that CH_4 conversion is similar in both catalysts (A_{cat} and B_{cat}). However, A_{cat} revealed higher C_2 selectivity and yield than B_{cat}, passing by a maximum at temperature of 750 ^oC. This behaviour was also observed when A_{cat} and B_{cat} were tested in a larger inner diameter reactor. However, using a smaller inner diameter reactor led to higher C_2 selectivity and yield. As suggested in chapter V, this behaviour would be associated with an increase of the gas flow rate caused by a smaller diameter. Nevertheless, the maximum C_2 selectivity and yield were again observed at 750 ^oC.

As mentioned above, O_2^{2-} and O^- surface oxygen species were found, respectively, on A_{cat} and C_{cat} respectively (Table 6.1). It was demonstrated in Chapter III and IV that these surface species play an important role in the activity and C_2 selectivity. The O^- species were attributed to be responsible for the selective oxidative coupling of methane in B_{cat}. Nevertheless, A_{cat} containing the peroxide anion (O_2^{2-}) showed also to be selective to form C_2

hydrocarbons. It was reported that O_2^{2-} itself is not able to promote the selective oxidative coupling of methane [30]. However, O_2^{2-} and O^- species may exist in equilibrium which depends on the nature of the catalyst [31]. Thus, O_2^{2-} can undergo decomposition into O^- at temperatures high enough (> 600 ^oC) according to the following equation:

$$O_2^{2-} \rightarrow 2O^- \qquad 6.1$$

Therefore, the higher C_2 selectivity and yield observed in A_{cat} can be attributed to the formation O^- species from the decomposition of peroxide anion (O_2^{2-}) at high temperature.

6.3.2.2 Effect of steam on the OCM reaction

The effect of the amount of water added to the reaction stream over A_{cat}, B_{cat}, and C_{cat} was studied. The catalytic tests were carried out at the temperature of maximum CH_4 conversion and C_2 selectivity in the absence of steam (see section 6.3.2.1 and 5.3.2.2). OCM reaction parameters are shown in table 6.2 and Figure 6.4. In the case of A_{cat}, it can be observed that CH_4 conversion as well as C_2 selectivity and yield slightly increased as the amount of steam increased. However, an opposite behaviour was observed in $B_{cat.}$ It is known that there are two kinds of reaction process in the OCM reaction: the heterogeneous catalytic reaction, which gives methyl radicals; and the noncatalysed gas-phase reaction to form C_2 and CO_x products.

In the low temperature range the former is predominant, producing C_2 hydrocarbons by methyl radical coupling. However, at high temperatures, the latter is enhanced and part of CH_4 and C_2 products are oxidised to form CO_x products. Therefore, the catalytic results obtained in presence of steam are discussed in terms of its eventual effect on the catalyst surface chemistry (where the heterogeneous reaction occurs) and on the gas-phase reactions.

Chang et al. [32] reported that the presence of steam has a positive effect in OCM which would be related with the presence of O_2^{2-} and O^- surface oxygen species. This effect was observed in the temperature range of 550-600 ^oC. They suggested that at 550 ^oC steam reacts with O_2^{2-} forming O^- and surface hydroxyl groups. In other words, Chang et al. suggested that the presence of steam is necessary to produce O^- at temperature around

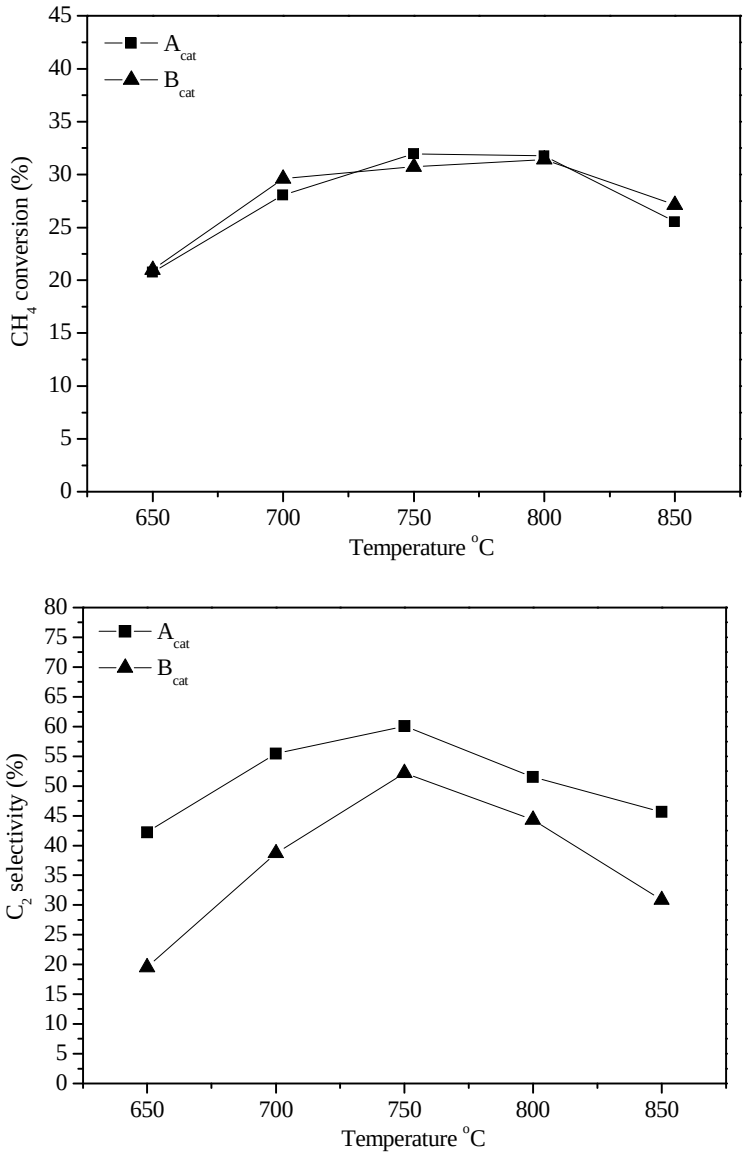

Figure 6.4 Effect of temperature over the catalytic performance of A_{cat} and B_{cat} for OCM.

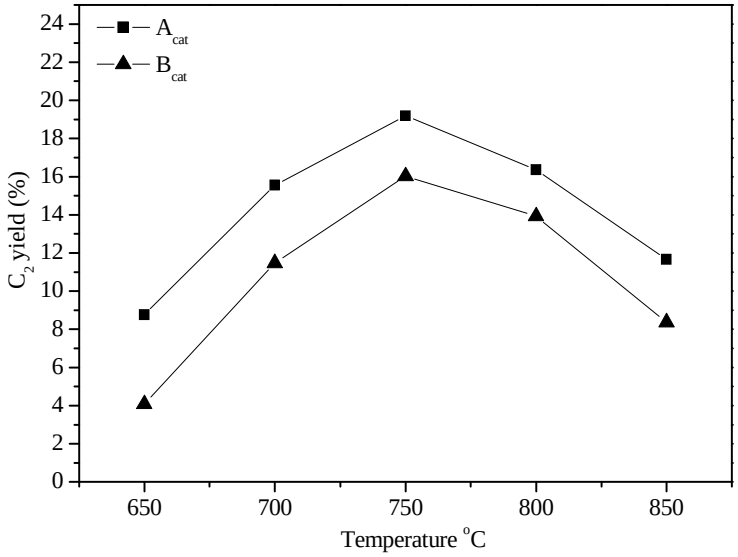

Figure 6.4 (cont) Effect of temperature over the catalytic performance of A_{cat} and B_{cat} for OCM.

Table 6.2 Effect of steam on the OCM reaction performance (T = 750 °C)

H_2O (%)	Acat					Bcat				
	CH_4 Conv. (%)	Selectivity (%)			C_2 yield (%)	CH_4 conv. (%)	Selectivity (%)			C_2 yield (%)
		C_2	CO	CO_2			C_2	CO	CO_2	
0	32.4	60.2	4.8	35.0	19.5	29.0	54.4	4.4	41.2	15.8
5	32.4	62.4	4.5	33.0	20.2	29.0	45.2	4.9	49.9	13.1
10	32.4	63.0	3.8	33.2	20.4	29.4	43.9	4.7	51.4	12.9
15	33.9	62.0	5.4	32.6	21.0	29.8	44.6	5.2	50.3	13.3
20	34.6	62.5	6.0	31.4	21.6	29.2	44.5	4.5	51.0	13.0
25	35.0	62.7	6.1	31.1	22.0	28.5	43.4	4.2	52.4	12.4

550-600 °C, to maintain the supply of O^{-}. However, they point out that at high temperatures (>600 °C), the presence of steam probably may not favour the formation of O^{-} and hydroxyl groups. It would explain why a significant effect of steam was not observed in A_{cat}. The reaction temperature in this latter was 750 °C, thus the O_2^{2-} species probably are not decomposed

to form O^- species. However, the decomposition of O_2^{2-} to form O^- (Eq. 6.1) can proceed in the same way like it occurs in the absence of steam, i.e., the presence of steam is not required to improve significantly the OCM performance. Similarly, this analysis can be applied in the case of B_{cat}. In addition, this latter only exhibited O^- species which means that steam is not also required. Moreover, steam seems to have a poisoning effect on the $B_{cat.}$

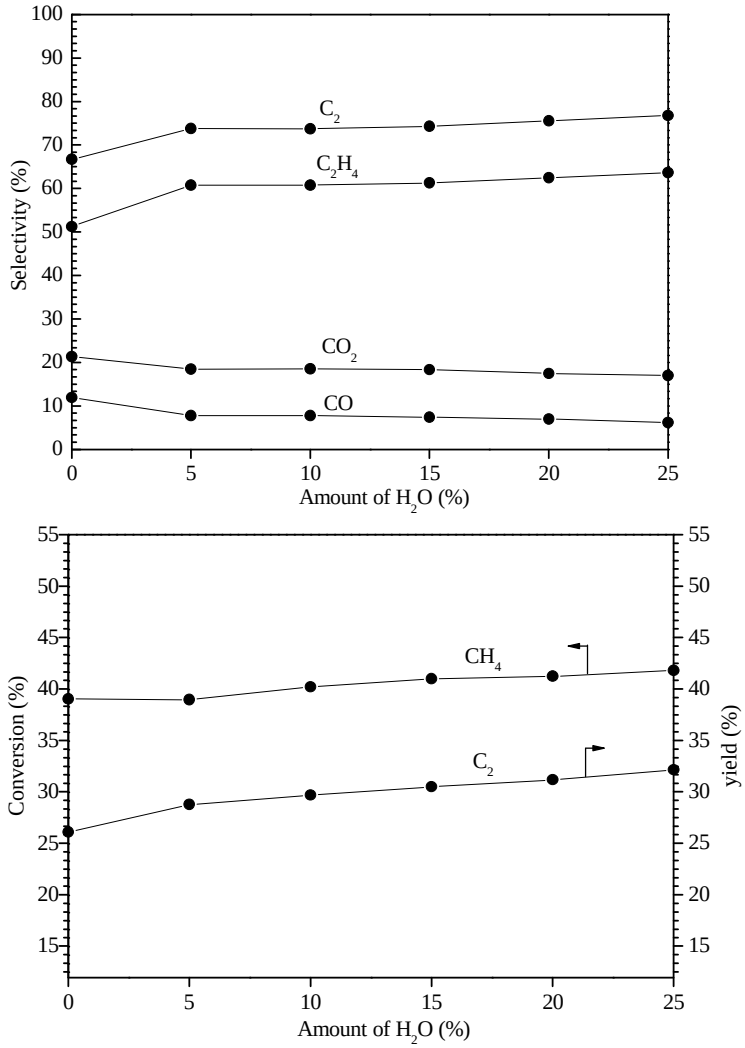

Figure 6.5 Effect of steam on C_2, C_2H_4, CO, CO_2 selectivity, CH_4 conversion and C_2 yield over C_{cat} at 800 ^oC.

On the other hand, the addition of steam had an important effect on C_{cat}, since the CH_4 conversion as well as C_2 selectivity and yield were found to increase with the amount of steam at 800 ^oC (Figure 6.5). These results

suggest that the beneficial effect of the presence of steam is specific for $C_{Cat.}$ As shown in Table 6.1, Ccat did not exhibit O_2^- and O_2^{2-} species. The surface chemistry of this catalyst is different from that of A_{cat} and B_{cat} in agreement with literature regarding types of species active for the OCM. A mechanism, until now proposed for this kind catalysts, is based in a redox cycle which allows generating methyl radicals from CH_4. It seems that the reduction of W^{6+}/W^{4+} or W^{6+}/W^{5+} plays an important role for CH_4 activation in presence of the O^{2-} active surface species [33-35]. These species are formed from activation of gas phase O_2 on a reducible metal ion, since there are no reports on their formation from H_2O at 800 ºC. Therefore, in this work it was assumed that H_2O does not affect the heterogeneous catalytic reaction on C_{cat}. However, Haitao et al. [36] reported that the presence of steam had a positive effect on C_2 selectivity and yield over a similar catalyst at 800 ^oC. They indicated that steam, in addition to a dilution effect on oxygen, also suppresses the deep oxidation in the gas phase. Steam seems to promote moderated temperature in the catalyst bed during reaction. Therefore, a moderate temperature is created in the bed, suppressing the total oxidation of CH_4 in the gas-phase, leading to more C_2 product at the outlet. On the other hand, Shahri and Pour [37] suggested that the addition of Ce could promote the performance of the catalysts for the OCM reaction, and inhibited the gas phase oxidation of methane.

Finally, one might ask why the suppression of CH_4 and C_2 hydrocarbon oxidation to form CO_x products was not observed on A_{cat} and B_{cat}. This could be related to the temperature, which influences the exothermic reaction of OCM, eventually leading to the formation of hot spots in the catalyst bed. Then, hot spots can increase the bed temperature which also depends of catalyst nature. Thus, it is probable that more hot spots are developed at 800 ^oC in the C_{cat} bed increasing the bed temperature making more predominant the gas-phase reaction to form CO_x when compared to A_{cat} and B_{ca}. Therefore, the effect of steam to suppress deep oxidation is more significant in C_{cat} when compared to A_{cat} and B_{ca}.

6.4 Conclusions

Oxidative coupling of methane was studied under humid atmosphere. The co-feeding of steam with CH_4 and O_2 was advantageous to the OCM reaction over C_{cat}. The presence of steam enhanced CH_4 conversion, C_2 selectivity as

well as yield. This is due probably to the effect of temperature distribution in the catalyst bed at high temperature suppressing the predominant gas-phase reaction to form CO_x products. On the other hand, it is suggested that O_2^{2-} species are not decomposed into O^- species in the presence of water. Therefore, steam did not improve significantly the OCM performance over A_{cat} at 750 ^oC. Steam showed to have a poisoning effect over B_{cat}.

This work allows to suggesting that A_{cat} and C_{Cat} can be used in a system where OCM reaction can be integrated into a process to produce useful products besides C_2 hydrocarbons under humid atmosphere. However, additional studies are necessary, such as catalytic stability tests and CH_4/O_2 ratio effect.

References

[1] Keller GE, Bhasin MM, *Synthesis of ethylene via oxidative coupling of methane: I. Determination of active catalysts*. Journal of Catalysis **73** (1982) 9-19.

[2] Dissanayake D, Lunsford JH, Rosynek MP, *Oxidative Coupling of Methane over Oxide-Supported Barium Catalysts*. Journal of Catalysis **143** (1993) 286-298.

[3] Ito T, Wang J, Lin CH, Lunsford JH, *Oxidative dimerization of methane over a lithium-promoted magnesium oxide catalyst*. Journal of the American Chemical Society **107** (1985) 5062-5068.

[4] Lunsford JH, *The catalytic conversion of methane to higher hydrocarbons*. Catalysis Today **6** (1990) 235-259.

[5] Gholipour Z, Malekzadeh A, Hatami R, Mortazavi Y, Khodadadi A, *Oxidative coupling of methane over (Na_2WO_4+Mn or Ce)/SiO_2 catalysts: In situ measurement of electrical conductivity*. Journal of Natural Gas Chemistry **19** (2010) 35-42.

[6] Wu J, Zhang H, Qin S, Hu C, *La-promoted Na_2WO_4/Mn/SiO_2 catalysts for the oxidative conversion of methane simultaneously to ethylene and carbon monoxide*. Applied Catalysis A: General **323** (2007) 126-134.

[7] Zheng W, Cheng D, Zhu N, Chen F, Zhan X, *Studies on the structure and catalytic performance of S and P promoted Na-W-Mn-Zr/SiO_2*

catalyst for oxidative coupling of methane. Journal of Natural Gas Chemistry **19** (2010) 15-20.

[8] Leyshon DW (1991) Thin Bed Reactor for Conversion of Methane to Higher Hydrocarbons. In: A. Holmen KJJ, Kolboe S (eds) Studies in Surface Science and Catalysis, vol Volume 61. Elsevier, pp 497-507. doi:10.1016/s0167-2991(08)60116-0

[9] van Looij F, Mulder A, Boon AQM, Scheepens JF, Geus JW (1993) Fixed Bed Catalytic Reactors Based on Sintered Metals. In: L. Guczi FS, P T (eds) Studies in Surface Science and Catalysis, vol Volume 75. Elsevier, pp 1377-1389. doi:10.1016/s0167-2991(08)64458-4

[10] Mleczko L, Pannek U, Niemi VM, Hiltunen J, *Oxidative Coupling of Methane in a Fluidized-Bed Reactor over a Highly Active and Selective Catalyst*. Industrial & Engineering Chemistry Research **35** (1996) 54-61.

[11] Coronas J, Menendez M, Santamaria J, *Development of ceramic membrane reactors with a non-uniform permeation pattern. Application to methane oxidative coupling*. Chemical Engineering Science **49** (1994) 4749-4757.

[12] Lu Y, Dixon AG, Moser WR, Ma YH, Balachandran U, *Oxygen-permeable dense membrane reactor for the oxidative coupling of methane*. Journal of Membrane Science **170** (2000) 27-34.

[13] Garagounis I, Kyriakou V, Anagnostou C, Bourganis V, Papachristou I, Stoukides M, *Solid Electrolytes: Applications in Heterogeneous Catalysis and Chemical Cogeneration*. Industrial & Engineering Chemistry Research **50** (2010) 431-472.

[14] Stoukides M, *Methane conversion to C_2 hydrocarbons in solid electrolyte membrane reactors*. Res Chem Intermed **32** (2006) 187-204.

[15] Vayenas CG, Bebelis S, Yentekakis IV, Lintz HG, *Non-faradaic electrochemical modification of catalytic activity: A status report*. Catalysis Today **11** (1992) 303-438.

[16] Tsiakaras P, Vayenas CG, *Oxidative Coupling of CH_4 on Ag Catalyst-Electrodes Deposited on ZrO_2 (8 mol% Y_2O_3)*. Journal of Catalysis **144** (1993) 333-347.

[17] Caravaca A, de Lucas-Consuegra A, González-Cobos J, Valverde JL, Dorado F, *Simultaneous production of H_2 and C_2 hydrocarbons by gas phase electrocatalysis*. Applied Catalysis B: Environmental **113–114** (2012) 192-200.

[18] Aoki A, Ohno S, Muramatsu Y, *Preparation of YBaCu oxide precursor by the citrate gel process*. Journal of Non-Crystalline Solids **147–148** (1992) 720-723.

[19] Marcilly C, Courty P, Delmon B, *Preparation of highly dispersed mixed oxides and oxide solid solutions by pyrolysis of amorphous organic precursors*. Journal of the American Ceramic Society **53** (1970) 56-57.

[20] Yu M, Lin J, Zhou YH, Wang SB, *Citrate–gel synthesis and luminescent properties of $ZnGa_2O_4$ doped with Mn^{2+} and Eu^{3+}*. Materials Letters **56** (2002) 1007-1013.

[21] Segal D, *Chemical synthesis of ceramic materials*. Journal of Materials Chemistry **7** (1997) 1297-1305.

[22] Hu C, Gao Z, Yang X, *One-pot low temperature synthesis of MFe_2O_4 (M=Co, Ni, Zn) superparamagnetic nanocrystals*. Journal of Magnetism and Magnetic Materials **320** (2008) L70-L73.

[23] Peng Q, Dong Y, Deng Z, Sun X, Li Y, *Low-Temperature Elemental-Direct-Reaction Route to II−VI Semiconductor Nanocrystalline ZnSe and CdSe*. Inorganic Chemistry **40** (2001) 3840-3841.

[24] Yáñez-Vilar S, Sánchez-Andújar M, Gómez-Aguirre C, Mira J, Señarís-Rodríguez MA, Castro-García S, *A simple solvothermal synthesis of MFe_2O_4 (M=Mn, Co and Ni) nanoparticles*. Journal of Solid State Chemistry **182** (2009) 2685-2690.

[25] Silva A, Machado B, Gomes H, Figueiredo J, Dražić G, Faria J, *Pt nanoparticles supported over Ce–Ti–O: the solvothermal and photochemical approaches for the preparation of catalytic materials*. Journal of Nanoparticle Research **12** (2010) 121-133.

[26] Wang L, Tomura S, Ohashi F, Maeda M, Suzuki M, Inukai K, *Synthesis of single silica nanotubes in the presence of citric acid*. Journal of Materials Chemistry **11** (2001) 1465-1468.

[27] Ji S-f, Xiao T-c, Li S-b, Xu C-z, Hou R-l, Coleman KS, Green MLH, *The relationship between the structure and the performance of Na-W-Mn/SiO_2 catalysts for the oxidative coupling of methane*. Applied Catalysis A: General **225** (2002) 271-284.

[28] Chen F, Zheng W, Zhu N, Cheng D-g, Zhan X, *Oxidative Coupling of Methane Over Na–W–Mn–Zr–S–P/SiO_2 Catalyst: Effect of S, P Addition on the Catalytic Performance*. Catal Lett **125** (2008) 348-351.

[29] Li Z, Zhu Y, *Surface-modification of SiO_2 nanoparticles with oleic acid*. Applied Surface Science **211** (2003) 315-320.

[30] Yamashita H, Machida Y, Tomita A, *Oxidative coupling of methane with peroxide ions over barium-lanthanum-oxygen mixed oxide*. Applied Catalysis A: General **79** (1991) 203-214.

[31] Palmer MS, Neurock M, Olken MM, *Periodic Density Functional Theory Study of Methane Activation over La_2O_3: Activity of O^{2-}, O^-, O_2^{2-}, Oxygen Point Defect, and Sr^{2+}-Doped Surface Sites*. Journal of the American Chemical Society **124** (2002) 8452-8461.

[32] Chang YF, Somorjai GA, Heinemann H, *Oxidative Coupling of Methane over Mg-Li Oxide Catalysts at Relatively Low Temperature - The Effect of Steam*. Journal of Catalysis **141** (1993) 713-720.

[33] Wu J, Li S, Niu J, Fang X, *Mechanistic study of oxidative coupling of methane over Mn_2O_3-$Na_2WO_4SiO_2$ catalyst*. Applied Catalysis A: General **124** (1995) 9-18.

[34] Jiang Z-c, Gong H, Li S-b (1997) Methane activation over Mn_2O_3-Na_2WO_4/SiO_2 catalyst and oxygen spillover. In: Can L, Qin X (eds) Studies in Surface Science and Catalysis, vol Volume 112. Elsevier, pp 481-490.

[35] Li S-B, *Oxidative Coupling of Methane over W-Mn/SiO_2 Catalyst*. Chinese Journal of Chemistry **19** (2001) 16-21.

[36] Liu H, Wang X, Yang D, Gao R, Wang Z, Yang J, *Scale up and stability test for oxidative coupling of methane over Na_2WO_4-Mn/SiO_2 catalyst in a 200 ml fixed-bed reactor*. Journal of Natural Gas Chemistry **17** (2008) 59-63.

[37] Shahri SMK, Pour AN, *Ce-promoted $Mn/Na_2WO_4/SiO_2$ catalyst for oxidative coupling of methane at atmospheric pressure*. Journal of Natural Gas Chemistry **19** (2010) 47-53.

7 Catalytic performance of 5wt%Ce-5wt%Na_2WO_4/SiO_2 catalyst in a solid electrolyte-fixed bed reactor configuration for the simultaneous production of H_2 and C_2 hydrocarbons[1]

In this chapter, an active and selective catalyst powder (5wt%Ce-5wt%Na_2WO_4/SiO_2) was evaluated in a combined single chamber solid electrolyte plus fixed bed reactor configuration for the simultaneous production of H_2 and C_2 hydrocarbons under a humidified CH_4 atmosphere. Hence, a Pt/YSZ/Ag solid electrolyte cell has been placed on top of the catalyst powder bed. H_2 was produced via steam electrolysis in a Pt cathode of the solid electrolyte cell ($H_2O + 2e^- \rightarrow H_2 + O^{2-}$). Simultaneously, the produced O^{2-} ions were electrochemically pumped to the Ag anode, leading to the production of C_2 hydrocarbons (ethane and ethylene), via oxidative coupling of CH_4 ($4CH_4 + 3O^{2-} \rightarrow C_2H_4 + C_2H_6 + 3H_2O + 6e^-$). Additionally, oxygen molecules desorbed to the gas phase ($O^{2-} \rightarrow O_2 + 2e-$) reacted with CH_4 on the 5wt%Ce-5wt%Na_2WO_4/SiO_2 catalyst bed leading to an increase of C_2 hydrocarbons yield. The influence of different reaction parameters (applied current, temperature and composition) on the catalytic performance of the system was investigated. In addition, long-term reaction experiments confirmed the stability of the overall configuration (solid electrolyte cell + catalyst bed) for long operation times in view of a practical application.

---

[1]Caravaca A, Ferreira VJ, de Lucas-Consuegra A, Figueiredo JL, Faria JL, Valverde JL, Dorado F, Simultaneous production of H_2 and C_2 hydrocarbons by using a novel configuration solid-electrolyte + fixed bed reactor. International Journal of Hydrogen Energy **38** (2013) 3111-3122.

7.1 Introduction

The direct conversion of methane to C_2 hydrocarbons remains a challenging problem in heterogeneous catalysis and chemical reaction engineering. Among various approaches, the OCM is one of the few processes that is capable of converting methane into higher hydrocarbons in a single step [1]. A lot of research work on the OCM process has been carried out since the work of Keller and Bhasin in 1982 [2]. The development of active and selective catalysts has been pursued in order to achieve high yields in this process. However, the main problem in OCM is the deep oxidation of CH_4 and C_2 hydrocarbons to form CO_x ($CO + CO_2$) products. Hence, different alternatives have been introduced in the last years to increase the C_2 yield and C_2 selectivity vs. CO_2 formation [3]. For instance, solid electrolyte membrane reactors (SEMR) seem to be a suitable configuration for the OCM [4-7]. A SEMR consists mainly of a ceramic solid electrolyte membrane (e.g. O^{2-} or H^+ conductor in most cases), with two porous metal or metal oxide electrodes on both sides of the membrane. Such configurations allow to supply electrochemically one of the reactants, (e.g., O^{2-} for the oxidative coupling reaction) by a Faradaic operation, and present several advantages such as: enhanced catalytic activity and selectivity, better process integration, reduced feedstock and easy reaction rate control. Hence, many solid electrolyte membrane reactor configurations have been studied for the oxidative coupling of methane [4-12].

On the other hand, a recent study showed the possibility of using a single chamber solid electrolyte membrane reactor for the simultaneous production of H_2 and C_2 hydrocarbons by the integration the OCM with the steam electrolysis process [13]. In that work, H_2O was used instead of O_2 for the coupling reaction and hence, the active O^{2-} ions for the OCM reaction were in-situ electrochemically produced in the cathode from H_2O through a steam electrolysis process ($H_2O + 2e^- \rightarrow H_2 + O^{2-}$). Simultaneously, the produced O^{2-} ions were electrochemically pumped to the Ag anode, leading to the production of C_2 hydrocarbons (ethane and ethylene), via oxidative coupling of CH_4 ($4CH_4 + 3O^{2-} \rightarrow C_2H_4 + C_2H_6 + 3H_2O + 6e^-$). The possibility of simultaneously producing H_2 and C_2 hydrocarbons in a single reactor step from a humidified methane stream is of great economical and technical interest. The main advantages can be summarized as follows:

-This configuration would reduce the cost of the overall process since no pure O_2 is required for feeding the reactor (the feed stream consists of a humidified CH_4 stream).

-At the same time it would allow to produce a high valuable chemical, i.e., H_2.

-It allows combining an exothermic reaction (oxidative coupling) with an endothermic one (steam electrolysis) by the heat transfer of all the gas components in the well mixed single chamber reactor configuration.

-The optimization of the C_2 yield and selectivity of the system at varying reaction conditions could easily be carried out by a simple modification of the applied current.

However, two limitations were also identified from that work [13]:

-Relatively low C_2 yields (around 8 %) were obtained at the optimal conditions.

-Relatively low H_2 faradaic efficiencies (up to 12 %) were obtained for H_2 production, due to the recombination of the H_2 produced and the free O_2 in the single chamber reaction atmosphere.

Thus, in order to increase the overall efficiency of the process, an active and selective catalyst can be used by combining a solid electrolyte membrane and conventional heterogeneous catalysis.

Several catalysts were developed for the OCM in previous Chapters. Then, the best catalysts were tested under a wet atmosphere. It was concluded that two catalysts, $Ca_{0.5}Ce_{0.5}O$ and 5wt%Ce-5wt%Na_2WO_4/SiO_2, can be used in these conditions. However, the last catalyst showed additional improvement in its performance when tested in the presence of steam.

Hence, in this work the 5wt%Ce-5wt%Na_2WO_4/SiO_2 catalyst bed was located next to a single chamber SEMR to enhance the reaction between O_2 molecules produced in the electrolysis process and methane, in order to increase the overall efficiency of the process for the production of H_2 and C_2 hydrocarbons. Thus, the influence of the presence of the catalyst bed, together with the reaction temperature, the applied current and the gas phase composition has been studied. Finally, a long term experiment was carried

out in order to study the durability and stability of the proposed novel configuration.

7.2 Experimental section

7.2.1 Preparation of the catalyst powder

Catalyst ($5Ce\text{-}5Na_2WO_4/SiO_2$) preparation was carried out in two steps. First, a SiO_2 support was sythetised using a reported procedure [14]. Then, metal precursors were dispersed on the SiO_2 support by the incipient wetness impregnation method. The preparation procedure is described in detail in section 5.2.1.

7.2.2 Preparation of solid electrolyte

The reaction experiments were carried out in a combined solid electrolyte-fixed bed reactor as shown in Figure 7.1. The preparation of the solid electrolyte cell is as described in literature [13]. Briefly, it consisted of a porous and continuous Pt thin film (working electrode, geometric area of 2.01 cm^2) deposited over one side of a 19-mm-diameter, 1-mm-thick YSZ (Yttria-stabilized Zirconia) disc (Tosoh-Zirconia). The Ag counter electrode (geometric area of 2.01 cm^2) was deposited on the other side of the electrolyte.

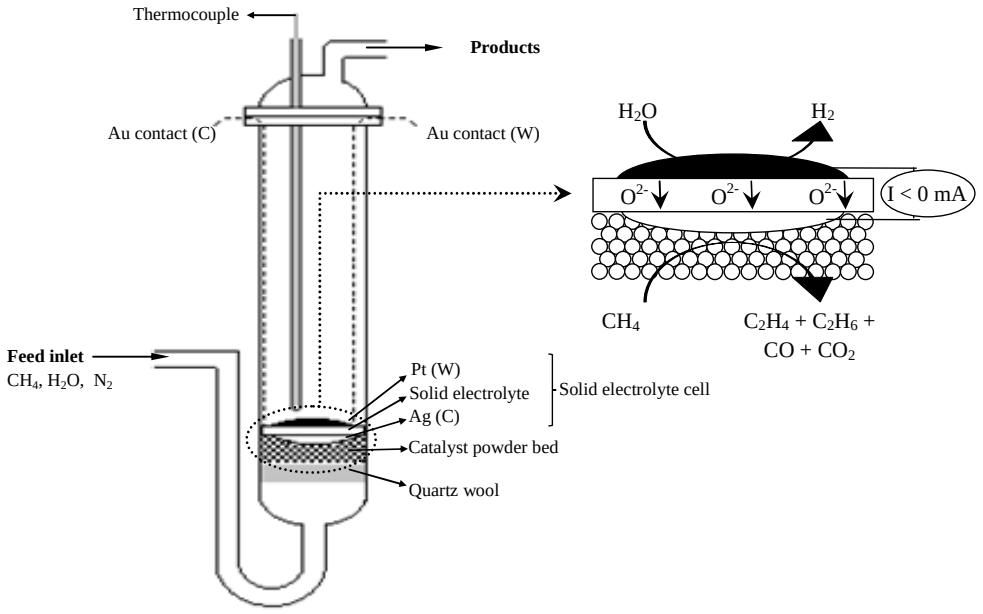

Figure 7.1 Scheme of the single chamber solid electrolyte cell reactor.

At first, the Ag electrode was deposited by application of thin coatings of Ag paste (Fuel Cell Materials), followed by two calcination steps, at 300 ºC (2 h) and 850 ºC (2 h). The final Ag loading was around 10 mg/cm^2. Then, the Pt film was deposited, as described in detail elsewhere [15], by successive steps of deposition and thermal decomposition (in two steps, 550 ºC for 1 h and 850 ºC for 2 h) of a H_2PtCl_6 precursor solution. The final Pt loading was 1.5 mg/cm^2. Gold wires were sealed to both electrodes with Ag paste in order to connect them to the potentiostat-galvanostat Voltalab 21 (Radiometer Analytical).

7.2.3 Catalyst characterisation

Textural and morphology properties of the catalyst powder were assessed by N_2 adsorption and scanning electron microscopy (SEM). Then, phases present in the catalyst powder were identified by X-Ray Diffraction (XRD).

Thus, BET surface areas of the samples were measured from the corresponding N_2 equilibrium adsorption isotherms, determined at -196 °C with a Quantachrome Instruments NOVA 4200e apparatus. The surface morphology of the samples was investigated by using Scanning Electron Microscopy (SEM). The SEM apparatus, FEI Quanta 400FEG ESEM/EDAX Genesis X4M instrument, was equipped with an Energy-Dispersive X-ray analyzer (EDX) to define the composition of the catalyst powder. Finally, X-ray diffraction patterns of the fresh powder were recorded on a Philips PW 1710 instrument using Ni-filtered Cu Kα radiation.

7.2.4 Catalyst evaluation

As mentioned above, the reaction experiments were carried out in a combined solid electrolyte-fixed bed reactor. The cell reactor was made of a quartz tube with appropriate feed-through and was operated at atmospheric pressure. The solid electrolyte cell was supported over the active OCM catalyst bed. First, 0.2 g of the powder catalyst bed was placed on a fritted quartz disk (21 mm in diameter). Then, the solid electrolyte cell was placed above the catalyst bed. Since the silver electrode is the active catalyst in the oxidative coupling reaction, the position of the solid electrolyte cell was chosen in order to allow contact of the Ag electrode with the catalyst powder. Hence, this reactor configuration allowed to partially separate the steam electrolysis process (that occurs on the active Pt catalyst-electrode)

and the oxidative coupling one, which occurs on both the Ag electrode and the active Ce-Na_2WO_4/SiO_2 catalyst bed.

The reaction gases (Praxair, Inc.) were certified standards of 10 % CH_4/N_2 and N_2 (99.999% purity) used as carrier gas. The gas flow was controlled by a set of calibrated mass flowmeters (Brooks 5850 E and 5850 S) while water was introduced into the feed stream by means of a saturator in order to achieve liquid-vapour equilibrium. The water content in the reaction mixture was controlled by the vapour pressure of H_2O at the temperature of the saturator (45 ºC). All lines placed downstream from the saturator were heated above 100 ºC to prevent condensation. The reactants were introduced into the reactor with the following concentrations: CH_4 (0.2-1 %), H_2O (10 %), N_2 (balance), with an overall gas flow rate of 50 cm^3 min^{-1}. All the catalytic experiments were carried out between 750-800 ºC at atmospheric pressure. Reactant and product gases were analysed with a micro gas-chromatograph (Varian CP-4900) equipped with two columns (Molsieve and Poraplot Q column) and two thermal conductivity detectors (TCD). The main detectable products were C_2H_6, C_2H_4, CO_2, CO and H_2. The CH_4 conversion, C_2 selectivity and yield were calculated as shown in Eqs. 2.1-2.3.

On the other hand, in order to evaluate the efficiency of the single chamber steam electrolysis cell, an apparent Faradaic efficiency (Λ) as defined in [13], which relates the amount of experimentally measured H_2 leaving the reactor with the applied current:

$$\Lambda = (rH_2 - r_0H_2)/(I/2F) \quad (7.1)$$

where rH_2 and r_0H_2 are the hydrogen reaction rates under closed circuit and open circuit conditions, respectively, and F is Faraday's constant.

7.3 Results and discussion

7.3.1 Characterisation and catalytic activity of the 5wt%Ce-5wt%Na_2WO_4 catalyst

The BET surface area and pore volume of the silica support (SiO_2) were measured to be 15.0 m^2 g^{-1} and 0.051 cm^3 g^{-1}, respectively. Data for the 5wt%Ce-5wt%Na_2WO_4/SiO_2 catalyst were 9.3 m^2 g^{-1} and 0.012 cm^3 g^{-1}. These results revealed that both the silica support and the catalyst powder exhibited low porosity. Moreover, a decrease in the textural parameters was

observed in the calcined powder. It is in good agreement with the results obtained by Gholipour et al. [16] who studied the structural properties of Na_2WO_4 + Mn or Ce /SiO_2 samples using commercial silica as the support. They attributed the decrease in the textural parameters of the calcined catalyst to the crystallization of amorphous silica, which yielded an almost nonporous material.

On the other hand, the XRD spectrum of the fresh catalyst powder is shown in Figure 7.2. As discuted in section 5.3.1.3, it was found that the amorphous phase present in the silica support partialtly changed to α-cristobalite after calcination at 800 °C, according to JCPDS standards. On the other hand, the crystalline phase of Na_2WO_4 was also observed on the fresh catalyst, which indicates that Na has affinity to be combined with WO_4. Cerium oxide phase was detected to be CeO_2 by the presence of the corresponding diffraction peaks. As reported in literature [16], phase transition from amorphous to crystalline silica appears to be an importante requirement for an effective catalyst, switching the oxidation properties of the transition metals (W) in favor of the oxidative coupling reaction.

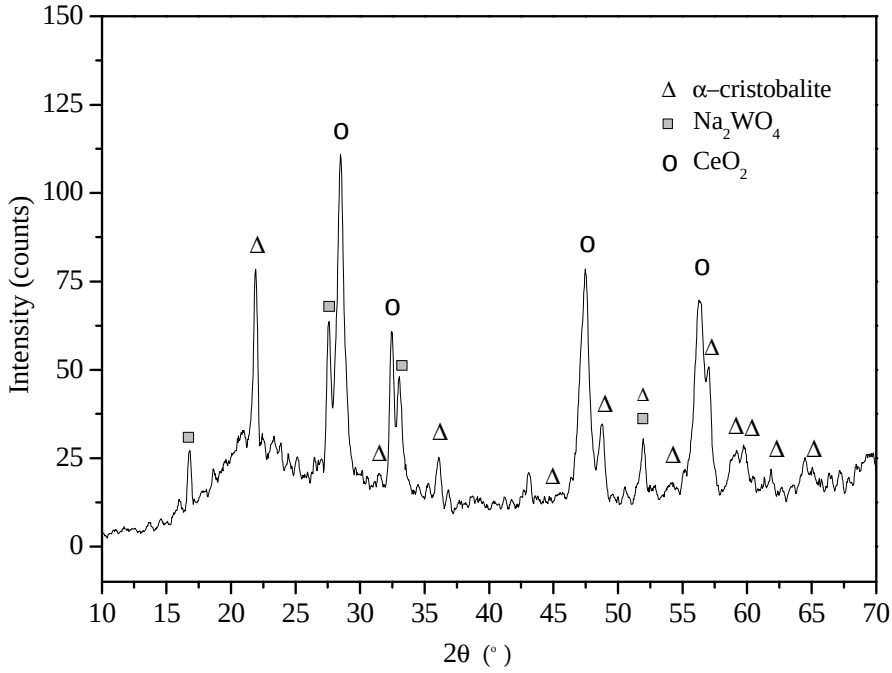

Figure 7.2 XRD pattern of the 5wt%Ce-5wt%Na_2WO_4/SiO_2 catalyst.

Moreover, the presence of the alkali ion (Na^+), which is used as a structural promoter, should facilitate the crystallization of the catalyst, which would in turn adjust the oxidation properties of the catalyst and make it more selective for the OCM reaction [17-19].

Finally, SEM analysis of the 5wt%Ce-5wt%Na_2WO_4/SiO_2 catalyst (Figure 7.3a) showed relatively homogeneous species of Ce and Na/W embedded into the silica matrix without apparent agglomeration. It was supported by the energy-dispersive x-ray spectroscopy analysis (EDX) of the highlighted area, which confirmed the presence of Ce, Na and W (Figure 7.3b).

a)

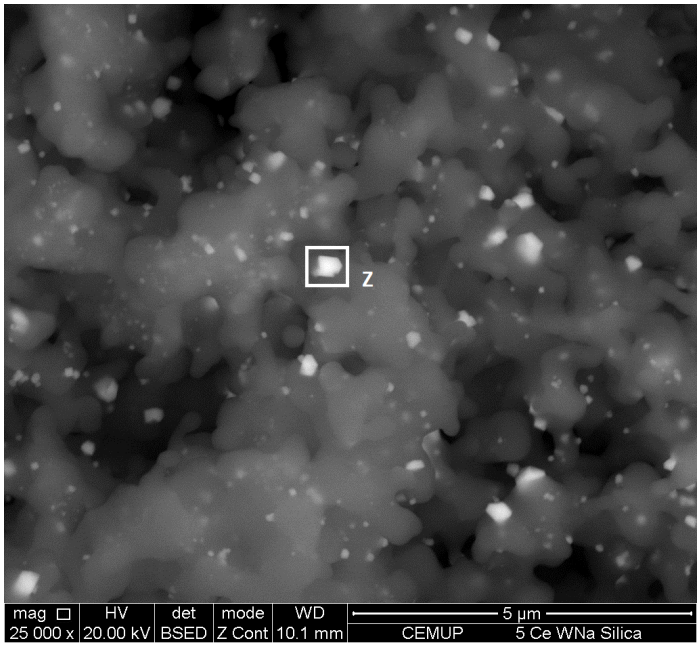

Figure 7.3 Scanning electron micrograph of a) 5wt%Ce-5wt%Na_2WO_4/SiO_2catalyst and b) EDX obtained from analysis of the 5wt%Ce-5wt%Na_2WO_4/SiO_2 catalyst in the zone labelled “Z” in the SEM image (a).

b)

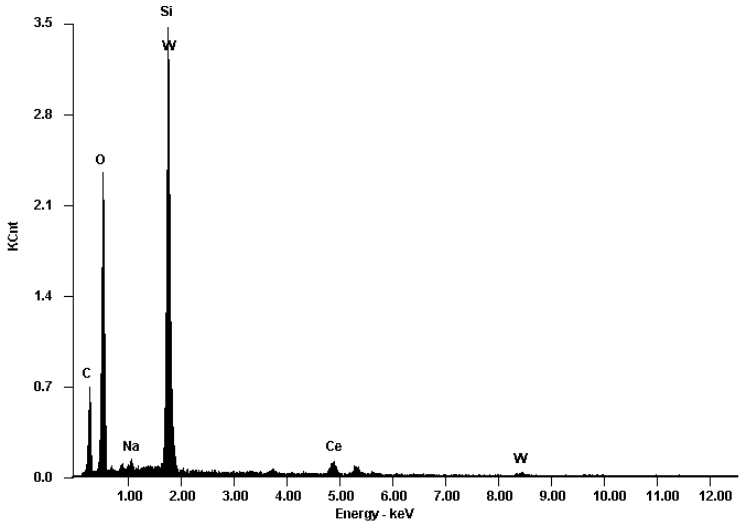

Figure 7.3 (Cont.) Scanning electron micrograph of a) 5wt%Ce-5wt%Na_2WO_4/SiO_2catalyst and b) EDX obtained from analysis of the 5wt%Ce-5wt%Na_2WO_4/SiO_2 catalyst in the zone labelled "Z" in the SEM image (a).

Although the 5wt%Ce-5wt%Na_2WO_4/SiO_2 catalyst was previously tested in the OCM reaction under similar operating conditions (see Chapter VI), a preliminary experiment was carried out. Table 7.1 shows the variation of the main reaction parameters of the OCM process (CH_4 conversion, C_2 yield and selectivity towards C_2 and CO_x) and the hydrogen production at three different reaction temperatures by feeding a mixture of $CH_4/O_2/H_2O$: 2 %/0.5 %/10 % (total flow rate 50 cm^3min^{-1} with N_2 as the carrier gas). In this case water was introduced in the feed stream in order to simulate the composition to be used in the subsequent electro-catalytic experiments (a mixture of CH_4 and H_2O and O_2 electrochemically produced from steam electrolysis process). The results of Table 7.1 reveal that methane conversion as well as the selectivity to C_2 hydrocarbons and C_2 yield increase with the reaction temperature. On the contrary, it seems that the CO and the CO_2 selectivities followed an opposite trend, decreasing as the reaction temperature increases. As expected, the catalyst powder resulted to be active in the oxidative coupling process under humid atmosphere.

Table 7.1 Catalytic performance of the 5wt%Ce-5wt%Na_2WO_4/SiO_2 on the OCM reaction at three different reaction temperatures.

Temp. (ºC)	CH_4 Conv. (%)	Selectivity (%)			C_2 yield %	(rH_2 mol s^{-1}) x10^8
		C_2	CO_2	CO		
750	16.0	50.5	29.3	20.2	8.1	0.82
775	19.6	57.4	23.3	19.3	11.3	1.13
800	22.7	61.0	22.0	17.0	13.9	1.15

The CH_4 conversion, C_2 selectivity and yield incresed, while CO_x (CO + CO_2) decreased with the reaction temperature in the range from 750 to 800 ºC. In this sense, the production of CO and CO_2 could be attributed to the partial and deep oxidation processes, respectively, which strongly competed with the coupling reaction. Also, it should be mentioned that the maximum C_2 yield achieved at 800 ºC was around 13.9 %, in contrast with results reported in Chapter VI and in literature [16]. However, the difference is not significant since contact times and reactor geometry are not comparable. On the other hand, it can be also observed that some amount of hydrogen was produced under the different reaction conditions. The hydrogen production rate was lower but of the same order as that the CO. In this sense, some studies have reported the simultaneous production of ethylene and syngas (CO + H_2) with a similar sodium tungstate based catalyst [20], in which the H_2 production could be attributed to the activity for methane partial oxidation. However, the amount of hydrogen produced here was very low compared to that obtained in previous study regarding the simultaneous production of H_2 and C [13], in which most of the hydrogen produced was attributed to the steam electrolysis process. Once the OCM activity of the 5wt%Ce-5wt%Na_2WO_4/SiO_2 was checked, a solid electrolyte cell was placed on the catalyst bed for the simultaneous production of H_2 and C_2 hydrocarbons by using a humidified gas stream as the feed. This way, O_2 was produced in-situ via electrolysis, consequently leading to the simultaneous production of H_2.

7.3.2 Electro-catalytic tests

First, a galvanostatic transient experiment was carried out at a constant temperature of 750 ºC with both the Pt/YSZ/Ag solid electrolyte cell (SEC from now on), and with the combined system of the solid electrolyte cell and the powder catalyst Pt/YSZ/Ag+5wt%Ce-5wt%Na_2WO_4/SiO_2 (SEC + PC from now on) as described in the experimental section. This experiment was performed by step changes in the applied current from 0 to -150 mA and under the following gas mixture in the feed stream: CH_4/H_2O: 1 %/10 %, overall flow rate 50 cm^3 min^{-1}, with N_2 as a vector gas. Hence, Figure 7.4 shows the variation the H_2 (a), CO_x (CO + CO_2) (b) and C_2 hydrocarbons (Ethane + Ethylene) (c) production rates vs. time under the application of the different currents. It can be observed that under open circuit conditions, i.e., Current = 0 mA (no O_2 was present in the reaction atmosphere) the catalytic activity of both the electrochemical catalyst and the catalyst bed was negligible towards the methane steam reforming process, since it was not observed any important syn-gas (H_2 + CO) production. On the other hand, regarding the SEC system, Figure 7.4 shows an increase in the production of all the reaction products with the increase of the applied current. As explained in [13], since the Pt layer and the silver catalyst were connected as working and counter electrodes, respectively, the application of negative currents led to the steam electrolysis in the Pt film. This process led to the formation of H_2 and oxygen ions (O^{2-}) [21]. While hydrogen migrates to the gas phase as a reaction product, the O^{2-} ions migrate from the Pt electrode to the Ag one. Hence, it explains the almost linear trend followed by the H_2 production for the SEC system with the increasing applied current, since the hydrogen production was mainly due to the electrochemical process of steam electrolysis. Thus, the oxygen ions reacted in the Ag electrode with methane to produce a mixture of carbon derived products (according to the scheme of Figure 7.5a). Then, an increase of the applied current led to an increase in the amount of oxygen ions (O^{2-}) supplied to the Ag electrode, therefore improving the methane reaction rate, with the subsequent positive effect in the formation of CO, CO_2, C_2H_4 and C_2H_6 [11]. In this sense, similar results were found in previous study with a similar solid electrolyte cell [13]. Then, the slight differences observed between the results obtained in this work for the Pt/YSZ/Ag solid electrolyte cell and the ones obtained in the previous work

could be attributed to the different performance regarding the position of the cell (different gas reactant bypass in the electrodes).

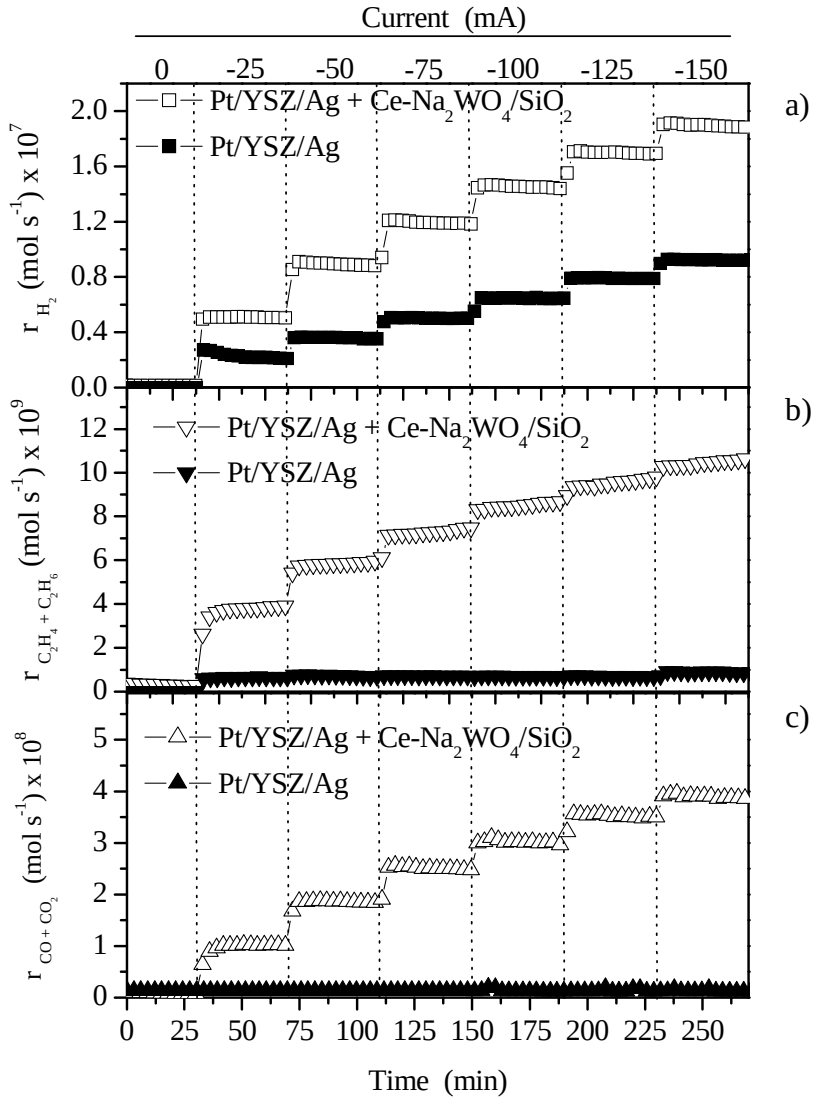

Figure 7.4 Influence of the applied current on the dynamic values of H_2 (a), C_2H_6 and C_2H_4 (c) and CO + CO_2 (b), reaction rates vs. time for both the Pt/YSZ/Ag and the Pt/YSZ/Ag+Ce-Na_2WO_4/SiO_2 systems. Conditions: CH_4/H_2O: 1 %/10 %, Total flow = 50 cm^3 min^{-1} (N_2 balance), Temperature = 750 ºC.

On the other hand, it could be observed that the yield of all the reaction products strongly increased at the different polarizations under the presence of the 5wt%Ce-5wt%Na_2WO_4/SiO_2 powder catalyst. This point clearly demonstrates the possibility of coupling catalysis and electrocatalysis in a single chamber reactor configuration for the production of H_2 and C_2 hydrocarbons. As explained in the previous study [13], one of the main drawbacks related with the use of a single chamber solid electrolyte cell is the drop in the apparent faradaic efficiency (i.e. in the final H_2 production) due to the recombination of the H_2 produced by steam electrolysis and the free O_2 ($O_{2\ free}$) present in the reaction atmosphere as a consequence of oxygen O^{2-} evolution in the Ag electrode. Hence, according to the results obtained in Figure 7.4, it seems that the presence of the catalyst bed led to a strong increase in both the faradaic efficiency of the system (since the H_2 production increased at all the currents studied) and the CH_4 oxidation (CO_x) and coupling (C_{2s}) products. It can be attributed to the reaction of $O_{2\ free}$ with the inlet CH_4 at the Ce-Na_2WO_4/SiO_2 powder catalyst bed (as schematized in Figure 7.5b), since, as previously explained in Table 7.1, this catalyst showed a good performance for the oxidative coupling reaction even under the presence of water in the feed stream. Thus, an increase in the applied current would lead to a higher amount of free O_2, increasing methane conversion over the powder catalyst towards carbon derived products, and leading to the observed increase of the CO_x and C_2 hydrocarbons reaction rates. On the other hand, due to the decrease of free O_2 present in the reaction atmosphere, H_2 production increased at all the polarizations studied (important increase in the electrolysis Faradaic efficiency).

One can find in literature some efforts to increase the efficiency of silver based solid electrolyte cell towards the C_2 coupling products by addition of active powder catalysts [22]. However, in this case the powder catalyst was introduced in the matrix of the Ag electrode, loading only to a slight increase in C_2 hydrocarbons production. Thus, the reaction performance shown in the present study can be considered as a strong advance regarding the simultaneous production of hydrogen and C_2 hydrocarbons.

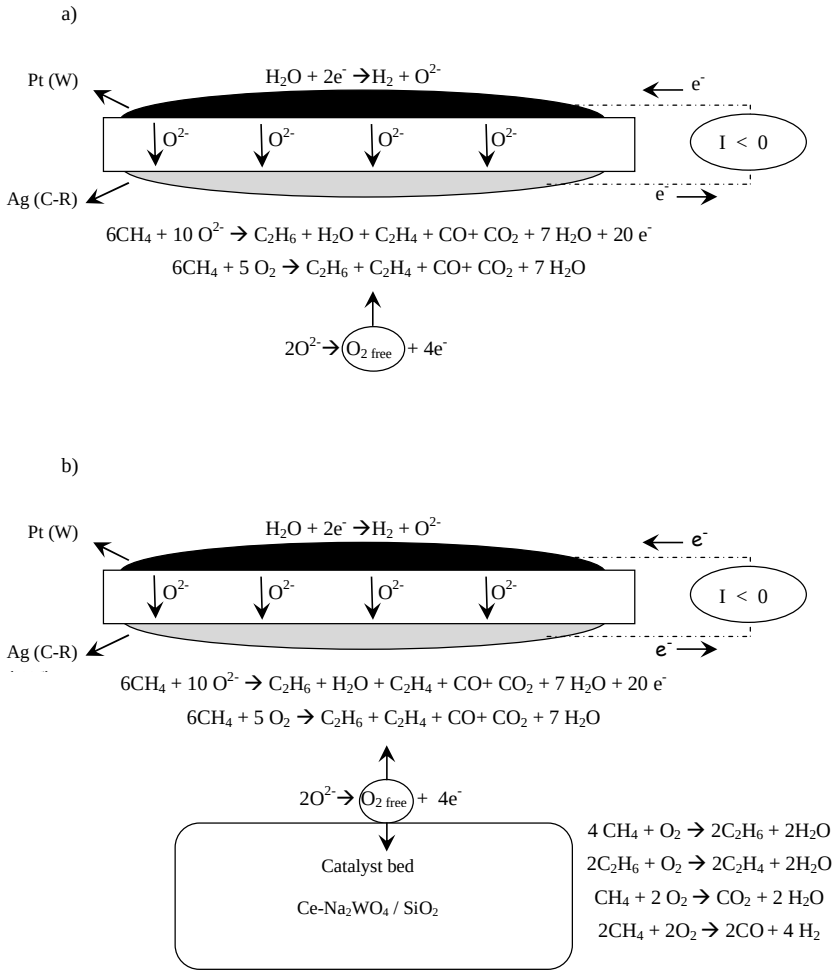

Figure7.5 Schematic representation of the main processes involved during the cathodic polarizations for the Pt/YSZ/Ag and the Pt/YSZ/Ag+Ce-Na_2WO_4/SiO_2 systems.

The presence of the catalyst powder enhanced both the energetic and the catalytic efficiency of the Pt/YSZ/Ag solid electrolyte cell.

The influence of the reaction temperature was studied for both, the electrolysis and the coupling processes. Thus, Figure 7.6 shows the response of the steady state values (after 1 h of polarization at a fixed current) of the following parameters: CH_4 conversion (a), C_2 yield (b) and C_2H_4/C_2H_6 ratio (c) with the reaction temperature and the applied current for both the Pt/YSZ/Ag (SEC) and the Pt/YSZ/Ag + catalyst powder (SEC + PC)

configurations. These experiments were carried out under the same feed stream used in the previous experiment (CH_4/H_2O: 1 %/10%), and in the reaction temperature range from 750 to 800 ºC. For both systems, Figure 7.6a shows an increase in methane conversion with the applied current and the reaction temperature. Regarding the solid electrolyte cell, a similar trend was observed in the previous study [13], which was attributed to an increase in the kinetics toward both the CO_x and the C_2 products. However, as shown in Figure 7.6, the introduction of the catalyst bed in the reaction system led to a strong enhancement of the methane reaction rate, and then in the methane conversion under all the explored reaction temperatures. As previously explained, this could be attributed to the reaction of the inlet methane with free O_2 present in the reaction atmosphere over the catalyst powder bed. Thus, the maximum methane conversion was obtained, for the SEC + PC system, at the reaction temperature of 800 ºC and at a constant current of -150 mA. A similar trend was observed in the parameters depicted on Figures 7.6b and 6c for both systems. Thus, the C_2 yield obtained with both devices (Figure 7.6b) increases with the applied current and the reaction temperature. A similar trend for the solid electrolyte cell was observed in the aforementioned previous study [13]. One can calculate the selectivity of the C_2 products taking into account the methane conversion and the C_2 yield. This parameter generally decreased (for both the SEC and the SEC + PC systems), at a constant temperature, with the increase in applied current. As explained in previous studies for electrochemical [11,13] and conventional catalysts [21], this could be attributed to the competition between combustion and the coupling reaction with the increase in the oxygen supplied to the coupling chamber (higher cathodic currents).

Hence, as the amount of O_2 electrochemically supplied to the Ag electrode increased, the ratio of the coupling vs. the combustion reaction decreased (lower C_2 selectivity) but the overall C_2 yield increases, therefore leading to a higher amount of C_2 hydrocarbons.

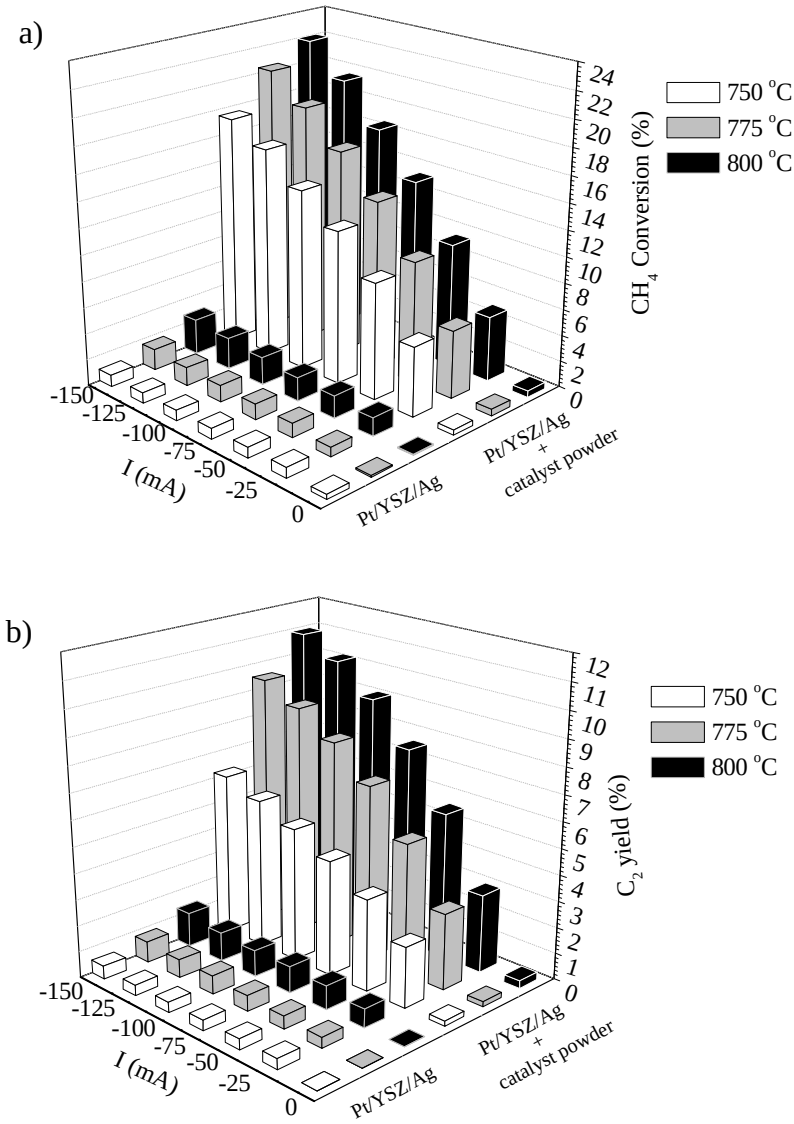

Figure 7.6 Influence of the reaction temperature and the imposed current for the Pt/YSZ/Ag and the Pt/YSZ/Ag+Ce-Na_2WO_4/SiO_2 systems on: a) CH_4 conversion, b) C_{2s} yield and c) C_2H_4/C_2H_6 ratio. Conditions: CH_4/H_2O: 1 %/10 %, Total flow = 50 cm^3 min^{-1} (N_2 balance), Temperature = 750 - 800 ºC.

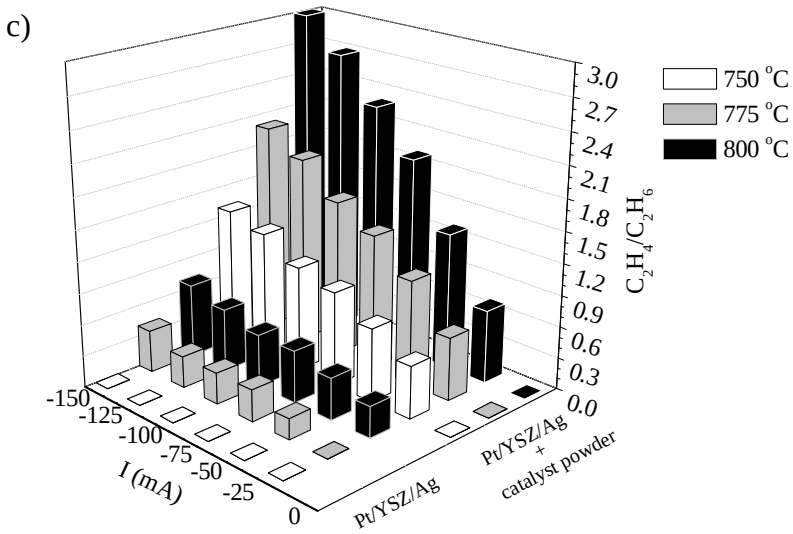

Figure 7.6 (Cont.) Influence of the reaction temperature and the imposed current for the Pt/YSZ/Ag and the Pt/YSZ/Ag+Ce-Na_2WO_4/SiO_2 systems on: a) CH_4 conversion, b) C_{2s} yield and c) C_2H_4/C_2H_6 ratio. Conditions: CH_4/H_2O: 1 %/10 %, Total flow = 50 cm^3 min^{-1} (N_2 balance), Temperature = 750 - 800 ºC.

Thus, as occurred for methane conversion, the presence of the catalyst powder led to higher C_2 hydrocarbons yield under all the reaction conditions studied. This is clearly supported by the results obtained with the powder catalyst (see Table 7.1) and the SEC system (Figure 7.6b) both of them showing an increase of the C_2 yield with the reaction temperature and the applied current. The maximum yield achieved for the SEC + PC system was around 11 %. In this sense, one can estimate that most of the catalytic activity towards C_2 production results from the presence of the catalyst bed, since the yield achieved with the solid electrolyte cell was lower than 2 %.

Finally, as showed in Figure 7.6c, an increase in the applied current and the reaction temperature led to a higher ethylene/ethane ratio for both systems. This behaviour can be also observed in Figure 5.7c, and can be attributed to the homogeneous-heterogeneous pathways of the oxidative coupling reaction, which led to the oxidative dehydrogenation of ethane (ODE) to produce ethylene [23,24].

Then, it seems that the increase of the applied current (and therefore the amount of O_2 supplied to the Ag electrode) and the reaction temperature enhance this process, as observed in previous study for the solid electrolyte cell [13]. However, further studies should be carried out to clarify this point by studying the reaction of ODE over the Ce-Na_2WO_4/SiO_2 catalyst.

Figure 7.7 depicts the H_2 production rates for the same experiments of Figure 7.6 at the different explored reaction temperatures. An almost linear increase of the H_2 production rate with the applied current can be observed for both systems under all working temperatures. This demonstrates the electrochemical nature of hydrogen formation, which was mostly due to the steam electrolysis process in the Pt film under the imposed current [13,25]. It can be observed that the presence of the catalyst lead to a strong increase in the H_2 production at the different reaction temperatures, increasing more than twice the average H_2 faradaic efficiency (see inset figures). This increase in the H_2 reaction rate might be due to some steam reforming or partial oxidation of methane over the catalyst bed. However, as shown in Table 7.1, the catalytic activity towards hydrogen production under the presence of oxygen and steam was around one order of magnitude lower than the values obtained in these experiments. Moreover, the negligible activity towards H_2 production under OCV conditions (Current = 0 mA) supports the negligible methane steam reforming activity of the catalyst bed. Thus, as previously explained in Figures 7.4 and 7.5, the strong increase in the overall methane reaction rate over the catalyst powder in the SEC + PC system, compared to SEC, led to a decrease of free O_2 present in the reaction atmosphere, thus increasing the observed apparent faradaic efficiency of this system.

Taking into account methane conversion towards the combustion and coupling products, the oxygen consumption can be obtained [13]. An average of oxygen conversion is calculated as the ratio between the O_2 reacted with methane and O_2 produced by the electrolysis process, i.e., I/4 F. Thus, although methane conversion increased with the reaction temperature in the SEC + PC system, the average O_2 conversion decreased from 28 % to 25 % when the reaction temperature increased from 750 to 800 ºC. However, as previously observed in Figure 7.6b, the C_2 yield strongly increased with the reaction temperature.

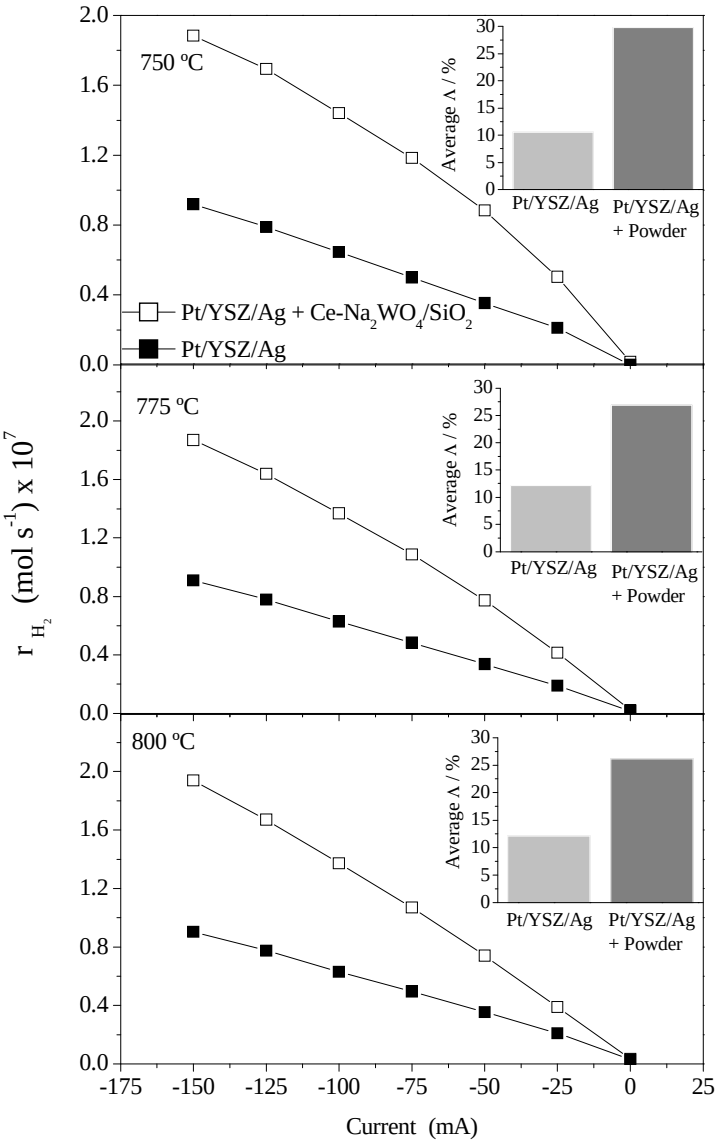

Figure 7.7 Influence of the temperature and the imposed current on the H_2 rate for the Pt/YSZ/Ag and the Pt/YSZ/Ag+Ce-Na_2WO_4/SiO_2 systems. The Inset figures depict the average apparent Faradic efficiency. Conditions: CH_4/H_2O: 1 %/10 %, Total flow = 50 cm^3 min^{-1} (N_2 balance), Temperature = 750 - 800 ºC.

This can be attributed to an enhancement of the C_2 selectivity with the increase of the reaction temperature, which increased around 15 % at all the applied currents. Thus, since oxygen conversion slightly decreased with the

reaction temperature, the amount of free O_2 present in the reaction atmosphere increased, therefore decreasing the apparent faradaic efficiency for the SEC + PC system as observed in the inset on Figures 7.7a-c. Moreover, one can find that the values of λ are similar to the oxygen conversion above mentioned. It demonstrates, firstly, that most of the non-converted oxygen reacted with H_2 due to the mixing properties of the single chamber configuration and, on the other hand, the electrochemical nature of H_2 produced via steam electrolysis. As a result, the hydrogen reaction rate was more than one order of magnitude higher than that of CO produced, leading to H_2/CO ratios between 12 and 15.

Finally, it should be mentioned that no mass transfer limitations were present in the polarization curves at the different reaction temperatures (not shown here), since no limiting current was observed in the cell potential range studied (from 1 V to 2 V).

In order to optimize both the H_2 and the C_2 hydrocarbon production rates, a new experiment was carried out at a constant temperature of 800 ºC by step changes in the inlet methane concentration from 0.2 to 1 %, and under the application of a constant current of -150 mA in the combined SEC + PC system. Figure 7.8 shows the variation of the H_2 and the CH_4 reaction rates (a) and C_2 yield (b) with the CH_4 feed concentration and with the equivalent CH_4/O_2 ratio in the secondary abscissa axis (calculated as a function of the inlet methane concentration and the applied current). As can be observed in Figure 7.8a, the increase in the methane concentration led to a growing H_2 production rate. Taking into account the increase in the methane reaction rate, and according to the previously obtained results, this could be attributed to the decrease in free O_2 due to the increasing methane consumption.

Hence, it led to a higher faradaic efficiency towards hydrogen production. Regarding the coupling products, an increase in C_2 yield with methane concentration from 0.2 to 0.6 % can be observed in Figure 7.8b. At higher inlet CH_4 concentrations this parameter remained almost constant at around 11 %, suffering a slight decrease at CH_4 concentrations higher than 0.9 %. Based on the reaction products, the optimum achieved in this parameter could be explained by the aforementioned competition between methane coupling and combustion.

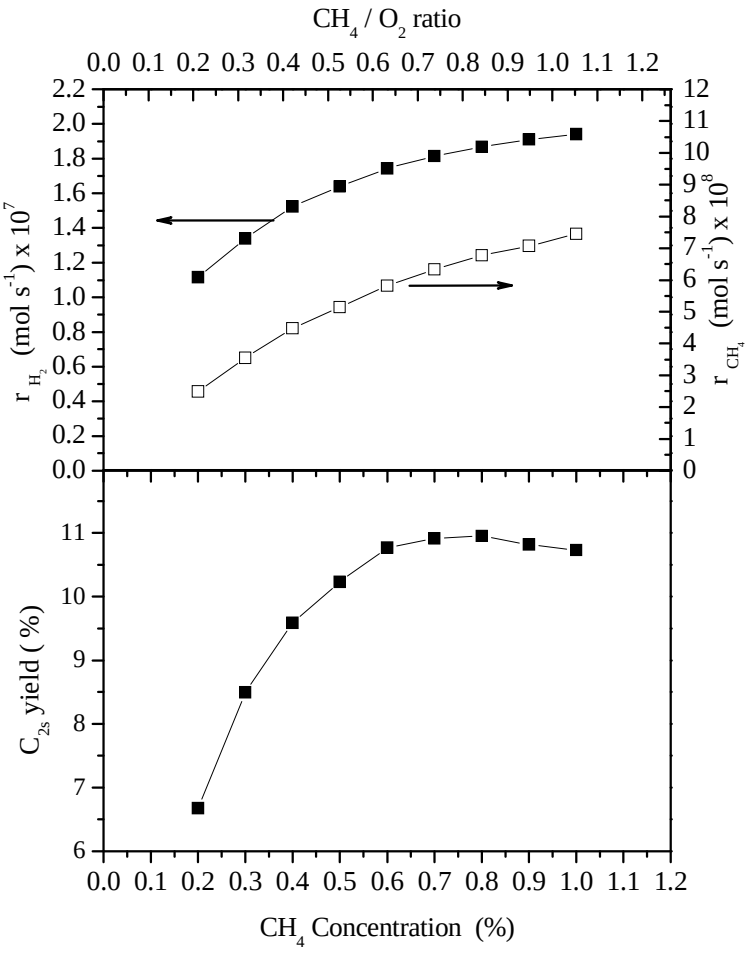

Figure 7.8 Influence of the inlet CH_4 concentration at constant imposed current on the H_2 and CH_4 reaction rates (a), and on C_2 hydrocarbon yield (b) for the Pt/YSZ/Ag+Ce-Na_2WO_4/SiO_2 system. Conditions: CH_4/H_2O: 0.2-1 %/10 %, Total flow = 50 cm^3 min^{-1} (N_2 balance), Temperature = 800 ºC. Imposed current = -150 ma.

Thus, although the overall methane reaction rate increased, the selectivity towards the C_2 hydrocarbons decreased, leading to an optimum C_2 yield. In this point it should be mentioned that the optimum CH_4/O_2 ratio was higher (around 0.85) in comparison with the optimum ratio found in our previous study (0.24) [13], which demonstrate again the higher conversion of free O_2 with methane due to the presence of the catalyst bed. Since the C_2 hydrocarbon production was almost the same at methane concentrations higher than 0.6 %, and higher the hydrogen production increased in this

concentration range, the following conditions were chosen as the optimal feed stream conditions for the simultaneous production of H_2 and C_2 hydrocarbons: methane concentration of 1 %, Current = -150 mA.

One can note that the maximum yield obtained under these conditions is slightly lower than the value reported in Table 7.1 for the powder catalyst (11 % vs. 13.9 %). Taking into account the faradaic efficiency (around 27 %), it seems that an important part of the free O_2 did not react with CH_4, decreasing the observed H_2 production. Thus, probably the counter-current flow of O_2 vs. the feed stream prevents complete conversion of the free O_2 in the catalyst, slightly decreasing the C_2 hydrocarbon production. Nevertheless, the drop in the C_2 yield for the SEC + PC system was not remarkable, being accompanied by an important H_2 production rate. Hence, further studies should be carried out to improve the reactor design using the same concept (combination of a catalyst bed and a solid electrolyte cell) in order to enhance the conversion of free O_2 with inlet methane. It probably would lead to a strong enhancement of the overall efficiency of the system towards the production of H_2 and C_2 hydrocarbons.

Taking into account the data of the previous Figures (7.6 and 7.8), the kinetics of the methane oxidation process (i.e., by coupling or combustion processes) was investigated (as shown in Figure 7.9), at a constant temperature of 800 ºC. Briefly, Figures 7.9a and b show the effect of CH_4 concentration on the rates of formation of CO, CO_2, C_2H_6 and C_2H_4 at fixed O_2 concentration (corresponding to the application of -150 mA) over the EC + PC system. In this figure it can be observed that the production of all the above compounds show positive order dependence to methane. A similar trend was observed by Tsiakaras and Vayenas [11], who studied the kinetics

of the oxidative coupling reaction over a silver electrochemical catalyst. They observed a similar relative reaction order for ethane and ethylene, and a lower reaction order for the CO_2 production, as in the present study. On the other hand, the effect of the O_2 concentration at constant methane concentration is shown in Figures 7.9c and d. A positive order of all the reaction products with respect to oxygen supplied to the Ag layer and the catalyst can also be observed. Thus, as reported in previous studies, the significantly higher reaction order for ethylene vs. ethane suggests that the

first one is a secondary product, resulting from the oxidative dehydrogenation of ethane [13,11].

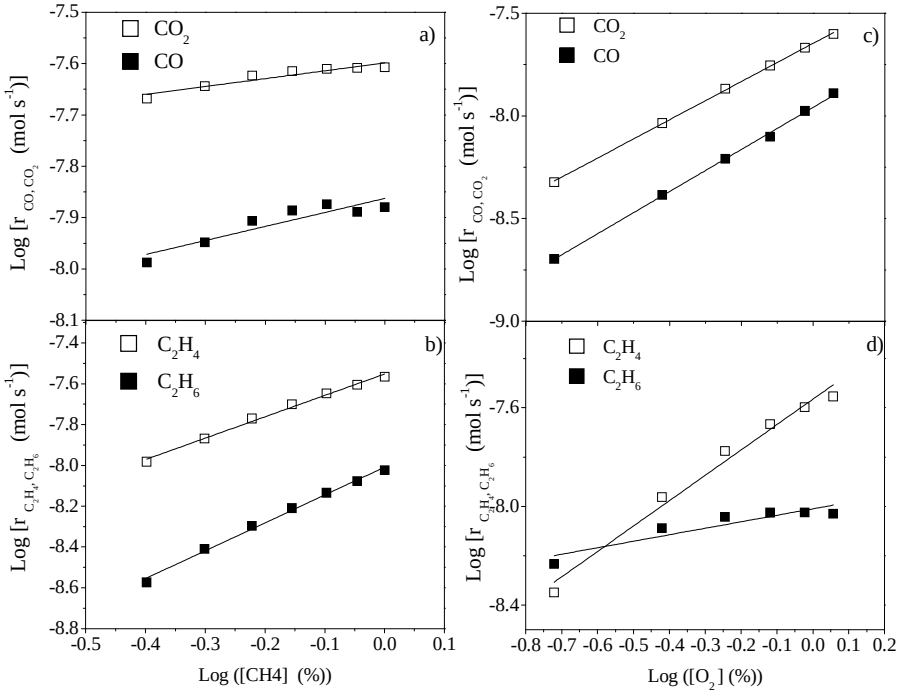

Figure 7.9 Effect of CH_4 concentration (a and b) and O_2 concentration (c and d) on the rates of formation of CO, CO_2, C_2H_4 and C_2H_6 for the Pt/YSZ/Ag+Ce-Na_2WO_4/SiO_2 system. Conditions: [H_2O]: 10 %, Total flow = 50 cm^3 min^{-1} (N_2 balance), Temperature = 800 ºC.

Finally, the stability of the combined SEC + PC system was examined under the optimal reaction conditions obtained in Figure 7.8, i.e., at 800 °C, under the application of a constant current of -150 mA and with the following feed stream: CH_4/H_2O: 1%/10%. Thus, Figure 7.10 shows the reaction rates of the obtained products during 24 h, confirming that 5wt%Ce-5wt%Na_2WO_4/SiO_2 presents a suitable activity and stability for the production of H_2 and C_2 hydrocarbons under the explored reaction conditions, and showing a high potential for the practical development of the system.

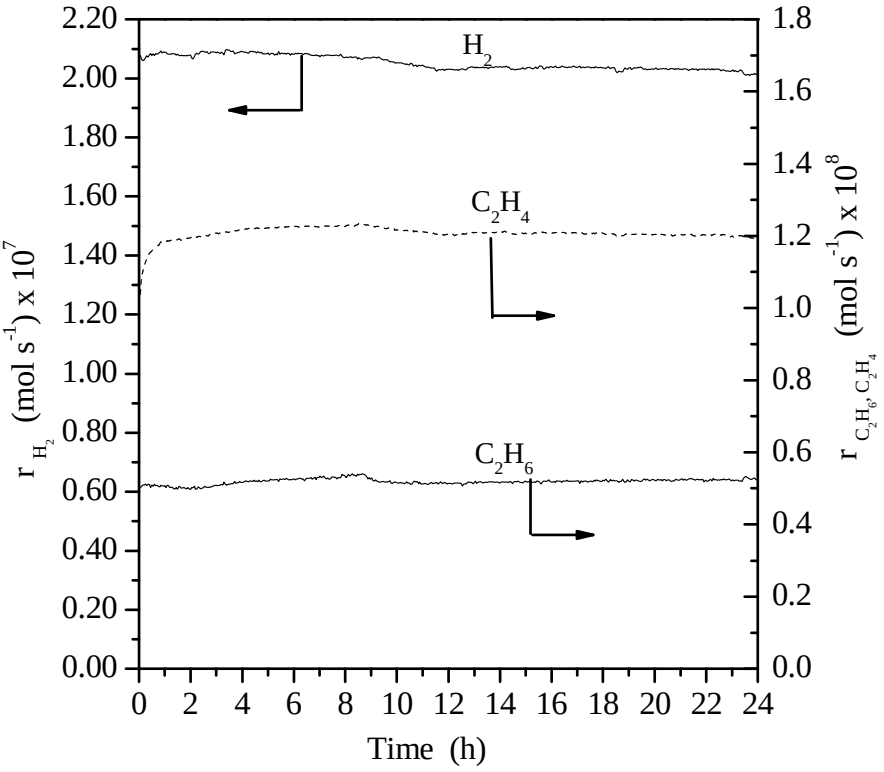

Figure 7.10 Variation of the H_2, CO, CO_2, C_2H_6 and C_2H_4 reaction rates with time during a durability study. Conditions: CH_4/H_2O: 1 %/10 %, Total flow = 50 cm^3 min^{-1} (N_2 balance), Temperature = 800 ºC, Current = -150 mA.

7.4 Conclusions

The performance of the 5wt%Ce-5wt%Na_2WO_4 /SiO_2 catalyst was evaluated in a solid electrolyte-fixed bed reactor configuration which combined electrocatalysis and conventional heterogeneous catalysis. Hence, a catalyst bed was placed next to the Pt/YSZ/Ag solid electrolyte. This system was used for the effective simultaneous production of H_2 and C_2 hydrocarbons under humidified CH_4 gas stream. The presence of the 5wt%Ce-5wt%Na_2WO_4 /SiO_2 catalyst bed strongly increased the catalytic activity towards C_2 hydrocarbon production and the efficiency of the single chamber steam electrolysis process. On the other hand, an increase in both the reaction temperature and cathodic current imposition led to higher production of desired compounds. On the other hand, the overall

configuration (solid electrolyte cell + catalyst bed) was found to be stable for long operation times (24 h).

References

[1] Holmen A, *Direct conversion of methane to fuels and chemicals*. Catalysis Today **142** (2009) 2-8.

[2] Keller GE, Bhasin MM, *Synthesis of ethylene via oxidative coupling of methane. I. Determination of active catalysts*. Journal of Catalysis **73** (1982) 9-19.

[3] Choudhary VR, Uphade BS, *Oxidative conversion of methane/natural gas into higher hydrocarbons*. Catalysis Surveys from Asia **8** (2004) 15-25.

[4] Garagounis I, Kyriakou V, Anagnostou C, Bourganis V, Papachristou I, Stoukides M, *Solid electrolytes: Applications in heterogeneous catalysis and chemical cogeneration*. Industrial and Engineering Chemistry Research **50** (2011) 431-472.

[5] Stoukides M, *Methane conversion to C_2 hydrocarbons in solid electrolyte membrane reactors*. Research on Chemical Intermediates **32** (2006) 187-204.

[6] Stoukides M, *Solid-Electrolyte Membrane Reactors: Current Experience and Future Outlook*. Catalysis Reviews - Science and Engineering **42** (2000) 1-70.

[7] Kokkofitis C, Ouzounidou M, Skodra A, Stoukides M, *High temperature proton conductors: Applications in catalytic processes*. Solid State Ionics **178** (2007) 507-513.

[8] Otsuka K, Yokoyama A, Morikawa A, *Catalytic activity- and selectivity-control for oxidative coupling of methane by oxygen-pumping through yttria-stabilized zirconia*. Chemistry Letters **14** (1985) 319-322.

[9] Otsuka K, Suga K, Yamanaka I, *Electrochemical enhancement of oxidative coupling of methane over LiCl-doped NiO using stabilized zirconia electrolyte*. Catal Lett **1** (1988) 423-428.

[10] Vayenas CG, Bebelis S, Yentekakis IV, Lintz HG, *Non-faradaic electrochemical modification of catalytic activity: A status report*. Catalysis Today **11** (1992) 303-438.

[11] Tsiakaras P, Vayenas CG, *Oxidative Coupling of CH4 on Ag Catalyst-Electrodes Deposited on ZrO2 (8 mol% Y_2O_3).* Journal of Catalysis **144** (1993) 333-347.

[12] Lapeña-Rey N, Middleton PH, *The selective oxidation of methane to ethane and ethylene in a solid oxide electrolyte reactor*. Applied Catalysis A: General **240** (2003) 207-222.

[13] Caravaca A, de Lucas-Consuegra A, González-Cobos J, Valverde JL, Dorado F, *Simultaneous production of H_2 and C_2 hydrocarbons by gas phase electrocatalysis*. Applied Catalysis B: Environmental **113–114** (2012) 192-200.

[14] Wang L, Tomura S, Ohashi F, Maeda M, Suzuki M, Inukai K, *Synthesis of single silica nanotubes in the presence of citric acid*. Journal of Materials Chemistry **11** (2001) 1465-1468.

[15] Dorado F, de Lucas-Consuegra A, Vernoux P, Valverde JL, *Electrochemical promotion of platinum impregnated catalyst for the selective catalytic reduction of NO by propene in presence of oxygen*. Applied Catalysis B: Environmental **73** (2007) 42-50.

[16] Gholipour Z, Malekzadeh A, Hatami R, Mortazavi Y, Khodadadi A, *Oxidative coupling of methane over (Na2WO4+Mn or Ce)/SiO2 catalysts: In situ measurement of electrical conductivity*. Journal of Natural Gas Chemistry **19** (2010) 35-42.

[17] Palermo A, Holgado Vazquez JP, Lee AF, Tikhov MS, Lambert RM, *Critical influence of the amorphous silica-to-cristobalite phase transition on the performance of $Mn/Na_2WO_4/SiO_2$ catalysts for the oxidative coupling of methane*. Journal of Catalysis **177** (1998) 259-266.

[18] Malekzadeh A, Dalai AK, Khodadadi A, Mortazavi Y, *Structural features of Na_2WO_4–MOx/SiO_2 catalysts in oxidative coupling of methane reaction*. Catalysis Communications **9** (2008) 960-965.

[19] Wang J, Chou L, Zhang B, Song H, Zhao J, Yang J, Li S, *Comparative study on oxidation of methane to ethane and ethylene*

over Na_2WO_4–Mn/SiO_2 catalysts prepared by different methods. Journal of Molecular Catalysis A: Chemical **245** (2006) 272-277.

[20] Zhang H, Wu J, Xu B, Hu C, *Simultaneous Production of Syngas and Ethylene from Methane by Combining its Catalytic Oxidative Coupling over Mn/Na_2WO_4/SiO_2 with Gas Phase Partial Oxidation*. Catal Lett **106** (2006) 161-165.

[21] Campbell KD, Lunsford JH, *Contribution of gas-phase radical coupling in the catalytic oxidation of methane*. The Journal of Physical Chemistry **92** (1988) 5792-5796.

[22] Lapeña-Rey N, Middleton PH, *The selective oxidation of methane to ethane and ethylene in a solid oxide electrolyte reactor*. Applied Catalysis A: General **240** (2003) 207-222.

[23] Choudhary VR, Mulla SAR, *Coupling of thermal cracking with noncatalytic oxidative conversion of Ethane to Ethylene*. AIChE Journal **43** (1997) 1545-1550.

[24] Chao Z-S, Ruckenstein E, *Noncatalytic and catalytic conversion of ethane over V-Mg oxide catalysts prepared via solid reaction or mesoporous precursors*. Journal of Catalysis **222** (2004) 17-31.

[25] Mulla SAR, Buyevskaya OV, Baerns M, *A comparative study on non-catalytic and catalytic oxidative dehydrogenation of ethane to ethylene*. Applied Catalysis A: General **226** (2002) 73-78.

8 Coupling catalysis and gas phase electrocatalysis for the simultaneous production and separation of pure H_2 and C_2 hydrocarbons from methane and natural gas over 5wt%Ce-5wt%Na_2WO_4 /SiO_2[1]

In this Chapter the simultaneous production of pure H_2 and C_2 hydrocarbons (ethane and ethylene) was studied by means of an Ag/YSZ/Ag double chamber solid oxide electrolysis cell coupled with an active and selective 5wt%Ce-5wt%Na_2WO_4 /SiO_2 catalyst bed. To this end, two feed streams were supplied, H_2O to the inner and CH_4 outer chamber. Thus, two kinds of products streams were obtained separately. Steam was electrolyzed on the inner Ag electrode of the electrochemical cell (cathode), producing pure H_2 and O^{2-} ions, which were electrochemically supplied through the YSZ solid electrolyte to the outer Ag electrode (anode). On this latter, the reaction of the O^{2-} ions formed molecular oxygen which was evolved with the methane stream leading production of C_2 hydrocarbons together with CO and CO_2 as secondary combustion products. The C_2 yield of this outer stream was strongly enhanced by the addition of 5wt%Ce-5wt%Na_2WO_4 /SiO_2 catalyst to obtain the second product stream. The influence of the Oxidative Coupling Catalyst powder bed, the reaction temperature and the gas phase composition was studied. Finally, the system was optimized varying the concentration of methane which allowed to obtain a C_2 yield of 10 % at 775 ^{o}C.

---

[1] Caravaca A, de Lucas-Consuegra A, Ferreira VJ, Figueiredo JL, Faria JL, Valverde JL, Dorado F, Coupling catalysis and gas phase electrocatalysis for the simultaneous production and separation of pure H_2 and C_2 hydrocarbons from methane and natural gas. Applied Catalysis B: Environmental **142–143** (2013) 298-306.

8.1 Introduction

Ethylene has a large market and is the most produced organic compound in the world. Thus, there is a strong demand growth for ethylene registered both in developed and developing countries [1]. Steam cracking of different liquid feedstock, especially naphtha, is the process conventionally used to produce ethylene in the petrochemical industry. However, since the work carried out by Keller and Bhasin [2], much attention has been paid to the catalytic methane oxidative coupling process for the production of C_2 hydrocarbons (mainly ethylene). In this sense, during last the 30 years, worldwide efforts have been focused on improving the performance of the catalytic OCM reaction, including catalysts and new reactor configurations. Thus, a large variety of catalysts has been evaluated for their performance in OCM with the objective developing a highly active catalyst [3-9]. However, few catalysts are close to the target for the industrial application of the OCM process: single-pass conversions of methane of at least 30% and C_2 selectivity of around 80% (see Figure 1.4).

On the other hand, the use of solid electrolyte membrane reactors has been demonstrated to be a promising technology for the production of these compounds via catalytic oxidative coupling process [10-14]. The option of using this kind of reactors presents several advantages such as: enhanced catalytic activity and selectivity, better process integration, and easy reaction rate control. Such systems allow performing oxidation and partial oxidation reactions (methane coupling) without feeding pure O_2 to the reactor (by an in-situ steam electrolysis process). Hence, the use of this kind of reactor configuration has allowed the simultaneous production of H_2 along with the C_2 hydrocarbons [10,11,13,14] .

Caravaca et al. [13] were the first to demonstrate this concept by using a single chamber solid electrolyte in which the active O^{2-} ions for the OCM reaction were in situ electrochemically produced from H_2O through a steam electrolysis process. However, low yields of C_2 hydrocarbons were obtained. Therefore, the introduction of an active and selective catalyst in this type of configuration is crucial for the overall system improvement. This was confirmed by the research group of Valverde [13] and Stoukides [10]. In both works, the catalyst used was 5wt%Ce-5wt%Na_2WO_4/SiO_2. This catalyst was developed and tested in OCM during the research work of the

present thesis using a conventional reactor (see Chapters V and VI). The possibility of increasing the C_2 yield in a single chamber solid electrolyte membrane reactor using a 5wt%Ce-5wt%Na_2WO_4/SiO_2 catalyst bed was described in detail in the previous chapter. The study showed lower electrical energy requirements of the solid electrochemical membrane reactor to produce the same amount of H_2 and C_2 hydrocarbons when the active catalyst powder bed was used. Nevertheless, low faradaic efficiency values were still obtained for H_2 production (around 25 %) associated with the undesired reaction of H_2 with the other products (CO_2 and O_2) in the single chamber atmosphere cell. In addition, H_2 and the other products (CO, CO_2, O_2 and C_2 hydrocarbons) were mixed in a unique product stream. Therefore, further separation steps should be required for the valorization of the desired products.

In this chapter, 5wt%Ce-5wt%Na_2WO_4/SiO_2 catalyst is introduced into Ag/YSZ/Ag double chamber steam electrolysis cell. This configuration allows to combine catalysis and gas-phase electrocatalysis for the simultaneous production and separation of a completely pure H_2 stream and a C_2 hydrocarbons rich stream. Thus, the influence of the Oxidative Coupling Catalyst powder bed, the reaction temperature and the gas phase composition was studied. Finally, the system was studied at different methane concentrations for C_2 yield optimization.

8.2 Experimental section

8.2.1 Catalyst preparation

Catalyst powder (5wt%Ce-5wt%Na_2WO_4/SiO_2) preparation was carried out in two steps. First, the SiO_2 support was sythetised using a method reported in literature. Then, metal precursors were dispersed on the SiO_2 support using the incipient wetness impregnation method. The preparation procedure is described in detail in section 5.2.1.

8.2.2 Preparation of combined solid electrolyte cell-fixed be reactor

The solid electrolyte cell consisted of an Yttria-Stabilized Zirconia (YSZ) tube closed at one end, with 15 cm length, 1.8 cm internal diameter, and 1.5 mm thickness. On both faces of the tube closed side (Figure 8.1), two Ag porous electrodes were prepared by application of thin coatings of Ag paste

(Fuel Cell Materials), followed by two calcination steps, at 300 ºC (2 h) and 850 ºC (2 h). The final Ag loading of each electrode was around 10 mg Ag/cm^2. The electrical contact of both electrodes was carried out by gold wires, which were in turn connected to a Voltalab 21 (Radiometer Analytical) potentiostat-galvanostat. Hence, the inner Ag electrode acted as a working electrode and as a cathode, while the outer Ag layer acted as a counter electrode and as anode of the solid electrolyte cell. In this work, all the experiments were carried out under galvanostatic imposition mode. The reaction experiments were carried out in a double chamber solid oxide electrolysis cell coupled with a catalyst powder bed, as shown in Figure 8.1. The cell reactor was made of a quartz tube with appropriate feed-through incorporating an inner fritted quartz. First, 0.2 g of the powder catalyst (5wt%Ce-5wt%Na_2WO_4/SiO_2) was placed on the fritted quartz (22 mm in diameter). Then, the solid electrolyte cell was placed above the catalyst bed (at around 5 mm). The inner Ag working electrode (W) was exposed to a H_2O/N_2 mixture, whereas the outer face, the Ag counter electrode (C), was exposed to a CH_4/N_2 or natural gas/N_2 feed stream. Hence, both reactions atmospheres were completely isolated. No gas permeation occurred between the two chambers, as confirmed by blank H_2 leak measurements.

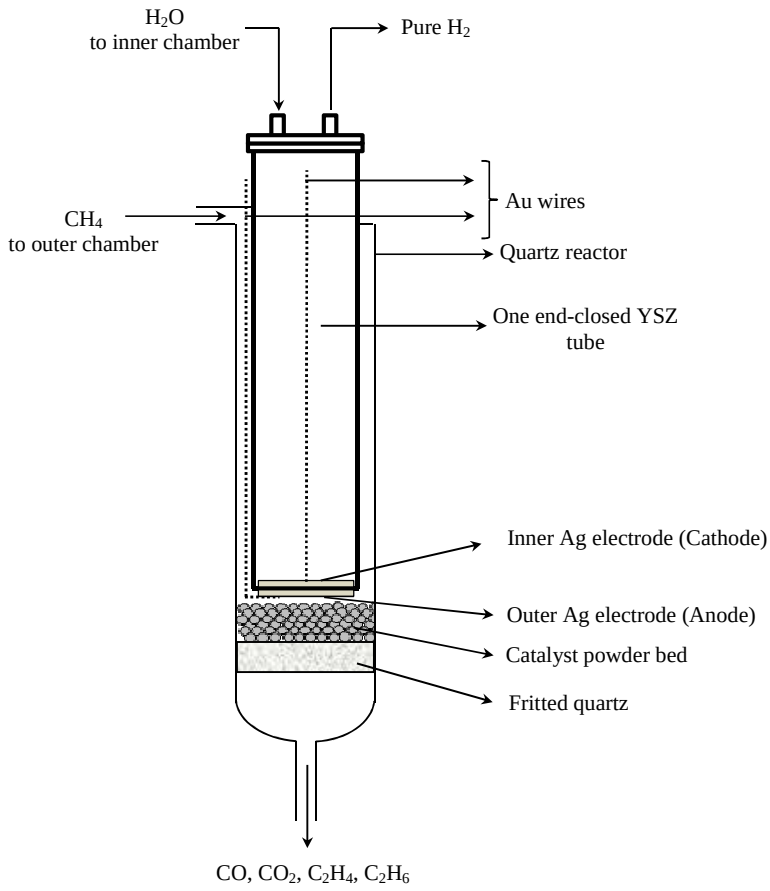

Figure 8.1 Scheme of double chamber solid electrolyte cell reactor.

8.2.3 Catalyst evaluation

The reaction gases (Praxair, Inc.) were certified standards of 10% CH_4/N_2, natural gas, and N_2 (99.999% purity) used as carrier gas. The gas flow was controlled by a set of calibrated mass flowmeters (Brooks 5850 E and 5850 S) while water was introduced into the feed stream by means of a saturator in order to achieve liquid-vapour equilibrium. Its content was controlled by the vapour pressure of H_2O at the temperature of the saturator (45 ºC). Thus, 10% water was introduced in a 50 mL min^{-1} feed stream. All lines placed downstream from the saturator were heated above 100 ºC to prevent condensation. Regarding the outer chamber, the reactants were introduced with the following concentrations: CH_4 (0.2-1.5 %), N_2 (balance), with an

overall gas flow rate of 50 cm^3 min^{-1}. It led to a gas hourly space velocity (GHSV) of 15000 cm^3 g^{-1} h^{-1} with respect to the catalyst powder bed. All the catalytic experiments were carried out at atmospheric pressure and at reaction temperatures between 750-800 ºC. Hydrogen produced in the inner chamber was calculated on the basis of Faraday's law. Reactant and product gases of the outer chamber were analysed with a micro gas-chromatograph (Varian CP-4900) equipped with two columns (Molsieve and Poraplot Q column) and two thermal conductivity detectors (TCD). The main detectable products of the outer side stream were C_2H_6, C_2H_4, CO_2, CO and H_2. The deviation associated to the carbon balance did not exceed 2%, which indicated no significant formation of other oxygenated species and/or coking of the catalyst-electrodes. CH_4 conversion, C_{2s} selectivity and C_{2s} yield were calculated by Eqs. 2.1-2.3.

8.3 Results and discussion

First, a dynamic galvanostatic transient experiment was carried out at a constant temperature of 750 ºC. It was performed under current imposition step changes between -10 and -45 mA by passing the following streams: 1 % CH_4 to the outer chamber and 10 % H_2O for the inner chamber, both of them balanced with N_2 at a total flow rate of 50 cm^3 min^{-1}.

Figure 8.2a (left) depicts the variation of the products reaction rates with time on stream under different current impositions, and figure 8.2b represents the scheme of the different reactions and processes that occurred on the system. The dense box simulates the separation between the inner and the outer chamber. It should be mentioned that for all the studied systems, the activity under open circuit conditions (not shown here), i.e., at current = 0 mA, was negligible due to the absence of any oxygen electrochemically supplied to the outer chamber. Hence, methane catalytic decomposition activity was not provided either by the Ag electrodes or by the active catalyst powder materials at the explored temperature range. On the other hand, it could be observed that an increase in the applied current led to a strong increase in the production rate for all the products. This can be easily understood with the scheme shown in Figure 8.2b.

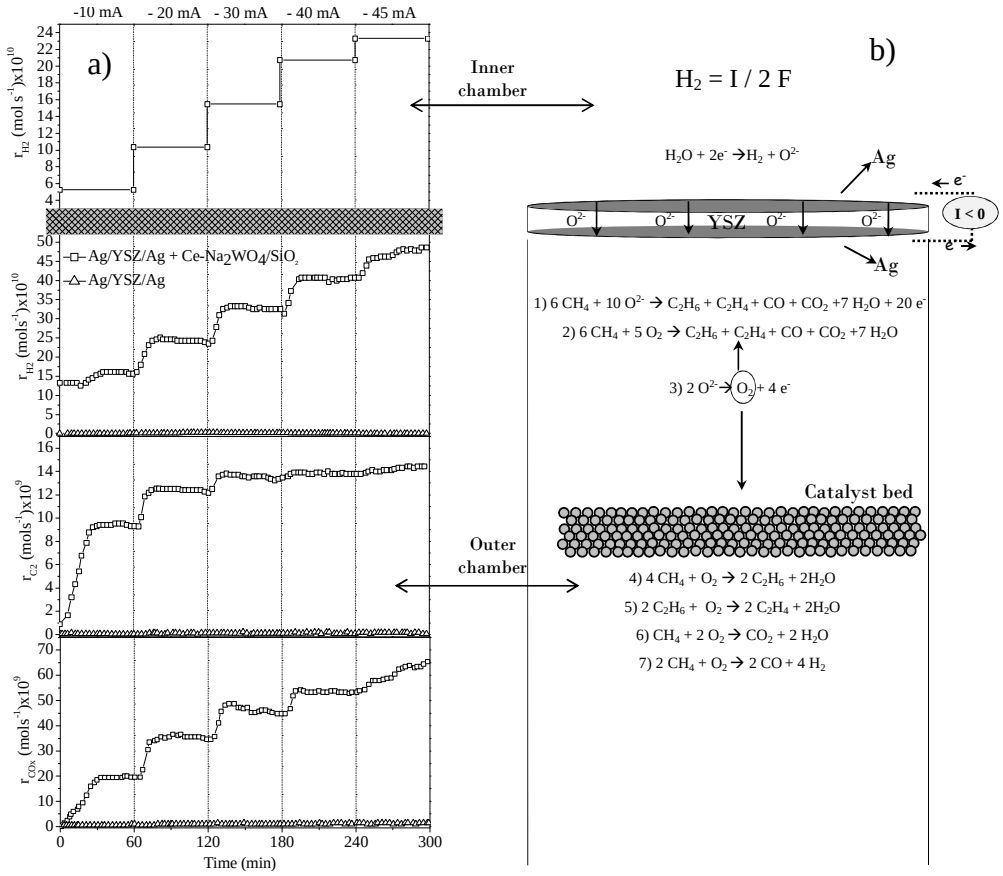

Figure 8.2 a) Influence of the applied current on the dynamic value of the inner (pure H_2) and the outer chamber products (H_2, C_{2s} and CO_x) for the Ce-Na_2WO_4/SiO system b). Schematic representation of the main processes involved during the cathodic polarizations for the above mentioned systems . Conditions: Outer chamber CH_4 = 1%, Inner chamber H_2O = 10%, Total flow in both chambers = 50 cm^3 min^{-1} (N_2 balance), Temperature = 750 ºC.

The YSZ solid electrolyte can be considered as a pure O^{2-} conductor. Thus, the application of negative currents (the inner Ag electrode being the working and the outer Ag electrode being the counter electrode) led to the steam electrolysis process in the Ag inner electrode, with production of pure gaseous H_2 and O^{2-} ions [13,14]. Hence, the H_2 production rate in the inner chamber could be calculated on the basis of Faraday's (rH_2= I/2 F), where I is the applied current, and F is Faraday's constant. Then, an increase of the applied current led to a proportional increase of both pure hydrogen produced and the amount of electrochemically pumped O^{2-} ions from the inner to the outer Ag electrode. It led to the production of carbon derived

products according to the global reactions depicted in Figure 8.2b. Regarding the solid electrolyte cell (SEC from now on), these O^{2-} ions could directly react in the Ag outer electrode with methane (reaction 1) to produce a mixture of C_2 hydrocarbon and CO_x [13,14]. Moreover, as proposed by Tsiakaras and Vayenas [15] the formation of oxygen dissolved species could activate the Ag catalyst to form ethane. Then, it would react with the oxygen evolved to the gas phase (reaction 3) to form ethylene and CO_2 (reaction 2). However, as observed in Figure 8.2a, the production rate of oxidative coupling (C_2 hydrocarbons) and combustion (CO_x) products was practically negligible in the SEC system in comparison with the reaction rate of these compounds under the presence of the active catalyst powder bed in the outer chamber (SEC + PC system from now on). This may be attributed to the reaction of the free oxygen evolved to the gas phase (reaction 3) with methane in the catalyst bed, strongly increasing the catalytic activity of the system (reactions 4-7). Hence, an increase of the applied current, with the concomitant increase in the O_2 pumping rate from the inner to the outer chamber, led to an increase of methane conversion via oxidative coupling (reactions 4 and 5), total oxidation (reaction 6) and partial oxidation (reaction 7), increasing the production rate of C_2 hydrocarbons, CO_x ($CO+CO_2$) and H_2. In addition, it can be observed that the H_2 production rate in the outer chamber via partial oxidation was around two orders of magnitude lower than the H_2 produced via electrolysis in the inner chamber.

In a previous study with a single chamber configuration (chapter VII), it was demonstrated that the SEC performance can be improved for H_2 and C_2 hydrocarbons production by introduction of the 5wt%Ce-5wt%Na_2WO_4/SiO_2 catalyst. In this work, this reaction is performed in a similar system in which two useful products are simultaneously produced and separated. Thus, the experiment shown in Figure 8.2a demonstrates the possibility of simultaneously producing and separating hydrogen and C_2 hydrocarbons with a YSZ-based solid electrolyte cell. In this sense, other electro-catalytic and membrane based systems have been used in literature for the simultaneous production/separation of H_2 and C_2 hydrocarbons [10,11,16]. In the study carried out by the group of Stoukides [10] this concept was demonstrated with solid electrolyte proton conductors using similar 5wt%Ce-5wt%Na_2WO_4/SiO_2 catalyst. This, was a first version of the catalyst which was provided to the group of Stoukides. In their work, Au

plus 5wt%Ce-5wt%Na_2WO_4/SiO_2 were used as anodic catalyst. Au is added because the 5wt%Ce-5wt%Na_2WO_4/SiO_2 catalyst has low electric conductivity. Then, they performed tests with Au alone and Au - 5wt%Ce-5wt%Na_2WO_4/SiO_2 composite. This latter reported to be catalytically more active than alone Au which demonstrates the important role of this type of catalyst in a system where C_2 hydrocarbons and another useful product as H_2 are produced. However, in the Stoukides group configurations [10,11], low current densities (accompanied with low hydrogen production) and low C_2 hydrocarbon yield (around 2.5%) were obtained. Moreover, a recent study carried out by Cao et al. [16] used a similar system as that proposed in this work. It consisted of a double chamber configuration separated by a BSCF oxygen-permeable membrane and coupled with a Mn doped Na_2WO_5/SiO_2 powder catalyst. In that study, the oxygen produced in the inner chamber from thermal water splitting was transported through the BSCF membrane, being consumed in the methane oxidative coupling process occurring in the catalyst bed placed in the outer chamber. However, the results obtained revealed lower C_2 hydrocarbon yield (by 6.5% at 950 ^oC) compared to those reported in this work (by 10% at 775 ^oC). On the other hand, water splitting at high temperatures is a thermodynamically controlled reaction, and hence only small amounts of hydrogen can be generated at equilibrium due to the very low equilibrium constant [16].

Next, the influence of the applied current and reaction temperature on the performance of the system was studied. In order to fix current application range at each temperature, the steady state current-potential curves (in absolute values) of the solid electrolyte cell were obtained at three different operation temperatures (750, 775 and 800 ºC) under the same feed stream conditions of the previous experiment (1% CH_4 in the outer chamber, and 10% H_2O in the inner chamber). The polarization curves were performed until a maximum cell potential of |2 V| in order to preserve stability and to avoid reduction of the YSZ solid electrolyte. Thus, maximum currents of -45, -60 and -70 mA were obtained at 750, 775 and 800 ºC, respectively, at a cell potential close to -2 V (Figure 8.3).

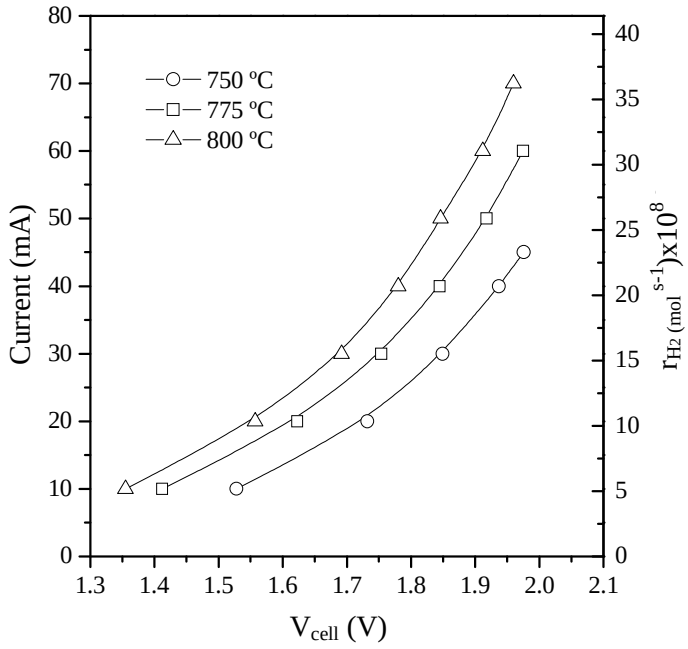

Figure 8.3 Influence of the reaction temperature on both the polarization curves and the H_2 production for the Ag/YSZ/Ag solid electrolyte cell.

In addition, the secondary Y axis shows the equivalent pure H_2 production rate obtained in the inner chamber (calculated via Faraday's law) for each polarization. It may be observed that no mass transfer limitations occurred at any temperature, since no limiting current at the studied potential range was observed [17]. Moreover, as expected, a reaction temperature increase led to a current increase at a fixed cell potential and, consequently, to a higher H_2 production rate. This can be attributed to an enhancement of the reaction rate for the steam electrolysis process and the increase of the O^{2-} ionic conductivity of the YSZ solid electrolyte.

Thus, the influence of the applied current on the main reaction parameters of the oxidative coupling process at the outer chamber for the SEC and the SEC + PC systems for three temperatures (750, 775 and 800) ^oC is shown in Figures 8.4, 8.6 and 8.7, respectively. In all these Figures, a third X axis shows the CH_4/O_2 ratio. Feed stream compositions were the same as described for previous experiments. The explored current application range at each temperature was selected according to the previously obtained current-potential curves (Figure 8.3).

In the first place, it can be observed that methane conversion over the outer Ag electrode was almost negligible at all the explored reaction temperatures. Then, the activity was mainly provided by the addition of the catalyst, which is in good agreement with the experiments shown in Figure 8.2. On the other hand, the CH_4 conversion increases as the applied current increases (Figure 8.4).

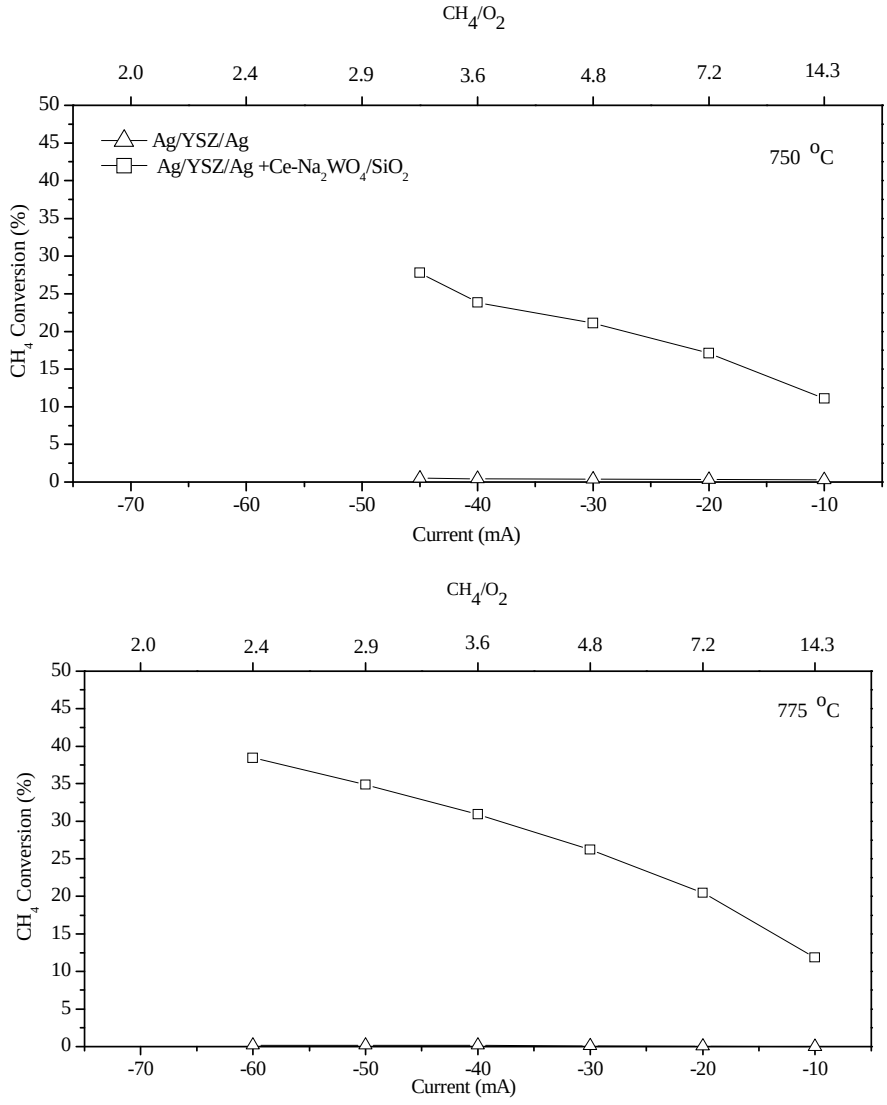

Figure 8.4 Influence of the reaction temperature and the current imposition for the Ag/YSZ/Ag, Ag/YSZ/Ag + Ce-Na_2WO_4/SiO_2 systems on CH_4 conversion. Conditions: Outer chamber CH_4 = 1%, Inner chamber H_2O = 10%, Total flow in both chambers = 50 cm^3 min^{-1} (N_2 balance).

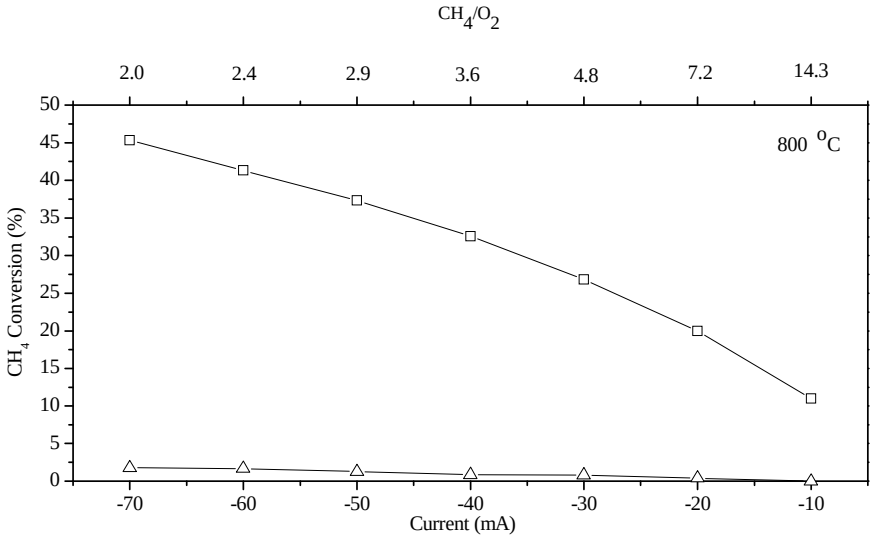

Figure 8.4 (Cont.) Influence of the reaction temperature and the current imposition for the Ag/YSZ/Ag, Ag/YSZ/Ag + Ce-Na_2WO_4/SiO_2 systems on CH_4 conversion. Conditions: Outer chamber CH_4 = 1%, Inner chamber H_2O = 10%, Total flow in both chambers = 50 cm^3 min^{-1} (N_2 balance).

In other words, CH_4 conversion increases as CH_4/O_2 decreases. This behaviour agrees with literature. This dependence is common to various catalysts and reactor designs which can be explained by the different apparent reaction orders of primary selective and non-selective reaction steps with respect to oxygen and methane (see section 1.7.2). In addition, it can be observed in Figure 8.5 that CH_4 conversion increases with the rise of temperature at CH_4/O_2 ratio of 3.6. However, a slight decrease in CH_4 conversion decrease is observed above CH_4/O_2 = 4.8. This may be related to the consecutive reactions of oxidation which occur also in the gas phase. Taking into account the O_2 balance, oxygen conversion was enhanced over this catalyst bed. As reported by Choudhary and Mulla [18], an increase of the oxygen present in the reaction atmosphere led to a lower selectivity towards C_2 hydrocarbons in benefit of the CO_x selectivity , which would be a consequence of the homogeneous oxidation of C_2 products. Therefore, a decrease of selectivity at high temperatures, caused by oxidation of C_2 hydrocarbons, is also associated to a decrease of methane conversion. [19].

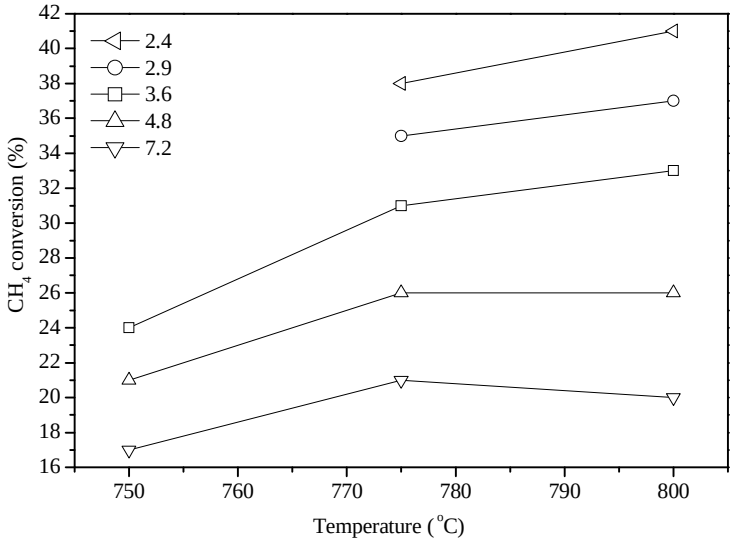

Figure 8.5 Effect of temperature and CH_4/O_2 on CH_4 conversion.

Figure 8.6 shows influence of the current on C_2 yield. A similar trend of C_2 yield with CH_4 conversion at 750 ^oC is observed. However, at temperatures of 775 and 800^oC, C_2 yield increased up to a determined CH_4/O_2 ratio and then a slight decrease was observed. This is because C_2 selectivities exhibited the same behaviuor. As mentioned above, a decrease of selectivity at high temperatures is caused by oxidation of C_2 hydrocarbons. However, the dependence of C_2 yield on CH_4/O_2 ratios is still accompanied with methane conversion, as the highest C_2 yields are achieved at the highest conversion of methane but not at the highest C_2 selectivities.

The variation of the ethylene/ethane ratio under the different conditions studied is shown in Figure 8.7. The increase of the reaction temperature and the applied current had a positive effect on this ratio. Moreover, the obtained values for the system were relatively high (ethylene/ ethane > 4) for most of the explored currents, if they are compared to those obtained in similar studies reported in the literature, with ethylene/ethane ratios ranging from 2 to 3 [20,14]. This may be attributed to the homogeneous oxidative dehydrogenation of ethane reached with this reactor configuration (ODE). As reported in literature an important activity for the non-catalytic or homogeneous ODE reaction could be found in the reaction temperature range studied in this work.

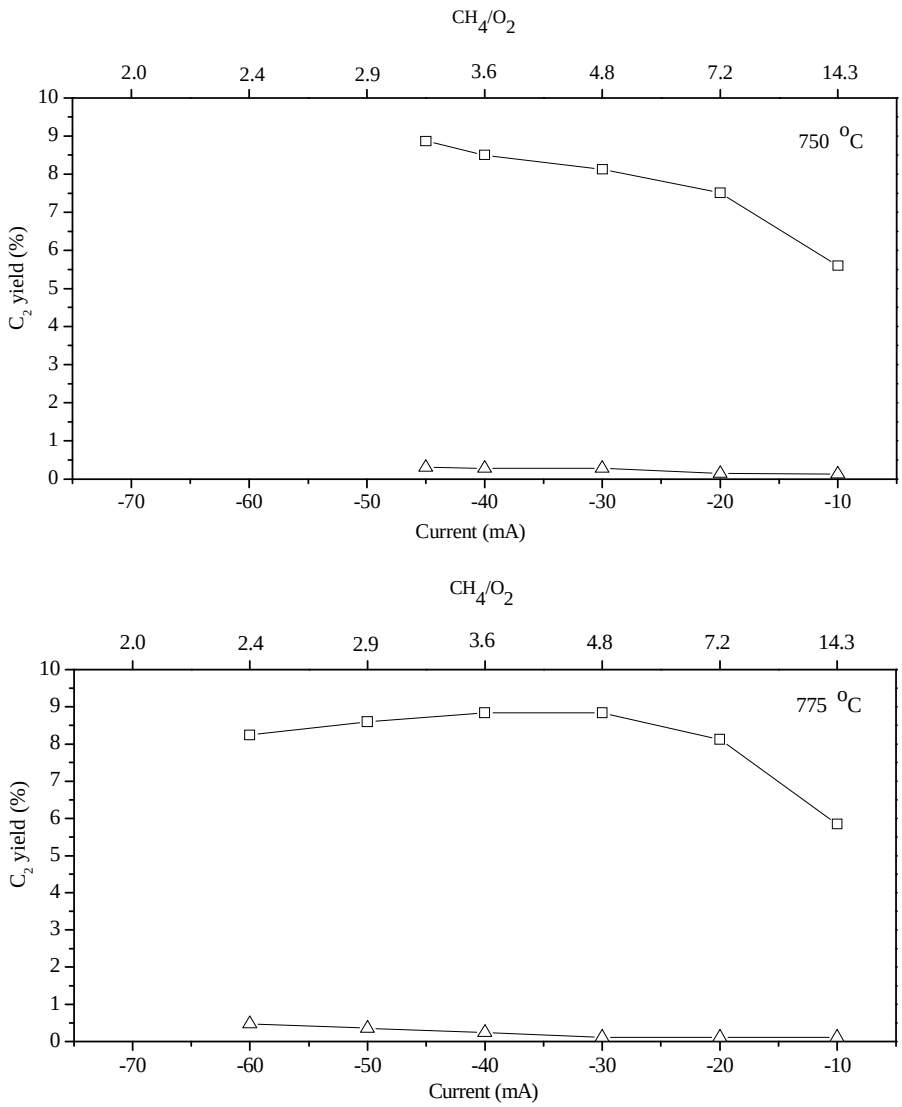

Figure 8.6 Influence of the reaction temperature and the current imposition for the Ag/YSZ/Ag, Ag/YSZ/Ag + Ce-Na_2WO_4/SiO_2 systems on C_2 yield. Conditions: Outer chamber CH_4 = 1%, Inner chamber H_2O = 10%, Total flow in both chambers = 50 cm^3 min^{-1} (N_2 balance).

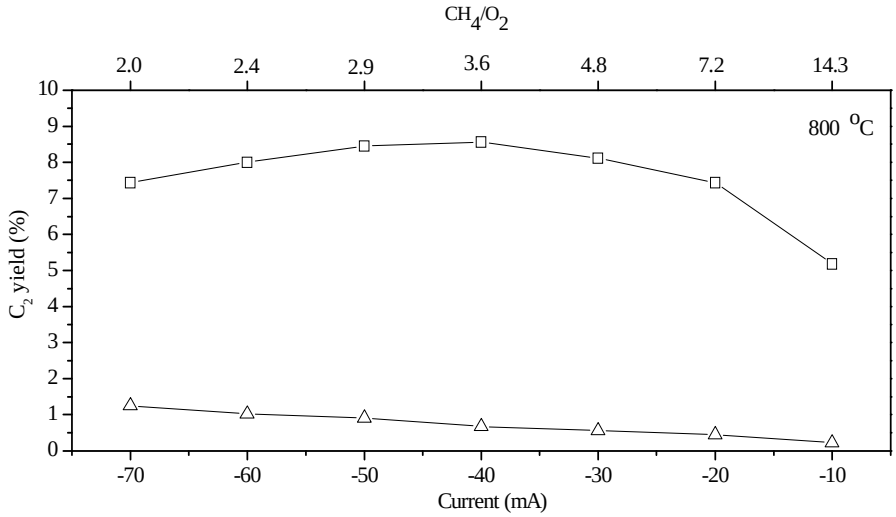

Figure 8.6 (Cont.) Influence of the reaction temperature and the current imposition for the Ag/YSZ/Ag, Ag/YSZ/Ag + Ce-Na_2WO_4/SiO_2 systems on C_2 yield. Conditions: Outer chamber CH_4 = 1%, Inner chamber H_2O = 10%, Total flow in both chambers = 50 cm^3 min^{-1} (N_2 balance).

The maximum C_2 yield (about 10%) for the 5wt%Ce-5wt%Na_2WO_4/SiO_2 catalyst was found at 775 ºC (higher temperatures enhanced the methane combustion in detriment of the oxidative coupling process). Hence, in order to optimize the reaction parameters as a function of the composition, methane concentration was changed considering a fixed oxygen partial pressure under a constant current application and the same feed stream conditions in the inlet chamber (10% H_2O, 50 cm^3 min^{-1}, N_2 balance), at the aforementioned temperatures.

Finally, the C_2 yields obtained for the SEC + PC system at the different methane concentrations are shown in Figure 8.8. As observed in this Figure, the production of C_2 hydrocarbons passed through a maximum. Based on the reaction products, the optimum could be explained attending to the competition between the methane coupling and combustion processes. Thus, although the overall methane reaction rate increased with the methane concentration, the selectivity towards C_2 hydrocarbons slightly decreased, leading to an optimum C_2 yield (10.4%). On the other hand, it should be mentioned that the CH_4/O_2 ratio that optimizes the C_2 yield for the SEC system coupled with the 5wt%Ce-5wt%Na_2WO_4/SiO_2 powder catalyst was established at 3.95. This value is different from that reported in a previous

work performed with the same catalyst powder in a single chamber configuration (0.85) [14]. This can be attributed to the double chamber reactor configuration used here, which improved the contact between methane and the oxygen electrochemically supplied.

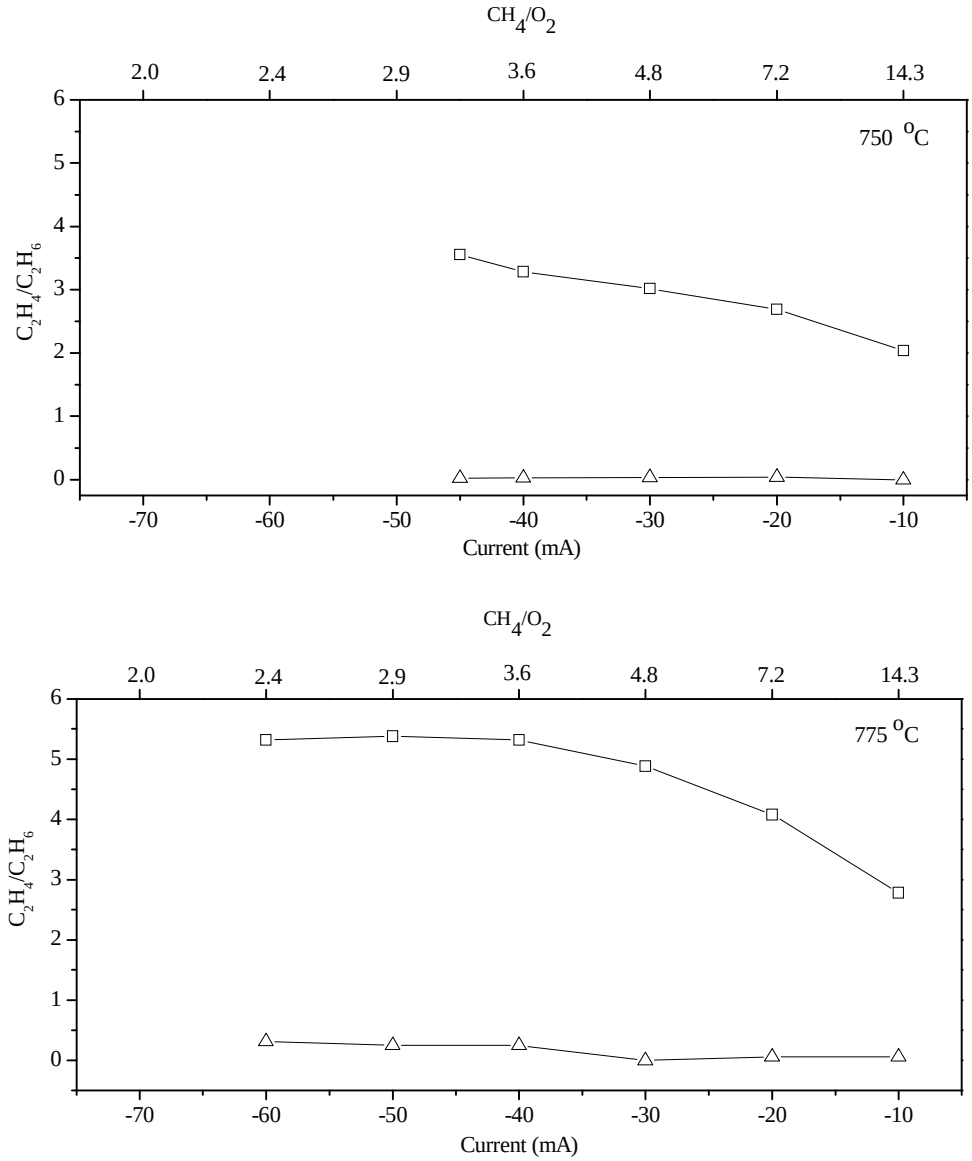

Figure 8.7 Influence of the reaction temperature and the current imposition for the Ag/YSZ/Ag, Ag/YSZ/Ag + Ce-Na_2WO_4/SiO_2 systems on C_2H_4/C_2H_6 ratio. Conditions: Outer chamber CH_4 = 1%, Inner chamber H_2O = 10%, Total flow in both chambers = 50 cm^3 min^{-1} (N_2 balance).

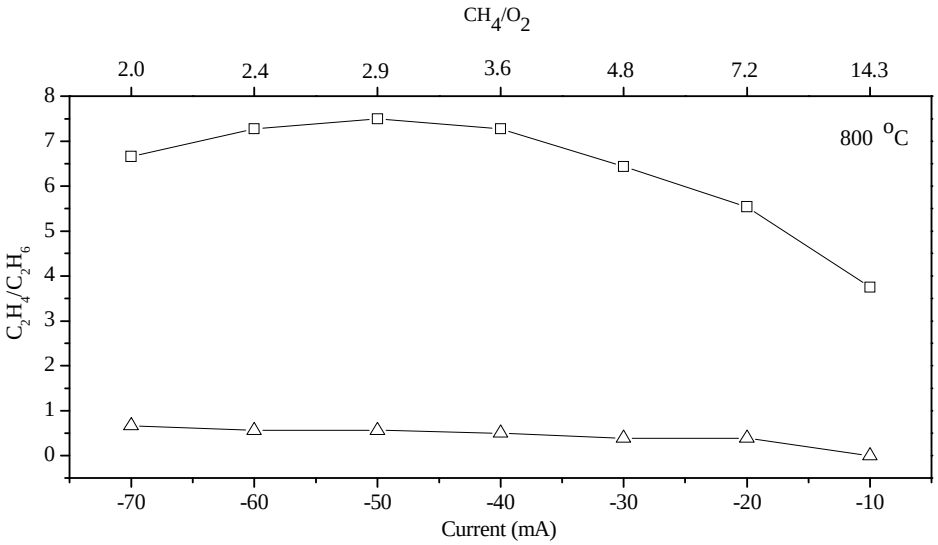

Figure 8.7 (Cont.) Influence of the reaction temperature and the current imposition for the Ag/YSZ/Ag, Ag/YSZ/Ag + Ce-Na_2WO_4/SiO_2 systems on C_2H_4/C_2H_6 ratio. Conditions: Outer chamber CH_4 = 1%, Inner chamber H_2O = 10%, Total flow in both chambers = 50 cm^3 min^{-1} (N_2 balance).

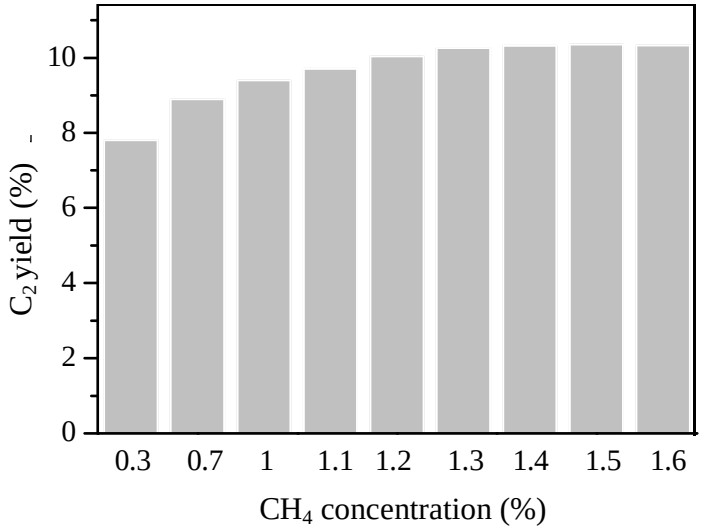

Figure 8.8 Influence of the inlet CH_4 concentration under fixed current imposition on the C_2 yield for the Ag/YSZ/Ag + Ce-Na_2WO_4/SiO_2 system. Operating conditions: Outer chamber CH_4 = 0.3-1.6%, Inner chamber H_2O = 10%, Total flow in both chambers = 50 cm^3 min^{-1} (N_2 balance), Temperature = 775.

8.4 Conclusions

In this work, pure H_2 and C_2 hydrocarbons were simultaneously produced and separated by means an Ag/YSZ/Ag double chamber solid oxide electrolysis cell. As expected, electrolyzed steam on the inner Ag electrode of the electrochemical cell allowed to produce pure H_2. On the other hand, the presence of the 5wt%Ce-5wt%Na_2WO_4 /SiO_2 catalyst (system SEC+PC) proved to be crucial to obtain higher C_2 yield when compared to SEC. Reaction temperature and gas phase composition were optimized. The optimal C_2 yield was ca.10% at 775 oC and CH_4/O_2 = 3.95.

References

[1] Paul Mann C, Walsh PR, Mackey PJ, Jaising V, Hwang HH, Chen JC, Maheshwari M, Dan CA, *Petrochemicals Preparing for a Supercycle*. Morgan stanley blue pape (October 2010)

[2] Keller GE, Bhasin MM, *Synthesis of ethylene via oxidative coupling of methane: I. Determination of active catalysts*. Journal of Catalysis **73** (1982) 9-19.

[3] Au PCT, Liu YW, Ng CF, *Raman Spectroscopic and TPR Studies of Oxygen Species over BaO- and BaX2(X=F, Cl, Br)-Promoted Nd_2O_3Catalysts for the Oxidative Coupling of Methane*. Journal of Catalysis **176** (1998) 365-375.

[4] Kondratenko EV, Maksimov NG, Selyutin GE, Anshits AG, *Oxidative coupling of methane over oxides of alkali earth metals using N_2O as oxidant*. Catalysis Today **24** (1995) 273-275.

[5] Kuś S, Otremba M, Taniewski M, *The catalytic performance in oxidative coupling of methane and the surface basicity of La_2O_3, Nd_2O_3, ZrO_2 and Nb_2O_5*. Fuel **82** (2003) 1331-1338.

[6] Myung-Jin Lee J-HJ, Jin-Seung Jung, Yong-Rok Kim, Lee aS-H, *Catalytic Activities of Perovskite-type $LaBO_3$ (B = Fe, Co, Ni) Oxides for Partial Oxidation of Methane*. Bull Korean Chem Soc **26** (2005) 1591-1596.

[7] Shamsi A, Zahir K, *Oxidative coupling of methane over perovskite-type oxides and correlation of Tmax for oxygen desorption with C_2 selectivity*. Energy & Fuels **3** (1989) 727-730.

[8] Traykova M, Davidova N, Tsaih J-S, Weiss AH, *Oxidative coupling of methane – the transition from reaction to transport control over La_2O_3/MgO catalyst*. Applied Catalysis A: General **169** (1998) 237-247.

[9] Yamamura M, Okado H, Tsuzuki N, Wakatsuki T, Otsuka K, *Oxidative coupling of methane over ternary metal oxide catalysts consisting of Groups I, III and V elements in the Periodic Table*. Applied Catalysis A: General **122** (1995) 135-149.

[10] Kyriakou V, Athanasiou C, Garagounis I, Skodra A, Stoukides M, *Production of H_2 and C_2 hydrocarbons from methane in a proton conducting solid electrolyte cell using a Au–5Ce–5Na_2WO_4/SiO_2 anode*. International Journal of Hydrogen Energy **37** (2012) 16636-16641.

[11] Kyriakou V, Athanasiou C, Garagounis I, Skodra A, Stoukides M, *Production of C_2 hydrocarbons and H2 from CH_4 in a proton conducting cell*. Solid State Ionics **225** (2012) 219-222.

[12] Stoukides M, *Methane conversion to C2 hydrocarbons in solid electrolyte membrane reactors*. Res Chem Intermed **32** (2006) 187-204.

[13] Caravaca A, de Lucas-Consuegra A, González-Cobos J, Valverde JL, Dorado F, *Simultaneous production of H_2 and C_2 hydrocarbons by gas phase electrocatalysis*. Applied Catalysis B: Environmental **113–114** (2012) 192-200.

[14] Caravaca A, Ferreira VJ, de Lucas-Consuegra A, Figueiredo JL, Faria JL, Valverde JL, Dorado F, *Simultaneous production of H2 and C2 hydrocarbons by using a novel configuration solid-electrolyte + fixed bed reactor*. International Journal of Hydrogen Energy **38** (2013) 3111-3122.

[15] Tsiakaras P, Vayenas CG, *Oxidative Coupling of CH4 on Ag Catalyst-Electrodes Deposited on ZrO_2 (8 mol% Y_2O_3)*. Journal of Catalysis **144** (1993) 333-347.

[16] Cao Z, Jiang H, Luo H, Baumann S, Meulenberg WA, Voss H, Caro J, *Simultaneous overcome of the equilibrium limitations in BSCF oxygen-permeable membrane reactors: Water splitting and methane coupling*. Catalysis Today **193** (2012) 2-7.

[17] Bockris JOM, Reddy AKN, Modern Electrochemistry. Springer; 2nd edition Edited by Bockris JOM, (1998) 828

[18] Choudhary VR, Mulla SAR, *Coupling of thermal cracking with noncatalytic oxidative conversion of Ethane to Ethylene*. AIChE Journal **43** (1997) 1545-1550.

[19] Mleczko L, Baerns M, *Catalytic oxidative coupling of methane—reaction engineering aspects and process schemes*. Fuel Processing Technology **42** (1995) 217-248.

[20] Gholipour Z, Malekzadeh A, Hatami R, Mortazavi Y, Khodadadi A, *Oxidative coupling of methane over (Na_2WO_4+Mn or Ce)/SiO_2 catalysts: In situ measurement of electrical conductivity*. Journal of Natural Gas Chemistry **19** (2010) 35-42.

9 Conclusions and future work

In this section a brief summary of the main results is presented and some conclusions are drawn regarding catalyst preparation, characterisation and testing (on conventional reactors and SEMRs) for the oxidative coupling of methane. Additionally, some guidelines for future work are suggested.

9.1 Main conclusions

In this research work, different catalysts were developed for the OCM reaction. The catalysts were tested in conventional reactors in which only C_2 hydrocarbons were produced. Then, the OCM reaction over the best catalyst was performed in an electrocatalytic system to produce simultaneously C_2 hydrocarbons and H_2.

Mixed oxide catalysts.

Several approaches were attempted for surface chemical and morphological modification of CeO_2 to obtain active and selective catalysts. To this end, alkali, alkaline earth and transition metals (Ti) were used as dopants. It was evidenced that incorporation of Li, Na and Ca in CeO_2 created different basic sites on the catalyst surface which were classified as weak, intermediate and strong basic sites.

Incorporation of the above metals led to a significant increase in the C_2 selectivity and yield when compared with CeO_2. In addition, it was found that C_2 selectivity and yield pass through a maximum in the range of temperatures between 700 and 800 ^oC. This behaviour was observed with the catalysts reported to have higher selectivity, namely $Li_{0.5}Ce_{0.5}O$, $Na_{0.5}Ce_{0.5}O$ and $Ca_{0.5}Ce_{0.5}O$. This latter showed the best performance in the OCM reaction, which could be attributed to its easy reducibility and large amount of intermediate basic sites.

These results indicate that incorporation of metals plays an important role in the creation of active sites on the CeO_2 surface for improving their performance in OCM. Thus, alkaline earth metals such as Mg, Ca and Sr were used to modify the CeO_2 surface. The incorporation of these metals as metal ions allowed the substitution of ions on the ceria surface, with the creation of oxygen "interstitial" species, namely O_2^{2-} and O_2^{-}.

A linear relationship between the total amount of basic sites and the relative amount of electrophilic oxygen species and lattice oxygen on the surface of the catalyst, $[(O_2^{2-} + O_2^{-})/ O^{2-}]$, was found. It was demonstrated that this ratio controls the amount of basic sites, CH_4 conversion, and selectivity to C_2H_6 and C_2H_4.

Then, active and selective Ce-doped La_2O_3 catalysts, with a Ce/La molar ratio of 1:3, were prepared by using two procedures, namely the citrate and

solvothermal methods. Both methods allowed the formation of a solid solution ($La_xCe_{1-x}O_{1.5+\delta}$) which means that Ce was incorporated into the La_2O_3 lattice as substitution ions, creating interstitial electrophilic oxygen species on the catalyst surface. The citrate method generated O^- and O_2^{2-} surface oxygen species, while the solvothermal method generated only O^- oxygen species. It was observed that the different oxygen species created are related with the different types of surface cerium ions (Ce^{3+} or Ce^{4+}). The catalyst prepared by the solvothermal method showed higher concentration of [Ce^{3+}].

Finally, the O^- oxygen species predominant on the $La_{0.75}Ce_{0.25}O$(SM) catalyst was suggested to be responsible for higher C_2 yield (by 10.5 %) at 750 ^oC in the oxidative coupling of methane.

Supported catalysts.

Three X%wt Ce-5%wtNa_2WO_4/SiO_2 catalysts were prepared by varying the amount of Ce in three concentrations (2, 5 and 7 %wt) resulting in materials with different proportions of amorphous and α-crystobalite silica phase. This resulted from the influence of the amount Ce which also led to the creation of different species active and selective towards C_2 hydrocarbons.

In order to enhance the C_2 yields and to compare with those reported in literature, a reactor of smaller inner diameter was used. Thus, higher C_2 selectivities were observed in the temperature range of 600 - 850 ^oC when compared to those obtained in the larger inner diameter reactor. This was attributed to the increase of the gas flow rate, which controls steep axial and radial temperature gradients to avoid reactor runaway condition. In other words, a higher gas flow rate allows to limit the possibility of deep oxidation of CH_4 and C_2 products.

The catalyst containing 5wt%Ce showed the best performance, since CH_4 conversion and C_2 yield presented maximum values (39 and 26 %, respectively) in the temperature range of 700-850 ^oC. This Ce concentration seems to be the appropriate amount of Ce to minimise its inhibiting effect on the α-cristobalite SiO_2 crystallisation. This allowed to create a mix constituted by amorphous and α-cristobalite SiO_2. Thus, tungstate-synthetized silica and tungstate-metal oxide interactions were formed during the crystallization process to create active centres to the OCM reaction.

Electrocatalytic simultaneous production of H_2 and C_2 hydrocarbons.

The $Ca_{0.5}Ce_{0.5}O$, $La0._{75}Ce_{0.25}O$ and 5wt%Ce-5wt%Na_2WO_4/SiO_2 catalysts, which had the best performance in OCM reaccion, were studied under a CH_4 wet atmosphere. Both $Ca_{0.5}Ce_{0.5}O$ and $La_{0.75}Ce_{0.25}O$ catalysts showed the maximum C_2 yield at 750 ^oC in the absence of steam. The presence of steam slightly improved the OCM performance over $Ca_{0.5}Ce_{0.5}O$. However, steam showed to have a poisoning effect over $La_{0.75}Ce_{0.25}O$. On the other hand, 5wt%Ce-5wt%Na_2WO_4/SiO_2 catalsyst had the highest C_2 yield of 32% at 800 ^oC in the presence of steam with 25% of water.

$Ca_{0.5}Ce_{0.5}O$ and 5wt%Ce-5wt%Na_2WO_4/SiO_2 catalysts can be used in a system where OCM reaction is integrated as a conventional heterogeneous catalytic process to produce C_2 hydrocarbons and H_2 under humid atmosphere. However, 5wt%Ce-5wt%Na_2WO_4/SiO_2 revealed the best performance.

Thus, the performance of 5wt%Ce-5wt%Na_2WO_4/SiO_2 catalyst was evaluated in a solid electrolyte-fixed bed reactor configuration which was used for the effective simultaneous production of H_2 and C_2 hydrocarbons under a humidified CH_4 gas stream.

The presence of 5wt%Ce-5wt%Na_2WO_4 /SiO_2 catalyst bed strongly increased the catalytic activity towards C_2 hydrocarbon production, and the efficiency of the single chamber steam electrolysis process. An increase in both the reaction temperature and the cathodic current imposed led to higher production of desired compounds (C_2 hydrocarbons and H_2). On the other hand, the overall configuration (solid electrolyte cell + catalyst bed) was found to be stable for long operating times (24 h).

Finally, pure H_2 and C_2 hydrocarbons were simultaneously produced and separated by means of an Ag/YSZ/Ag double chamber solid oxide electrolysis cell over 5wt%Ce-5wt%Na_2WO_4 /SiO_2 catalyst. The presence of the 5wt%Ce-5wt%Na_2WO_4 /SiO_2 catalyst (solid electrolyte cell + catalyst bed) resulted to be crucial to obtain higher C_2 yield when compared to solid electrolyte cell. Reaction temperature and gas phase composition were optimized, thus the optimal C_2 yield was 10% at 775 ^oC and CH_4/O_2 = 3.95.

In summary, Ce-based mixed oxide catalysts were successfully tested in the OCM reaction. In the case of modified CeO_2, the mechanism for the

selective production of C_2 hydrocarbons depends on the type of the surface oxygen created upon incorporation of doping metals. On the other hand, when Ce is used as doping agent on 5wt%N_2WO_4/SiO_2, the effect of the stronger metal-support interaction leads to the formation of mixed phases of amorphous SiO_2 and α-crystobalite and the possible formation of different Na-W species on the support surface when compared to 5%wtNa_2WO_4/SiO_2 surface species. The 5%wtCe-5%wtNa_2WO_4/SiO_2 resulted to be the most active and selective catalyst in OCM to form C_2 hydrocarbons. This improved significantly the overall configuration (solid electrolyte cell + catalyst bed) to produce simultaneously H_2 and C_2 hydrocarbons in both single and double chamber.

9.2 Future work

Oxidative coupling of methane has been denoted as an alternative route for the production of C_2 hydrocarbons from natural gas. However, the process is still economically unfeasible. High conversions and yields remain challenging and more fundamental work should be carried out for further insights.

It was observed that some Ce-based mixed oxides were adequate catalysts for the OCM reaction and that surface modifications by incorporation of earth alkaline metals play an important role in the catalyst performance which was attributed to enhanced basicity. Therefore, in order to take advantage of the basicity properties of modified CeO_2, exploratory screenning tests should be performed with different amounts of the best used dopant metals such as Ca, Na and Li.

The effect of amount of Ce on Na_2WO_4/SiO_2 was studied. It was confirmed that Ce has a significant influence on the crystalization of amorphous silica on Na_2WO_4/SiO_2. Thus, 5wt%Ce resulted to be the optimal concentration to achieve an adequate mixture of amorphous SiO_2 and α-crystobalite in the catalyst 5wt%Ce-5wt%Na_2WO_4/SiO_2. This result suggests that a total change of structure to α-crystobalite might not always be necessary for a good performance compared to literature. However, in order to improve the performance of this catalyst, additional studies are necessary.

To this end, a preliminary study is shown in appendix A. In this study, some effect of Mn on the amorphous silica crystallisation in 5%wtCe-

5%wtNa_2WO_4/SiO_2 was observed. Then, the new catalyst was coupled with an Ag/YSZ/Ag double chamber solid oxide electrolysis cell (as described in section 8.2.2) to separately produce C_2 hydrocarbons and H_2. A higher C_2 yield (16%) was observed when compared to 5%wtCe-5%wtNa_2WO_4/SiO_2 catalyst (10%) at 775 ^oC.

As mentioned in section 5.3.1.1, Na has been reported to be responsible for the phase transition. In addition, some works reported in literature, have denoted that the presence of W favour that transition. Mn is the transition metal frequently used in this type of catalysts (Mn-Na-W/SiO_2) because of its redox properties. However, in these studies Mn was reported as not influencing the phase transition of amorphous silica. Therefore, although addition of Mn leads to a more complex catalyst, it would be interesting to carry out further studies on the effect of Mn to form a catalyst of high crystallinity. This might create different synergic effects between Ce, Na and W for the OCM.

Regarding the practical application of the OCM reaction, the preliminary study allowed to carry out electro-catalytic experiments with natural gas over Mn-doped 5%wtCe-5%wtNa_2WO_4/SiO_2 catalyst. The results revealed hydrogen production and oxygen ions associated with the steam electrolysis ocorring in the inner chamber. The oxygen electrochemically supplied from the inner to the outer chamber led to a mixture of C_2 hydrocarbons and synthesis gas (CO + H_2), i.e., higher catalytic activity towards CO production was observed when natural gas was used. Therefore, in order to determine if the catalyst is responsible for the production of synthesis gas from natural gas, further tests should be carried out with oxygen supplied from the gas phase.

Development of catalysts for the OCM reaction was the main focus of this thesis. Among the developed catalysts, 5wt%Ce-5wt%Na_2WO_4/SiO_2 showed an acceptable performance when tested in a conventional reactor (39 % CH_4 conversion and 26% C_2 yield). It is remarkable that the combination of Ce, Na and W resulted also in a potential catalyst for the OCM reaction, particularly when used in a SEMR + conventional heterogeneous catalysis system to produce C_2 hydrocarbons and H_2. However, yields obtained in such system with 5%wtCe-5%wtNa_2WO_4/SiO_2 did not reach 25 %, which are required for industrial application. Therefore, the effects of metal concentration and SiO_2 precursor should be investigated, as well as the

activity of unsupported Ce or Mn-Na_2WO_4, since such study has not yet been reported in literature.

APPENDIX

Appendix A. Electro-catalytic experiments with natural gas over 5wt%Mn-5wt%Ce-5wt%Na_2WO_4 /SiO_2

The OCM reaction was combined with SEMRs to simultaneously and separately produce C_2 hydrocarbons and H_2. To this end, an active and selective catalyst (5wt%Ce-5wt%Na_2WO_4/SiO_2) was developed. However, yields $\geq$ 25%, required for a practical application, were not obtained. The objective of this study is to improve the catalytic performance of this catalyst using Mn as doping agent. In addition, in order to approach the system to a more practical one, the system was optimized and then analysed by feeding a synthetic gas stream (instead of CH_4).

The silica support was synthetized using the procedure described in section in section 5.2.1. Then, the active catalyst powder was prepared by incipient wetness impregnation of the synthesised silica support with aqueous solutions of the metal precursors. Thus, cerium, manganese and sodium tungsten impregnations to prepare the 5wt%Ce-5wt%Mn-5wt%Na_2WO_4/SiO_2 catalyst, was performed using aqueous solutions of $Ce(NO_3)_3$·6H2O (99% Aldrich), $Mn(NO_3)_2$·$4H_2O$ (97% Sigma-Aldrich) and Na_2WO_4·$2H_2O$ (99% Riedel-deHaën) with the appropriate concentration. Impregnated catalyst was dried at 120 °C after each impregnation overnight, followed by calcination at 800 °C during 8 h.

XRD was carried out as a preliminary characterization to determine the crystalline phases in the new catalyst powder. Thus, an X-ray diffraction analysis of fresh catalyst was performed on a Philips PW 1710 instrument using Ni-filtered Cu Kα radiation. XRD spectrum of fresh catalyst 5wt%Ce-5wt%Mn-5wt%Na_2WO_4/SiO_2 is shown in Figure A.1. The presence at 22^o of a peak corresponding to the presence of α-cristobalite can be again observed. As mentioned in section 5.3.1.1, transformation of amorphous silica to highly crystalline α-cristobalite occurs in the presence of an alkali like sodium tungstate acting as the mineralising agent. CeO_2 and Na_2WO_4 phases were also identified in both catalysts. In addition, the presence of crystalline Mn_2O_3 was observed in catalyst 5wt%Ce-5wt%Mn-5wt%Na_2WO_4/SiO_2.

However, a strong difference of the crystallinity between 5wt%Ce-5wt%Mn-5wt%Na_2WO_4/SiO_2 and 5wt%Ce-5wt%Na_2WO_4/SiO_2 is observed. Thus, the crystallinity of the Mn doped catalyst was higher than that for catalyst Ce-Na_2WO_4/SiO_2 (the peak at 22^o in the Mn doped catalyst difractogram shows a higher intensity).

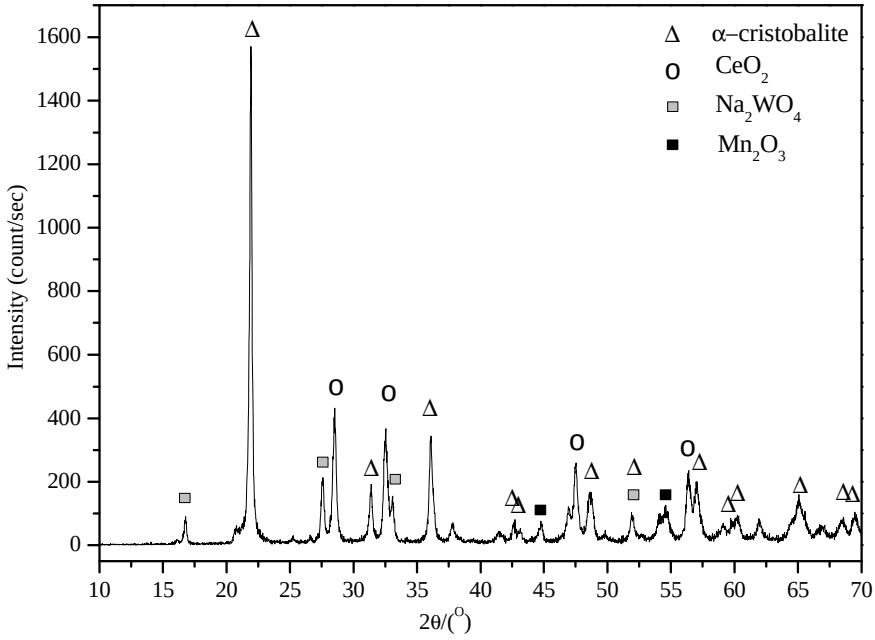

Figure A.1 XRD pattern of the fresh catalyst 5wt%Mn-5wt%Ce-5wt%Na_2WO_4/SiO_2.

The elements Mn and W have not been reported to induce the phase transition in catalysts such as Mn/SiO_2, W/SiO_2 or Na-W/SiO_2 [1]. However, in this preliminary study, Mn seems to have a positive influence in the crystallization of amorphous silica support in presence of the three elements Ce, Na and W. Thus, a research focusing the effect of Mn in this catalysts should necessary to explain this result.

Figure A2 depicts the influence of the reaction temperature on the main reaction parameters of the oxidative coupling process at the outer chamber for the SEC and the SEC + PC systems: methane conversion (Figure A2a) and C_2 hydrocarbons yield (Figure A2b).

Feed stream compositions were the same as described for previous experiments (see section 8.3). The explored current application range at each

temperature was selected according to the previously obtained current-potential curves (Figure 8.3).

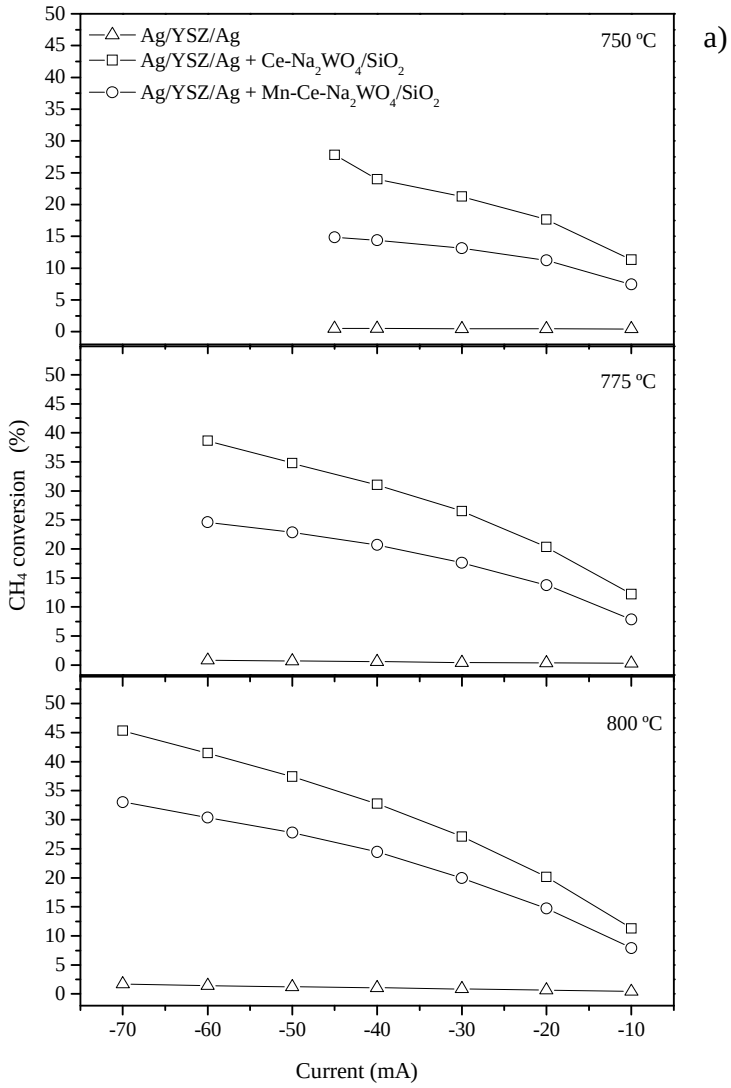

Figure A2 Influence of the reaction temperature and the current imposition for the Ag/YSZ/Ag, Ag/YSZ/Ag + Ce-Na_2WO_4/SiO_2 and Ag/YSZ/Ag + Mn-Ce-Na_2WO_4/SiO_2 systems on: a) CH_4 conversion, b) C_2 hydrocarbon. Conditions: Outer chamber CH_4 = 1%, Inner chamber H_2O = 10%, Total flow in both chambers = 50 cm^3 min^{-1} (N_2 balance).

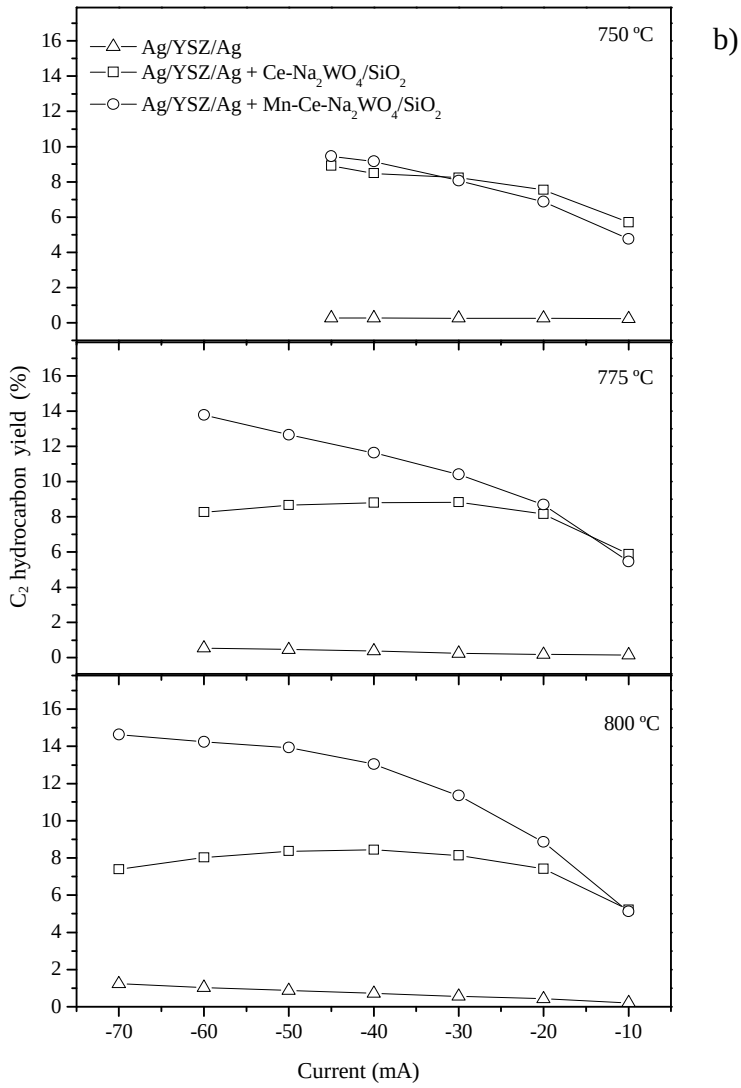

Figure A2 (cont.) Influence of the reaction temperature and the current imposition for the Ag/YSZ/Ag, Ag/YSZ/Ag + Ce-Na_2WO_4/SiO_2 and Ag/YSZ/Ag + Mn-Ce-Na_2WO_4/SiO_2 systems on: a) CH_4 conversion, b) C_2 hydrocarbon. Conditions: Outer chamber CH_4 = 1%, Inner chamber H_2O = 10%, Total flow in both chambers = 50 cm^3 min^{-1} (N_2 balance).

In first place, it can be observed that the methane conversion over the outer Ag electrode was almost negligible at all the explored reaction temperatures. Then, the activity was mainly provided by the addition of the catalyst powders. It can be also observed a higher methane conversion under the presence of the 5wt%Ce-5wt%Na_2WO_4/SiO_2 catalyst (Figure A2a).

However, higher activity towards methane oxidative coupling process was observed for the Mn doped catalyst (higher C_2 hydrocarbon yield, as observed in Figure A2b). This latter can be clearly observed at temperatures higher than 750 ºC, where similar C_2 hydrocarbon production rates were detected for both catalysts.

This higher activity could be explained according to the higher crystallinity observed for the Mn doped catalyst (Figure A1). Previous works have demonstrated that the phase transition from amorphous silica to crystalline form (α-cristobalite) is an essential requirement for an effective oxidative coupling catalyst. It was reported that amorphous SiO_2, with and without Na, is basically a total oxidation catalyst [1]. After the phase transition to α-cristobalite, the material can be considered as inert. In the case of Ce-Na_2WO_4/SiO_2 catalysts, it seems that the amorphous SiO_2 support partially crystallized into α-cristobalite during the calcination process. It supports, as observed in Figure A2a, the higher activity of catalyst 5wt%Ce-5wt%Na_2WO_4/SiO_2 towards methane combustion.

Although methane is the main component of the natural gas, there are other hydrocarbons that could strongly affect the activity of the catalytic system. Hence, preliminary experiments were performed considering 1% natural gas (50 cm^3 min^{-1}, N_2 balance) instead of methane as the outer chamber feed stream, and the SEC + PC system, accomplished with a bed of catalyst 5wt%Ce-5wt%Mn-5wt%Na_2WO_4/SiO_2. The composition of the natural gas is given in Table A1.

Table A1 Natural gas composition.

Hydrocarbon	Molecular formula	Concentration (%)
N-Butane	C_4H_{10}	0.30
Isobutane	C_4H_{10}	0.30
Propane	C_3H_8	1.49
Ethane	C_2H_6	4.94
Methane	CH_4	92.96

The feed stream of the inner chamber was the same as that used in the previous experiments (10% H_2O, 50 cm^3 min^{-1}, N_2 balance).

Figure A3 shows the response of a dynamic galvanostatic transient experiment on the main reaction products obtained in the outer compartment, at a constant temperature of 800 ºC.

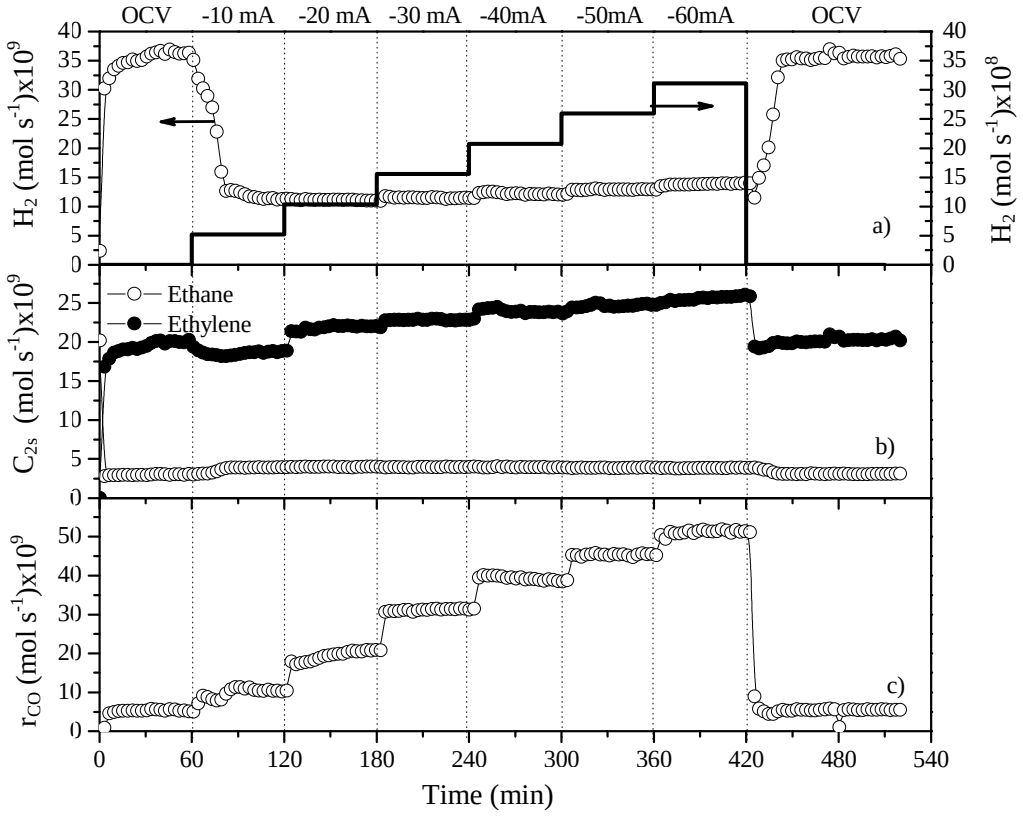

Figure A3 Influence of the applied current on the dynamic value of the outer chamber products (H_2, C_2H_6, C_2H_4, CO_x) for the Ag/YSZ/Ag + Mn-Ce-Na_2WO_4/SiO_2 system. Conditions: Outer chamber Natural gas = 1%, Inner chamber H_2O = 10%, Total flow in both chambers = 50 cm^3 min^{-1} (N_2 balance), Temperature = 800 ºC.

The secondary axis of Figure A3 depicts the theoretical H_2 produced at the inner chamber as a function of the Faraday's law, as previously explained in Figure 8.2. Considering the composition of the natural gas, under open circuit potential conditions (OCV, current = 0 mA), a strong increase of the ethylene production rate was observed. In this sense, the outlet ethylene concentration under these conditions was similar to the inlet ethane concentration in the outer chamber feed stream. On the other hand, a strong increase of the hydrogen produced under OCV conditions was also observed.

These results suggest that the main route for ethylene production was that of the thermal cracking of ethane [2] since there is no oxygen electrochemically supplied to the outer chamber under OCV conditions. Moreover, the hydrogen production was higher than the corresponding to the above mentioned process, which could be attributed to the cracking or dehydrogenation of other hydrocarbons present in the natural gas. In addition, it is interesting to note that a small amount of CO_x was produced under OCV conditions, which would indicate that a slight spontaneous O_2 flux took place under these conditions. On the other hand, the application of currents from -10 to -60 mA led to a decrease of the hydrogen production respect the OCV conditions, with a progressive increase of the C_2 hydrocarbons and CO_x reaction rates, which could be again attributed to the enhancement of the kinetics corresponding to the methane oxidative coupling and partial or total combustion processes. Finally, Figure A3 shows that the polarization effect was totally reversible, since the catalytic activity under the final OCV conditions were very similar to those considered at the beginning of the experiment.

The main parameters related to the catalytic activity of the SEC + PC system in the outer chamber were studied for the experiments described above. Figure A4a depicts the ethylene yield variation with the applied current at 800 ºC. First, a general increase of this parameter for both systems with the increase of the applied current can be observed. However, it seems that the system was more active towards ethylene production when natural gas was fed to the outer chamber. As previously mentioned, it could be attributed to the additional ethylene production from the heterogeneous/homogeneous oxidative dehydrogenation mechanism of the ethane present in the raw natural gas stream. On the other hand, the catalytic activity towards CO production is shown in Figure A4b. Similarly to the trend observed in Figure A4a, a general increase of this parameter was found when natural gas was fed to the outer chamber. The CO yield was around 1.5-2 times higher for the case of using natural gas than that for the case of using methane. It could be attributed to the partial oxidation of other hydrocarbons (apart from methane) with the O_2 supplied from the inner to the outer chamber by the

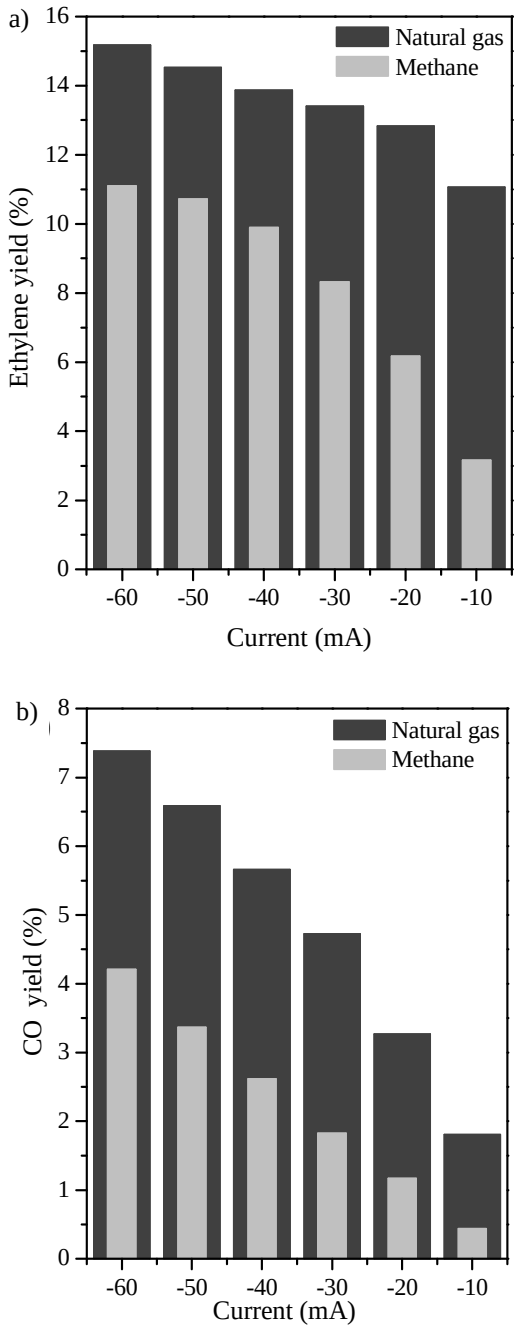

Figure A4 Influence of the applied current on the steady state values of ethylene yield, CO yield and H_2/CO ratio of the outer chamber products for the Ag/YSZ/Ag + Mn-Ce-Na_2WO_4/SiO_2 system. Conditions: Outer chamber Natural gas = 1%, Inner chamber H_2O = 10%, Total flow in both chambers = 50 cm^3 min^{-1} (N_2 balance), Temperature = 800 ºC.

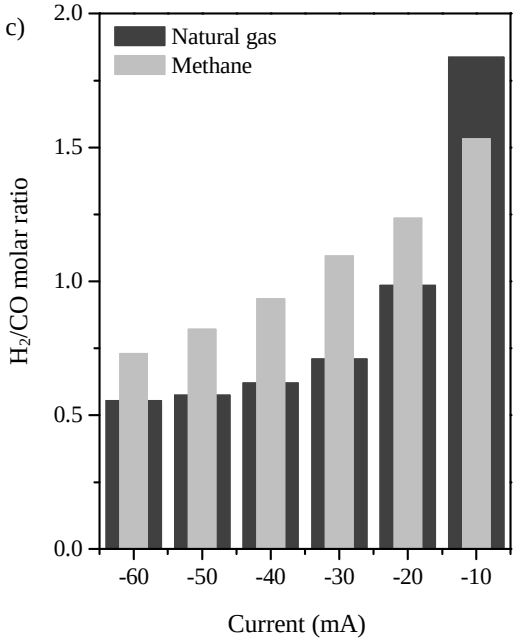

Figure A4 (cont.) Influence of the applied current on the steady state values of ethylene yield (a), CO yield (b) and H_2/CO ratio (c) of the outer chamber products for the Ag/YSZ/Ag + Mn-Ce-Na_2WO_4/SiO_2 system. Conditions: Outer chamber Natural gas = 1%, Inner chamber H_2O = 10%, Total flow in both chambers = 50 cm^3 min^{-1} (N_2 balance), Temperature = 800 ºC.

steam electrolysis process since both, ethane and propane, are more reactive than methane [3].

Finally, an important parameter to be evaluated is the H_2/CO ratio, which defines the quality of the produced synthesis gas. As it can be observed in Figure A4c, the H_2/CO ratio decreased as the applied current increased. It may be due to the enhancement of the total combustion process in detriment of the partial oxidation. Moreover, it is interesting to note that the natural gas fed to the system led to a broad range of H_2/CO ratios. Syngas is a versatile feedstock that can be used to produce a variety of fuels and chemicals, such as methanol, Fischer–Tropsch fuels, ethanol, and dimethyl ether (DME) [4]. In this sense, H_2/CO ratios close to 1 are used in literature to produce lower alkenes In general, for DME production and oxygenated compounds, a syngas ratio of 1 is also needed, whereas for Fischer–Tropsch synthesis, the required syngas ratio varies from 1 to 2.1 depending on the catalyst and pressure used [5].

The configuration used in this study with the new catalyst led to a mixture of C_2 hydrocarbons and synthesis gas from natural gas. Therefore, further research is necessary to optimize this catalyst and consequently use natural gas instead of methane for a practical development of this new technology.

References

[1] Arndt S, Otremba T, Simon U, Yildiz M, Schubert H, Schomäcker R, *$Mn–Na_2WO_4/SiO_2$ as catalyst for the oxidative coupling of methane. What is really known?* Applied Catalysis A: General **425–426** (2012) 53-61.

[2] Choudhary VR, Mulla SAR, *Coupling of thermal cracking with noncatalytic oxidative conversion of Ethane to Ethylene*. AIChE Journal **43** (1997) 1545-1550.

[3] Demoulin O, Le Clef B, Navez M, Ruiz P, *Combustion of methane, ethane and propane and of mixtures of methane with ethane or propane on Pd/γ-Al2O3 catalysts*. Applied Catalysis A: General **344** (2008) 1-9.

[4] Gangadharan P, Kanchi KC, Lou HH, *Evaluation of the economic and environmental impact of combining dry reforming with steam reforming of methane*. Chemical Engineering Research and Design **90** (2012) 1956-1968.

[5] C.H. Park, W.I. Lee, Nicolais L, Manufacturing: Economic Consideration, in: Wiley Encyclopedia of Composites. Edited by John Wiley & Sons I, (2011)

LIST OF PUBLICATIONS AND COMUNICATIONS

Papers published in International Journals

Ferreira VJ, Tavares P, Figueiredo JL, Faria JL (2012), Effect of Mg, Ca, and Sr on CeO_2 Based Catalysts for the Oxidative Coupling of Methane: Investigation on the Oxygen Species Responsible for Catalytic Performance. Ind. Eng. Chem. Res. **51** (2012) 10535-10541

Caravaca A**, Ferreira VJ**, de Lucas-Consuegra A, Figueiredo JL, Faria JL, Valverde JL, Dorado F, Simultaneous production of H_2 and C_2 hydrocarbons by using a novel configuration solid-electrolyte + fixed bed reactor. International Journal of Hydrogen Energy **38** (2013) 3111-3122.

Caravaca A, de Lucas-Consuegra A, **Ferreira VJ**, Figueiredo JL, Faria JL, Valverde JL, Dorado F, Coupling catalysis and gas phase electrocatalysis for the simultaneous production and separation of pure H_2 and C_2 hydrocarbons from methane and natural gas. Applied Catalysis B: Environmental **142–143** (2013) 298-306.

Paper submitted in International Journals

Ferreira VJ, Tavares P, Figueiredo JL, Faria JL, Ce-Doped La_2O_3 based catalyst for the oxidative coupling of Methane. Catalysis Communications (2013) (accepted).

Publications in national and international congress and conferences

V.J. Ferreira J.L. Figueiredo and J.L. Faria, "**Ce-Na_2WO_4/SiO_2 catalyst for the production of H_2 and C_2 hydrocarbons**", IV Iberian Symposium on Hydrogen, Fuel Cells and advanced Batteries (HYCELTEC 2013), Estoril/Portugal Jun, 2013.

V.J. Ferreira J.L. Figueiredo and J.L. Faria, **"Cerium based catalysts for synthesis of H_2 and C_2 hydrocarbons from a wet CH_4 atmosphere",** 9^o National meeting of catalyse and porous materials, Porto/Porugal May, 2013.

V.F. Ferreira, J.L. Figueiredo and J.L. Faria, **"Effect of steam on the performance of the oxidative coupling of methane using Ce-Na_2WO_4/SiO_2 catalyst"**, International Congress of Chemical Engineering, Seville/Spain June, 2012.

V.F. Ferreira, J.L. Faria, J.L. Figueiredo, **"Modificação de Catalisadores de CeO_2 para o Acoplamento Oxidativo do Metano"**, SPQ National Meeting XXII, Braga, Portugal July, 2011.

V.F. Ferreira, J.L. Faria, J.L. Figueiredo, **"Dopado de catalizadores basados en CeO_2 para el acoplamiento oxidativo de metano"**, XVII Luso-Galego Meeting of Chemistry, Ponte Vedra/ Spain November, 2011.

V.F. Ferreira, J.L. Faria, J.L. Figueiredo, **"Effect of Ca and Mg doping of CeO_2 based catalysts for the Oxidative Coupling of Methane"**, Europa Cat X, Glasgow, Scotland August, 2011.

V.F. **Ferreira**, Bruno F. Machado, Joaquim L. Faria, José L. Figueiredo, **"Catalyst Development for the Oxidative Coupling of Methane"**. XVI Luso – Galego Meeting of Chemistry, Aveiro/Portugal 10-12, November, 2010.